AN INTRODUCTION TO FLUID MECHANICS FOR CARDIOVASCULAR ENGINEERING

GIANNI PEDRIZZETTI

University of Trieste, Italy

PREMISE

This textbook is based on the lecture notes of my course held at the University of Trieste. It is an introductory course on fluid mechanics with emphasis to cardiovascular applications. It develops from preliminary information needed when dealing with flows to the laws governing the dynamics of incompressible flows. It then presents main results of these laws for fundamental problems and to problems typical of cardiovascular flows. Finally, the text introduces the fundamental elements of vortex dynamics to allow a qualitative understanding of complex flows of cardiovascular interest that are discussed in the final clinical-oriented chapters.

By my personal attitude, these notes are synthetic aimed to provide a thread along the material treated, from theoretical background to clinical examples. The topic is so wide that coverage of arguments is certainly incomplete and some important references may be missed.

The material contained in this textbook is still in a preliminary and draft form. The written text can contain numerous inaccuracies due to the rapid writing by a non-native speaker. Besides the written language, many pictures are subjected to copyright.

Last revision: Saturday, July 25, 2020.

TABLE OF CONTENT

A. INTRODUCTORY ELEMENTS

1. Basic Concepts

1.1. Mechanics and continuum

Mechanics is about the law of motion, or equilibrium of momentum. This general field can be divided into three main subjects:

1. *statics*, that deals about equilibrium of forces in absence of motion;
2. *kinematics*, that deals about the description of motion irrespective of the applied forces that create such motion;
3. *dynamics*, the most important and comprehensive part, that regards the relationship between forces and motion.

The term "dynamics" derives from the ancient Greek (δυναμικός) and was renewed in the French word *dynamique* by Leibnitz (1646-1716) where it got the meaning of "pertaining with forces producing motion". The concept of mechanics was addressed in mathematical terms by Newton who demonstrated that forces are the entities that change the motion, or that produce accelerations. Newton laws of classical mechanics were carefully developed for individual point particles of finite mass; they were then extended to rigid bodies and to deformable material. Here we will have to revise these classical laws of mechanics for their applications to fluid elements.

The course is about classical mechanics, it will ignore modern developments like quantum mechanics and theory of relativity whose corrections are largely negligible for objects of size much larger than individual sub-atomic constituent of matters moving with velocities well below the speed of light. We will also deal with pure mechanics and avoid discussing thermic and chemical phenomena, with the exception of a few mentions that are reported where appropriate.

The course is specifically about biological fluids; which are mainly air, water and blood. However, it is important to remark from the beginning that the concept of "fluid" is a "model" used to describe certain phenomena encountered in reality. Fluids and solids represent the main classes of the wider model of "continuum". No material is really a continuum, it is made of individual molecules that are made of atoms, that are made of sub-atomic particle; however, the model of continuum is used to describe macroscopic phenomena whose modification occurs on scales that are much larger than those of individual constituents.

Air and water have molecules whose size is of the order of nanometers (1 nm=10^{-9} m); for them, the scheme of continuum is appropriate when studying macroscopic phenomena whose size is much larger than that. In this sense, macroscopic scales range can be as small in absolute terms as little fractions of a millimeters.

Blood is different; blood is a particulate fluid mixture composed by a percentage of about 50% by plasma (that is essentially water) and another percentage about 50% of red blood cells (this percentage is called hematocrit), plus minor percentages of white cells and other constituents. Red blood cells, transport oxygen in the whole body and are much larger than water molecules. They have a discoidal shape of radius about 8 micrometer (1 μm=10^{-6} m), thicker around the circumference, with thickness about 2 μm, and a thin membrane at the center. It can also be seen as a donut whose hole is covered by a membrane that extends from the surface of the outside ring to the center (see figure 1.1). Thus, the volume of a red blood cell is approximately 10^{-7} mm^3 and, if blood cells covers 50% of blood volume, there are about 5×10^6 red blood cells in one mm^3 of blood.

Based on these figures, blood motion should be described with a corpuscular or a continuous models depending on the size of the vessel under analysis. Large vessels have a diameter ranging from centimeter to millimeters, here the continuum model is appropriate; smaller vessels have a size that can contain some tens of red blood cells across. At the smaller end, the diameter of capillaries is less than 10 μm; here red blood cells flow one after the other in a row, even squeezing to be able to pass through, and the corpuscular nature of blood is fundamental (see figure 1.2).

However, the physiological sites of greater clinical interest, and where the mechanical phenomena take a fundamental relevance, are the heart chambers and the large vessels, like Aorta and carotid for example. In the heart and large vessels blood dynamics can be confidently modelled as that of a continuous fluid. Nevertheless, some phenomena that may still be influenced by its corpuscular nature should be considered separately. This simplified representation of blood allows employing a rich theoretical background of continuous mechanics and differential mathematics that represents the basic tools of most achievements in fluid dynamics.

Figure 1.1. Red Blood Cells (Source: *Anatomical Travelogue*).

The continuous model is appropriate for describing the large scale phenomena of motion, when changes in the fluid motion occurs over distances that are orders of magnitudes larger than individual constituents. A continuous mean can be characterized by either its global properties or its local properties. Examples of global, or integral, properties are the volume V or the mass M of the portion of material under analysis. The density ρ, mass per unit volume, given by the ratio M/V can also be a seen as global property of a volume of fluid. More correctly, however, the density of a volume of fluid represents the average value over that volume, because density is a local property that takes different values at different position inside the volume. The density can be defined locally at every point as

$$\rho = \lim_{V \to 0} \frac{M}{V} = \frac{dM}{dV}. \tag{1.1}$$

The second equality in (1.1) used the differential form of a ratio between infinitesimal quantities that implicitly assume the limit $dV \to 0$; here it should be remarked once again that in the continuous model the infinitesimal volume is still much larger than the individual constituents of the material. Needless to remind that global properties can be evaluated by integration of local ones, like the mass of a volume

$$M = \int_V \rho dV.$$

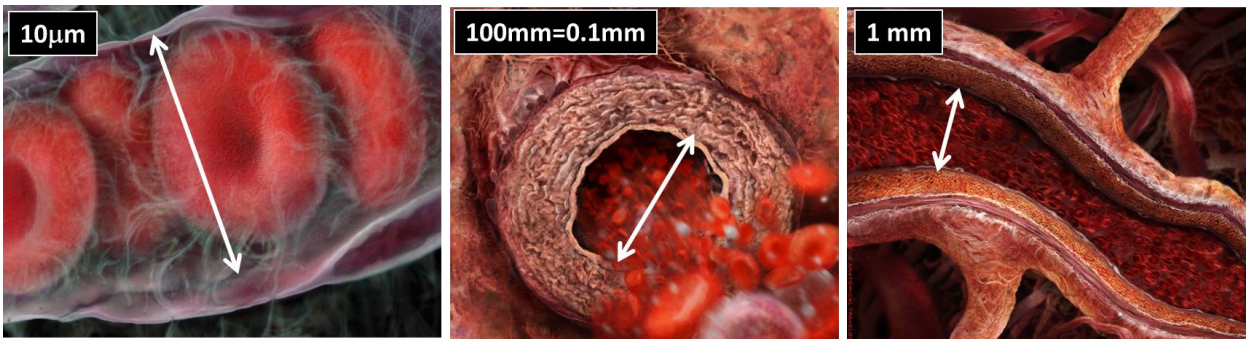

Figure 1.2. Red Blood Cells flowing in vessels of varying size. (Source: *Anatomical Travelogue*)

Local properties provide the most comprehensive description of the continuum, they are also called "fields" that are quantities that vary in time and space, like temperature $T(\boldsymbol{x}, t)$ or pressure $p(\boldsymbol{x}, t)$ where t is the time coordinate and $\boldsymbol{x}$ is the space coordinate; similarly, velocity $v(\boldsymbol{x}, t)$ is a vector field.

The physical laws that govern the mechanics of a continuum are the conservation of mass and the conservation of momentum and of angular momentum (both are expressions of the Newton law). Given the limited changes in temperature inside the circulatory system, we simplify the discussion by neglecting thermodynamics phenomena. We also assume that the material does not undergo transformations (state, chemical or else) and remains the same material everywhere in the space region of interest as time progresses. Under these simplified conditions, the only form of energy coming into play is the mechanical energy in its manifestations of kinetic and potential energy. Other forms of energy like those associated with heat transport or chemical reactions are neglected; this means that any non-mechanical propertie, like temperature or concentration of a solute, is transported passively with the fluid and does not influence the motion. In this purely mechanical scenario, the conservation of momentum can be recast to express the conservation of energy that is not an additional conservation law.

The conservation laws must be combined with the equation of state that characterizes the specific continuous material under analysis. The equation of state is the law that relates volume, pressure and temperature. A well known example is the law $pV = RT$ of ideal gas. In a continuum, it is preferable to express the equation of state with local variable, or fields, as a relation between density, pressure and temperature

$$\rho = f(p, T). \tag{1.2}$$

The role of temperature in (1.2) is typically associated with the decrease of density in regions with an increase of temperature. This effect, not considering local sources of thermal energy, is important in large environments like the atmosphere or the oceans where it gives rise to stratification with the quote and is responsible for buoyancy effects. Differently, to our present purpose thermodynamics

effects will be ignored, which means that temperature is considered constant or non-influent such that (1.2) reduces to

$$\rho = f(p), \tag{1.3}$$

which expresses the intuitive phenomenon that density increases when pressure increases and vice versa.

Let us quantify this point a little more carefully: consider a generic volume V of material (for example, a cylinder), that is in equilibrium with the external pressure, and apply a pressure increment Δp on the surrounding surface of such volume (for example pushing a piston in the cylinder). The volume will be compressed and experience a decrease of volume, $-\Delta V$, that increases with increasing pressure Δp. The compressibility of a material is thus measured by the ratio between increase of pressure and the corresponding change in volume, which must be expressed relative to its initial volume V because the same pressure acts on every infinitesimal element. This is the modulus of cubic compressibility (or bulk modulus) defined as

$$\varepsilon = \frac{\Delta p}{-\Delta V/V} = \rho \frac{dp}{d\rho}; \tag{1.4}$$

which is larger for stiffer materials, when a large increase of pressure is required to have a small decrease of volume. The second equality in (1.4) used the relation between volume and density, $V = M/\rho$ with the mass M being constant, to transform the volume variations into density. Moreover, for mathematical generality differences, denoted by Δ, have been transformed to differentials, indicated with d. The previous equation can be rearranged to express the relative change of density

$$\frac{d\rho}{\rho} = \frac{dp}{\varepsilon} = \frac{dp}{\rho c^2}; \tag{1.5}$$

where the last equality used the definition of velocity of propagation of sound (Kundu et al., 2012), $c = \sqrt{dp/d\rho}$, in the material that gives $\varepsilon = \rho c^2$.

In the case of liquid materials, the modulus ε is large because a small reduction of volume requires extremely large increase of pressure that are typically not physiological. To state it differently, pressure variations induced by flow are proportional to ρv^2 (where v is the fluid velocity, see chapter 6), therefore relative changes in density $d\rho/\rho$ in (1.5) turn out to be proportional to the ratio between the squares of fluid velocity and velocity of sound, $(v/c)^2$. Physiological velocities are much lower than the velocity of sound (that in water is about 1500 m/s and in dry air about 345 m/s); the condition that $v \ll c$, which amplified for square velocities, implied from (1.5) that $d\rho \ll \rho$. Thus variation of density becomes negligible and we can focus the attention to the limiting case "incompressible material" (or $\varepsilon \to \infty$). Therefore, the equation of state to our purpose takes the simple form

$$\rho = constant \tag{1.6}$$

where the density takes values about 10^3 Kg/m^3 in water, 1.05×10^3 Kg/m^3 for blood and about 1.2 Kg/m^3 in air at 20°C and atmospheric pressure.

1.2. Fluids and solids

The discussion so far applies to a generic continuum, which can be a model for either a solid or a fluid material. It is time to clarify the difference between solids and fluid so that we can focus on the latter with no ambiguity.

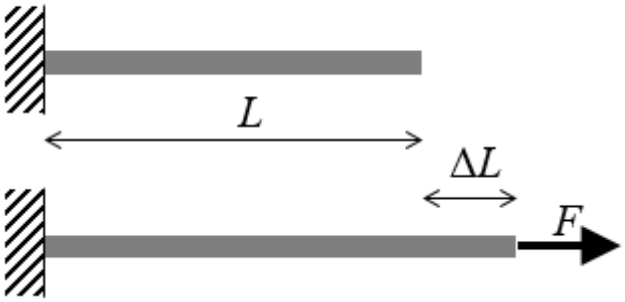

Figure 1.3. Elasticity in solids: material deforms under the action of a force.

A solid material, such as biological hard tissue like a bone or a soft tissue like a muscle, is presents its own shape due to a natural geometric organization of the constituting elements. When the relative position of these elements is altered by a small amount, internal stresses develop in an effort to restore the elements to their original, stress-free state. For example, with reference to figure 1.3, a rod of elastic material of length L stretches under the action of a force F and returns to its original length when the force ceases. This distinctive property of solids where internal stresses develop in response to a deformation is generally called "elasticity". Elastic energy is a form of potential energy, it is stored in the deformed structure composing the material and it is returned when the deformation goes back to zero. Indeed, an elastic deformation is normally completely reversible. Elastic deformation, or strain, $s = \Delta L/L$, is related to the amount of stress, $\tau = F/A$, proportional to the force and inversely proportional to the area of the cross section. In general, solid materials are characterized by a stress-strain relationship as shown in figure 1.4, which represents the "consititutive law" characterizing the elastic behavior of a solid material. For small enough deformation the stress-strain relationship can be considered as linear and, for one-dimensional deformation, is written $\tau = Es$, where the proportionality coefficients E is the Young modulus. Most biological tissues, however, present a hyperelastic behavior as shown in figure 1.4. Hyperelasticity means an increase of stiffness when the material is subjected to increasingly large deformations; therefore, it represents a protective property that limits the entity of deformation in the event of extreme overloads.

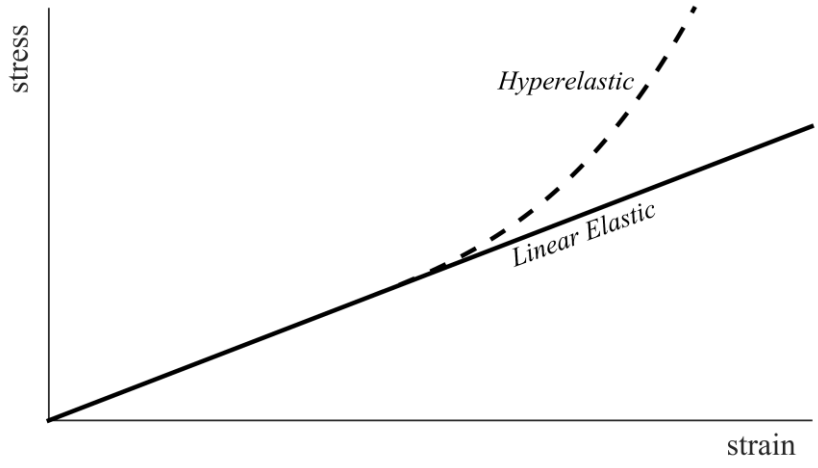

Figure 1.4. Elasticity in solids: stress-strain relationship.

Fluids are different and do not present an elastic behavior. The most distinctive property of fluids, which include liquids and gases, is that a fluid has not a preferred shape. A fluid offers no resistance to taking the shape of its container, irrespective of any geometry it had previously. The individual elements constituting a fluid have not preferred relative positions; thus, they may organized in infinitely many stress-free states. Fluids do not develop stresses for a relative displacement of its constituting elements; instead, fluids develop an internal resistance during their relative motion. Indeed the distinctive property of fluids is the development of internal stresses in response to a "rate of deformation", to a differential velocity between nearby elements. This property of fluids takes the name of "viscosity". A fluid thus experiences a viscous resistance during the motion caused by the sliding of the individual fluid elements one on the other. Viscous stresses represent a frictional phenomenon that appears during motion, when the motion ceases also stress cease and there is no mechanism taking the system to its original position as it happened in solids. The mechanical energy used to deform the fluid elements has not been stored anywhere, it is dissipates by internal viscous friction and irreversibly transformed into heat and dispersed away.

In analogy to what previously shown for elasticity, fluids are characterized by a relationship between stress and rate-of-strain. Consider a simple experiment of a thin layer of fluid between two walls (infinitely extended to avoid introducing end-effects), the lower wall being fixed and the upper wall sliding with constant velocity U, as sketched in figure 1.5. The upper wall is maintained at constant velocity under the action of a shear action τ, given by the force per unit area. Such shear increases when velocity U increases and when the thickness d decreases, it eventually depends on the ratio U/d. If the thickness is small enough such ratio is the velocity derivative and, with reference to figure 1.5, one can write

$$\tau = f\left(\frac{U}{d}\right) = f\left(\frac{dv_x}{dy}\right) \tag{1.7}$$

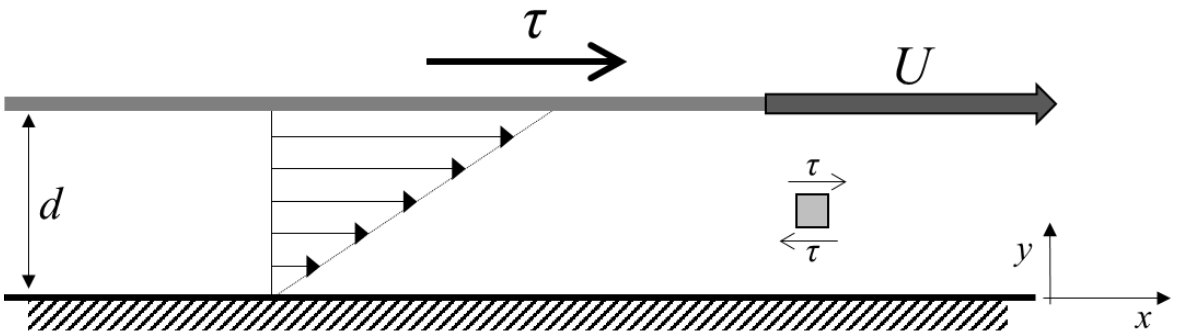

Figure 1.5. Viscosity in fluids: shear frictions between fluid elements sliding with different velocity.

This relationship between shear stress and shear rate is the "constitutive law" that characterizes the viscous fluid properties as shown in figure 1.6 for typical examples. Fluid that follow a simple linear relationship are called "Newtonian fluids" for which (1.7) becomes

$$\tau = \mu \frac{dv_x}{dy} \tag{1.8}$$

and the proportionality coefficient μ is the "dynamic viscosity" or simply "viscosity". Luckily, most common fluids like water and air behave as a Newtonian fluids with small viscosity (that takes value about 10^{-3} Kg/m·s for water and 1.8×10^{-5} Kg/m·s for air).

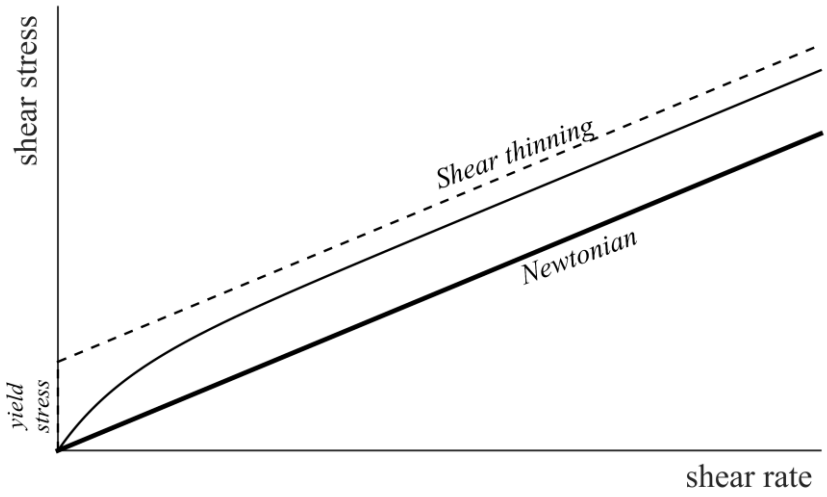

Figure 1.6. Viscosity in fluids: shear stress depends on shear rate.

Blood is more a shear thinning fluid where the corpuscular nature influences the value of viscosity, which cannot be assumed to be circumstantially constant. In fact, the apparent blood viscosity is not an intrinsic material property and thus its value depends on the type of motion the blood is experiencing at the different sites. For example, blood behaves as a Newtonian fluid in regions with a high shear rate when the blood cells undergo an intense mixing and average friction is not directly influenced by the corpuscular structure. Conversely, at low shear rate the interaction between individual cells gives rise to higher friction and higher apparent viscosity; a behavior that is sometime modelled by a static yield stress. Viscosity is also function of the local hematocrit because a higher percentage of red blood cells reflects into a higher average friction.

Such variability is further influenced by several concurring factors and still lacks a complete and general description. However, in large vessels, where shear rates are normally high, these variations are small and the mathematics would present a significant increase in complexity when accounting for a variable viscosity. Therefore, at least for flow in large vessels, blood is normally treated as a Newtonian fluid with constant viscosity $\mu = 3.3 \times 10^3$ Kg/m $\cdot$ s, about three times greater than the viscosity of water.

Dynamic viscosity is a proportionality coefficient in (1.8) between a dynamic quantity, the shear stress that involves the tree dimensional units (mass, length, time) and the shear rate that involves only kinematic units (length, time). When dealing with the description of motion, it is sometime useful to introduce the "kinematic viscosity" defined as

$$\nu = \frac{\mu}{\rho} \tag{1.9}$$

that is the viscosity coefficient directly involved in the description of fluid motion, whereas the dynamic viscosity enters when such motion must be translated into dynamic actions like forces and stresses. Kinematic viscosity takes value about $\nu = 10^{-6}$ m^2/s for water and $\nu = 1.5 \times 10^{-5}$ m^2/s for air showing that the motion of water is less viscous that air's although the involved shear stresses are larger. The value of kinematic viscosity for blood when assumed as a Newtonian fluid is $\nu = 3.3 \times 10^{-6}$ m^2/s that is often expressed $\nu = 3.3 \times 10^{-2}$ cm^2/s.

It must be clear in mind that these are interpretative models and the distinction between fluids and solids is not always so immediate. Most materials present both elastic and viscous characteristics. Some material can be intrinsically viscoelastic (for example gels). Some materials should be even be described as fluids in some conditions and as solids in another. A glacier is a solid if one can walk on it, yet it flows like a fluid during its slow motion detectable over the years. It is thus important to remind that solids and fluids, elasticity and viscosity, are conceptual models used to describe the behavior of specific materials under the specific situation of interest.

1.3. Overview of Bio-flow Domains

The eventual objective of this book is that of a rigorous application of fluid dynamics principles to blood flow in the cardiovascular system. For completeness, we provide here a quick overview of the circulatory system for the inexperienced reader. This is intentionally an extremely superficial synthesis and the reader is directed to the numerous other texts for more comprehensive descriptions.

Circulation is a systems aimed to distribute nutrients (mainly oxygen) transported by blood to every cell in the entire body. For reaching all regions in the body, circulation uses two main mechanisms: transport and diffusion. Transport allows covering relatively large distances, from the heart to other body regions up to limbs. Blood is transported with the local velocity U along the cardiovascular network and allow travelling a distance $\ell_{\text{transp}} \sim Ut$ in a time interval t. This mechanism is efficient until velocity is high enough and becomes progressively less efficient in small vessels where velocity is small. Indeed velocity necessarily decreases at smaller scales in order to avoid development of excessive shear stresses that are proportional to U/d, with d the vessel diameter (as shown by relationship 1.7). On the opposite end, diffusion is more efficient to cover small distances and permits the local distribution from capillary to interstitial space up to individual cells through a diffusive behavior that rapidly covers small distances covering in a time t a length $\ell_{\text{diff}} \sim \sqrt{2\nu t}$. Comparative results, reported in the table below, show how transport is best suited to cover large distances traveling along large vessels where velocity can be of the order of cm/s, when the vessels become small and velocities are reduced to values of few mm/s or smaller diffusion becomes progressively more efficient to cover small distances.

t	ℓ_{transp} (U=10 cm/s)	ℓ_{transp} (U=1 mm/s)	ℓ_{diff} (ν=0.04 cm^2/s)
10^{-3} s	0.1 mm	1 μm	90 μm
10^{-2} s	1 mm	10 μm	0.28 mm
10^{-1} s	1 cm	0.1 mm	0.9 mm
1 s	10 cm	1 mm	2.8 mm
1 min	6 m	6 cm	2.2 cm
1 hour	360 m	3.6 m	17 cm

The entire circulatory system is composed of the systemic and the pulmonary circulation systems that are at the same time are in parallel and in series. Figure 1.7 presents a sketch of the main vessels. Systemic circulation starts from the left heart, that receives low pressure oxygenated blood from the pulmonary veins and pushes at higher pressure in the Aorta, the first systemic artery. Aorta branches into smaller arteries that redirect blood into different regions of the body, these in turn branch into smaller arteries then to arterioles and into capillaries that are close enough to any cell of the body to which oxygen is delivered and cells' refuses collected. Capillaries then merge together into venules that merge into progressively larger veins up to inferior vena cava and superior vena cava (from the lower and upper part of the body, respectively) that eventually enter the right heart. From the right

heart blood is pushed into the pulmonary arteries and then across the lungs, where red blood cells leave the refuses and collect oxygen, and reaches the left heart to restart its cycle. The two circulations are also in parallel because the left and right sides of the heart are part of the same organ and work in synergy.

Mechanical analysis is principally dedicated to the transport mechanism in the larger vessels that also represent the sites of greater clinical interest; thus across the heart, in the larger arteries and the larger veins. There are important differences between arterial and venous networks. Blood flows in arteries through an unsteady, pulsatile motion forced by the heartbeat rhythm and fills arteries at high pressure (75 to 120 mm_{Hg}, that can be expressed as 1.0 to 1.6×10^{-5} Pa or 1 to 1.6 m_{H2O}, thus blood may jump this high when an artery is punched). Differently, blood reaches the venous system after having passed though the capillary bed; there blood experienced large frictional resistances, it loses its unsteadiness and loses pressure. Thus, the venous flow is essentially a steady one and pressure is low (as immediately verifiable by pushing the superficial veins). This is also a reason why arteries have thicker walls and are protected, deep in the body, while veins are closer to the surface.

The diameter of arteries of higher pato-physiological interest range from few centimeters (Aorta) to one centimeter or several millimeters (carotid bifurcation, iliac arteries) where unsteady velocities reach peaks of about 1 m/s or more. Fluid dynamics phenomena that are relevant to blood flow in the heart chambers and in the main vessels represent the main topics covered in later chapters.

This book will focus on blood flow in the large vessels of the cardiovascular system due to its paramount relevance with respect to other potential clinical application of fluid dynamics. Nevertheless, microcirculation as well as other aspects of biological fluid dynamics are gaining increasing attention for their potential relevance in clinical applications. Main examples include:

- Pulmonary circulation deals with the forced oscillatory motion of air across the pulmonary airways to the pulmonary alveoli. The main issues are the presence of dysfunctional/insufficient alveoli, or the collapse of air vessels under extreme thrusts. In the same field, some attention is devoted to the fluid mechanics of main external airways (nasal sinuses, turbinate) for the numerous and common pathologies that affect these areas.
- Biomechanics of the eye received particular attention during last years. The dynamics of the aqueous humour (a fluid similar to water) in the anterior chamber of the eye regulates the intraocular pressure and is involved in the development of glaucoma. The vitreous humour, a water-gel fluid that flows in the vitreous chamber during eye movements. It has important roles for eye function while a liquefied vitreous may be connected with retinal detachment.
- Blood perfusion represents the small scale dynamics of blood into the organs. There range from the liver, to kidney, to muscles, up to the myocardial muscle. Perfusion analysis can be of interest to recognize and assess regions with insufficient blood supply (ischemic areas) following injury or a disease, or to assess potential absorption of drugs. Models of these are still at early stages for clinical application; more importantly dedicated clinical imaging modalities allow direct evaluation of perfusion levels in numerous organs.
- Industrial fluid dynamics is a large part of clinical or biotechnological environments, in either laboratories or plants, in either large or microscopic domains. It is therefore important to known the fundamental aspects of fluid dynamics to understand their fundamental function.

These topics are not covered here, and the reader is redirected to other books for a wider spectrum of fluid mechanics phenomena in biological environments (Fung, 1997; Rubenstein et al., 2015).

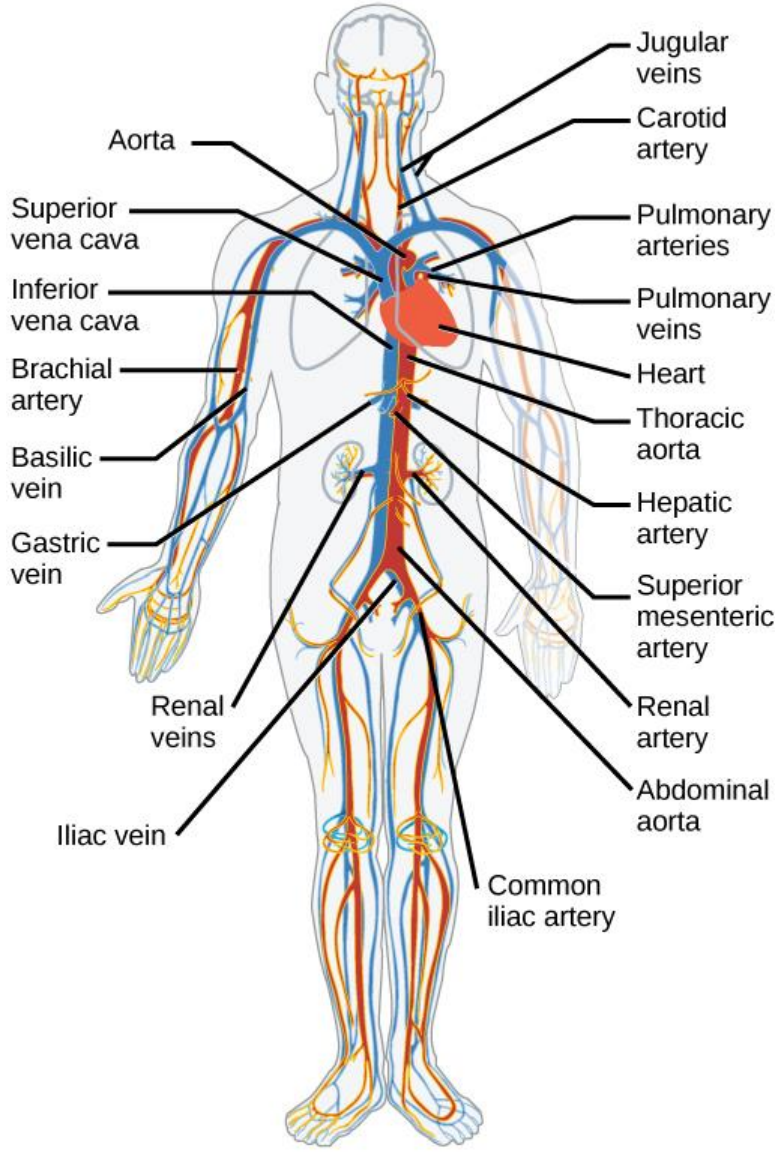

Figure 1.7. Overview of the circulatory anatomy. (Source: *opentextbc.ca/biology/chapter/11-3-circulatory-and-respiratory-systems/*)

1.4. Dimensional Analysis

It is worth dedicating some words to the topic of dimensional analysis. Dimensional analysis explores the implication of dimensional congruence for physical laws, and it is interesting to notice how this apparently trivial consideration can sometime allow simplifying or even uncovering relationships between physical variable. The topic of dimensional analysis is quickly introduced here for providing a tool that will be employed later in this book. However, this apparently trivial topic is more powerful than what described here (Barenblatt, 2003).

Any physical property can be expressed in general as the product between a pure number and a dimensional measurement unit. To be explicit, a property X can be expresses as $X=A\times\text{UNIT}_1$ or $X=B\times\text{UNIT}_2$. Usage of different units brings to a different numerical coefficient; however, the physical property is evidently not affected by a change in the description. For example, a person height

X=1.80m can be expressed as X=180cm or as X=70.87inch but the physical property itself, the height of that person, is evidently independent from the unit chosen to describe it.

Similarly, a "physical law" reflects a physical phenomenon that is independent from the units used to describe it. As before, this is a trivial affirmation; however, this simple concept is a constraint that allows simplification of the physical laws itself.

Let us use one example to show the power of dimensional analysis. Consider fluid flow in a cylindrical vessel, the fluid reduces its pressure (potential energy) while moving downstream due to the viscous friction experienced by fluid along its motion. We are willing to express how the loss of pressure per unit length depends on the parameters of the vessel and of the stream. Without any knowledge of the physical laws governing fluid dynamics, we can state that this phenomenon must be expressed by a physical law of the type

$$\frac{dp}{dx} = f(D, U, \rho, \mu) \tag{1.10}$$

that relates the pressure gradient (pressure loss per unit length) $\frac{dp}{dx}$, with all the properties that may influence it: the vessel diameter D, the flow velocity U, and the fluid characteristics, density ρ and viscosity μ. Assuming a simple configuration (cylindrical vessel with no bend, obstacles etc.), there are no other quantities coming into play. Thus a physical law (1.10) must exist although its specific form may be unknown. This law depends on 4 parameters, if you had to find it by experiments, considering to test (as a minimum) 10 values for each parameters, you had to make 10^4 experiments to fill this 4-dimensional parameters space. Requiring multiple experimental apparatuses with different diameters D and different fluids to vary ρ and μ.

Here dimensional analysis can help. Equation (1.10) is a physical law, thus it does not depend on the specific unit of length, L, of time, T, and mass, M, chosen to express it. You can choose standard units (L = m, T = sec, M = Kg) or Anglo-Saxon units (L = ft, T = sec, M = lb) or any other one; the resulting law would be unaffected by this choice. Once the units are decided, the physical law would express a relationship between the numerical coefficients expressing the quantities in those units and the law is automatically consistent because a physical law is independent from the choice of units: units on the left and the right side of (1.10) must be the same in a physical law.

However, it is not necessary to use units previously defined by some international standard in a separate context. It is actually smarter to use units that are natural to the specific application. In this case, one could use the diameter D as unit of length, the ratio D/U as the unit of time and ρD^3 as unit of mass

$$\mathrm{L} = D \quad \mathrm{T} = \frac{D}{U} \quad \mathrm{M} = \rho D^3. \tag{1.11}$$

Even with this special choice, the physical law will express a relationship between the numerical coefficients of every quantity in those units. Thus, express each quantity in (1.10) as the product between the numerical coefficients and its units (1.11), where the numerical coefficient is trivially obtained by dividing the dimensional quantity by its units. The dimensional quantities are thus expressed as

$$\frac{dp}{dx} = \frac{D}{\rho U^2}\frac{dp}{dx} \cdot \left[\frac{\mathrm{M}}{\mathrm{L^2T^2}}\right], \quad D = 1 \cdot [\mathrm{L}], \quad U = 1 \cdot \left[\frac{\mathrm{L}}{\mathrm{T}}\right], \quad \rho = 1 \cdot \left[\frac{\mathrm{M}}{\mathrm{L^3}}\right], \quad \mu = \frac{\mu}{\rho UD} \cdot \left[\frac{\mathrm{M}}{\mathrm{LT}}\right].$$

Then insert these into (1.10) to obtain the relationship between the numerical coefficients because the units are automatically satisfied being it a physical law

$$\frac{D}{\rho U^2}\frac{dp}{dx} = f\left(1,1,1,\frac{\mu}{\rho UD}\right) = f\left(\frac{\mu}{\rho UD}\right). \quad (1.12)$$

Equation (1.12) represents the same physical law (1.10), but it is now expressed as a relationship between dimensionless quantities. Expressed this way it has reduced the number of independent variable from 4 to a single one. Thus, you can establish the physical law making just N experiments instead of N^4 that could even be performed, for example, just with one fluid in one vessel and varying the fluid velocity only.

This simplification allowed by dimensional congruence is a general rule: expressing a physical law in dimensionless terms allows reducing the number of variables by a number equal to the number of independent dimensional units involved in the law. In the previous case, a relationship between 5 variables involving 3 units has been simplified in a relationship between 2 dimensionless variables.

It is easy to demonstrate that the resulting law is independent from the specific units selected. In the previous example we could use, for example, a different unit time unit

$$\mathrm{L} = D \quad \mathrm{T} = \frac{\rho D^2}{\mu} \quad \mathrm{M} = \rho D^3$$

These give

$$\frac{dp}{dx} = \frac{\rho D^3}{\mu^2}\frac{dp}{dx}\cdot\left[\frac{\mathrm{M}}{\mathrm{L^2T^2}}\right], \quad D = 1\cdot[\mathrm{L}], \quad U = \frac{\rho DU}{\mu}\cdot\left[\frac{\mathrm{L}}{\mathrm{T}}\right], \quad \rho = 1\cdot\left[\frac{\mathrm{M}}{\mathrm{L^3}}\right], \quad \mu = 1\cdot\left[\frac{\mathrm{M}}{\mathrm{LT}}\right];$$

that inserted into (1.10) gives

$$\frac{\rho D^3}{\mu^2}\frac{dp}{dx} = f\left(1,\frac{\rho DU}{\mu},1,1\right),$$

that can be recast as

$$\frac{D}{\rho U^2}\frac{dp}{dx} = \left(\frac{\rho UD}{\mu}\right)^{-2} f\left(\frac{\rho DU}{\mu}\right) = f\left(\frac{\mu}{\rho DU}\right),$$

to give a result functionally identical to (1.12).

It is actually a general result for fluid flowing in smooth cylindrical vessels that the pressure loss per unit of length is expressed in general as

$$\frac{dp}{dx} = \frac{\rho U^2}{2D} f(Re), \quad (1.13)$$

Where f is known as the (Darcy) friction factor and $Re = \frac{UD}{\nu}$ is the Reynolds number, a classical dimensionless number indicating the relative importance of kinetic energy with respect to viscous frictions that we will encounter several times later.

It should be underlined that it was possible to obtain the general resistance law (1.12) or (1.13) based on dimensional consideration only without using any knowledge of fluid dynamics. This example demonstrates the power of the simple concept of dimensional analysis. Fluid dynamics theory may be then advocated to better specify the function $f(Re)$; however, we will see that this is not immediate in most of the cases and (1.12) may become the only theoretical result to be integrated by physical experiments.

It is therefore of fundamental importance to formulate any physical law in dimensionless terms.

If we extend the example (1.10) to consider a pulsatile flow with period T,

$$\frac{dp}{dx} = f(D, U, \rho, \mu, T) \tag{1.14}$$

Selection of the same units (1.11) gives the dimensionless relationship

$$\frac{D}{\rho V^2}\frac{dp}{dx} = f(Re, St) \tag{1.15}$$

showing that pressure changes as before due to friction (dependence on the Reynolds number, Re) and it also depends on the frequency of oscillation that is expressed by the Strouhal number $St = \frac{D}{UT}$ in dimensionless form.

Dimensional analysis permits to reduce the number of independent variable to their minimum and to recognize the dimensionless number that characterizes the phenomenon under analysis. It is a powerful tool in complex conditions, for example when mathematical equations do not lead to a closed solutions. It will be used in some occasions to progress across critical passages that cannot be solved otherwise.

2. Fluid Statics

2.1. Pressure distribution

Fluid statics deals with the forces exerted by fluids in absence of motion. These are of enormous importance in numerous applications, from industrial to biological, as they represent the basic stress state in every fluid domain. Motion, when it occurs, may induce modification on top of this fundamental state.

Statics means that the velocity vector field is identically zero, $\boldsymbol{v}(\boldsymbol{x}, t) \equiv 0$. As we have seen in the definition of fluids and of viscosity, shear stresses develop in consequence of differential velocities (shear rate, or rate of deformation). Therefore, in static conditions, shear stresses are also absent and the stress made by still fluid over any surface has only a normal component

$$\boldsymbol{\tau} = p\boldsymbol{n}, \tag{2.1}$$

where $\boldsymbol{n}$ is the normal to the surface (a vector perpendicular to the surface, directed toward the surface and of unit modulus) and $p(\boldsymbol{x})$ is the pressure field. Let me remark that pressure is a scalar quantity that has no direction; pressure gives rise to a stress vector (2.1) only after it acts on a surface in which case the direction is given by the normal $\boldsymbol{n}$ directed toward the surface.

Statics obey the law of equilibrium, which states that the sum of volumetric forces and of surface forces acting on a generic volume V is zero

$$\int_V \boldsymbol{f} dV + \int_S p\boldsymbol{n} dS = 0 \tag{2.2}$$

where the surface S is that surrounding the volume V. Equation (2.2) is the integral balance equation of fluid statics.

Let's derive the same equation in differential form. Balance equation (2.2) is valid for an arbitrary volume. Consider an infinitesimal cube of size $dx \times dy \times dz$,

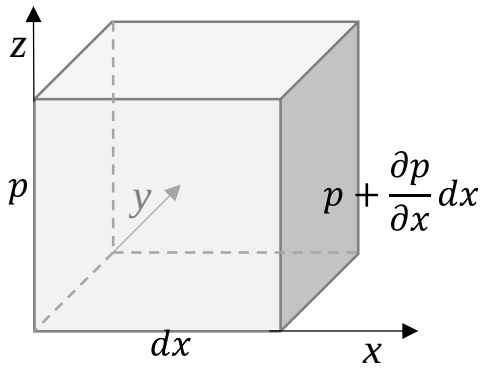

Figure 2.1. Balance applied on infinitesimal cube

the balance (2.2) along the *x*-direction

$$f_x dxdydz + pdydz - \left(p + \frac{\partial p}{\partial x} dx\right) dydz = 0$$

presents the x-component of the volume force, f_x, and the pressure force acts only on the two face, with normal $\boldsymbol{n} = [1, 0, 0]$ and $\boldsymbol{n} = [-1, 0, 0]$, respectively and becomes

$$f_x = \frac{\partial p}{\partial x}.$$

In general vector form, the differential equation of fluid statics reads

$$\boldsymbol{f} = \nabla p; \tag{2.3}$$

that expresses the balance on every fluid particle between the volumetric forces and the pressure gradient. It is immediate to verify that the result (2.3) could also be obtained directly from equation (2.2) by transforming the second terms therein into a volumetric integral and then extending the equality to the terms inside the integral for the arbitrariness of the volume (or using an infinitesimal volume). This requires the application of the Gauss theorem that will be recalled later in section 3.1

The volumetric force of greatest interest for normal applications is the gravitational force. It can be expresses as

$$\boldsymbol{f} = -\gamma \boldsymbol{k} = -\nabla \gamma z;$$

where $\boldsymbol{k}$ is the unit vector directed upwards against gravity, and z is the corresponding direction. In case of gravitational forces, equation (2.3) becomes

$$\nabla(p + \gamma z) = 0. \tag{2.4}$$

Equation (2.4) states that, in a fluid subjected to gravitational field only, pressure, $p(z)$, is constant on xy-planes at constant z and it increases linearly as the quote z decreases. An easier application of equation (2.4) comes with the introduction of a new quantity called the *static head* defined as

$$h = z + \frac{p}{\gamma}. \tag{2.5}$$

Using this definition, equation (2.4) expresses the first fundamental concept of fluid statics: *the static head remains constant inside a same fluid*; in other words, the value of the static head characterizes the specific potential energy (per unit of weight) of a volume of fluid. The constancy of the static head (or equation 2.4) allows evaluating the pressure difference between two points at different quote zzinside the same fluid. Consider two points then (2.4) tells

$$p_1 + \gamma z_1 = p_2 + \gamma z_2$$

thus

$$p_2 = p_1 + \gamma(z_1 - z_2)$$

pressure difference between two point is equal to the difference of quote multiplied by the specific weight; the pressure at the lower point is increased by the weight of the column of fluid above it.

Take point “1” at the free surface subjected to atmospheric pressure and “2” at a generic level z

$$p(z) = p_{Atm} + \gamma(z_{\text{surface}} - z)$$

if you define the depth $\zeta = z_{\text{surface}} - z$, then the pressure grows linearly with the depth ζ

$$p(\zeta) = p_{Atm} + \gamma\zeta.$$

It is often useful to use pressure relative to the atmospheric pressure instead of its absolute value, because atmospheric pressure is almost everywhere the reference value and disappears when dealing with pressure differences as happens in most cases. Assuming atmospheric pressure as the zero value of pressure, then one can write simply

$$p(\zeta) = \gamma\zeta.$$

It is also immediately evident from (2.5) that the level of the free surface where pressure is zero represents the value of the static head for that fluid.

The second fundamental concept of fluid statics is based on the equilibrium of the interface between two fluids. Assuming that surface tension is negligible (in absence of capillary phenomena that should be treated separately) an interface between two fluid is subjected only to pressure on the two faces and its equilibrium gives the result that *pressure is the same on the two faces at the interface between two fluids*.

These two principles make possible the evaluation of pressure difference between all places in fluid filled containers. Figure 2.2 shows on the left a simple case where pressure increases linearly with depth from the zero value at the surface. Differently, the right side shows pressure profile with a two immiscible fluids with different specific weight, γ_1 and $\gamma_2 > \gamma_1$, and non-zero pressure value at the free surface. It is easy to show that, with reference to figure symbols, pressure takes the value $p(\zeta_1) = p_0 + \gamma_1\zeta_1$ in the upper fluid and $p(\zeta_2) = p_0 + \gamma_1 H + \gamma_2\zeta_2$.

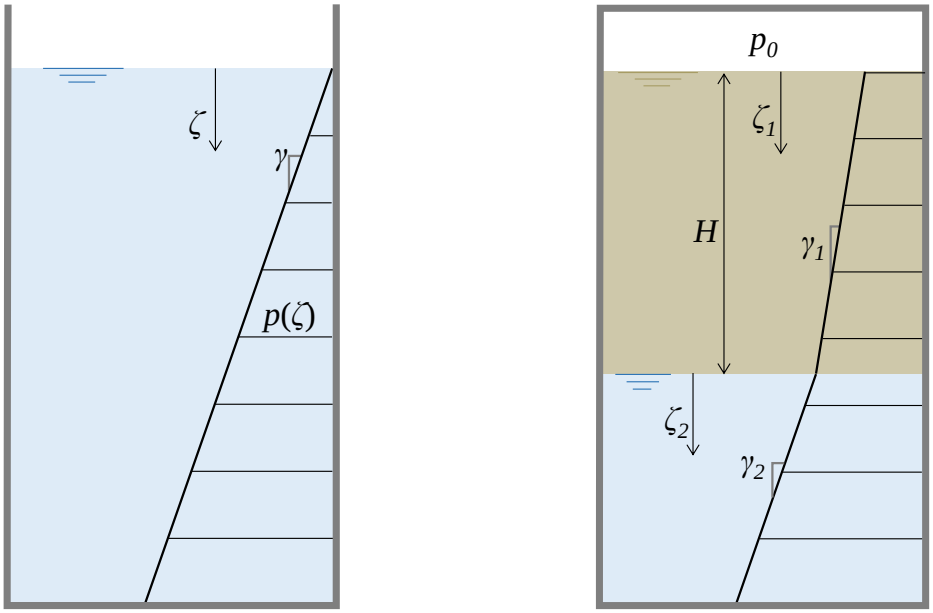

Figure 2.2. Pressure distribution with depth.

An interesting and technologically important case is the differential manometer shown in figure 2.3.

A tool that allows measuring the difference in static head between two reservoirs filled with a same fluid of specific weight γ connected by a small duct partially filled with a heavier fluid (typically mercury) of specific weight γ_m. The static head is constant inside each reservoir, thus we can use the points at the edge with the heavier fluid, and write by definition, with reference to figure 2.3

$$h_1 - h_2 = z_1 + \frac{p_1}{\gamma} - z_2 - \frac{p_2}{\gamma} = \frac{p_1 - p_2}{\gamma} - \Delta.$$

Now apply the conservation of h inside the heavier fluid to write

$$z_1 + \frac{p_1}{\gamma_\mathrm{m}} = z_2 + \frac{p_2}{\gamma_\mathrm{m}} \quad \Rightarrow \quad p_1 - p_2 = \gamma_\mathrm{m}\Delta$$

and substituting back

$$h_1 - h_2 = \left(\frac{\gamma_m - \gamma}{\gamma}\right)\Delta. \tag{2.6}$$

The reading of the difference of height Δ in the differential manometer permits to compute the difference of static head between the two chambers. Often one chamber has a known head (for example it is open to the atmosphere) and it is used as reference to measure directly the head in a second chamber. Once the head is known, pressure can be obtained at every point.

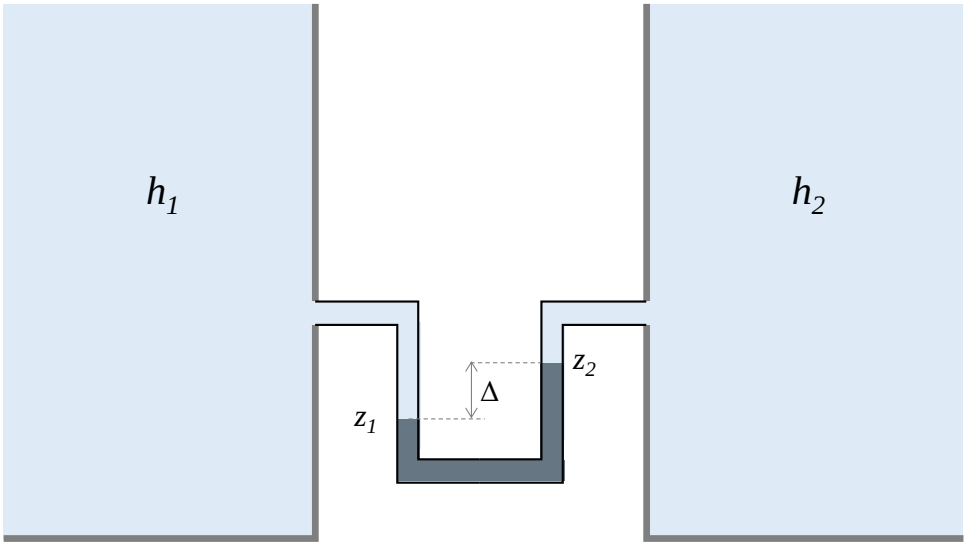

Figure 2.3. Differential manometer

2.2. Forces on Plane Surfaces

Consider a planar surface with area A and normal $\boldsymbol{n}$ directed towards the surface The force vector acting on the surface is

$$\boldsymbol{F} = \int_A p\boldsymbol{n}dA = F\boldsymbol{n}$$

it has modulus F and direction given by $\boldsymbol{n}$. Consider the surface wet by a single fluid whose pressure can be expressed in general as $p = p_0 + \gamma(z_0 - z)$

$$F = \int_A p(z)dA = p_0A + \gamma z_0 A - \gamma \int_A zdA = p_0A + \gamma(z_0 - z_G)A = p_GA$$

where we have used the definition for the center G of a surface for any coordinate $x_G = \frac{1}{A}\int_A xdA$. Thus the force on a plane surface has always modulus equal to pressure on the center of the surface multiplied by the area of the surface, and it is directed towards the surface.

$$\boldsymbol{F} = p_GA\boldsymbol{n}. \tag{2.7}$$

The distribution of pressure is equivalent to the force (2.7) applied to an application point C. However, let me remark with emphasis that such a point of application C is <u>not</u> the center G of the surface. The

point of application is the center of the pressure distribution that is usually below the center of the surface because pressure is higher at higher depth.

The point of application is needed to compute the torque T of the force about an axis. Consider a horizontal axis at depth ζ_1 and compute the torque for a vertical surface. By definition one can write

$$T = \int_A (\zeta - \zeta_1) p(\zeta) dA = (\zeta_C - \zeta_1) F \tag{2.8}$$

where ζ_C is the depth of the point of application. Choosing the reference $\zeta = 0$ at the position where $p = 0$, it is immediate to show that

$$\zeta_C = \frac{\int_A \zeta^2 dA}{\int_A \zeta dA} \tag{2.9}$$

and it is also immediate to show that equation (2.8) is valid when the surface is not vertical as well. The integrals in equation (2.8) are easy to evaluate when the surface is rectangular contained between two depths ζ_A and $\zeta_B > \zeta_A$.

$$\zeta_C = \frac{2}{3} \frac{\zeta_B^3 - \zeta_A^3}{\zeta_B^2 - \zeta_A^2} \tag{2.10}$$

Moreover, when the surface's upper edge is on the free surface the distribution of pressure is triangular and the center of pressure *C* is at a depth 2/3 the surface height; while, when the surface is horizontal, pressure is constant and application is on the surface center *C=G*.

In rectangular surfaces, it is sometime convenient to divide the pressure distribution as the sum of a rectangular profile, applied in the surface center, and a triangular profiles applied at two-third the depth; then compute the torque as the sum of the two individual ones. In more complex surfaces the torque can be computed by dividing it in a composition of simpler surfaces.

All these methods provide an immediate understanding of the expected results and are useful for design of for drawing approximate results in complex conditions when the calculation (2.8) is eventually computed by numerical integration.

2.3. Forces on Curved Surfaces

Consider now a generic surface S, with arbitrary curved shape. An infinitesimal force $d\boldsymbol{F} = p\boldsymbol{n}dS$ acts at every individual infinitesimal element of surface dS and local normal $\boldsymbol{n}$. Therefore, the total force acting on the surface S is the integral

$$\boldsymbol{F} = \int_S p\boldsymbol{n}dS. \tag{2.11}$$

Differently from the case of plane surfaces, the normal $\boldsymbol{n}$ is not a constant and the integral cannot be simplified like before. A method to compute (2.11) can be obtained by advocating the global balance (2.2).

Consider first the case of a *closed surface*: a surface S surrounding a volume V that is in equilibrium immersed in a fluid. The force is given by the integral (2.11) evaluated on the external side of the surface S. It is important to remind that the value of the integral is independent whether the internal volume V is occupied by a body (kept static by some mean) or it is a volume of fluid, because under static conditions the distribution of pressure depends on the depth of each point only. Consider first the case where V is of a volume of fluid and S is thus a mathematical surface with the same fluid on

both sides. We are under statics condition and the volume is in equilibrium; this means that the sum of all forces acting on the volume is zero. Following the integral equilibrium (2.2), these forces are the weight of the fluid volume S and the integral of pressure on the surface S

$$-\gamma V\boldsymbol{k} + \int_S p\boldsymbol{n}dS = 0. \tag{2.12}$$

with $\boldsymbol{k}$ the unit vector directed against gravity. Thus equilibrium tells that horizontal forces are zeros and vertical force is directed upward (buoyancy force)

$$\boldsymbol{F} = \gamma V\boldsymbol{k}. \tag{2.13}$$

When a body, kept in equilibrium by some external force, occupies the volume V the force made by the fluid on the surface of the body is given by the same integral that appears in the second term of (2.12), and the value of that integral is independent from the presence of the body and takes the same result (2.13). Equation (2.13) states Archimedes' principle (dated back to the 3rd century b. c.), which says that "a body immersed in a fluid is subjected to a force directed upward that is equal to the weight of the displaced fluid".

Consider a solid body with its own weight $\gamma_s V$, being γ_s the solid specific weight; when it is immerged in a fluid it is subjected to its weight and the buoyancy force (2.13). As a results, the apparent weight of a body immersed in a fluid is reduced and becomes $(\gamma_s - \gamma)V$. The value $(\gamma_s - \gamma)$ represent the apparent specific weight of an immersed body and it is often useful for immediate evaluations.

Let us now move to generic surface S that can be open and have fluid on one or the other side. The procedure to compute the force acting on the surface S, equation (2.11), is that of selecting a volume of fluid partly surrounded by S and partly closed by planar surfaces. That volume is in equilibrium and obeys the law (2.2) that represents a balance of forces. These forces comprise volumetric forces that can be calculated, forces on plane surfaces that we have learnt above to evaluate, and force of the curved surface that remains the only unknown in the balance (2.2).

This apparently complex procedure is relatively straightforward in practice. Consider for example a surface made of a quarter of a circumference like the one shown in figure 2.4.

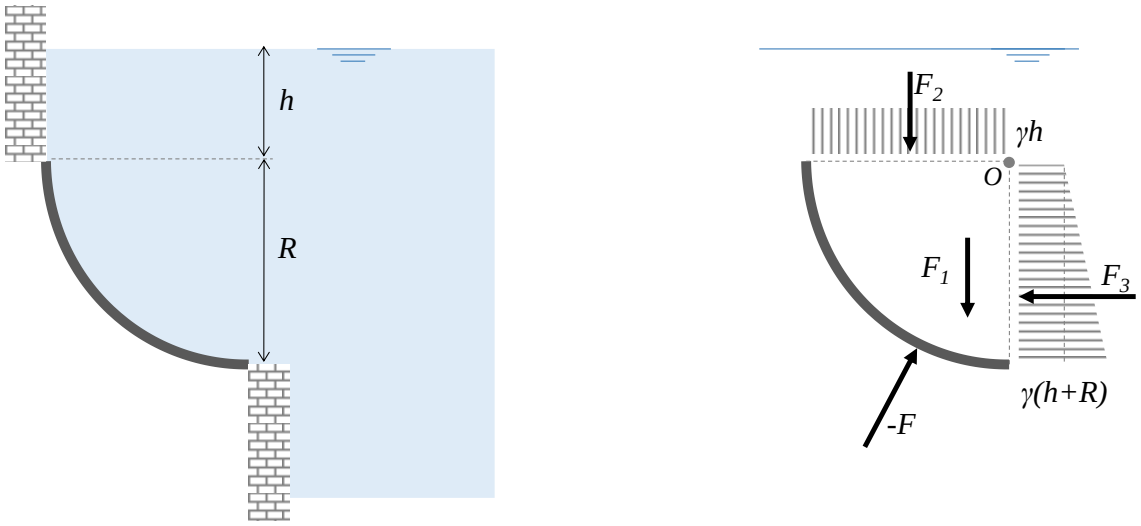

Figure 2.4. Calculation of the force on a curved surface

Select an arbitrary control volume to perform the balance of forces, for example the quarter of cylinder of radius R. The forces (per unit width) acting on that volume are:

- the weight of the fluid volume $F_1 = \gamma V$ directed downward;
- the force on the horizontal plane boundary F_2 where pressure is γh and the normal is directed downward,
- the force on the vertical boundary F_3 where pressure ranges from γh to $\gamma(h+R)$,
- the unknown force vector made by the curve surface to the fluid volume, that is equal in module and opposite in direction to the force $\boldsymbol{F} = [F_x, F_y]$ made by the fluid on the surface.

The balance along the horizontal rightward direction, x, and vertical upward direction, z, gives

$$F_x = -F_3 = -\gamma\left(h + \frac{R}{2}\right)R$$
$$F_z = -F_1 - F_2 = -\gamma\frac{\pi}{4}R^2 - \gamma hR$$

thus showing that the force on the surface is directed leftward and downward.

The result is always independent from the chosen volume, although some choices permit easier calculations. For example, in this case, it is immediate to see that the same result would have been achieved by selecting a volume extending up to the free surface; the force F_2 would be equal to the volume of fluid above and the horizontal forces on the two sides would be identical and opposite. We could also use a smaller volume bounded by the chord connecting the two extremes of the surface; calculations are less immediate but result is identical.

It is useful to always keep in mind that the force is the integral of pressure on the surface as defined by (2.11), and that such calculation must not necessarily be performed on a fluid volume that is effectively present in the current configuration. It is therefore advisable to idealize the problem under investigation: immerse the surface under analysis in an unbounded fluid and select a volume bounded by an ideal surface where the integral of pressure is identical to that looked for. For example, in figure 2.4, if the fluid was on the other side of the surface we could idealize the problem and consider the volume on the other side (a square minus a circle). But we could also consider exactly the same volume (a quarter of a circle) noticing that the distribution of pressure on the external face is identical and opposite to that on the internal face, because pressure depends on depth only. Thus the module is the same, and the direction opposite; the calculation could be the same as before and simply changing sign to the resulting force.

A balance like (2.2) can be rewritten in terms of the moment of forces, or torques, to evaluate the torque on a surface. Indeed, (2.8-2.9) permits to compute the moment of the force on planar surfaces and the moment of a weight is just a matter of computing center of mass.

Let us apply this concept to the example in figure 2.4 to evaluate the moment of the force on the surface S relative to the center O. The torque balance, assumed positive counterclockwise, can be written as

$$T_O = F_1 r_1 + F_2 r_2 - F_3 r_3 = \gamma\frac{\pi}{4}R^2 \cdot \frac{4R}{3\pi} + \gamma hR \cdot \frac{R}{2} - \gamma\left(h + \frac{R}{2}\right)R \cdot \left(\frac{2}{3}\frac{(h+R)^3 - h^3}{(h+R)^2 - h^2} - h\right)$$

where the definition (2.10) was used to evaluate the center of the force F_3. In the calculation of torque on rectangular surfaces it is sometime be easier to separate the trapezoidal force distribution as the sum, say $F_3 = F_{3a} + F_{3b}$, of a rectangular distribution that gives $F_{3a} = \gamma hR$ and whose arm is in this

case equal to $R/2$, plus the triangular distribution $F_{3b} = \gamma R^2/2$ whose arm is equal to $2R/3$, from which

$$T_O = F_1 r_1 + F_2 r_2 - F_{3a} r_{3a} - F_{3b} r_{3b} = \gamma \frac{\pi}{4} R^2 \cdot \frac{4R}{3\pi} + \gamma h R \cdot \frac{R}{2} - \gamma h R \cdot \frac{R}{2} - \gamma \frac{R^2}{2} \cdot \frac{2}{3} R$$

Both formulas are equivalent, although the second was easier to formulate, and compute the torque in the surface *S* about the point *O*. It is immediate to notice that in this specific case the torque is exactly zero. This result could be anticipated here because the curve is a portion of a cylinder and every individual (infinitesimal) force acting normally to its surface is directed along with the radius and present zero torque about the center *O* of the circumference.

2.4. Example calculation of static forces

We present some examples where the static force can be readily computed by simple application of the balance laws described above. When not expressly indicated, the subscripts $_H$ and $_V$ stands for horizontal and vertical, respectively

Example 1. Compute force and torque, per unit width, on the cylindrical body hinged in *A*. Consider H=2m; h=5m; R=1m; $\gamma = 10^4 N/m^3$.

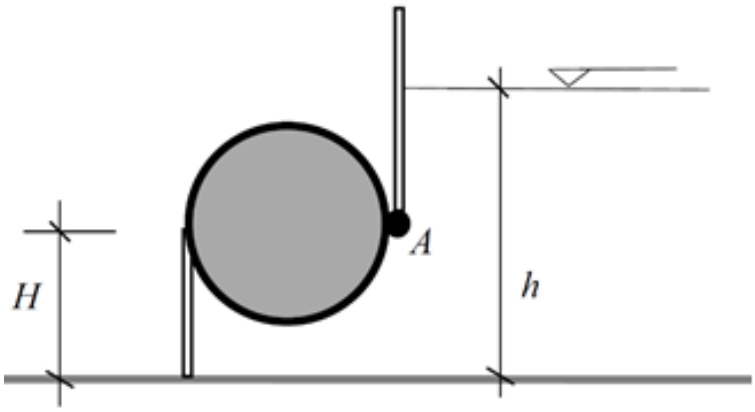

Solution:

$F_H = 0$,

$$F_V = \gamma V + \gamma (h - H) 2R = \gamma V + \gamma (h - H) 2R = \gamma \left(\frac{\pi}{2} R^2 + 2R(h - H) \right) = 7.57\ 10^4 \frac{\text{N}}{\text{m}},$$

$T_A = F_V \cdot R$.

Example 2. Compute force and torque, per unit width, for the entire surface, made of half a circle plus a straight part, hinged in *A*. Consider: h=6m; R=2m; $\gamma = 10^4$ N/m^3.

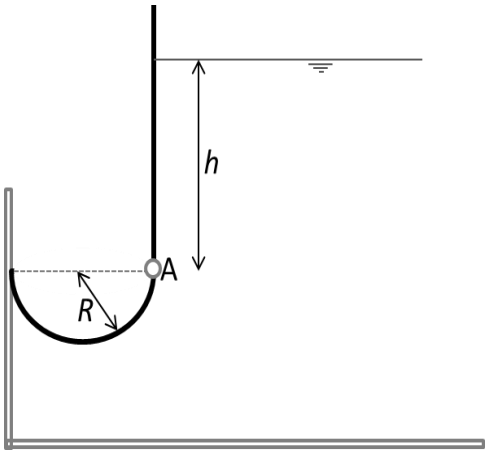

Solution:

$F_H = \gamma \frac{h^2}{2} = 18\ 10^4 \text{N}, \quad r_H = \frac{h}{3} = 2\text{m};$

$F_V = \gamma \left(2hR + \frac{\pi}{2} R^2\right) = 30.3\ 10^4\ \text{N}, \quad r_V = R = 2\text{m};$

$T_A = -F_H r_H + F_V r_V = 24.6\ 10^4\ \text{J}.$

Example 3. Compute force and torque, per unit width, for the surface made of two semicircles, hinged in upper edge *A*.

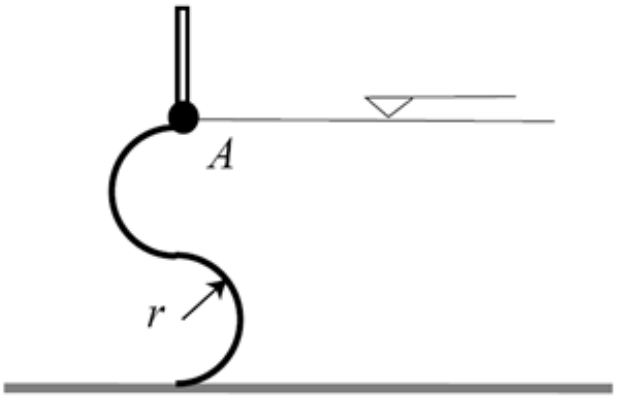

Solution:

$F_H = \gamma 8r^2, \quad r_H = \frac{2}{3} 4r, \quad F_V = \gamma \frac{\pi}{2} r^2 - \gamma \frac{\pi}{2} r^2 = 0;$

notice that F_V is a force couple with arm $r_V = \frac{4}{3\pi} r$.

$T_A = \gamma 8r^2 \cdot \frac{2}{3} 4r - \gamma \pi r^2 \cdot \frac{4}{3\pi} r = 20\ \gamma r^3.$

Example 4. Define the volume V of the sphere, of negligible weight, such that its buoyancy is as strong as the downward force on the lower surface of area A.

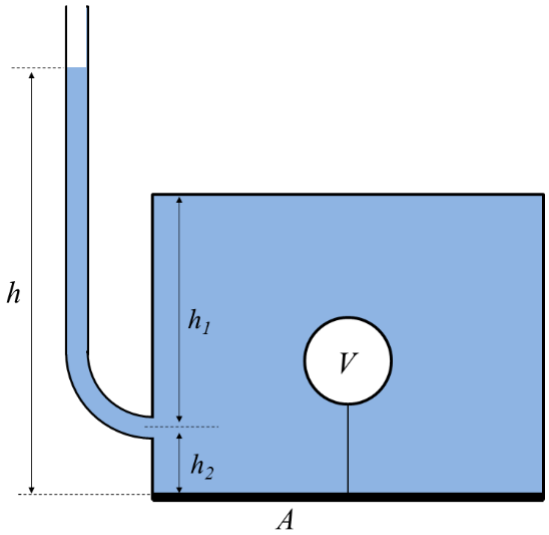

Solution:

$\gamma hA = \gamma V, \quad V = hA.$

Example 5. A plane surface, made of homogeneous material of negligible thickness, and hinged in point C, separates two reservoirs. Compute the weight W of the surface (per unit of width) to ensure that it remains in equilibrium. Consider HA=1.0 m, HB=2.0 m.

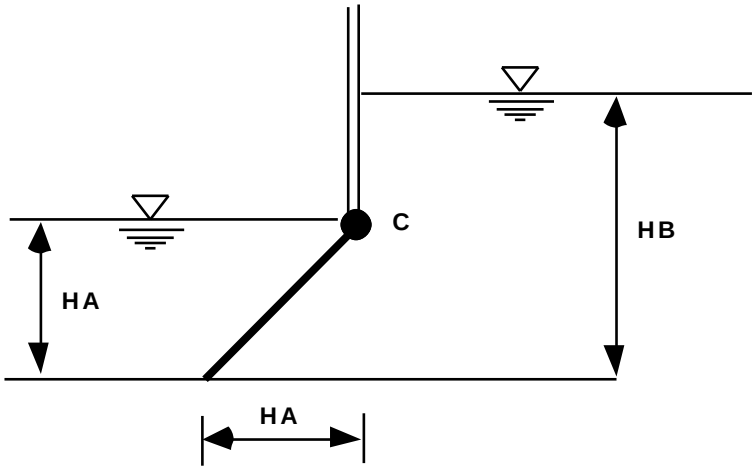

Solution:

Fluid torque is

$$F = \gamma(\mathrm{HB} - \mathrm{HA})\mathrm{HA}\sqrt{2}, \quad r = \mathrm{HA}\frac{\sqrt{2}}{2}, \quad T_f = F \cdot r = \gamma(\mathrm{HB} - \mathrm{HA})\mathrm{HA}^2;$$

the same result could be found considering separately the left and right sides of the surface

$$F_L = \gamma \mathrm{HA}^2 \frac{\sqrt{2}}{2}, \quad r = \frac{2\sqrt{2}}{3}\mathrm{HA}, \quad M_L = \gamma \frac{2}{3}\mathrm{HA}^2;$$

$$F_{R1} = \gamma(\mathrm{HB} - \mathrm{HA})\mathrm{HA}\sqrt{2}, \quad r = \frac{\sqrt{2}}{2}\mathrm{HA}, \quad M_{R1} = \gamma(\mathrm{HB} - \mathrm{HA})\mathrm{HA}^2;$$

$$F_{R2} = \gamma\mathrm{HA}^2\frac{\sqrt{2}}{2}, \quad r = \frac{2\sqrt{2}}{3}\mathrm{HA}, \quad M_{R2} = \gamma\frac{2}{3}\mathrm{HA}^2;$$

noticing that F_{L} and F_{R2} cancel each other.

Solid weight torque is

$$T_s = W\frac{\mathrm{HA}}{2}.$$

Equilibrium

$$W = 2\gamma(\mathrm{HB} - \mathrm{HA})\mathrm{HA} = 20\ \mathrm{KN}.$$

Example 6. Evaluate the weight of the cover such that it equilibrates the force exerted by the fluid from below. Consider γ_{water}=10^4 N/m^3 e γ_{oil}=6800 N/m^3; let heights be h_1=2m e h_3=36cm, and diameters D=5m, d=20cm.

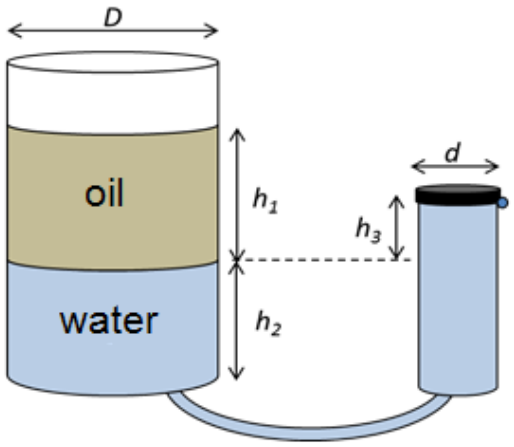

Solution:

$$F = (\gamma_{\mathrm{oil}}h_1 - \gamma_{\mathrm{water}}h_3)\pi\frac{d^2}{4} = 314\mathrm{N}.$$

Example 7. Compute force and torque relative to the hinge in A, per unit width, on the surface of the object, made of half a cylinder or radius R=2m with a cylindrical cavity of radius $r = R/4$. Consider the fluid of specific weight γ=10^4 N/m^3.

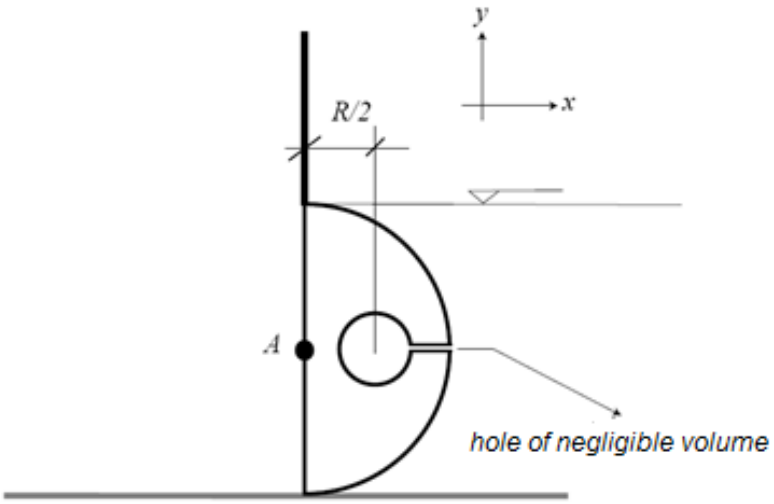

Solution:

$$F_x = -\gamma 2R^2, \quad F_y = \gamma\left(\pi\frac{R^2}{2} - \pi r^2\right).$$

Pressure on the outer cylindrical surface acts radially and gives no momentum. Momentum about A is only due to the pressure on the inner cylinder surface:

$$T_A = \gamma\pi r^2\frac{R}{2}.$$

Example 8. Compute the torque acting on the rectangular cover of length d=50cm, and unitary width. Consider the specific weigh of fluid γ=10^4 N/m^3 and that of mercury γ_m=130 N/dm^3, in the differential manometer whose reading is Δ=40 mm. Consider the following dimensions h_1=1.12m, h_2=62cm, a=120cm, b=50dm.

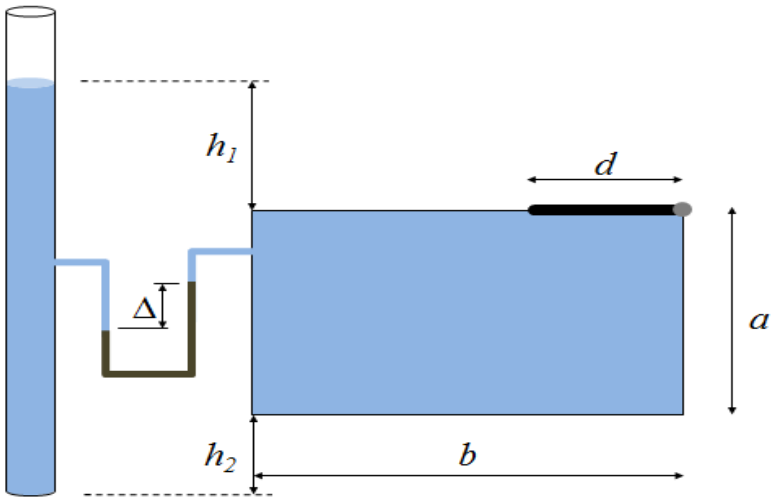

Solution:

$$h = h_1 - \left(\frac{\gamma_m - \gamma}{\gamma}\right)\Delta = 0.64\text{m}, \quad F = \gamma h d = 3.2\text{KN}, \quad T = F\frac{d}{2} = 800\text{J}.$$

Example 9. Compute the tilting moment on the structure. Consider γ=10^4 N/m^3 and measures h=6m, b=50 cm, B=2m.

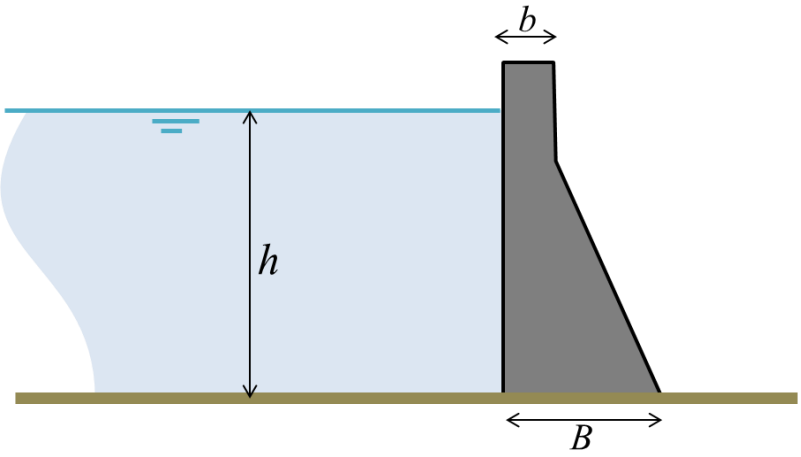

Solution:

$$M = \gamma \frac{h^2}{2}\frac{h}{3} = \gamma \frac{h^3}{6} = 3.6\ 10^5 \text{J}.$$

Example 10. Compute the torque, relative to the basis, made by the fluid on the oblique septum. Geometric measures are a=2m, b=4m, e Δ=20cm. The fluid specific weight is γ=9810N/m^3, pressure in the gas chamber is P_1=10^4Pa at height h_1=1m.

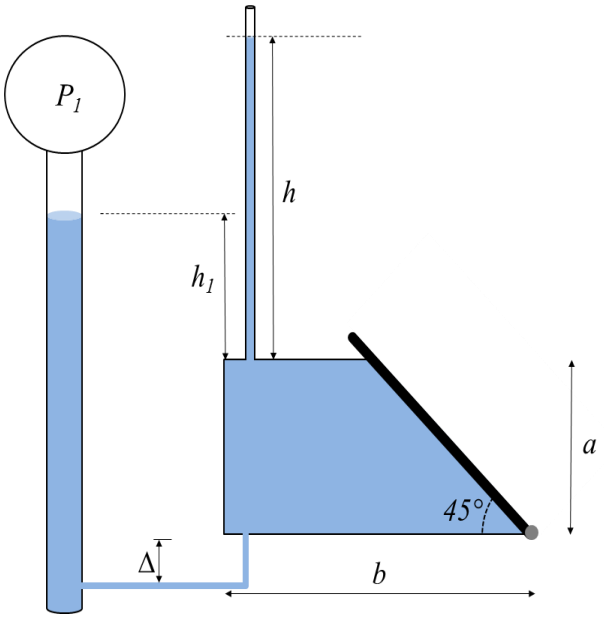

Solution:

$$h = h_1 + \frac{P_1}{\gamma} = 2.02\text{m}, \qquad F = \gamma\left(h + \frac{a}{2}\right)a\sqrt{2} = 83.78\text{KN},$$

$$\zeta_C = \frac{2}{3}\frac{(h+a)^3 - h^3}{(h+a)^2 - h^2} = 3.13\text{m}, \quad r = (h + a - \zeta_C)\sqrt{2} = 1.258\text{m}, \quad T = F \cdot r = 105\text{KJ}.$$

Torque could be evaluated by considering separately the contribution of the square and triangular distribution of pressure

$$F_{sq} = \gamma h a\sqrt{2} = 56\text{KN}, \quad T_{sq} = F_{sq}\frac{a}{2}\sqrt{2} = 79\text{KJ},$$

$$F_{tr} = \gamma\frac{a}{2}a\sqrt{2} = 28\text{KN}, \quad T_{tr} = F_{tr}\frac{a}{3}\sqrt{2} = 26\text{KJ}, \quad T = T_{sq} + T_{tr} = 105\text{KJ}.$$

Example 11. Define the width X of the base such that the surface is in equilibrium to rotation with respect to the rightmost edge.

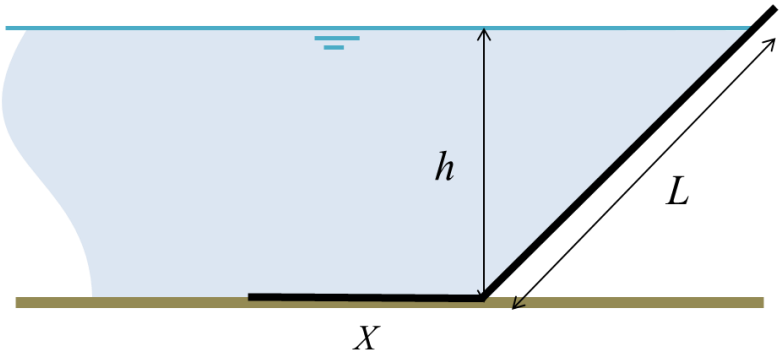

Solution:

$$\gamma\frac{hL}{2}\frac{L}{3} = \gamma h X\frac{X}{2}, \quad X = \frac{L}{\sqrt{3}}.$$

Example 12. Compute the force on the semisphere at the base of bowl. Assume γ=9810 N/m^3 and pressure on the upper gas P_0=9810Pa; fluid height is h=2.2m and radius at the base R=1m.

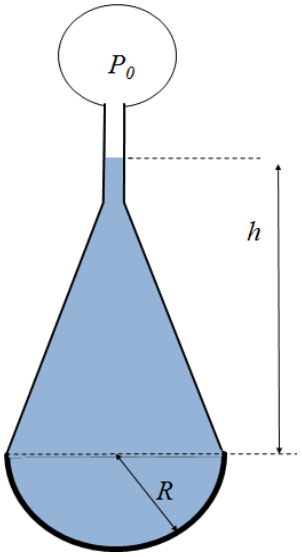

Solution:

$$H = h + \frac{P_0}{\gamma} = 3.2\text{m}, \quad F = \gamma H \pi R^2 + \gamma \frac{2}{3}\pi R^3 = 120\text{KN}.$$

Example 13. Consider the rigid surface, made of a horizontal wall of width L and a vertical wall of height h. Compute the value of the former such that it is in equilibrium to ration around the hinge A.

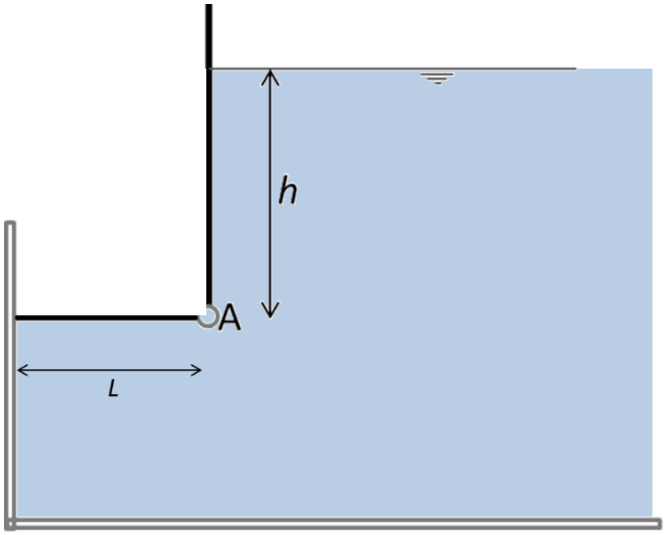

Solution:

$$\gamma \frac{h^3}{6} = \gamma h \frac{L^2}{2}, \quad L = \frac{h}{\sqrt{3}}.$$

Example 14. Compute the torque about the hinge in A for the surface made of two rectangular walls and a central semicircle. Consider $D=6m$, and $\gamma=10^4\ N/m^3$.

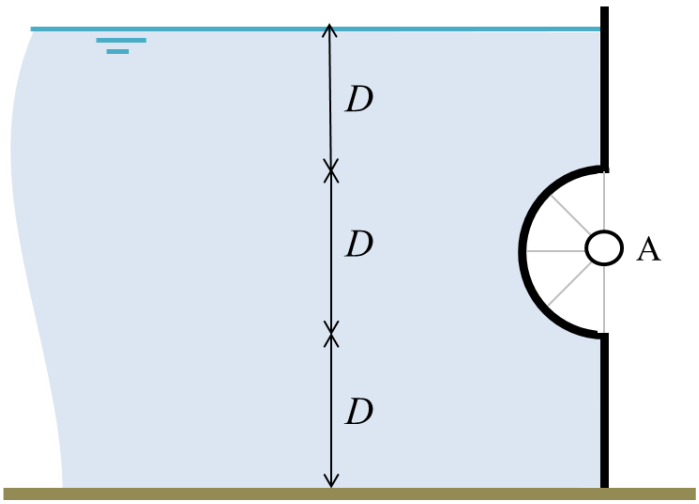

Solution:

The circular surface does not generate torque about A. The upper and lower straight walls give, respectively

$$T_u = \gamma \frac{D^2}{2}\left(\frac{D}{3}+\frac{D}{2}\right) = 9\ 10^5\text{J},$$

$$T_l = \gamma \frac{D^2}{2}\left(\frac{2}{3}D+\frac{D}{2}\right) + \gamma 2D^2\left(\frac{D}{2}+\frac{D}{2}\right) = 55.8\ 10^5\text{J},$$

$$T = T_l - T_u = 46.8\ 10^5\text{J}.$$

Example 15. Compute the ratio between vertical and horizontal components of the force made by fluid on the wall made of a rectangular wall above a semi cylindrical surface. Consider $H = D/2$.

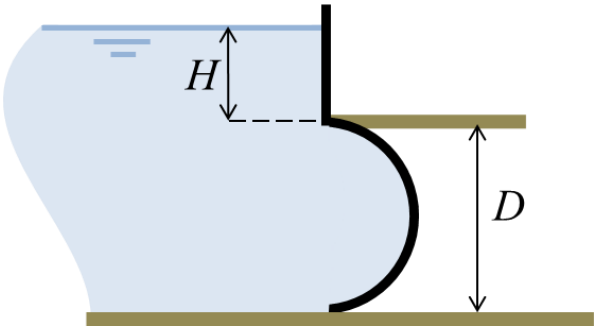

Solution:

$$F_H = \gamma\left(H+\frac{D}{2}\right)D + \gamma\frac{H^2}{2} = \frac{9}{8}\gamma D^2, \quad F_V = \gamma\pi\frac{D^2}{8}, \quad \frac{F_V}{F_H} = \frac{\pi}{9}.$$

Example 16. Compute the function $M(h)$, of the tilting moment about the hinge A, per unit width, of the oblique wall as a function of the height h. Consider the quote $a = 2h/3$ and gas pressure in the chamber $P_0 = \gamma h$.

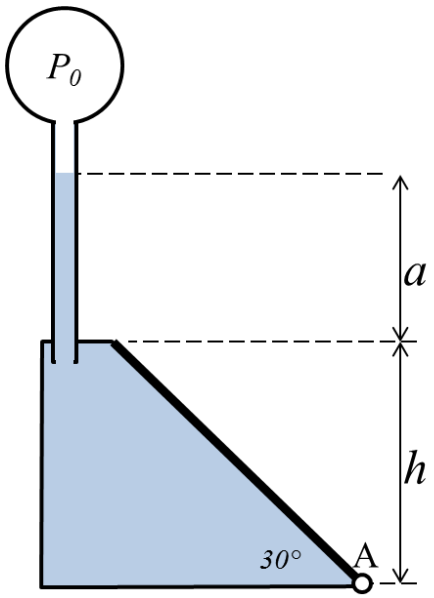

Solution:

The length of the wall is $L = \frac{h}{\sin(30°)} = 2h$, and pressure at the top of the wall is equal to that given by a depth H below a free surface, where

$$H = a + \frac{P_0}{\gamma} = \frac{5}{3}h,$$

Considering the pressure distribution as the sum of square plus triangular profiles, respectively

$$F_{sq} = \gamma HL, \quad M_{sq} = \gamma HL \cdot \frac{L}{2} = \frac{10}{3}\gamma h^3,$$
$$F_{tr} = \gamma h\frac{L}{2}, \quad M_{tr} = \gamma h\frac{L}{2}\cdot\frac{L}{3} = \frac{2}{3}\gamma h^3;$$

from which the result follows

$$M(h) = \frac{10}{3}\gamma h^3 + \frac{2}{3}\gamma h^3 = 4\gamma h^3.$$

The same result could be found considering the momentum of the entire force acting con the center C of pressure distribution

$$F = \gamma\left(H + \frac{h}{2}\right)L = \frac{13}{3}\gamma h^2, \quad \zeta_C = \frac{2}{3}\frac{(h+H)^3 - H^3}{(h+H)^2 - H^2} = \frac{86}{39}h, \quad r = 2(H + h - \zeta_C) = \frac{12}{13}h;$$

from which the same result follows

$$M(h) = F \cdot r = \frac{13}{3}\gamma h^2 \cdot \frac{12}{13}h = 4\gamma h^3.$$

Example 17. Compute force and torque, about the hinge in A, on the vertical surface (per unit width). Consider P_0=150*mmHg*, h=5m, a=2m; and the specific weight γ=10KN/m^3.

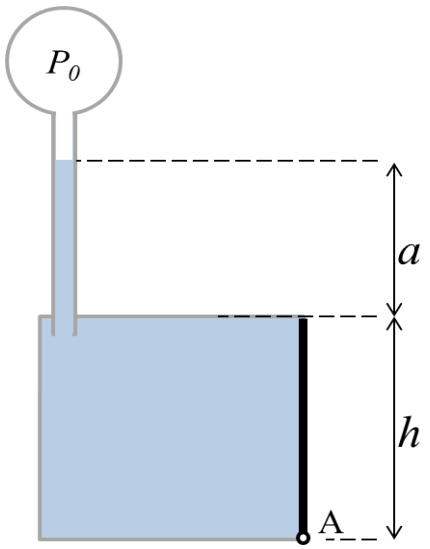

Solution:

$$P_0 = 150\text{mmHg} = 20\text{KPa} = \gamma \cdot 2\text{m},$$

Considering the pressure distribution as the sum of square plus triangular pressure profiles, respectively

$$F = F_{sq} + F_{tr} = (P_0 + \gamma a)h + \gamma\frac{h^2}{2} = 200\text{KN} + 125\text{KN} = 325\text{KN},$$

$$T = F_{sq}\cdot\frac{h}{2} + F_{tr}\cdot\frac{h}{3} = 500\text{KJ} + 208\text{KJ} = 708\text{KJ}.$$

In alternative, considering the entire force at once

$$h_1 = \frac{P_0}{\gamma} + a = 4\text{m}, \quad h_2 = h_1 + h = 9\text{m}, \quad h_C = \frac{2}{3}\frac{h_2^3 - h_1^3}{h_2^2 - h_1^2} = 6.82\text{m}, = 2.18\text{m};$$

$$F = \left(P_0 + \gamma\left(a + \frac{h}{2}\right)\right)h = 325\text{KN}, \quad T = F\cdot(h_2 - h_C) = 708\text{KJ}.$$

Example 18. Compute the static force acting on the semispherical surface. Consider H=3.6m, R=1.6m, γ=9810 N/m^3.

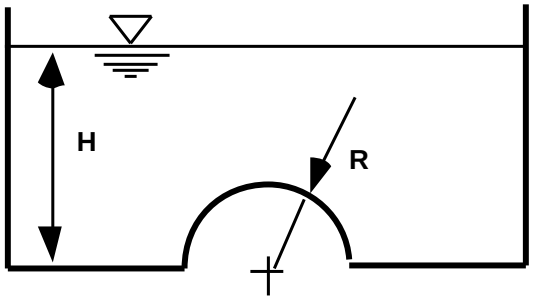

Solution:

$$F = \gamma V = \gamma\left(\pi\text{R}^2\text{H} - \frac{2}{3}\pi\text{R}^3\right) = 200\text{KN}.$$

Example 19. Compute the horizontal and vertical components of the force made by the fluid on the semispherical surface. Assume *H=50cm H=1m* and the fluid specific weight γ=9810 N/m^3.

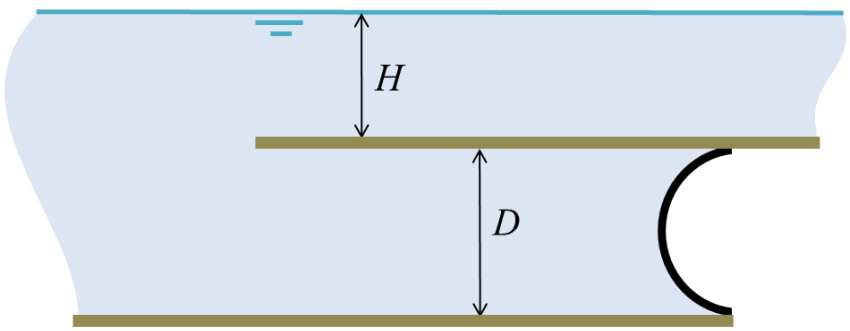

Solution:

$$F_H = \gamma\left(H + \frac{D}{2}\right)\pi\frac{D^2}{4} = 7705\text{N}, \quad F_V = \gamma\frac{2}{3}\pi\frac{D^3}{8} = 2568\text{N}\cdot$$

Example 20. Compute the force acting on the semispherical surface at the bottom of the bowl. Consider the following relationships $\gamma_{oil} = 2/3\gamma$, $h_1 = 1.8R$, $h_2 = 0.2R$, $h_3 = 1.5R$, where R=3m and γ=9810N/m^3.

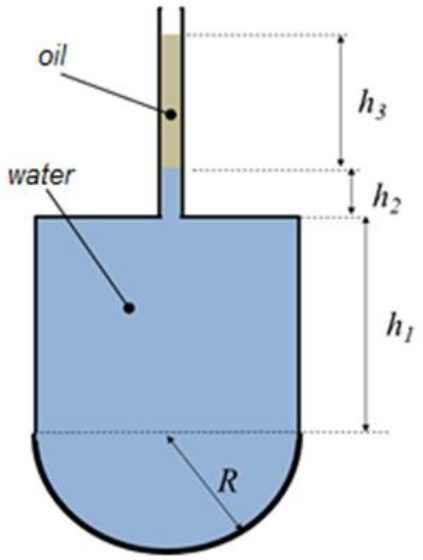

Solution:

$$h = h_1 + h_2 + \frac{\gamma_{oil}}{\gamma}h_3 = 3R, \quad F_H = 0, \quad F_V = \gamma h\pi R^2 + \gamma\frac{2}{3}\pi R^3 = \gamma\frac{11}{3}\pi R^3 = 3.06\text{MN}\,.$$

3. Fluid Kinematics

3.1. Recalls of differential vector calculus

Let us recall some basic notions of differential vector calculus that are extensively used afterwards.

The differential vector operator *nabla* is useful to perform derivatives in three-dimensional (3D) fields. In Cartesian coordinates the operator nabla is defined as

$$\nabla = \begin{bmatrix} \frac{\partial}{\partial x} \\ \frac{\partial}{\partial y} \\ \frac{\partial}{\partial z} \end{bmatrix}.$$

The *gradient* of a scalar field $f(\boldsymbol{x})$ is a vector field, ∇f, obtained by applying the operator Nabla to the field. In Cartesian coordinates the gradient is a vector

$$\nabla f = \begin{bmatrix} \frac{\partial f}{\partial x} \\ \frac{\partial f}{\partial y} \\ \frac{\partial f}{\partial z} \end{bmatrix} \tag{3.1}$$

and describes how the field f changes in space. For example, if ∇f has one component it means that the field f changes along that component. In other words, the gradient vector is always perpendicular to the lines or surfaces where f is constant. Knowledge of the gradient vector permits the evaluation of partial derivatives along an arbitrary direction, say $\boldsymbol{n}$, by projection

$$\frac{\partial f}{\partial n} = \nabla f \cdot \boldsymbol{n} \,. \tag{3.2}$$

Gradient vector fields are important in physics. Some vector field, $\boldsymbol{F}$, can be expressed as the gradient of a scalar field, $\boldsymbol{F} = \nabla f$; in this case, the field $\boldsymbol{F}$ is a conservative field and the scalar field f is called the potential of $\boldsymbol{F}$. It is immediate to verify that when $\boldsymbol{F} = \nabla f$, its integral along a curve is trivially the difference of the potential f at the two ends and does not depend from the path itself, which is the definition of conservative field.

We have seen that the gradient of a scalar field is a vector field; indeed the gradient operation increases the dimensionality. Similarly, the gradient of a vector field, $\boldsymbol{v}(\boldsymbol{x})$, is a tensor field, $\nabla \boldsymbol{v}$**,** whose component *i*,*j* in Cartesian coordinates is

$$(\nabla \boldsymbol{v})_{ij} = \frac{\partial v_i}{\partial x_j}. \tag{3.3}$$

The *divergence* of a vector field, $\boldsymbol{v}(\boldsymbol{x})$, is a scalar field, $\nabla \cdot \boldsymbol{v}$, obtained by performing formally the scalar product of $\boldsymbol{v}$ with nabla. In Cartesian coordinates the divergence is

$$\nabla \cdot \boldsymbol{v} = \frac{\partial v_x}{\partial x} + \frac{\partial v_y}{\partial y} + \frac{\partial v_z}{\partial z} = \sum_{i=1}^{3} \frac{\partial v_i}{\partial x_i} = \frac{\partial v_i}{\partial x_i} \tag{3.4}$$

where in the last expression the summation on repeated indices it is implicitly assumed (Einstein notation). The name divergence comes because a positive divergence at a point means that the vector (relative to the point) is directed radially away from that point, thus it diverges. For example consider

the 2D case, $\frac{\partial v_x}{\partial x} + \frac{\partial v_y}{\partial y} > 0$, means that v_x is negative before and positive after and that v_y is negative below and positive above.

Vector fields with zero divergence are called *solenoidal* (name coming from electromagnetism) and take particular relevance in fluid dynamics as will be shown shortly.

The divergence reduces the dimensionality; thus, the divergence of a tensor field $\mathbb{T}$ is a vector field.

$$(\nabla \cdot \mathbb{T})_i = \frac{\partial \mathbb{T}_{ij}}{\partial x_j}. \tag{3.5}$$

Last vector operator is the *curl* that is applied to a vector field and produces another vector field; it does not change the dimensionality. The curl or a vector field is $\nabla \times \boldsymbol{v}$, obtained by performing formally the internal product with nabla. In Cartesian coordinates the curl is

$$\nabla \times \boldsymbol{v} = \begin{bmatrix} \frac{\partial v_z}{\partial y} - \frac{\partial v_y}{\partial z} \\ \frac{\partial v_x}{\partial z} - \frac{\partial v_z}{\partial x} \\ \frac{\partial v_y}{\partial x} - \frac{\partial v_x}{\partial y} \end{bmatrix}. \tag{3.6}$$

When the vector $\boldsymbol{v}(\boldsymbol{x})$ is the velocity, the curl represents twice the angular velocity at a point.

The curl of velocity takes a special relevance in fluid dynamics and deserved its own name; the *vorticity vector field* $\boldsymbol{\omega}(\boldsymbol{x})$

$$\boldsymbol{\omega}(\boldsymbol{x}) = \nabla \times \boldsymbol{v}\ ; \tag{3.7}$$

which will be treated with attention in Chapter 10 to analyze the most advanced phenomena in cardiovascular flows. In particular, vector fields whose curl is zero are called *irrotational*; such especially simple fields can be expressed as a gradient field. It is immediate to verify that the divergence of a curl field is identically zero (vorticity is a solenoidal field) and that the curl of a gradient is zero (conservative fields are irrotational fields)

$$\nabla \cdot (\nabla \times \boldsymbol{v}) = 0, \quad \nabla \times (\nabla f) = 0.$$

Let us briefly recall two fundamental theorems involving the integral applications of these operators.

3.2. The Gauss theorem in integral calculus

The Gauss theorem (or divergence theorem) states that the divergence of a vector field $\boldsymbol{v}(\boldsymbol{x})$ inside a volume V is equal to the flux of that vector across the boundary surface S of that volume

$$\int_V \nabla \cdot \boldsymbol{v}\, dV = \int_S \boldsymbol{v} \cdot \boldsymbol{n}\, dS\ . \tag{3.8}$$

where $\boldsymbol{n}$ is unit normal, directed outward. Despite the apparent mathematical complexity, the physical interpretation of the Gauss theorem is intuitive: if a vector field has some divergence inside a volume, necessarily it has to point outside that volume. It can be seen immediately when the volume is a small cube (or a square, in 2D): if the vector field points outward that cube then the field diverges, it has positive divergence inside the cube. The Gauss theorem permits to transform the calculation of a volume integral into a calculation on its boundary that is usually simpler to perform; therefore, represents a powerful mathematical tool in many contexts.

A simple application the Gauss theorem permits to compute the volume of an arbitrary shape by the integral on its surface. For this, consider a field with unit divergence, $\nabla \cdot \boldsymbol{v} = 1$, for example taking $\boldsymbol{v} = \boldsymbol{x}/3$, then we find that the volume can be computed by a surface integral

$$V = \int_V \, dV = \frac{\mathbf{1}}{3} \int_S \, \boldsymbol{x} \cdot \boldsymbol{n} \, dS. \tag{3.9}$$

Similarly, the center $\overline{\boldsymbol{x}}$ of a volume can be computed as (Messner and Taylor, 1980)

$$\overline{\boldsymbol{x}} = \frac{\mathbf{1}}{4V} \int_S \, \boldsymbol{x}(\boldsymbol{x} \cdot \boldsymbol{n}) dS. \tag{3.10}$$

The same method can be used in 2D for computing the area of a generic figure; the surface integral becomes a line integral that reads

$$A = \int_A \, dA = \frac{\mathbf{1}}{2} \oint_C \, \boldsymbol{x} \cdot \boldsymbol{n} \, ds = \frac{\mathbf{1}}{2} \oint_C \, (x dy - y dx), \tag{3.11}$$

where we used that $\boldsymbol{n} ds = [dy, -dx]$.

The Gauss theorem can be rearranged to provide a number of different relationships between volume and surface integral. A typical examples is the integral of a curl

$$\int_V \, \nabla \times \boldsymbol{v} \, dV = - \int_S \, \boldsymbol{v} \times \boldsymbol{n} dS. \tag{3.12}$$

that is obtained by applying (3.8) to a vector $u_j = \varepsilon_{ijk} v_k$, a , for an arbitrary value of $i = 1,2,3$ and repeating it for the three coordinates $i = 1,2,3$, (where ε_{ijk} is the fully antisymmetric tensor, or Levi-Civita tensor, equal to $+1$ when the three indices are a cyclic permutation of 1,2,3, equal to -1 if an anticylcic permutation and zero is two indices are equal).

Another example is the integral of a gradient field

$$\int_V \, \nabla f \, dV = \int_S \, f \boldsymbol{n} dS. \tag{3.13}$$

obtained as before by applying (3.8) to a vector $v_j = \delta_{ij} f$, (where δ_{ij} is the identity tensor, equal to $+1$ when the two indices are equal and zero otherwise).

The Gauss theorem can also be used to compute the volume integral of a divergence-free vector field $\boldsymbol{v}$ that becomes

$$\int_V \, \boldsymbol{v} \, dV = \int_S \, (\boldsymbol{v} \cdot \boldsymbol{n}) \boldsymbol{x} dS. \tag{3.14}$$

This is obtained by applying (3.8) to the vector $u_j = v_j x_i$

$$\int_V \, \nabla \cdot (\boldsymbol{v} x_i) \, dV' = \int_V \, x_i \nabla \cdot \boldsymbol{v} + \boldsymbol{v} \cdot \nabla x_i \, dV' = \int_V \, v_i \, dV' = \int_S \, x_i \boldsymbol{v} \cdot \boldsymbol{n} dS;$$

which gives (3.14) once repeated for the three coordinates $i = 1,2,3$,

The Stokes theorem (or circulation theorem) states that the circulation of a vector along a closed curve *C* is equal to the integral of its curl on any surface *S* bounded by that curve

$$\oint_C \, \boldsymbol{v} \cdot d\boldsymbol{s} = \int_S \, (\nabla \times \boldsymbol{v}) \cdot \boldsymbol{n} \, dS \, . \tag{3.15}$$

where the curve direction of integration and its normal are related by the right-hand rule. The Stokes theorem can also be derived from the Gauss theorem, in particular it is a 2D version of the result

(3.12). The physical interpretations is similarly straightforward: the total rotation (circulation) is given by the summation of the individual rotations (curl of the vector) contained within. As a trivial example, take the rigid rotation of a circular plate with angular velocity Ω, the rotation velocity at a distance r from the center is $v=\Omega r$, the Stokes equality states that $2\pi rv=\pi r^2\omega$. From which it follows that the vorticity, previously introduced in (3.7), has only the component normal to the plane and its value is twice the angular velocity $\omega=2\Omega$.

3.3. Breaking down elementary motion

Consider the velocity $\boldsymbol{v}(\boldsymbol{x})$ a point $\boldsymbol{x}$ and let's describe the nearby velocity, at infinitesimal distance $d\boldsymbol{x}$, to define the elementary types of motion that can be encountered in general. Using Taylor expansion

$$\boldsymbol{v}(\boldsymbol{x}+d\boldsymbol{x})=\boldsymbol{v}(\boldsymbol{x})+\nabla\boldsymbol{v}\cdot d\boldsymbol{x}+O(dx^2); \tag{3.16}$$

the velocity is equal to the velocity at the original point, plus its gradient in the direction of the new point, plus second order terms that will be neglected from now on as we implicitly work in the limit $dx\to 0$. In index notation (3.16) can be rewritten equivalently

$$v_i(\boldsymbol{x}+d\boldsymbol{x})=v_i(\boldsymbol{x})+\frac{\partial v_i}{\partial x_j}dx_j\ ; \tag{3.17}$$

where summation on repeated indices (here index j) is implicitly assumed.

The velocity gradient tensor can be divided as the sum of a symmetric $\mathbb{D}$ and an asymmetric tensor $\boldsymbol{\Omega}$

$$\frac{\partial v_i}{\partial x_j}=\frac{1}{2}\left(\frac{\partial v_i}{\partial x_j}+\frac{\partial v_j}{\partial x_i}\right)+\frac{1}{2}\left(\frac{\partial v_i}{\partial x_j}-\frac{\partial v_j}{\partial x_i}\right),\quad \nabla\boldsymbol{v}=\mathbb{D}+\boldsymbol{\Omega}\ ; \tag{3.18}$$

equation (3.16) can thus be rewritten

$$\boldsymbol{v}(\boldsymbol{x}+d\boldsymbol{x})=\boldsymbol{v}(\boldsymbol{x})+\mathbb{D}\cdot d\boldsymbol{x}+\boldsymbol{\Omega}\cdot d\boldsymbol{x}; \tag{3.19}$$

or in an equivalently from (3.17) in an indexed form.

Let us look at the three terms in (3.19) that sum up to describe the velocity about a point. The first term describes the *rigid translation* of the small region where all points share the same velocity. The last term is driven by $\boldsymbol{\Omega}$ that is a 3x3 asymmetric tensor, which in Cartesian coordinates reads

$$\boldsymbol{\Omega}=\begin{bmatrix} 0 & +\frac{1}{2}\left(\frac{\partial v_x}{\partial y}-\frac{\partial v_y}{\partial x}\right) & +\frac{1}{2}\left(\frac{\partial v_x}{\partial z}-\frac{\partial v_z}{\partial x}\right)\\ -\frac{1}{2}\left(\frac{\partial v_x}{\partial y}-\frac{\partial v_y}{\partial x}\right) & 0 & +\frac{1}{2}\left(\frac{\partial v_y}{\partial z}-\frac{\partial v_z}{\partial y}\right)\\ -\frac{1}{2}\left(\frac{\partial v_x}{\partial z}-\frac{\partial v_z}{\partial x}\right) & -\frac{1}{2}\left(\frac{\partial v_y}{\partial z}-\frac{\partial v_z}{\partial y}\right) & 0 \end{bmatrix}=\frac{1}{2}\begin{bmatrix} 0 & -\omega_z & +\omega_y\\ \omega_z & 0 & -\omega_x\\ -\omega_y & +\omega_x & 0 \end{bmatrix}.$$

Being asymmetric, this tensor is described by 3 independent terms only, and these 3 terms are equal to the components of the vorticity (3.6-3.7), module a ½ factor. It can be immediately verified that the scalar product $\boldsymbol{\Omega}\cdot d\boldsymbol{x}=\frac{1}{2}\boldsymbol{\omega}\times d\boldsymbol{x}$. Rewriting (3.19) this way

$$\boldsymbol{v}(\boldsymbol{x}+d\boldsymbol{x})=\boldsymbol{v}(\boldsymbol{x})+\mathbb{D}\cdot d\boldsymbol{x}+\frac{1}{2}\boldsymbol{\omega}\times d\boldsymbol{x};$$

it is immediate to notice that the last terms is the expression corresponds to a *rigid rotation* with angular velocity $\frac{1}{2}\boldsymbol{\omega}$. Rigid translation and rigid rotation do not produce local deformations; it follows that the deformation of the fluid element is only due to the second term. In fact, the symmetric tensor $\mathbb{D}$ is the *rate of deformation tensor*, which in Cartesian coordinates reads

$$\mathbb{D} = \begin{bmatrix} \frac{\partial v_x}{\partial x} & \frac{1}{2}\left(\frac{\partial v_x}{\partial y} + \frac{\partial v_y}{\partial x}\right) & \frac{1}{2}\left(\frac{\partial v_x}{\partial z} + \frac{\partial v_z}{\partial x}\right) \\ \frac{1}{2}\left(\frac{\partial v_x}{\partial y} + \frac{\partial v_y}{\partial x}\right) & \frac{\partial v_y}{\partial y} & \frac{1}{2}\left(\frac{\partial v_y}{\partial z} + \frac{\partial v_z}{\partial y}\right) \\ \frac{1}{2}\left(\frac{\partial v_x}{\partial z} + \frac{\partial v_z}{\partial x}\right) & \frac{1}{2}\left(\frac{\partial v_y}{\partial z} + \frac{\partial v_z}{\partial y}\right) & \frac{\partial v_z}{\partial z} \end{bmatrix}. \tag{3.20}$$

The scalar product $\mathbb{D} \cdot d\boldsymbol{x}$ represents the (rate of) deformation of the fluid element. The diagonal terms of the tensor are associated with elongation/shortening in the corresponding direction and the off-diagonal are shear motion. The change of volume of the fluid element is due to the combination of elongations/shortening, that is given by the trace of the rate of deformation tensor (the sum of the elements on the diagonal), while a tensor with zero trace does not give change of volume. The trace of the deformation tensor is the divergence of the velocity field, therefore it is useful to rewrite (3.19) in its final form as

$$\boldsymbol{v}(\boldsymbol{x} + d\boldsymbol{x}) = \boldsymbol{v}(\boldsymbol{x}) + \frac{\nabla \cdot \boldsymbol{v}}{3}\mathbb{I} \cdot d\boldsymbol{x} + \left(\mathbb{D} - \frac{\nabla \cdot \boldsymbol{v}}{3}\mathbb{I}\right) \cdot d\boldsymbol{x} + \frac{1}{2}\boldsymbol{\omega} \times d\boldsymbol{x}. \tag{3.21}$$

Expression (3.21) allows recognizing the different elementary motions of an infinitesimal fluid element. We have seen that the first terms describes rigid translation and the last term is the rigid rotation. The second term is pure expansion/compression that is responsible for the local change of volume; it will be shown shortly that this terms is zero in an incompressible fluid. The third term is the pure deformation, with no change of volume; this terms is the only responsible for internal viscous stresses that are due to the relative sliding motion of fluid particles.

Before concluding this section about the description of fluid motion, let us define and specify differences between trajectories and streamlines. *Trajectories*, as by the normal language, are the curves in space occupied by a same particle during its motion; therefore, trajectories are curves traveled by particles during time from a specified initial particle position. Differently, *streamlines* are curves drawn at one instant of time that are everywhere tangent to the local velocity; therefore, streamlines change during time. In steady flow trajectories and streamlines coincides and can be used interchangeably. In general, trajectories follow the time-course of individual material particle (what is called Lagrangian description) while streamlines the instantaneous flow paths at fixed points in space (Eulerian description); these descriptions are different and provide different information.

3.4. Lagrangian and Eulerian description

The laws of physics are commonly expressed in terms of the conservation of quantities associated with material elements. Following this line, elementary mechanics typically refers to individual particles with given mass that are followed in time while they change their velocity and other properties like, for example in thermodynamics, their temperature. Mechanics of rigid bodies also considered the translation and rotation of a given volume mad of material elements. This approach is used in general for the analysis of solid deformable bodies where the changes in the position, and relative position, of individual material elements are followed during their motion.

The natural description of dynamics is thus expressed by *following the individual elements* composing the body under analysis. In such a perspective, that is called *Lagrangian description*, each individual

material element is identified by its position $\boldsymbol{X}_0$ at a certain reference time, say t=0, and is then described at subsequent times by its position $\boldsymbol{X}(t, \boldsymbol{X}_0)$ and by the value of properties associated to that element $G(t, \boldsymbol{X}_0)$ identified by the initial position $\boldsymbol{X}_0$. The Lagrangian approach is well suited for solid mechanics, where the material has an internal structure characterized by the relative arrangement of individual elements.

In fluid mechanics, the individual fluid elements do not have a preferable relative arrangement; they undergo to large relative motion and cannot be followed during time. Individual blood cells follow independent paths; they separate in arterial bifurcations, some enter in an organ others in another and so forth. Therefore, a Lagrangian description based on following individual elements is generally not feasible with fluids. The natural description of fluid dynamics is made in terms of properties measured at points fixed in space, which is called *Eulerian description*. The wind velocity is measured at the anemometer position, water temperature is measured at the thermometer position, blood velocity is measured across a valve; all these are Eulerian measurements made at fixed spatial locations that do not refer to the original position of individual particles that pass through.

Indicate with lowercase letters the Eulerian properties measures at time t at spatial location $\boldsymbol{x}$, the property $g(t, \boldsymbol{x})$ represents the Eulerian counterpart of the Lagrangian property $G(t, \boldsymbol{X}_0)$. However, both correspond to different descriptions of the same physical property. The Eulerian is more appropriate for measuring and describing fluid properties, whereas conservation laws are more naturally expressed in Lagrangian terms.

The relationship between Lagrangian and Eulerian description is

$$G(t, \boldsymbol{X}_0) = g\big(t, \boldsymbol{X}(t, \boldsymbol{X}_0)\big). \tag{3.22}$$

Relation (3.22) simply states that the properties of the particle $\boldsymbol{X}_0$ at time t is the same found at the spatial position $\boldsymbol{X}(t, \boldsymbol{X}_0)$ occupied by the particle at time t. Equation (3.22) is important because it provides a bridge between Lagrangian to Eulerian descriptions. Conservation laws are commonly expressed in terms of the time variation of particle properties; for example, acceleration of a fluid particle is the time derivative of velocity of a particle. Relation (3.22) permits to evaluate the time derivative associated with fluid particles in terms of Eulerian quantities. Take the time derivative of (3.22), using the chain rule,

$$\frac{dG}{dt} = \frac{\partial g}{\partial t} + \frac{\partial g}{\partial x}\frac{dX}{dt} + \frac{\partial g}{\partial y}\frac{dY}{dt} + \frac{\partial g}{\partial z}\frac{dZ}{dt} = \frac{\partial g}{\partial t} + v_x\frac{\partial g}{\partial x} + v_y\frac{\partial g}{\partial y} + v_z\frac{\partial g}{\partial z},$$

or

$$\frac{dG}{dt} = \frac{\partial g}{\partial t} + \boldsymbol{v} \cdot \nabla g. \tag{3.23}$$

The right hand side of (3.23) is the Lagrangian time derivative written in Eulerian terms, which is sometime called *material* or *substantial* time derivative. Equation (3.23) states that the material property of a particle passing through a fixed location $\boldsymbol{x}$ can increase either because the property is increasing at the location or because the particle is moving in the direction along which the property increases in space, i.e. when its gradient is aligned with the velocity vector.

As a fundamental application, let us apply the (3.23) to the fluid velocity to compute the acceleration of a fluid particle at position $\boldsymbol{x}$

$$\boldsymbol{a}(t, \boldsymbol{x}) = \frac{\partial \boldsymbol{v}}{\partial t} + \boldsymbol{v} \cdot \nabla \boldsymbol{v}. \tag{3.24}$$

This shows that a particle can accelerate either when velocity increases in time at the position $\boldsymbol{x}$ or, even in steady flow, when the particle is moving toward a region with higher velocity. This point is sketched in figure 3.1, the first term of (3.24) is the *inertial acceleration*, because it is associated with the increase of fluid inertia, the second term is the *convective acceleration*, because due to the convection of fluid.

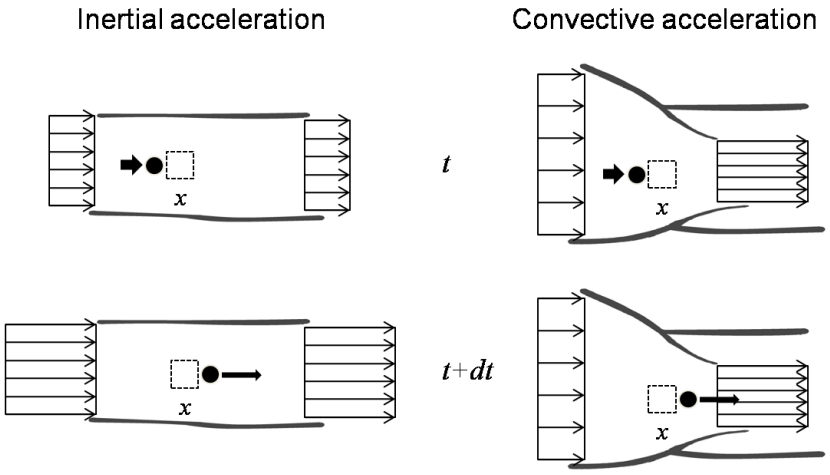

Figure 3.1. Inertial and convective acceleration

This concept can be extended from individual particles to the integral expressions applied to finite volume. Integral conservation laws typically apply to a (Lagrangian) material volume of fluid that deforms during its motion, whereas fluid balances are necessarily applied to (Eulerian) spatially defined regions, like a portion of a duct between two cross-sections.

The Reynolds' *Transport theorem* permits to express the time variation of a property associated to a material fluid volume in terms of variations in a spatially fixed volume. Consider a volume of fluid $V_F(t)$ and a fixed volume V that described the location of the volume of fluid at time t, $V = V_F(t)$, bounded by a fixed surface S. We can prove that

$$\frac{d}{dt}\int_{V_F(t)} G(t) = \int_V \frac{\partial g}{\partial t} dV + \int_S g\, \boldsymbol{v}\cdot\boldsymbol{n} dS \qquad (3.25)$$

where $\boldsymbol{n}$ is the outward normal to the surface S.

The intuitive demonstration of (3.25) is as follow. Express the time derivative at the incremental ratio (dt is infinitesimal and implicitly includes the limit to $dt \to 0$)

$$\frac{d}{dt}\int_{V_F(t)} G(t) = \frac{1}{dt}\left(\int_{V_F(t+dt)} g(t+dt)dV - \int_V g(t)dV\right) =$$

divide the first integral on the right-hand-side in two parts

$$= \frac{1}{dt}\left(\int_V g(t+dt)dV + \int_{V_F(t+dt)-V} g(t+dt)dV - \int_V g(t)dV\right) =$$

the second integral is over the thin space between the volume at time t and $t+dt$, whose infinitesimal volume portion dV is spanned by the infinitesimal surface dS on the boundary of volume V, multiplied by the length travelled normally to that surface in the period dt. In formulas $dV = dS(\boldsymbol{v}\cdot\boldsymbol{n})dt$; thus the previous formula becomes

$$= \int_V \frac{\partial g}{\partial t} dV + \int_S g(\boldsymbol{v} \cdot \boldsymbol{n}) dS$$

where the first integral combined the formerly first and last terms, and the higher order infinitesimal terms disappeared in the limit of dt approaching 0. This completed the proof of (3.25).

The transport theorem (3.25) can be rewritten with volume integrals with the aid of the Gauss theorem (3.8),

$$\frac{d}{dt} \int_{V_F(t)} G(t) = \int_V \left\{ \frac{\partial g}{\partial t} + \nabla \cdot (g\, \boldsymbol{v}) \right\} dV. \tag{3.26}$$

Equation (3.25) and (3.26) will be fundamental to express the (Lagrangian) conservation laws in terms of (Eulerian) fluid volumes fixed in space.

B. FLUID DYNAMICS: CONSERVATION LAWS

4. Conservation of Mass

4.1. Mass balance in integral form

The first law of conservation to consider is the conservation of mass. Given a generic volume V_F of a continuum, the mass of that volume is by definition

$$\int_{V_F(t)} \rho dV$$

where ρ is the density. Conservation of mass states that the mass of a volume of material does not change during time, which reads

$$\frac{d}{dt}\int_{V_F(t)} \rho dV = 0 \tag{4.1}$$

The law (4.1) applies to a material volume of fluid (or any continuum) deforming during its motion. Application of the transport theorem (3.25) to (4.1) gives the *integral law of conservation of mass*

$$\int_V \frac{\partial \rho}{\partial t} dV + \int_S \rho\, \boldsymbol{v} \cdot \boldsymbol{n} dS = 0 \tag{4.2}$$

where V is a spatial volume fixed in space and S is the surface surrounding that volume. Equations expressing mass conservation are also called *continuity equation*, because mass conservation ensures the continuity to the material that cannot disappear from one region.

As mentioned before, we will only deal with fluids whose density is constant in time and uniform in space. These fluids are generically referred here as incompressible fluids (although more rigorously, fluids can be incompressible even with spatially variable density). For them, conservation of mass (4.2) simplifies in

$$\int_S \boldsymbol{v} \cdot \boldsymbol{n} dS = 0. \tag{4.3}$$

The integral equation of mass conservation for incompressible fluids, equation (4.3), states that given a spatially fixed volume, the amount of fluid that enters through a part the boundary of such volume is equal to the amount that leaves through the remaining boundary.

This concept can be expressed in different integral terms. If we have a container of volume $V(t)$ bounded by surface $S(t)$ composed of a solid surface S_0, moving with boundary velocity $\boldsymbol{v}_b$, and open sections of area S_{open} allowing the fluid to flow with fluid velocity $\boldsymbol{v}$, we can rewrite the instantaneous balance (4.3) as

$$\int_{S_0} \boldsymbol{v}_b \cdot \boldsymbol{n} dS + \int_{S_{\text{open}}} \boldsymbol{v} \cdot \boldsymbol{n} dS = 0;$$

being $S = S_0 + S_{\text{open}}$. Consider now that the open boundary of the varying volume $V(t)$ also moves with a velocity $\boldsymbol{v}_b$ that represents its geometric displacement then we can divide the fluid velocity therein as the sum of the boundary velocity plus the relative velocity $\boldsymbol{v} = \boldsymbol{v}_b + (\boldsymbol{v} - \boldsymbol{v}_b)$ the previous balance can be recast as

$$\int_S \boldsymbol{v}_b \cdot \boldsymbol{n} dS + \int_{S_{\text{open}}} (\boldsymbol{v} - \boldsymbol{v}_b) \cdot \boldsymbol{n} dS = \frac{dV}{dt} + \int_{S_{\text{open}}} (\boldsymbol{v} - \boldsymbol{v}_b) \cdot \boldsymbol{n} dS = 0;$$

where the first integral is over the entire bounding surface S. This can be written more simply as

$$\frac{dV}{dt} = Q_{\text{in}} - Q_{\text{out}}; \tag{4.4}$$

where Q_{in} is the total entering discharge, rate of fluid flow relative to the moving boundary, across the open section S_{in} through which flow enters and Q_{out} is the total exiting discharge across S_{out}, $\left(S_{\text{open}} = S_{\text{in}} + S_{\text{out}}\right)$

$$Q_{\text{in}} = -\int_{S_{\text{in}}} (\boldsymbol{v} - \boldsymbol{v}_b) \cdot \boldsymbol{n} dS\,, \quad Q_{\text{out}} = +\int_{S_{\text{out}}} (\boldsymbol{v} - \boldsymbol{v}_b) \cdot \boldsymbol{n} dS; \tag{4.5}$$

and we remind that we considered the normal $\boldsymbol{n}$ pointing outward. It is important to remark that when writing (4.4) and (4.5) the fluid velocities $\boldsymbol{v}$ are Eulerian quantities: absolute values measured relative to a spatially fixed reference. Thus the discharges (4.5) are written using the relative velocity of fluid with respect to possibly moving boundaries.

As an instructive example, consider a left ventricle (LV), whose total volume is $V_{\text{LV}}(t)$ increases during filling (diastole) while blood enters through the mitral valve of area A_{MV}. Application of (4.4) reads

$$\frac{dV_{\text{LV}}}{dt} = A_{\text{MV}} \left(v_{\text{MV}} + v_{b\,\text{MV}}\right); \tag{4.6}$$

where v_{MV} is the *fluid* velocity across the mitral valve (here assumed positive downward, entering the chamber); this is the velocity measured by imaging methods, like Doppler echocardiography or Phase-Contrast CMR (Cardiac Magnetic Resonance). The value $v_{b\,\text{MV}}$ is the velocity of the mitral valve boundary (assumed positive upward) during ventricular expansion. In common applications this terms is neglected because it is assumed to be much smaller that the fluid velocity. This is commonly realistic, although introduces an approximation that may not be always valid. A balance like (4.6) can be applied to ventricular contraction during flow ejection through the aortic valve, as well as to other chambers or portions of a vessel. It is particularly useful to properly relate measurements of fluid velocity, tissue velocity and chamber dimension.

4.2. Mass balance for a vessel

Consider the flow in a vessel, this type of motion is predominantly one-dimensional (1D), with the velocity component along the vessel axis much larger than the transversal components. In such cases, it is often useful to consider properties characterizing the whole cross section (area, average velocity, discharge, average pressure etc,) expresses as a function of the single spatial coordinate, say x, that defines the position along the vessel.

Consider an infinitesimal length dx of such a 1D stream of cross section area $A(t,x)$ and discharge $Q(t,x) = A(t,x)U(x,t)$ being $U(x,t)$ the velocity averaged over the cross-section. And apply the conservation of mass (4.4) to quasi-cylindrical short element with volume $V = A(t,x)dx$. The flow entering from the first section is $Q_{\text{in}} = Q(t,x)$ and that existing is $Q_{\text{out}} = Q(t,x) + \frac{\partial Q}{\partial x} dx$, equation (4.4) reads

$$\frac{dA}{dt} dx = Q(t,x) - \left(Q(t,x) + \frac{\partial Q}{\partial x} dx\right);$$

that becomes

$$\frac{dA}{dt} + \frac{\partial Q}{\partial x} = 0. \tag{4.7}$$

Equation (4.7) expresses the *law of conservation of mass for 1D streams*. It can also be rewritten

$$\frac{dA}{dt} + U\frac{\partial A}{\partial x} + A\frac{\partial U}{\partial x} = 0. \qquad (4.7b)$$

Equation (4.7) expresses the conservation of mass along a 1D vessel in absence of lateral inflow/outflow; it states that discharge decreases downstream when the vessel enlarges, or vice versa, as sketched in figure 4.1.

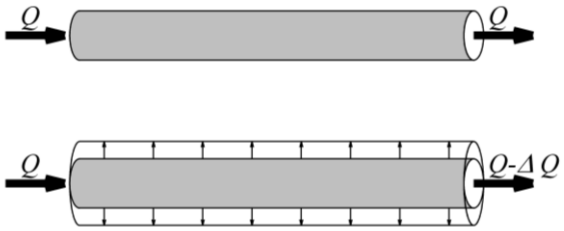

Figure 4.1. Reduction of discharge along a vessel for mass conservation

In perfectly rigid ducts conservation of mass says the discharge is constant along the vessel, Therefore conservation of mass between two arbitrary sections, say 1 and 2, of a rigid duct with varying cross sections permits to evaluate the corresponding changes in mean velocity

$$Q_1 = Q_2 \quad \Rightarrow \quad U_1 A_1 = U_2 A_2 \quad \Longrightarrow \quad U_2 = U_1 \frac{A_1}{A_2};$$

stating that velocity increases when the area decreases and vice versa.

In elastic vessels, the increase of area is a consequence of an increase of pressure. Therefore, equation (4.7) says that the fluid rate of blood reduces downstream when accompanied by a pressure increase. This is what happens, for example, along the Aorta. Blood enters as a pulse of discharge during ventricular systole accompanied by a pressure pulse (systolic pressure), with no flow during diastole when aortic valve is closed and pressure decreases (diastolic pressure). During systole the vessel enlarges and accommodates part of the incoming fluid; at the end of the flow pulse, when pressure decreases, the stored blood is releases and flow increases downstream. The result of this phenomenon is the transformation of the sharp flow pulsation into a smoother time profile downstream that is non-zero even during diastole.

4.3. Mass balance in differential form

Equation (4.3) states a balance of the flow exiting and entering across the surface bounding a volume V. The same balance can be rewritten, with the aid of the Gauss theorem (3.8), in terms of a volume integral

$$\int_V \nabla \cdot \boldsymbol{v}\, dV = 0.$$

Mass conservation applies to any arbitrary volume either large or infinitesimal; for the previous integral being zero for any volume V means that the integrand must be identically zero. This leads to the *law of conservation of mass in differential form*

$$\nabla \cdot \boldsymbol{v} = 0\,; \qquad (4.8)$$

that is more commonly called the *continuity equation*. Equation (4.8) implies that the velocity field of an incompressible flow has zero divergence at every point (velocity field is solenoidal).

The same result could be obtained by applying (4.3) to an infinitesimal cube. Figure 4.2 shows the balance of flow across the two faces with normal *x*, performing the same operation on the 6 faces $-v_x dydz + \left(v_x + \frac{\partial v_x}{\partial x} dx\right) dydz - v_y dxdz + \left(v_y + \frac{\partial v_y}{\partial y} dy\right) dxdz - v_z dxdy + \left(v_z + \frac{\partial v_z}{\partial z} dz\right) dxdy =$
$= \left(\frac{\partial v_x}{\partial x} + \frac{\partial v_y}{\partial y} + \frac{\partial v_z}{\partial z}\right) dxdydz = 0$

it ends up with the same result (4.8) in Cartesian coordinates

$$\frac{\partial v_x}{\partial x} + \frac{\partial v_y}{\partial y} + \frac{\partial v_z}{\partial z} = 0 \,. \tag{4.9}$$

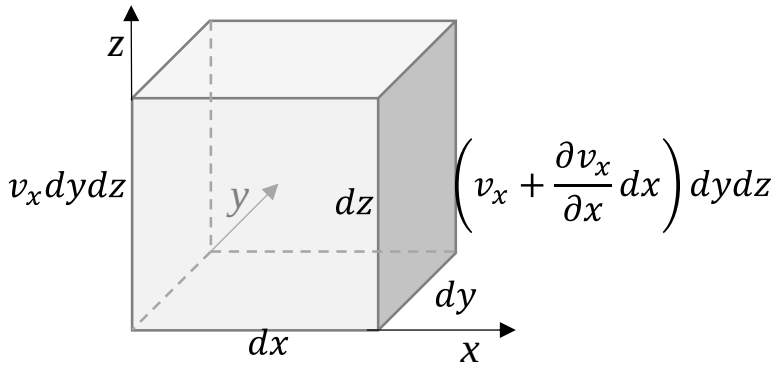

Figure 4.2. Balance of mass in an infinitesimal cube

The condition (4.8), or (4.9), is an important constraint to the possible realization of the velocity vector field. Looking at the description of flow kinematics in equation (3.15), the velocity field locally can only translate and rotate rigidly and deform without change of volume because the flow has zero divergence. If velocity field converges from one direction to a point it must similarly diverge on another direction.

As a simple example, if a jet is directed toward a wall, velocity present a convergence in that direction because it is positive upstream and zero at the wall for impermeability. As a consequence of mass conservation, the flow must diverge on the opposite direction, i.e. parallel to the wall velocity must be directed away from the impact region to create a splash effect on the wall.

5. Conservation of Momentum

5.1. Momentum balance in integral form

The second law of conservation to consider is the conservation of momentum. This corresponds to the second Newton law (expressed by $\boldsymbol{F} = m\boldsymbol{a}$ for a single particle) that has to be rewritten for a fluid continuum. Given a generic volume of fluid V_F, the momentum of that volume is defined

$$\int_{V_F(t)} \rho \boldsymbol{v} dV.$$

Conservation of momentum states that the momentum of a volume of material can only change in time in consequence of the application of forces

$$\frac{d}{dt}\int_{V_F(t)} \rho \boldsymbol{v} dV = \int_V \boldsymbol{f} dV + \int_S \boldsymbol{\tau} dS. \tag{5.1}$$

The term on the left hand side is the variation of momentum (the equivalent of the product between mass and acceleration for a particle). The first term on the right side are volumetric forces that act at time t on the volume of fluid, $V = V_F(t)$, and the field $\boldsymbol{f}(\boldsymbol{x}, t)$ is the force per unit volume; the second term are the surface forces applied on the boundary S of the same volume.

Application of the transport theorem (3.25) to (5.1) gives

$$\int_V \frac{\partial \rho \boldsymbol{v}}{\partial t} dV + \int_S \rho \boldsymbol{v}(\boldsymbol{v} \cdot \boldsymbol{n}) dS = \int_V \boldsymbol{f} dV + \int_S \boldsymbol{\tau} dS; \tag{5.2}$$

which is the *integral law of conservation of momentum*

Before moving forward with applications, it can be useful to show that this law it can be rewritten in an alternate expression where the first term is a surface integral. This is feasible in the case of incompressible flows, when velocity has zero divergence and density is a constant. In this case, application of the Gauss theorem, in particular of its expression (3.14), permits to transform one component of the first integrand in (5.2) into a surface integral

$$\int_V \frac{\partial v_i}{\partial t} dV = \int_V \nabla \cdot \left(x_i \frac{\partial \boldsymbol{v}}{\partial t} \right) dV = \int_S x_i \left(\frac{\partial \boldsymbol{v}}{\partial t} \cdot \boldsymbol{n} \right) dS.$$

Then, insertion of this into (5.2) leads to an expression for the integral law of conservation of momentum (5.2) for incompressible flows

$$\int_S \rho \boldsymbol{x} \left(\frac{\partial \boldsymbol{v}}{\partial t} \cdot \boldsymbol{n} \right) dS + \int_S \rho \boldsymbol{v}(\boldsymbol{v} \cdot \boldsymbol{n}) dS = \int_V \boldsymbol{f} dV + \int_S \boldsymbol{\tau} dS. \tag{5.3}$$

that expresses the entire change of momentum in terms of velocity values evaluated on boundaries without the need of knowing velocities in the interior of the volume (Pedrizzetti, 2019). Formulation (5.3) can be useful in several situations involving unsteady flows, as it is often the case in the cardiovascular circulation.

Symbolically, equation (5.2) or (5.3) is often expresses as

$$\mathbf{I} + \mathbf{M} = \mathbf{G} + \mathbf{\Pi};$$

with

$$\begin{aligned}
\mathbf{I} &= \int_V \frac{\partial \rho \boldsymbol{v}}{\partial t} dV = \int_S \rho \boldsymbol{x} \left(\frac{\partial \boldsymbol{v}}{\partial t} \cdot \boldsymbol{n} \right) dS, \\
\mathbf{M} &= \int_S \rho \boldsymbol{v} (\boldsymbol{v} \cdot \boldsymbol{n}) dS, \\
\mathbf{G} &= \int_V \boldsymbol{f} dV, \\
\mathbf{\Pi} &= \int_S \boldsymbol{\tau} dS.
\end{aligned} \tag{5.4}$$

The first term is called the local inertia and it can be expressed in terms of volume integral or surface integral, accordingly to equations (5.2) or (5.3), respectively. The second term is the flux of momentum across the boundary, third term is the volume force and last term is the surface force. The balance (5.2), or (5.3), is useful to compute the dynamic forces acting on rigid elements. This represents an extension of the calculation of static forces. The static analysis (seen in Chapter 2) analyzed in detail the last two terms of volumetric and surface forces; the dynamics analysis includes the addition of the first two terms associated to the change of momentum due to the fluid velocity.

Let's see now a few instructive example to show application of the balance (5.3) for the calculation of dynamic forces, to better explore the meaning of the terms in (5.4) and the ways of computing them.

Consider a circular duct with constant cross section A, presenting a 90° bent on the horizontal plane as sketched in figure 5.1. A steady flow, with velocity U, provokes a thrust on the lateral surface of the duct; that is then transferred to the boundaries where the curve is attached to the rest of the system. Application of the dynamic balance (5.3) permits to compute the force exerted by flow on the curved duct. First, $\mathbf{I} = 0$, because flow is steady, velocity is constant in time and its time derivative is zero. The flux of momentum at the entrance is given by

$$\mathrm{M}_x = -\int_A \rho \, v_x^2 dA = -\rho \beta U^2 A; \tag{5.5}$$

where the minus sign in front is due to $\boldsymbol{v} \cdot \boldsymbol{n} = -v_x$, because velocity v_x enters the volume while the normal is directed outward. When the flow is a mostly unidirectional stream, like in this case, the flux of momentum is often in a compact form in terms of global quantities introducing a velocity-correction coefficient β embodying the effect of velocity variation over the cross-section.

$$\mathrm{M}_x = -\rho \beta U^2 A; \quad \beta = \frac{\frac{1}{A}\int_A v^2 dA}{\left(\frac{1}{A}\int_A v dA\right)^2} = \frac{\int_A v^2 dA}{U^2 A}. \tag{5.6}$$

Such a momentum velocity-correction factor β reflects the difference between the average of velocity square and the square of the average velocity. The calculation of the integral of square velocity would require the knowledge of the spatial distribution of velocity that may not be available. In such cases, the introduction of this coefficient allows a simpler formulation based on global properties and leaves the problem of not knowing the transversal profile to means of estimating β. This coefficient approaches the unit value when the velocity approaches a uniform profile. This is increasingly valid in steady turbulent flow or near the entrance of a duct; whereas it can be very different from that in unsteady flows. Details of the velocity profiles will be studies later; nevertheless, in many situations (and when we have no information to suggest a different number) it can be assumed approximately equal to 1.

Using the same approach, the flux of momentum at the exit is written

$$\mathrm{M}_y = \int_A \rho \, v_y^2 dA = \rho \beta U^2 A.$$

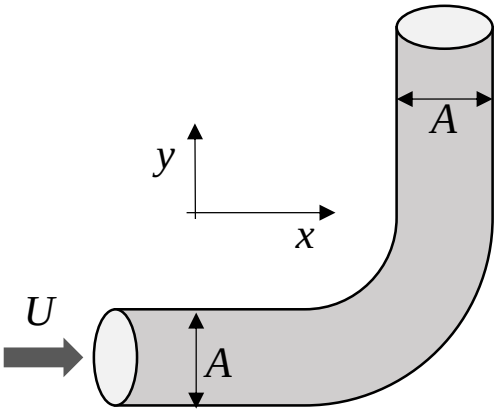

Figure 5.1. Force on a curved vessel

The volume force, **G**, assumed due to gravity only, has only the vertical component given by the static weight of the volume. The surface force term is composed of three terms: pressure p_1 acting on the inflow cross-section having the normal to the surface directed in the positive x-direction; pressure p_2 acting on the outflow cross-section with normal directed in the negative y-direction; and the force made by the lateral duct surface that is equal and opposite to the force vector $\boldsymbol{F} = [F_x, F_y, F_z]$ made by flow on that surface. In formulas

$$\Pi_x = p_1 A - F_x, \quad \Pi_y = -p_2 A - F_y \quad \Pi_z = -F_z.$$

The overall balance (5.3) in the three directions is as follows

$$-\rho\beta U^2 A = p_1 A - F_x, \quad \rho\beta U^2 A = -p_2 A - F_y \quad 0 = -\gamma V - F_z.$$

Therefore, the force made by flow on the curved vessel is

$$F_x = p_1 A + \rho\beta U^2 A, \quad F_y = -\rho\beta U^2 A - p_2 A, \quad F_z = -\gamma V. \tag{5.8}$$

The force along x is made by the static force $p_1 A$ plus the dynamic force caused by the deviation of the entire income momentum, i.e. the impact of the incoming flow to the bent. The force along y is made by the static force $p_1 A$ that pushes in the negative direction plus the recoil due to the generation of momentum. The vertical force is simply the weight of the fluid volume.

A second instructive example is the case of a rectilinear rigid vessel presenting a reduction of the cross section along its axis, as shown in figure 5.2, from an initial area A_1 to a final $A_2 < A_1$. Let us calculate the terms in the balance (5.3) for this case.

Let us start from the inertial term, that is non-zero because the flow is unsteady. To this aim, consider the time-varying discharge $Q(t)$ that for mass conservation does not vary along the vessel axis, indicated with x, and can be evaluated at any generic section with area $A(x)$ including inlet or outlet sections

$$Q(t) = \int_{A(x)} v_x dA = U_1(t) A_1 = U_2(t) A_2.$$

The component of the inertial term along the vessel axis becomes

$$\mathrm{I}_x = \int_V \frac{\partial \rho v_x}{\partial t} dV = \rho \int_1^2 \int_{A(x)} \frac{\partial v_x}{\partial t} dA\, dx = \rho \int_1^2 \frac{d}{dt} \left\{ \int_{A(x)} v_x dA \right\} dx.$$

Noticing that term in curl brackets is the discharge $Q(t)$, this eventually gives

$$\mathrm{I}_x = \rho \frac{dQ}{dt} L; \tag{5.9}$$

where $L = x_2 - x_1$ is the length of the vessel portion.

The same result could be obtained by the second expression in (5.4) based on surface integral.

$$\mathrm{I}_x = \int_S \rho\, x \left(\frac{\partial \boldsymbol{v}}{\partial t} \cdot \boldsymbol{n}\right) dS = \int_{A_2} \rho x_2 \frac{\partial v_x}{\partial t} dA - \int_{A_1} \rho x_1 \frac{\partial v_x}{\partial t} dA = \rho(x_2 - x_1) \frac{dQ}{dt}.$$

The flux of momentum is written using (5.5), assuming β=1 for simplicity, for the two sections as

$$\mathrm{M}_x = \rho Q^2 \left(\frac{1}{A_2} - \frac{1}{A_1}\right).$$

The pressure terms is due to pressure values at the two sections plus the force made by the lateral wall to the fluid, that is equal and opposite to the force F_x made by the fluid on the lateral wall

$$\Pi_x = p_1 A_1 - p_2 A_2 - F_x.$$

Inserting these terms in the balance (5.3) along x, the force made by flow on the vessel is

$$F_x = p_1 A_1 - p_2 A_2 - \rho Q^2 \left(\frac{1}{A_1} - \frac{1}{A_2}\right) - \rho \frac{dQ}{dt} L. \tag{5.10}$$

The first two terms are the difference of the static force acting on the two sections; the flux of momentum is negative and represent the reaction of the higher flux of momentum at the exit; last inertial term reflects the force associated to the acceleration/deceleration of the whole fluid.

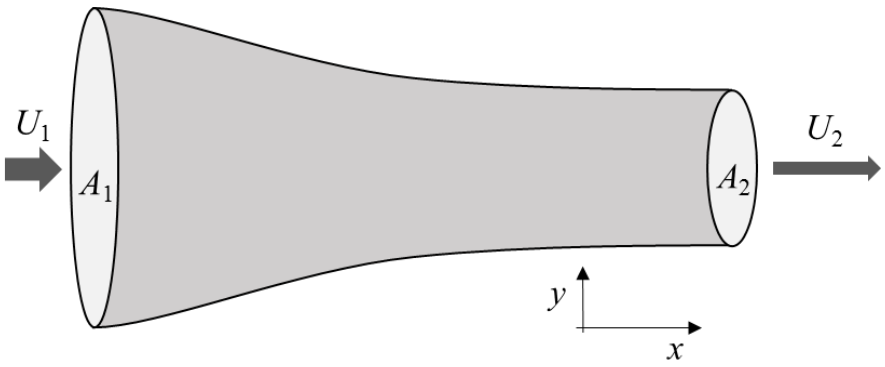

Figure 5.2. Force on a rectilinear vessel with varying section

This example can also be used to evaluate the force when the contraction is very sharp as it can be the case of an orifice placed transversally in the vessel, which can represent a model for a valve. In that case, formula (5.10) provides an estimation for the force pushing on the upstream surface of orifice wall.

For a final simple example compute the force produced by a fluid jet toward a planar surface as in figure 5.3. Consider a steady jet with mean velocity U and area A, directed perpendicular to a flat plate. With reference to figure 5.3, take the volume bounded by the inlet section, the boundary of the flow adjacent to the air at atmospheric pressure, the plate and the exit sections that are directed transversally to the inflow; and write the balance for this volume in the direction of the jet. Inertia is zero because the flow is steady. The flux of momentum is $\mathrm{M} = -\rho\beta U^2 A$, given by the inlet, while the outlet does not contribute to this direction (and is zero for symmetry in the transversal direction).

Body force (gravity) is also zero in this direction. Surface force are not present on the lateral boundaries because pressure is zero (or equal to the atmospheric value that would be present as a constant value everywhere and gives zero after integration). Similarly pressure is zero all around the jet and remains zero inside the inlet section (this can be demonstrated rigorously later) and the same at the outlet sections. Therefore surface pressure is only the force given by the obstacle $\Pi = -F$.

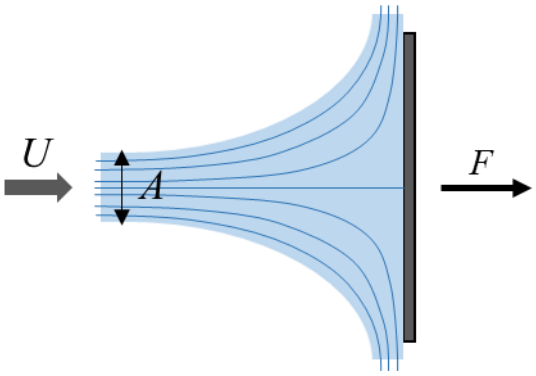

Figure 5.3. Force of a jet impacting on a flat plate

Insertion of these findings in the balance (5.3) shows that the force on the plate is only given by the deviation of the incoming momentum

$$F = \rho U^2 A = \rho Q U. \tag{5.11}$$

These simple cases were presented to show appropriate simple means of evaluating the terms (5.4) under typical conditions. In more general situations, the integrals (5.4) must be evaluated.

The balance (5.2) can be extended to provide the balance of angular momentum. In which case every term must be multiplied with the corresponding arm of the force. The details of this extension are not reported here as they are not of primary interest for the topic of this book and do not bring conceptual challenges. However, such extension is immediate to draw in most situations using the same approach described above.

5.2. Momentum balance for a vessel

Following the same approach that we used above for conservation of mass, let us rearrange the balance of momentum (5.2) for the special important case of flow in a vessel. Indicating, as before, x as the longitudinal direction, this is a predominantly 1D stream of cross section area $A(t,x)$. The transversal velocities are thus negligible with respect to the longitudinal ones and we remind that the average velocity is defined

$$U(x,t) = \frac{1}{A}\int_A v_x dA. \tag{5.12}$$

Consider an infinitesimal length dx of such a vessel and let us evaluate the component along the vessel of each individual term in (5.4). Remind that the balance is made on a spatial volume (instantaneously fixed). This volume is bounded upstream by the cross-surface $A(t,x)$, where velocity is $U(x,t)$ and average pressure is $p(x,t)$. It is bounded downstream by the cross-surface $A(t,x+dx) = A(t,x) + \frac{\partial A}{\partial x}dx$, where velocity is $U(t,x+dx) = U(t,x) + \frac{\partial U}{\partial x}dx$, and pressure is $p(t,x+dx) = p(t,x) + \frac{\partial p}{\partial x}dx$ and it is also bounded laterally by the perimeter curve $C(t,x)$ that extends over the length dx.

The inertial term is integrated over the volume $dV = dAdx$ and reads

$$\mathrm{I} = \int_V \frac{\partial \rho v_x}{\partial t} dV = \rho \int_A \frac{\partial v_x}{\partial t} dA\, dx = \rho \frac{\partial}{\partial t} \int_A v_x dA\, dx = \rho A \frac{dU}{dt} dx. \tag{5.13}$$

The flux of momentum across the two cross-sections and the lateral contour

$$\mathrm{M} = -\int_{A(x)} \rho v_x^2 dA + \int_{A(x)+\frac{\partial A}{\partial x}dx} \rho \left(v_x + \frac{\partial v_x}{\partial x} dx\right)^2 dA + \int_{C(x)} \rho v_x v_n dC dx =$$

is simplified assuming that the velocity is uniform over the cross section, which means β=1, and ignoring all terms of order dx^2

$$= -\rho U^2 A + \rho \int_A \left(v_x^2 + 2 v_x \frac{\partial v_x}{\partial x} dx\right) dA + \int_{\frac{\partial A}{\partial x}dx} \rho \left(v_x^2 + 2 v_x \frac{\partial v_x}{\partial x} dx\right) dA + \int_C \rho v_x v_n dC dx =$$

$$= -\rho U^2 A + \rho U^2 A + \rho 2U \frac{\partial U}{\partial x} A dx + \rho U^2 \frac{\partial A}{\partial x} dx + \int_C \rho v_x v_n dC dx =$$

last integral above can be rewritten considering that the integral of $v_n dC$ is the rate of increase of the cross-area, $\frac{\partial A}{\partial t}$. Rearranging all terms

$$= \rho U \frac{\partial U}{\partial x} A dx + \rho U \frac{\partial U}{\partial x} A dx + \rho U^2 \frac{\partial A}{\partial x} dx + \rho U \frac{\partial A}{\partial t} dx = \rho U \frac{\partial U}{\partial x} A dx + \rho U \left(A \frac{\partial U}{\partial x} + U \frac{\partial A}{\partial x} + \frac{\partial A}{\partial t}\right) dx$$

It is immediate to verify that the terms in bracket in last term are equal to zero because of mass conservation (4.7) and the whole flux of momentum becomes simply

$$\mathrm{M} = \rho U \frac{\partial U}{\partial x} A dx \tag{5.14}$$

Surface forces are composed of pressure acting on the two cross-sections, of the wall shear stress acting on the lateral surface and of the pressure acting on the lateral surface; the latter may presents a longitudinal component only when the cross-section is not constant. Surface forces are

$$\Pi = pA - \left(p + \frac{\partial p}{\partial x} dx\right)\left(A + \frac{\partial A}{\partial x} dx\right) - \tau_w C dx + \left(p + \frac{1}{2}\frac{\partial p}{\partial x} dx\right) n_x dS_{LAT} =$$

Last but one term has is the average wall shear stress exerted by the lateral solid boundary to the fluid; it has a negative sign as we conventionally indicate with τ_w the stress made by fluid to the wall. Last term is the pressure on the lateral surface (taken as the mean between x and $x + dx$) and n_x is the x component of the normal unit vector on the lateral surface dS_{LAT} (notice that here we did not use the simplification $dS_{LAT} = C dx$ to remark the relevance of the change of cross section along dx, the tilting of the later surface, whereas C is the average value along the length dx). It can be noticed that the terms $n_x dS_{LAT}$ is the component of the lateral surface facing x, thus it corresponds to the increase of cross-surface $n_x dS_{LAT} = \frac{\partial A}{\partial x} dx$.

Ignoring the higher order terms in *dx* and simplifying

$$\Pi = pA - pA - \frac{\partial p}{\partial x} A dx - p \frac{\partial A}{\partial x} dx - \tau_w C dx + p \frac{\partial A}{\partial x} dx = -A \frac{\partial p}{\partial x} dx - \tau_w C dx\,. \tag{5.15}$$

Finally, the volume force, assumed imputable to gravity only $\boldsymbol{f} = -\gamma \nabla z$, gives the component along the vessel

$$\mathrm{G} = -\gamma A \frac{\partial z}{\partial x} dx; \tag{5.16}$$

where z stands for the vertical aligned with gravity. Combine all terms (5.13-5.16) of the momentum balance (5.4)

$$\rho A\frac{dU}{dt}dx + \rho U\frac{\partial U}{\partial x}Adx = -A\frac{\partial p}{\partial x}dx - \tau_w Cdx - \gamma A\frac{\partial z}{\partial x}dx;$$

divide by ρAdx to obtain

$$\frac{dU}{dt} + U\frac{\partial U}{\partial x} = -\frac{\partial}{\partial x}\left(\frac{p}{\rho} + gz\right) - \frac{\tau_w}{\rho}\frac{C}{A}. \tag{5.17}$$

Equation (5.17) is the *law of conservation of momentum for 1D streams*, under the assumption of uniform velocity over the cross-section and in presence of gravity only. The left-hand terms represent the (Lagrangian) acceleration of a 1D fluid element moving with velocity U expressed in terms of (Eulerian) derivatives in a fixed frame of reference.

The first term on the right hand side is the driving force that can be due either to a pressure gradient (negative, higher upstream and lower downstream) or to a difference of quote. This expression underlines again that pressure gradient and gravity play the same role in fluid motion. It is common habit using a generalized pressure that includes gravity, $p + \gamma z = \gamma h$, where h is the static head previously introduced with equation (2.5) in fluid statics. Then (5.17) is usually rewritten without explicit mention to gravity (or another conservative force) as

$$\frac{dU}{dt} + U\frac{\partial U}{\partial x} = -\frac{1}{\rho}\frac{\partial p}{\partial x} - \frac{\tau_w}{\rho}\frac{C}{A}; \tag{5.18}$$

where p stands for the generalized pressure. Then, if needed, the actual pressure can be recovered simply removing the gravity contribution $p - \gamma z$.

Last term is the friction on the lateral walls. This term depends on the velocity profile near the wall, as shown for example by equation (1.8) for a Newtonian fluid. The 1D model however deals with the mean velocity only, that is conventionally assumed as uniform over the cross section, and does not provide information about transversal velocity gradient. Therefore, the friction terms is often neglected (in which case the flow is without viscous resistance) or it must be provided explicitly as a function of velocity field *U*.

5.3. Momentum balance in differential form for a continuum: Cauchy equation

The balances of momentum presented above do not allows investigating the spatiotemporal details of fluid motion. These require the formulation of the balance at a punctual level or, more precisely, in differential form. To this purpose, we follow here the same procedure previously adopted for the conservation of mass and apply it to the conservation of momentum.

Start from the balance of momentum in global terms (5.2), divided by the constant density

$$\int_V \frac{\partial \boldsymbol{v}}{\partial t}dV + \int_S \boldsymbol{v}(\boldsymbol{v}\cdot\boldsymbol{n})dS = \frac{1}{\rho}\int_V \boldsymbol{f}dV + \frac{1}{\rho}\int_S \boldsymbol{\tau}dS; \tag{5.19}$$

at this point we want to transform the surface integrals, 2nd and 4th terms, as integrals over the volume. Such that, when all integrals refer to the same volume, we can eventually transfer the equality to the integrand terms. To this aim, take the generic i^{th} component of the second term, which can be transformed as follows

$$\int_S v_i\boldsymbol{v}\cdot\boldsymbol{n}dS = \int_V \nabla\cdot(v_i\boldsymbol{v})dV = \int_V v_i\nabla\cdot\boldsymbol{v} + \boldsymbol{v}\cdot\nabla v_i dV = \int_V \boldsymbol{v}\cdot\nabla v_i dV. \tag{5.20}$$

The first equality used the Gauss theorem (3.8) applied to the vector field $v_i \boldsymbol{v}$; the second equality is immediate to verify using the derivative of a product for vector terms, and last equality follows after cancelling the terms $\nabla \cdot \boldsymbol{v}$ that is identically zero for mass conservation (4.8).

Last term in (5.19) contains the stress vector $\boldsymbol{\tau}$ acting on the surface dS. Apparently, at a point there are infinite stress vectors that can act on surfaces with different orientations, and the identification of the vector $\boldsymbol{\tau}$ that acts on the specific surface dS may look like a complex task. However, such an infiniteness is only apparent because there is a single stress "state" about a point and the value of all these individual vectors come from a combination of such stress state and the orientation of the surface. Indeed, it can be demonstrated that the stress vector acting on a surface with normal $\boldsymbol{n}$ can be expressed in general as

$$\boldsymbol{\tau} = \mathbb{T} \cdot \boldsymbol{n} \tag{5.21}$$

where $\mathbb{T}$ is the stress the tensor. It characterizes the stress state at a point, such that the stress vector at that point acting on a surface with normal $\boldsymbol{n}$ is obtained by projecting the stress tensor over the direction $\boldsymbol{n}$, as by (5.21).

Result (5.21) is immediate to demonstrate using the Cauchy tetrahedron, which is build by the original surface dS and its projection on the Cartesian planes as shown in figure 5.4.

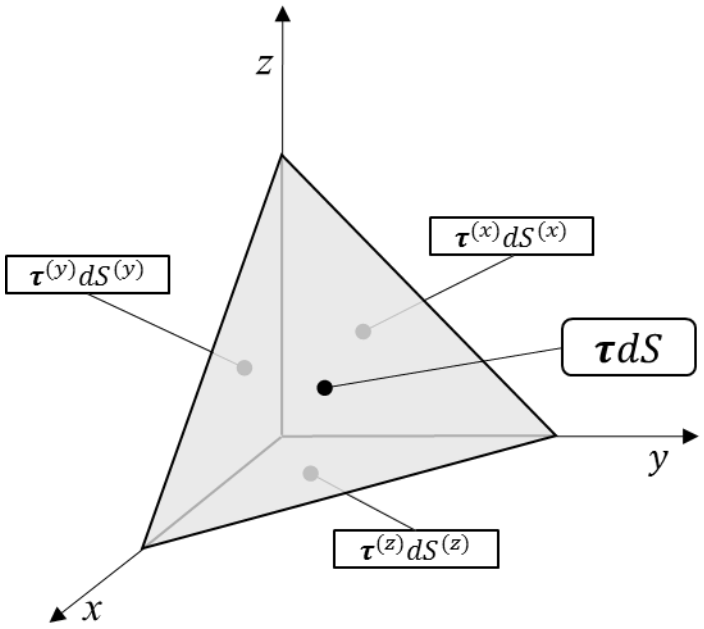

Figure 5.4. Cauchy tetrahedron

Indicate with $\boldsymbol{\tau}^{(x)}$ the stress vector acting on the surface $dS^{(x)}$, which is projection of dS on the y-z plane perpendicular to the x-axis; same for the other coordinate axes. First, we want to see whether the stress $\boldsymbol{\tau}$ on the original surface can be expressed as a combination of the stresses $\boldsymbol{\tau}^{(x)}$, $\boldsymbol{\tau}^{(y)}$, $\boldsymbol{\tau}^{(z)}$ acting on the surfaces normal to the Cartesian axes. Balance of the forces acting on the tetrahedron gives the equivalence of the surface forces

$$\boldsymbol{\tau} dS = \boldsymbol{\tau}^{(x)} dS^{(x)} + \boldsymbol{\tau}^{(y)} dS^{(y)} + \boldsymbol{\tau}^{(z)} dS^{(z)}. \tag{5.22}$$

It is then easy to verify by simple geometry that $dS^{(i)} = dS\, n_i$, where the n_i is the i^{th} component of the normal $\boldsymbol{n}$ to the surface dS. Introducing this into (5.22) gives

$$\boldsymbol{\tau} = \boldsymbol{\tau}^{(x)} n_x + \boldsymbol{\tau}^{(y)} n_y + \boldsymbol{\tau}^{(z)} n_z \tag{5.23}$$

If you define the stress tensor as a tensor made by three stress vectors placed in column $\tau_i^{(j)} = \mathbb{T}_{ij}$ then equation (5.23) corresponds to (5.21) that is thus proven.Using expression (5.21) the forth term in (5.19) can be rewritten as a volume integral through the Gauss theorem

$$\frac{1}{\rho}\int_S \boldsymbol{\tau} dS = \frac{1}{\rho}\int_S \mathbb{T}\cdot\boldsymbol{n}\, dS = -\frac{1}{\rho}\int_V \nabla\cdot\mathbb{T} dV. \tag{5.24}$$

where the minus comes out because the normal in Gauss theorem is outward directed. Introduction of (5.20) and (5.24) in the momentum balance (5.19) allows rewriting in terms of volume integrals

$$\int_V \frac{\partial \boldsymbol{v}}{\partial t} dV + \int_V \boldsymbol{v}\cdot\nabla\boldsymbol{v} dV = \frac{1}{\rho}\int_V \boldsymbol{f} dV - \frac{1}{\rho}\int_V \nabla\cdot\mathbb{T} dV.$$

This must be valid for any volume, including an infinitesimal volume, therefore the balance must apply to the integrands as well

$$\frac{\partial \boldsymbol{v}}{\partial t} + \boldsymbol{v}\cdot\nabla\boldsymbol{v} = \frac{1}{\rho}\boldsymbol{f} - \frac{1}{\rho}\nabla\cdot\mathbb{T}. \tag{5.25}$$

Equation (5.25) is the *Cauchy equation* that expresses the law of conservation of momentum for a continuum.

The same result could be obtained in Cartesian coordinates by applying the balance of momentum (5.19) to an infinitesimal cube of volume as shown in figure 5.5.

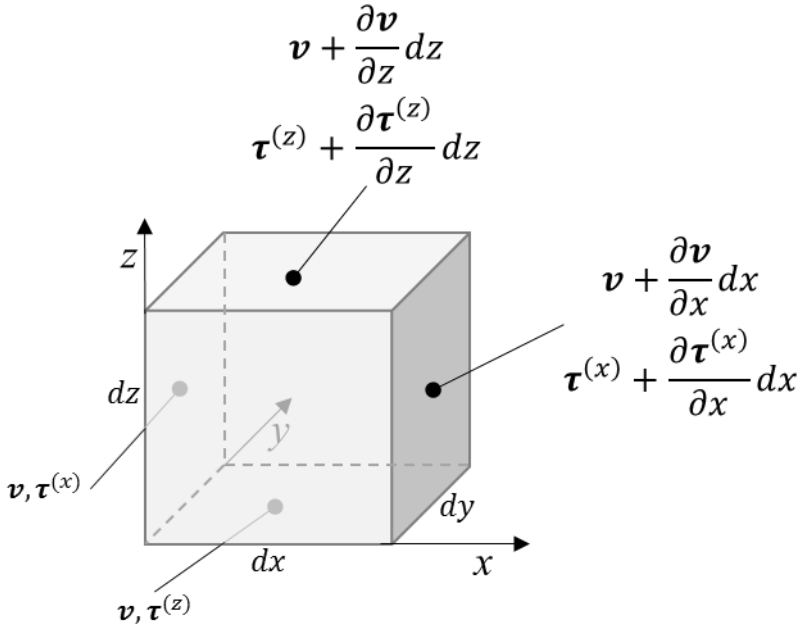

Figure 5.5. Balance of momentum in an infinitesimal cube
(values on the faces perpendicular to *y* are not shown to for clarity)

Consider, for example, the *x*-component (then results can be immediately extended to the other components). The first term in (5.19) applied to the infinitesimal cube, *V=dxdydz*, becomes

$$\int_V \frac{\partial v_x}{\partial t} dV = \frac{\partial v_x}{\partial t} dxdydz. \tag{5.26}$$

The second term includes the fluxes of momentum on the 6 faces

$$
\begin{aligned}
&\int_S v_x(\boldsymbol{v}\cdot\boldsymbol{n})dS = \\
&= -v_x v_x dydz - v_x v_y dxdz - v_x v_z dxdy + \left(v_x + \frac{\partial v_x}{\partial x}dx\right)\left(v_x + \frac{\partial v_x}{\partial x}dx\right)dydz + \\
&\quad + \left(v_x + \frac{\partial v_x}{\partial y}dy\right)\left(v_y + \frac{\partial v_y}{\partial y}dy\right)dxdz + \left(v_x + \frac{\partial v_x}{\partial z}dz\right)\left(v_z + \frac{\partial v_z}{\partial z}dz\right)dxdy = \\
&= \left(v_x\frac{\partial v_x}{\partial x} + v_x\frac{\partial v_x}{\partial x} + v_x\frac{\partial v_y}{\partial y} + v_y\frac{\partial v_x}{\partial y} + v_x\frac{\partial v_z}{\partial z} + v_z\frac{\partial v_x}{\partial z}\right)dxdydz = \\
&= (\boldsymbol{v}\cdot\nabla v_x + v_x\nabla\cdot\boldsymbol{v})dxdydz = \\
&= \boldsymbol{v}\cdot\nabla v_x\, dxdydz
\end{aligned}
\tag{5.27}
$$

The third term

$$
\int_V f_x dV = f_x dxdydz. \tag{5.28}
$$

Last term combines the stress forces on the six surfaces of the cube

$$
\begin{aligned}
&\int_S \tau_x dS = \\
&= \tau_x^{(x)}dydz + \tau_x^{(y)}dxdz + \tau_x^{(z)}dxdy - \left(\tau_x^{(x)} + \frac{\partial\tau_x^{(x)}}{\partial x}dx\right)dydz + \\
&\quad - \left(\tau_x^{(y)} + \frac{\partial\tau_x^{(y)}}{\partial y}dy\right)dxdz - \left(\tau_x^{(z)} + \frac{\partial\tau_x^{(z)}}{\partial z}dz\right)dxdy = \\
&= -\left(\frac{\partial\tau_x^{(x)}}{\partial x} + \frac{\partial\tau_x^{(y)}}{\partial y} + \frac{\partial\tau_x^{(z)}}{\partial z}\right)dxdydz = \\
&= -(\nabla\cdot\mathbb{T})_x dxdydz =
\end{aligned}
\tag{5.29}
$$

Where here we defined, as we did before in the Cauchy tetrahedron, the stress tensor $\mathbb{T}$ as made by the three stress vectors relative to the three coordinates.

Insertion of expressions (5.26)-(5.29) into the balance (5.19) gives again the Cauchy equation (5.25).

The two terms on the left hand side of the Cauchy equation (5.25) represent the acceleration of fluid particles that we previously introduced in equation (3.24). The two terms on the right hand side are the forces acting on such particles, caused by intrinsic volumetric forces and by the stresses made by the neighboring fluid elements.

The same procedure must now be performed for the conservation of angular momentum by writing the same expressions including the arms of the individual terms. The derivation is somehow lengthy and is not reported in details here. Nevertheless, the result is remarkably simple and important: the *conservation of angular momentum* implies that *the stress tensor* $\mathbb{T}$ *is a symmetric tensor*. It does not produce further differential equations and simply reduces the complexity of the 3×3 stress tensor from 9 components to 6 independent components.

5.4. Momentum balance for Newtonian fluids: Navier-Stokes equations

Let us recapitulate the set of equations describing the mechanics of a continuum (still we have not used any argument that this continuum is a fluid, only that it is incompressible). This is given by the conservation of mass (continuity equation) and the conservation of momentum (Cauchy equation)

$$
\begin{cases}
\nabla\cdot\boldsymbol{v} = 0, \\
\dfrac{\partial\boldsymbol{v}}{\partial t} + \boldsymbol{v}\cdot\nabla\boldsymbol{v} = \dfrac{1}{\rho}\boldsymbol{f} - \dfrac{1}{\rho}\nabla\cdot\mathbb{T};
\end{cases}
\tag{5.30}
$$

which is a set of 4 scalar equations. The unknowns are the 3 components of the velocity vector and the 6 components of the stress tensor, resulting in a number of 9 total unknowns. Thus this set is not complete, it cannot be solved, until some additional information is provided.

The set of equations (5.30) is valid for a generic continuum; it applies to both solids and fluids. In order to be refined for a specific material we must introduce information about such a material. In other terms, we must introduce the *constitutive law* that specifies how internal stresses develop from the behavior of the material. Below we'll specify the constitutive law for fluids, following the general properties described in section 1.2.

The first information for specifying the constitutive law comes from the statics of fluids. In chapter 2 we have seen that under static conditions the stresses on a surface is made by pressure and acts normally toward the surface, it is expressed as $\boldsymbol{\tau} = -p\boldsymbol{n}$ (the minus comes here for the convention of the outward normal). Comparison with (5.21) immediately shows that in the limit case of static conditions, the stress tensor is required to take the form

$$\mathbb{T} = p\mathbb{I} = p\begin{bmatrix}1 & 0 & 0\\ 0 & 1 & 0\\ 0 & 0 & 1\end{bmatrix}$$

where $\mathbb{I}$ is the identity matrix.

The second information comes from the kinematics of fluid. In chapter 3 we have shown that motion is composed by rigid translation and rotation plus a pure deformation. The latter is the only elementary action which involves the relative motion of fluid elements, thus the only that can be responsible for friction and stresses. Therefore, we can express in general the constitutive law for a fluid as

$$\mathbb{T} = p\mathbb{I} + f(\mathbb{D}); \tag{5.31}$$

where $\mathbb{D}$ is the symmetric deformation tensor (3.20). Relationship (5.31) states that the 6 unknown present in the tensor $\mathbb{T}$ can be expressed in terms of the velocity field plus a single unknown, the pressure p. Thus providing a closure (balance between equations and unknowns) to the system (5.30). Fluids following the law (5.31), where stress forces are due to rate of deformation, are called Stokes fluids.

The third information comes from the definition of viscosity for a Newtonian fluid. In section 1.2, we showed that the stress due to shear flow along x on a surface with normal y is given by formula (1.8); which that can be restated with the current formalism as

$$\mathbb{T}_{xy} = -\mu\frac{\partial v_x}{\partial y};$$

This expression is not symmetric and violates conservation of angular momentum; however, it can easily be made symmetric as

$$\mathbb{T}_{xy} = -\mu\left(\frac{\partial v_x}{\partial y} + \frac{\partial v_y}{\partial x}\right);$$

without contradicting the experimental result (1.8) because the transversal velocity v_y was zero. This is an off-diagonal term of a form compatible with (5.31), suggesting that the function $f(\mathbb{D})$ appearing in (5.31) is a linear one for Newtonian fluids.

Combining this set of information, the *constitutive law for Newtonian fluids* is written in general as

$$\mathbb{T} = p\mathbb{I} - 2\mu\mathbb{D}; \tag{5.32}$$

or in individual Cartesian components

$$\mathbb{T} = \begin{bmatrix} p - 2\mu\frac{\partial v_x}{\partial x} & -\mu\left(\frac{\partial v_x}{\partial y} + \frac{\partial v_y}{\partial x}\right) & -\mu\left(\frac{\partial v_x}{\partial z} + \frac{\partial v_z}{\partial x}\right) \\ -\mu\left(\frac{\partial v_x}{\partial y} + \frac{\partial v_y}{\partial x}\right) & p - 2\mu\frac{\partial v_y}{\partial y} & -\mu\left(\frac{\partial v_y}{\partial z} + \frac{\partial v_z}{\partial y}\right) \\ -\mu\left(\frac{\partial v_x}{\partial z} + \frac{\partial v_z}{\partial x}\right) & -\mu\left(\frac{\partial v_y}{\partial z} + \frac{\partial v_z}{\partial y}\right) & p - 2\mu\frac{\partial v_z}{\partial z} \end{bmatrix}.$$

Let us now look how to the surface force term in the Cauchy equation (5.25) can be written when the stress tensor is expressed by the constitutive law (5.32)

$$\begin{aligned} -\nabla\cdot\mathbb{T}|_x &= -\left(\frac{\partial \mathbb{T}_{xx}}{\partial x} + \frac{\partial \mathbb{T}_{xy}}{\partial y} + \frac{\partial \mathbb{T}_{xz}}{\partial z}\right) = \\ &= -\frac{\partial p}{\partial x} + 2\mu\frac{\partial^2 v_x}{\partial x^2} + \mu\frac{\partial^2 v_x}{\partial y^2} + \mu\frac{\partial^2 v_y}{\partial xy} + \mu\frac{\partial^2 v_x}{\partial z^2} + \mu\frac{\partial^2 v_z}{\partial zx} = \\ &= -\frac{\partial p}{\partial x} + \mu\left(\frac{\partial^2 v_x}{\partial x^2} + \frac{\partial^2 v_x}{\partial y^2} + \frac{\partial^2 v_x}{\partial z^2}\right) + \mu\frac{\partial}{\partial x}\left(\frac{\partial v_x}{\partial x} + \frac{\partial v_y}{\partial y} + \frac{\partial v_z}{\partial z}\right) = \\ &= -\frac{\partial p}{\partial x} + \mu\nabla^2 v_x \end{aligned} \quad . \tag{5.33}$$

Insertion of (5.33) into the Cauchy equation (5.25) gives the equations for conservation of momentum for Newtonian fluids: the *Navier-Stokes equation*

$$\frac{\partial \boldsymbol{v}}{\partial t} + \boldsymbol{v}\cdot\nabla\boldsymbol{v} = \frac{1}{\rho}\boldsymbol{f} - \frac{1}{\rho}\nabla p + \nu\nabla^2\boldsymbol{v}. \tag{5.34}$$

where $\nu = \frac{\mu}{\rho}$ is the kinematic viscosity previously defined in (1.9). This equation is also called the *law of motion* for an incompressible Newtonian fluid, and represents the rearrangement of the 2nd Newton law for this special material. The left hand side is the acceleration of a fluid particle, the terms on the right hand side are the force, per unit mass. Respectively they are the volumetric force, the thrust due to pressure difference and the resistance force due to internal viscous friction.

As discussed in chapter 1, blood is a complex material for which the assumption of a Newtonian constitutive relations is approximate. The reliability of this approximation was discussed therein and it is not recalled here. In what follows we will limit our treatise to Newtonian fluids that represent the foundation for understanding the majority of flow phenomena in the heart and large blood vessels.

When dealing with gravitational volume forces only, we have seen that the force can be rewritten in gradient form $\boldsymbol{f} = \gamma\nabla z$. Therefore they can be formally included in the pressure term

$$\frac{\partial \boldsymbol{v}}{\partial t} + \boldsymbol{v}\cdot\nabla\boldsymbol{v} = -\frac{1}{\rho}\nabla p + \nu\nabla^2\boldsymbol{v}. \tag{5.35}$$

where p is includes gravity and stands for the static head $\gamma h = p + \gamma z$.

The set of equations given by continuity equation (4.8) and Navier-Stokes equation (5.35) is now a complete set with the same number of equations (4 scalar equations) and unknowns (the 3 components of the velocity vector and pressure)

$$\begin{cases} \nabla\cdot\boldsymbol{v} = 0, \\ \frac{\partial \boldsymbol{v}}{\partial t} + \boldsymbol{v}\cdot\nabla\boldsymbol{v} = -\frac{1}{\rho}\nabla p + \nu\nabla^2\boldsymbol{v}; \end{cases} \tag{5.36}$$

This system of equations, continuity and motion, must be completed with the appropriate boundary conditions. The Navier-Stokes equation is a partial differential equation containing second order derivatives for velocity; therefore, roughly speaking, it requires two boundary conditions for velocity.

The first condition is the impermeability at the boundary between fluid and solid; this means that the normal component of the velocity must be zero (or equal to that of the boundary when it is moving). The second condition is the adherence to the wall; this means that the tangential velocity must go to zero at the wall. Adherence is a purely viscous phenomenon; this is congruent with the fact that the second condition follows from the presence of the viscous terms that is the only one containing 2nd order derivatives.

The viscous, frictional term in the Navier-Stokes equation produces energy dissipation. In a wider perspective, total energy is conserved and friction is a mechanism of transformation of kinetic energy into heat. Therefore, from the mechanical perspective, friction provokes a dissipation, a reduction of the mechanical energy.

The kinematic viscosity is a small coefficient $\nu=10^{-6}m^2/s=10^{-2}cm^2/s$ for water. Therefore, especially far from the boundaries, the viscous terms can be sometime neglected and fluid behave mostly like an inviscid one.

Consider now the limiting case when viscosity is zero, $\nu = 0$, that can be useful as a model in numerous applications. In this asymptotic limit, we talk of *ideal fluids* (also called inviscid or frictionless). The equation of motion for ideal fluids is the *Euler equation*

$$\frac{\partial \boldsymbol{v}}{\partial t} + \boldsymbol{v} \cdot \nabla \boldsymbol{v} = -\frac{1}{\rho}\nabla p; \tag{5.37}$$

that differs from the Navier-Stokes equation (5.35) for the absence of the viscous term only. The Euler equation does not present friction and therefore conserves mechanical energy. Thus, it describes reversible phenomena. Indeed, if the velocity pressure pair $(\boldsymbol{v}, p)$ is solution of the Euler equation forward in time, then the reversed pair $(-\boldsymbol{v}, -p)$ is also a solution backward in time. This was not true for the Navier-Stokes equation due to the friction term that does not reverse (reverse flow also has friction, it certainly does not transform heat back into kinetic energy).

Another important difference between Euler and Navier-Stokes is that the former is a 1st order partial differential equation because it contains 1st order derivatives only. This difference reflects into the fact that only one boundary condition can be imposed for the velocity. Namely, the adherence condition does not apply to the Euler equation; this is perfectly physically consistent because the adherence is a viscous phenomenon; ideal flows have no viscosity and cannot have viscous adherence.

Euler equation is important because it allows some simple solution to specific applications; however, care must be taken for applying the approximation of ideal flow. It can be usable over short regions, where the small viscosity may be effectively negligible, and far from boundaries outside the regions influenced by viscous adherence.

A last consideration about Navier-Stokes (and Euler) equation regards the frequent case of flows where velocity is predominantly along one direction. Consider a motion that is predominantly along the x-direction, thus $v_y \cong 0$ and $v_z \cong 0$, and write the Navier-Stokes equation over the direction transversal to the directions of motion, for example the y direction

$$\frac{\partial v_y}{\partial t} + v_x\frac{\partial v_y}{\partial x} + v_y\frac{\partial v_y}{\partial y} + v_z\frac{\partial v_y}{\partial z} = -\frac{1}{\rho}\frac{\partial p}{\partial y} + \nu\left(\frac{\partial^2 v_y}{\partial x^2} + \frac{\partial^2 v_y}{\partial y^2} + \frac{\partial^2 v_y}{\partial z^2}\right). \tag{5.38}$$

If we can neglect the velocity v_y and its derivatives; in other words, if *streamlines are straight and parallel*, then equation (5.38) reduces to

$$\frac{\partial p}{\partial y} = 0; \tag{5.39}$$

that, in presence of gravity, has the meaning

$$\frac{\partial}{\partial y}(p + \gamma z) = 0.$$

This is a general and important result. In regions where fluid motion is straight and parallel, the static head (2.5), given by pressure plus gravity if the latter is present, remains constant transversal to the direction of motion.

Put simpler, along the directions without motion (transversal to flow), the law of fluid statics (2.4) holds. This simple fact was sometime used in section 5.1 when computing dynamic forces, it tells about the average pressure value in the equation for a vessel in 5.2, and will be used several times later in the book.

6. Conservation of Energy (Bernoulli Balance)

6.1. Equation for conservation of mechanical energy

In a system where the only form of energy is mechanical energy, there are no other physical mechanisms, or physical laws, other than conservation of mass and of momentum that can be included to describe the behavior of the system. The unique transformation is about kinetic energy $\frac{1}{2}\rho v^2$ (per unit volume) and the potential energy $p + \gamma z$ (per unit volume). The latter again underlining that pressure plays the same role of gravity which is commonly assumed to be implicitly included for easier writing. The law of conservation of momentum already described the dynamic relationship between velocity (for kinetic energy) and pressure (for potential energy); therefore, in absence of other forms of energy, the conservation of energy must be in accordance with that.

In this special case, the law of conservation of energy can be obtained directly from the Cauchy equation (5.25), for a generic continuum, or from the Navier-Stokes equation (5.35), for a Newtonian fluid. Consider the i^{th} component of equation (5.25)

$$\frac{\partial v_i}{\partial t} + v_j \frac{\partial v_i}{\partial x_j} = \frac{1}{\rho} f_i + \frac{1}{\rho} \frac{\partial \mathbb{T}_{ij}}{\partial x_j}.$$

and make the scalar multiplication with the velocity (in index formalism, multiply the i^{th} component of the equation by the same component of velocity and perform summation for i=1,2,3)

$$\rho v_i \frac{\partial v_i}{\partial t} + \rho v_i v_j \frac{\partial v_i}{\partial x_j} = v_i f_i + v_i \frac{\partial \mathbb{T}_{ij}}{\partial x_j}.$$

that can be rewritten

$$\rho \frac{1}{2} \frac{\partial v_i v_i}{\partial t} + \rho v_j \frac{1}{2} \frac{\partial v_i v_i}{\partial v_j} = v_i f_i + v_i \frac{\partial \mathbb{T}_{ij}}{\partial x_j}.$$

$$\frac{\partial}{\partial t}\left(\frac{1}{2}\rho v_i v_i\right) + v_j \frac{\partial}{\partial v_j}\left(\frac{1}{2}\rho v_i v_i\right) = v_i f_i + \frac{\partial}{\partial x_j}\left(v_i \mathbb{T}_{ij}\right) - \mathbb{T}_{ij} \frac{\partial v_i}{\partial x_j}.$$

$$\frac{\partial}{\partial t}\left(\frac{1}{2}\rho v_i v_i\right) + v_j \frac{\partial}{\partial v_j}\left(\frac{1}{2}\rho v_i v_i\right) = v_i f_i + \frac{\partial}{\partial x_j}\left(v_i \mathbb{T}_{ij}\right) - \mathbb{T}_{ij} \mathbb{D}_{ij}.$$

where we used the rule of product derivative and, for the last term, the fact that the product between a symmetric and antisymmetric tensor is zero, thus only the symmetric part of the velocity gradient contributes. In final form the general equation for the conservation of mechanical energy is

$$\frac{\partial}{\partial t}\left(\frac{1}{2}\rho v^2\right) + \boldsymbol{v} \cdot \nabla\left(\frac{1}{2}\rho v^2\right) = \boldsymbol{v} \cdot \boldsymbol{f} + \nabla \cdot (\boldsymbol{v} \cdot \mathbb{T}) - \mathbb{T} : \mathbb{D}. \tag{6.1}$$

where the double scalar products is $\mathbb{T} : \mathbb{D} = \mathbb{T}_{ij} \mathbb{D}_{ij}$. The two terms on the left hand side are the (Lagrangian) time derivative of the kinetic energy on the moving fluid element. This can change for the work done by the volume force (first terms on the right hand side) by the surface forces (second terms), and for work spent to deform the fluid elements (last term). The last term represents the dissipation of mechanical energy.

In the case of Newtonian incompressible fluid, using (5.2), the rate of dissipation of kinetic energy can be expressed

$$\mathbb{T} : \mathbb{D} = 2\mu \mathbb{D} : \mathbb{D} = 2\mu \mathbb{D}_{ij} \mathbb{D}_{ij}. \tag{6.2}$$

This expression evidences that viscous energy dissipation is strictly a positive value because given by the sum of squares.

6.2. Bernoulli energy balance

An expression for the conservation of energy that is of immediate interpretation in simpler circumstances can be obtained directly from the Navier-Stokes equation under some specific hypotheses.

Consider the case of volume forces that are absent or limited to the gravitational forces and included into the pressure term without loss of generality. Now make the strong hypothesis of considering the motion of an ideal fluid with zero viscosity. The equation governing fluid motion is the Euler equation (5.37)

$$\frac{\partial \boldsymbol{v}}{\partial t} + \boldsymbol{v} \cdot \nabla \boldsymbol{v} = -\frac{1}{\rho} \nabla p.$$

The second term on the left hand side is nonlinear and can be rewritten in an alternate form as follows. Consider the x-component of that term in Cartesian coordinates

$$\boldsymbol{v} \cdot \nabla \boldsymbol{v}|_{\boldsymbol{x}} = v_x \frac{\partial v_x}{\partial x} + v_y \frac{\partial v_x}{\partial y} + v_z \frac{\partial v_x}{\partial z} =$$

add and remove the same quantity

$$= v_x \frac{\partial v_x}{\partial x} + v_y \frac{\partial v_x}{\partial y} + v_z \frac{\partial v_x}{\partial z} + v_y \frac{\partial v_y}{\partial x} - v_y \frac{\partial v_y}{\partial x} + v_z \frac{\partial v_z}{\partial x} - v_z \frac{\partial v_z}{\partial x} =$$

the 1st, 4th and 6th terms can be grouped as the derivative of squares, then evidence v_y from 2nd and 5th and v_z from 3rd and 7th

$$= \frac{1}{2}\frac{\partial}{\partial x}\left(v_x^2 + v_y^2 + v_z^2\right) + v_y\left(\frac{\partial v_x}{\partial y} - \frac{\partial v_y}{\partial x}\right) + v_z\left(\frac{\partial v_x}{\partial z} - \frac{\partial v_z}{\partial x}\right) =$$

the first term is the derivative of the square of the modulus of velocity $v^2 = v_i v_i = v_x^2 + v_y^2 + v_z^2$. Then notice that the other terms in parenthesis are components of vorticity, thus we get

$$= \frac{\partial}{\partial x}\frac{v^2}{2} - v_y \omega_z + v_z \omega_y = \left[\nabla \frac{v^2}{2} - \boldsymbol{v} \times \boldsymbol{\omega}\right]_x.$$

Insertion of this result into the Euler equation permit to rewrite it in the following alternate form

$$\frac{\partial \boldsymbol{v}}{\partial t} + \nabla\left(\frac{v^2}{2} + \frac{p}{\rho}\right) = \boldsymbol{v} \times \boldsymbol{\omega}. \tag{6.3}$$

Equation (6.3) is a vector equation, where the term on the right hand side is perpendicular to the velocity (and to vorticity) for the property of the cross product. Thus, if we project equation (6.3) in the direction of a streamline, i.e. if we take the scalar product of every term with the versor $\boldsymbol{s} = v^{-1}\boldsymbol{v}$, last term is zero and we are left with

$$\frac{\partial v_s}{\partial t} + \frac{\partial}{\partial s}\left(\frac{v^2}{2} + p\right) = 0. \tag{6.4}$$

Integration of equation (6.4) between two points, point 1 and point 2, along one streamline gives

$$\frac{p_1}{\rho} + \frac{v_1^2}{2} = \frac{p_2}{\rho} + \frac{v_2^2}{2} + \int_1^2 \frac{\partial v_s}{\partial t} ds\,. \tag{6.5}$$

which expresses the conservation of the mechanical energy. Equation (6.5) represents the *Bernoulli theorem* or *Bernoulli balance* and states that, in a gravitational field, under the hypothesis that viscous energy dissipations are negligible, the total mechanical energy is conserved along a streamline net of the last term (inertia) that is the energy spent to accelerate the fluid or acquired during its deceleration.

For an immediate interpretation, it is common to define the total head

$$H = \frac{v^2}{2g} + \frac{p}{\gamma} = \frac{v^2}{2g} + h; \tag{6.6}$$

which is a height that expresses the total mechanical energy per unit weight as the sum of kinetic energy $\frac{v^2}{2g}$ plus the potential energy h, which is the static head previously defined in section 2.1. Using the definition (6.6), the Bernoulli balance (6.5) can be written as

$$H_1 = H_2 + \frac{1}{g}\int_1^2 \frac{\partial v_s}{\partial t} ds\,, \tag{6.7}$$

stating that the total head can vary along a streamline only when there is inertia stored by fluid along that path.

The case of stationary fluid, $\frac{\partial \boldsymbol{v}}{\partial t} = 0$, when inertia is zero, takes particular relevance for numerous applications. In this case, last term in (6.6) is zero and the total head (6.6) is conserved along a streamline. This case presents only the transformation of kinetic energy into potential energy (pressure) and vice versa.

Consider the case of a large reservoir with a hole at its bottom as shown in figure 6.1.

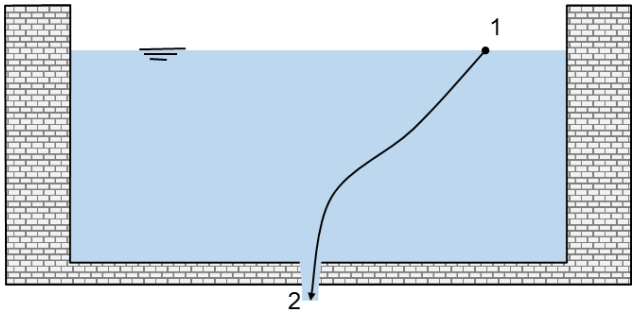

Figure 6.1. Flow existing from the bottom of a reservoir

Consider a streamline starting from the free surface and going to the outflow. Pressure is equal to the atmospheric pressure at the point 1 on the free surface and at the point 2 that is a unidirectional jet surrounded by atmospheric pressure. If the reservoir is large enough, we can also neglect the velocity (square) in point 1 with respect to that in 2, and consider the flow as approximately stationary. Application of Bernoulli balance (6.7) to this case gives

$$z_1 = z_2 + \frac{v_2^2}{2}\,.$$

Indicating with $h = z_1 - z_2$, the total head weighting on the exit the outflow velocity $v = v_2$ can be immediately evaluated as

$$v = \sqrt{2gh}\,. \tag{6.8}$$

Velocity (6.8) is called the Torricelli velocity; it is the free-fall velocity of a particle subjected to gravity only. Based on (6.8) it is possible to estimate the discharge exiting from the orifice as

$$Q = C_c A\sqrt{2gh}\,.$$

where A is the orifice area and C_c is the coefficient of contraction that accounts for the contraction of the cross-section of the existing jet, which for a sharp edge is about $C_c \cong 0.6$.

In a stationary flow, in general, the change of fluid kinetic energy is balanced by change in pressure. Therefore, for example, the fluid velocity increases in a horizontal converging vessel and pressure decreases accordingly to the conservation of the total head; vice versa, in an expanding vessel, velocity decreases downstream and pressure increases. Similarly, when you have a steady jet, with velocity v, that impacts on a solid surface, the stagnation point on the solid surface experiences an overpressure

$$\Delta p = \frac{1}{2}\rho v^2;$$

because all the kinetic energy transformed into an increase of pressure.

The Bernoulli balance is at the base of an important velocity measurement instrument called *Pitot tube* that is shown in figure 6.2. The Pitot tube is a small tube with a bullet-like leading edge facing the incoming stream. It is made of two concentric chambers: the inner chamber communicates to the outside from an opening at the front tip; the outer chamber communicates to the outside through openings on the lateral side. Then, the two chambers end internally with a differential manometer that reports their pressure difference.

With reference to the sketch in figure 6.2 we can apply the Bernoulli balance under steady conditions separately for the two chambers along two streamlines both starting from two points upstream that are very close each other, thus have the same velocity v and pressure p (point 0). One ending to the stagnation point (point 1) in front of the tube and the other passing to the side near the lateral holes (point 3).

Consider first the path starting from the upstream point 0, passing through point 1, and ending to point 2 on one side of the differential manometer. Apply the Bernoulli balance between 0 and 1,

$$\frac{p}{\rho} + \frac{v^2}{2} = \frac{p_1}{\rho} + \frac{v_1^2}{2}.$$

Velocity is zero at the stagnation point 1 and we obtain that pressure measured in 1 is equal to the upstream pressure augmented by the kinetic energy that is transformed into pressure at the stagnation point

$$p_1 = p + \rho\frac{v^2}{2}.$$

Then, inside the tube the fluid is at rest and the laws of fluid statics hold. Ignoring gravity (without loss of generality, because it can be included into pressure) we have that

$$p_2 = p_1 = p + \rho\frac{v^2}{2}.$$

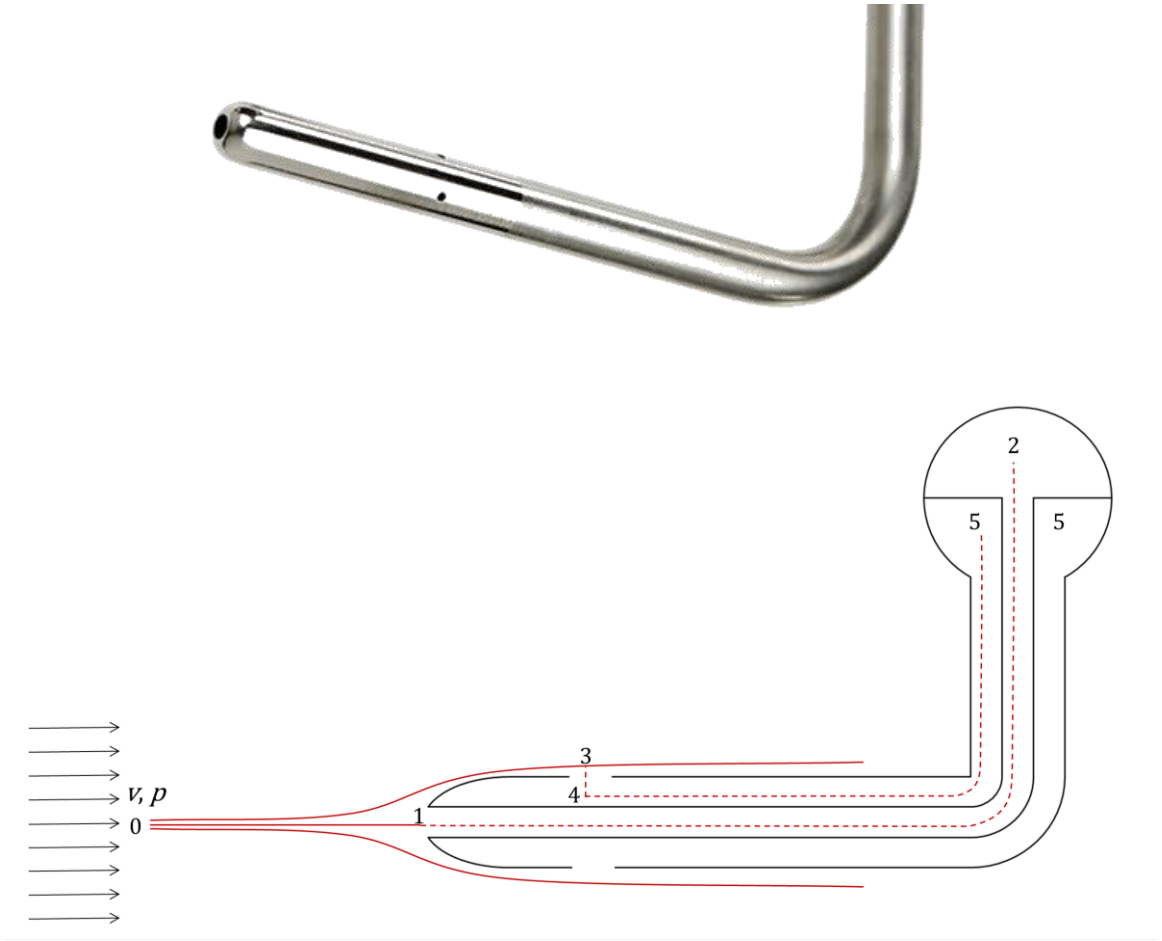

Figure 6.2. Pitot tube: Picture (above, https://www.unitedsensorcorp.com/images/Pitot-Stataic-probe.jpg); sketch for calculations (below).

Now consider the path starting from the upstream point 0, passing through points 3 and 4, and ending to point 5 on the other side of the differential manometer. The Pitot tube is small enough that it does not disturbs appreciably the fluid flow and we can assume that next to the tube $v_3 = v$ and $p_3 = p$. The Bernoulli balance cannot be applied between points 3 and 4 because there is no streamline connecting the two. However, the path from point 3 to point 4 moves transversally to the streamlines and we can apply the law of statics (5.39) transversal to the direction of flow. Then, once entered into the tube the same law of statics apply in the fluid at rest. This gives a constancy of pressure from the outside up the manometer

$$p_5 = p_4 = p_3 = p.$$

From these formulas, the pressure values measured at the two sides of the manometer are

$$p_2 = p + \rho \frac{v^2}{2}, \quad p_5 = p;$$

the former is often called the dynamic pressure, because it is the ambient pressure increased by the kinetic head; the latter is the static ambient pressure. The pressure difference reading from the manometer is

$$\Delta p = p_2 - p_5 = \rho \frac{v^2}{2}$$

that is immediate to transform into a velocity measurement

$$v = \sqrt{2\frac{\Delta p}{\rho}}. \tag{6.9}$$

The Pitot tube has an important applied relevance because it provides a measurement of velocity based on mechanical principles. It works without the need of an external source of energy like electricity or digital post processing of data. It thus equips most aircrafts and boats providing an independent velocity measurement to rely on under any circumstances up to the case of failure of electric support.

The Pitot tube represents the archetype of velocity and pressure measurements used in clinical practice through catheterization. Typically, clinical hemodynamic catheters are used inside the heart chambers or in large vessels and present side opening to measure pressure and possibly front opening to measure velocities.

The simplified form of the Bernoulli balance, where the time derivative term is absent, is used in stationary flows. However, it can also be used in unsteady flow at those time instants when the time derivative is zero. In cardiovascular pulsatile flows, it is commonly applied at the peak of the pulsation to compute the pressure drop across cardiac valves, for example.

In cardiovascular pulsatile flows, the simplified, stationary form of the Bernoulli balance is used for application during those time instants when the time derivative of velocity is zero. For example, it is commonly applied at the peak of the pulsation to compute the pressure drop across cardiac valves.

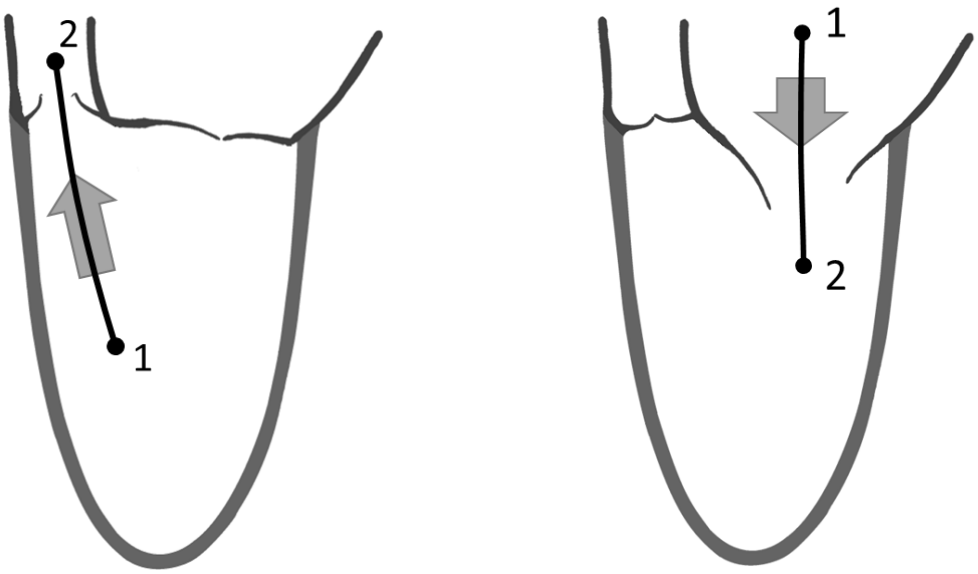

Figure 6.3. Flow across the aortic valve (left) or mitral valve (right)

With reference to figure 6.3 (left), select a streamline crossing the aortic valve during the maximum velocity of systolic contraction with the first point inside the ventricle and the other point at the exit of the valve. The same approach can be used for flow across the mitral valve (figure 6.3, right), The velocity is at its maximum and the time derivative is approximately zero, thus Bernoulli balance (6.5) reads

$$\frac{p_1}{\rho} + \frac{v_1^2}{2} = \frac{p_2}{\rho} + \frac{v_2^2}{2}.$$

Neglecting the upstream velocity (square) inside the chamber with respect to the velocity at the exit of the valvular tips the pressure drop $\Delta p = p_1 - p_2$ across the valve can be expressed as a function of the valvular velocity $v = v_2$ as

$$\Delta p = \rho \frac{v^2}{2}. \tag{6.10}$$

The velocity at the exit of the valve can be measured with relative ease, for example with Doppler ultrasound, and allows having an estimate of the transvalvular pressure drop. Formula (6.10) is dimensionally consistent; for example, when the valve velocity is measured in *m/s* and density in Kg/m^3 then pressure is given in *Pascal*. In clinical practice, it is very common to express this balance in dimensional form, with pressure drop measured in mm_{Hg} and velocity in *m/s*. Transformation from *Pascal* to mm_{Hg} requires a factor $133 Pa/mm_{Hg}$, and using density ρ=$1050 Kg/m^3$ then

$$\Delta p_{[mm_{Hg}]} = \frac{1050}{133 \times 2} v^2_{[\frac{m}{s}]} \cong 4\, v^2_{[\frac{m}{s}]}.$$

The simple formula $\Delta p = 4v^2$ often called the *simplified Bernoulli formula* (which we remark is valid only when pressure is measured in mm_{Hg} and velocity in *m/s*) is widely used in clinical cardiology to estimate transvalvular pressure gradients. Given its frequent use, it must be kept in mind that it was obtained under the hypotheses of the Bernoulli balance (ideal flow), with the additional assumptions that the upstream velocity is negligible and it is valid under static conditions, namely at the maximum of velocity.

The pressure drop evaluated at the instant of maximum velocity (6.10) is not necessarily the maximum pressure drop during the period of systolic outflow across the aortic valve, or diastolic inflow through the mitral valve. At a generic instant the time derivative cannot be neglected and the complete Bernoulli balance (6.5) applies

$$\Delta p = p_1 - p_2 = \frac{1}{2}\rho(v_2^2 - v_1^2) + \rho \int_1^2 \frac{\partial v_s}{\partial t} ds$$

which can be rewritten

$$\Delta p = \frac{1}{2}\rho(v_2^2 - v_1^2) + \rho \frac{\partial \overline{v_{12}}}{\partial t} L_{12}$$

where L_{12} is the distance traveled between the two points and $\overline{v_{12}}$ is the velocity averaged along that path. Under the assumption that the upstream velocity is negligible, $v_1^2 \ll v_2^2 = v^2$, and that the velocity increases linearly $\overline{v_{12}} \cong \frac{1}{2} v_2 = \frac{1}{2} v$, then we can approximate the unsteady pressure drop by

$$\Delta p = \frac{\rho}{2} v^2 + \rho \frac{\partial \overline{v_{12}}}{\partial t} L_{12} \cong \frac{\rho}{2} v^2 + \frac{\rho}{2} \frac{\partial v}{\partial t} L_{12}\ . \tag{6.11}$$

The first term is the pressure drop due to transformation of pressure into kinetic energy, the second is the energy stored into inertia. Typically, the two terms are comparable in magnitude and present different time phase. The former is in phase with velocity and dominates about the instants of maximum velocity; the latter is in quadrature of velocity and dominates during the acceleration/deceleration periods (Firstenberg et al., 2000; Tonti et al., 2001).

6.3. Bernoulli balance with dissipation: localized energy losses.

Among the hypotheses of the Bernoulli balance, the one that can be unrealistic under several conditions is main the assumption of ideal fluid. Fluids are never ideal and some form of viscous dissipation is always present.

For example, when the flow in a vessel passes across a reduction of area (like a valve or a pathologic narrowing or stenosis) the flow accelerates at the smaller area and decelerates afterwards where the vessel returns to its original size. Thus, potential energy (pressure) transforms into kinetic energy at the constriction where pressure reaches smaller values. The kinetic energy transforms back into pressure during the enlargement; however, while velocity (and kinetic energy) go back to their initial value, pressure does not get back to its initial value and display a net reduction. This reduction is due to the energy lost for friction along the short tracts presenting narrowing and expansion. We consider these as *localized* energy losses, because they occur in consequence of a local disturbance to the flow.

In general, dealing with friction requires the use of Navier-Stokes equation that introduces several complexities in the analysis. However, it is sometimes feasible simply adding an energy dissipation term in the Bernoulli balance (6.5) that can be rewritten as

$$p_1 + \rho\frac{v_1^2}{2} = p_2 + \rho\frac{v_2^2}{2} + \rho\int_1^2 \frac{\partial v_s}{\partial t} ds + \Delta E_{diss}\,, \tag{6.12}$$

including an explicit term ΔE_{diss} accounting for energy dissipation, or pressure loss. Equation (6.12) maintains the same form of the Bernoulli balance although it contains an additional term that is in principle unknown. However, under some circumstances the pressure loss can be expressed in simple form as a percentage of the available kinetic energy. In that case, the generalized balance (6.12) can be used in the same way as the normal Bernoulli balance.

An exemplary case where the energy losses can be evaluated with relative ease is the case of a sudden expansion and rigid walls as sketched in figure 6.4.

Figure 6.4. Sketch for evaluating energy loss in a sudden expansion

To this aim, the balance of momentum

$$\mathrm{I}_x + \mathrm{M}_x = \Pi_x$$

should be written for the cylindrical volume of cross-area A_2 and length L, indicated with dashed line in figure 6.4, starting adjacent to the expansion and ending in a downstream section where the flow is back to unidirectional.

The inertial term is

$$\mathrm{I}_x = \int_V \frac{\partial \rho v_x}{\partial t} dV = \rho \int_L \int_{A_2} \frac{\partial v_x}{\partial t} dA\, dx = \rho \frac{dU_2}{dt} A_2 L.$$

The flux of momentum occurs across the open part, of area A_1, of the upstream end and across the entire downstream section of area A_2

$$\mathrm{M}_x = -\rho U_1^2 A_1 + \rho U_2^2 A_2$$

assuming that the velocity is approximately uniform over the cross section (β=1).

The pressure term pushes upwards on the downstream surface of area A_2 where pressure is p_2; it also pushes, downward, on the entire upstream surface of area again equal to A_2, here pressure is equal to p_1 on the open part and it remains approximately constant on the closed part where flow is about stagnating, thus static

$$\Pi_x = p_1 A_2 - p_2 A_2.$$

Summing up these three terms and dividing by A_2 we obtain

$$p_1 - p_2 = \rho \frac{dU_2}{dt} L - \rho U_1^2 \frac{A_1}{A_2} + \rho U_2^2. \tag{6.13}$$

The balance (6.12) can be rewritten making the dissipation term explicit

$$\Delta E_{diss} = p_1 - p_2 + \rho \frac{v_1^2}{2} - \rho \frac{v_2^2}{2} - \rho \int_1^2 \frac{\partial v_s}{\partial t} ds\,, \tag{6.14}$$

then, assuming the flow sufficiently uniform we can exchange velocity and cross-section average velocity and rewrite (6.14)

$$\Delta E_{diss} = p_1 - p_2 + \rho \frac{U_1^2}{2} - \rho \frac{U_2^2}{2} - \rho \frac{\partial U_2}{\partial t} L\,. \tag{6.15}$$

Now substitute the pressure difference (6.13) into (6.15) to get

$$\Delta E_{diss} = \rho \frac{U_2^2}{2} + \rho \frac{U_1^2}{2}\left(1 - 2\frac{A_1}{A_2}\right).$$

that can be rewritten in terms of one velocity only

$$\Delta E_{diss} = \rho \frac{U_1^2}{2}\left(1 - \frac{A_1}{A_2}\right)^2 = \rho \eta \frac{U_1^2}{2}, \quad \eta = \left(1 - \frac{A_1}{A_2}\right)^2. \tag{6.16}$$

Equation (6.16) describes the loss of energy (per unit volume) in a sharp enlargement. It tells that energy losses are given by a fraction η of the incoming kinetic energy, while the remainder is transformed into potential energy (i.e. pressure). The entity of such fraction depends on the degree of the expansion; in the limit case of very large expansion, $A_2 \gg A_1$, then $\eta \cong 1$, the incoming kinetic energy is unable to significantly affect the wide downstream reservoir and the entire incoming kinetic energy is lost.

The result (6.16) is very instructive because it teaches that localized energy losses can be in general expresses as a fraction of the available kinetic energy

$$\Delta E_{diss} = \rho \eta \frac{U_1^2}{2}. \tag{6.17}$$

where the dimensionless dissipation coefficient η depends from the degree of disturbance created on the streaming flow. The dissipation coefficient cannot be easily expressed by mean of explicit formulas like (6.16). However, its value was determined experimentally in most situations of practical interests and can be often found in literature.

C. FUNDAMENTALS FOR MOSTLY UNIDIRECTIONAL FLOW

7. Unidirectional Flow in Rectilinear Vessels

7.1. Boundary layer

Viscosity is the only, unique mechanism for energy dissipation in fluids governed by the Navier-Stokes equation. In order to understand the role of viscosity in more depth, let us analyze in more depth at the flow near the boundary, in the simple case of flat, rigid wall. Consider the flow along the x-direction of a Cartesian set of coordinates, with the wall set at $y = 0$, and neglect the velocity and variations along the transversal z-component (two-dimensional flow). The stream-wise component of the Navier-Stokes equation is

$$\frac{\partial v_x}{\partial t} + v_x \frac{\partial v_x}{\partial x} + v_y \frac{\partial v_x}{\partial y} = -\frac{1}{\rho}\frac{\partial p}{\partial x} + \nu \left(\frac{\partial^2 v_x}{\partial x^2} + \frac{\partial^2 v_x}{\partial y^2} \right). \tag{7.1}$$

We have seen that the kinematic viscosity in front of the last term is a small number. Therefore, the viscous terms is often negligible locally. However, viscosity has a fundamental influence in the proximity of solid boundaries because it is associated to the boundary condition of adherence, which applies irrespective of the value of viscosity. As a result, viscosity has a fundamental role near the boundaries (because of adherence) while its role is expected to becomes progressively negligible away from them (because it is small). In other terms, there is always a region next to the wall boundary, which is called *boundary layer*, where the role of viscosity cannot be neglected. More quantitatively, the boundary layer is the region next to the boundaries where the viscous term is comparable with the other terms of the Navier-Stokes equation.

Consider a uniform unidirectional flow, of velocity U, that encounters a plane surface of negligible thickness. As shown in figure 7.1, when the incoming uniform profile gets in contact with the surface the velocity at the surface goes to zero because of adherence. As the fluid travels downstream, the slower fluid elements close to the boundary decelerate those immediately above thus extending the influence of adherence for a thickness over the surface. This process continues and the thickness of fluid influenced by the viscous adherence increases downstream. Roughly, the flow field can be divided in an external flow, not reached by the influenced of adherence, and a boundary layer that is directly affected by viscosity.

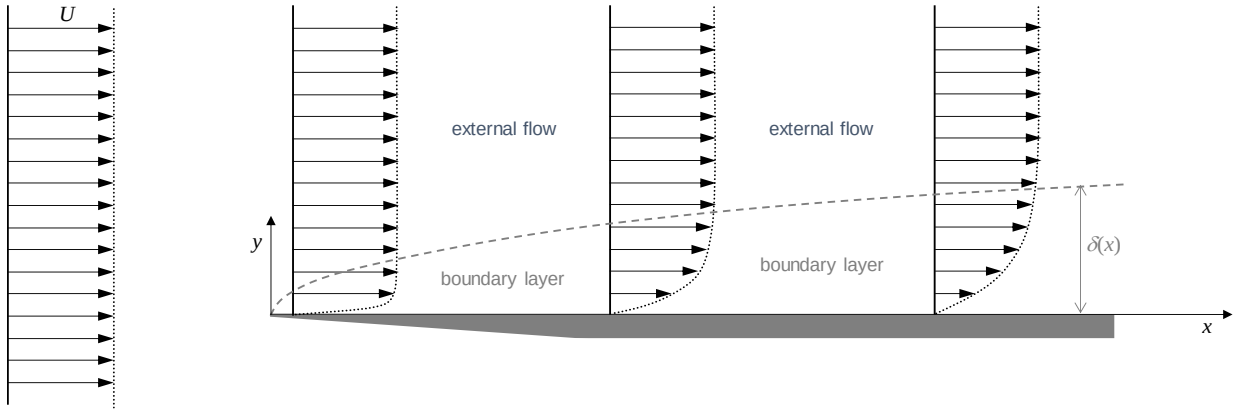

Figure 7.1. Boundary layer development on a flat plate.

The boundary layer thickness is indicated by $\delta(x)$ and it increases downstream. The order of magnitude of $\delta(x)$ can be obtained using the Navier-Stokes equation (7.1) and estimating the order

of magnitude of the different terms therein. By definition of boundary layer, the thickness is the region where the viscous term is comparable with the others.

The time derivative can be ignored because the flow is steady. For the first transport term you can consider that velocity upstream is U and downstream, say at a distance $2x$ inside the boundary layer, it is a fraction of U, say κU. Here κ is a number smaller than 1, but still a finite fraction of 1 and not infinitesimal (in order of magnitude arguments, κ is said to of the order of magnitude of 1). Thus, the derivative at x can be roughly estimated by the difference of velocity at $2x$ and at 0 divided by the distance and the velocity by the mean value

$$v_x \frac{\partial v_x}{\partial x} \sim \frac{\kappa U + U}{2} \cdot \frac{\kappa U - U}{2x} \sim \frac{U^2}{x}. \tag{7.2}$$

where the symbol ~ stands for "of the order of magnitude of" and coefficients that are about the order of unity are eventually left out.

The order of magnitude of the transversal velocity, v_x, can be obtained by the continuity equation that in 2D reads

$$\frac{\partial v_x}{\partial x} + \frac{\partial v_y}{\partial y} = 0. \tag{7.3}$$

The x-derivative can be estimated as above; the y-derivative from the unknown value v_y, minus the zero value at the wall, divided by the boundary layer thickness. Thus (7.3) suggests

$$\frac{U}{x} \sim \frac{v_y}{\delta}; \tag{7.4}$$

inserting these estimates in the second transport term

$$v_y \frac{\partial v_x}{\partial y} \sim v_y \frac{U}{\delta} \sim \frac{U\delta}{x} \frac{U}{\delta} \sim \frac{U^2}{x} \tag{7.5}$$

shows that this is of the same order of the other (7.2). Let us ignore for the moment the pressure term in (7.1), as the boundary layer develop even in absence of pressure gradient thus it should not play a key role.

Following the same lines, the viscous terms is

$$\nu \left(\frac{\partial^2 v_x}{\partial x^2} + \frac{\partial^2 v_x}{\partial y^2} \right) \sim \nu \left(\frac{U}{x^2} + \frac{U}{\delta^2} \right) \sim \nu \frac{U}{\delta^2}; \tag{7.6}$$

where we ignored the first term in parenthesis with respect to the second because we expect δ to be small.

In the boundary layer, the viscous term is of the same order of magnitude of the other terms. Equating (7.6) with (7.2) or (7.5) we obtain

$$\nu \frac{U}{\delta^2} \sim \frac{U^2}{x}$$

and therefore

$$\delta \sim \sqrt{\nu \frac{x}{U}} \tag{7.7}$$

The estimate (7.7) shows that the thickness of the boundary layer grows like the square root of the downstream distance. The boundary layer is thin when viscosity is small and gets thinner when

velocity is higher. The exact coefficient that is in front of the square root of (7.7) depends on the specific definition of boundary layer thickness. Some texts suggest setting the edge of the boundary layer where velocity differs of a small percentage to the external velocity, others use the velocity square. In any case, equation (7.7) demonstrated a general validity with the coefficient varying from about 3 to 5, depending on the definition of δ and on the specific situation under analysis.

Let us try to understand further the origin of the boundary layer thickness. The viscous term of the Navier Stokes equation represent a diffusion phenomenon. In this case it represents the diffusion of a disturbance to velocity (set to zero by adherence) away from the wall. Pure diffusion, in absence of velocity, of a whatsoever field $f(t, y)$ along the direction y, is described by the diffusion equation

$$\frac{\partial f}{\partial t} = D \frac{\partial^2 f}{\partial y^2}. \tag{7.8}$$

where D is the diffusion coefficient (in Navier-Stokes corresponding to the kinematic viscosity).

The connection between diffusion and boundary layer development is immediate considering the dual problem of a fluid over an infinite plate that is set abruptly in motion with velocity U. The boundary layer is now uniform and grows in time. The Navier-Stokes equation reads

$$\frac{\partial v_x}{\partial t} = \nu \frac{\partial^2 v_x}{\partial y^2}; \tag{7.9}$$

that is a diffusion equation like (7.8). This is a linear partial differential equation of parabolic type that was largely investigated in the past. The solution to (7.9) with boundary condition $v_x(0, t) = U$ is the error function

$$v_x(y, t) = U - \frac{U}{\sigma(t)} \int_0^y e^{-\frac{1}{2}\left(\frac{s}{\sigma(t)}\right)^2} ds, \tag{7.10}$$

with width

$$\sigma = \sqrt{2\nu t}. \tag{7.11}$$

The velocity profile (7.10) is shown in figure 7.2, it starts from U at the wall and decreases away from the wall reaching $v_x \approx 0.005U$ at $y = 2\sigma$.

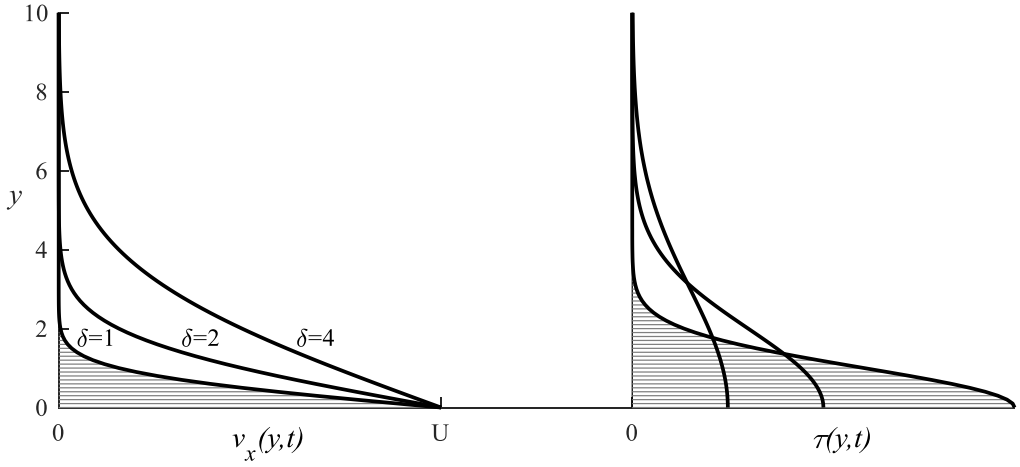

Figure 7.2. Velocity and shear stress above a moving wall.

Thus, we can consider the thickness of the boundary layer given by

$$\delta(t) = 2\sigma = 2\sqrt{2\nu t}. \tag{7.12}$$

The same solution (7.10)-(7.11) can be reached by a different perspective. Consider that the wall motion creates a jump in velocity equal to U, from U at the wall to zero infinitely above,

$$U = \int_0^\infty \frac{\partial v_x}{\partial y} dy. \tag{7.13}$$

that is produced by a wall shear stress $\tau = \mu \frac{\partial v_x}{\partial y}$ due to adherence. Shear stress is ideally infinite at $t = 0$, although with finite integral (7.13), when the wall sets in motion and progressively decreases to ensure the same velocity jump while it diffuses away from the wall. The propagation of shear stress is again a diffusion process ruled by the diffusion equation (7.8) for $f = \tau$. The solution to (7.8) with the constraint (7.13) is the well known Gauss function

$$\frac{\partial v_x}{\partial y} = \frac{U}{\sigma(t)} e^{-\frac{1}{2}\left(\frac{y}{\sigma(t)}\right)^2}, \tag{7.14}$$

in association with the width $\sigma(t)$ given by (7.11). Then the solution (7.10) can be recovered by integrating (7.14).

We have shown that the development of the viscous boundary layer is simply a phenomenon of diffusion of shear from the wall with thickness given by (7.12). The same concept can be applied to the previous case of a steady flow over a plane wall leading to the expression (7.7). In that case, the spatial variation under steady conditions can be transformed into the same diffusion problem by considering an observed moving with velocity U. This observer start at $t = 0$ from the edge of the plate where $\delta = 0$ and at time t reaches the position $x = Ut$ where the thickness is given by (7.7) that, by comparison with (7.12) can be expressed by

$$\delta = 2\sqrt{2\nu \frac{x}{U}}. \tag{7.15}$$

In a closed conduit, the boundary layer cannot grow indefinitely, because it saturates the available space. Therefore in a vessel of diameter say D, the boundary layer terminates its growth when $\delta \approx D/2$. Using formula (7.15) it is possible to estimate the length of the entry region as

$$x_E \approx \frac{1}{32}\frac{UD^2}{\nu} = \frac{Re}{32} D. \tag{7.16}$$

where $Re = \frac{UD}{\nu}$ is the Reynolds number. The boundary layer grows as by (7.15) from the start of the duct, at $x = 0$, to reach a steady thickness about x_E; afterwards, for $x > x_E$, the flow can be assumed as fully developed and not influenced by the distance from the start of the vessel.

These estimates are obtained under the assumption of steady flow and the unsteady case will be considered later. For providing estimates in real arteries, let us consider these estimates as acceptable, for the moment, when applied to the time-averaged flow. In the Aorta, mean velocity is about 50 cm/s and diameter about 3 cm; the entry flow length is nearly 200 diameters (about 1 meter), therefore the flow is never fully developed. Vice versa, in small arteries the boundary layer fills the entire vessel after less that one diameter downstream the entrance.

	U	*D*	x_E	
Aorta	50 cm/s	3 cm	142 *D*	Never fully developed
mid-vessel	10 cm/s	1 cm	10 *D*	
small-vessel	5 cm/s	2.5 mm	1 *D*	Immediately fully developed

7.2. Steady Uniform Planar Flows

Navier-Stokes equation cannot be solved in general; however, a solution can be found under special simple conditions that may present applied relevance. We present here the analytical solution of the Navier-Stokes equation for some few simple flows.

(i) Flow induced by a moving surface above a fixed wall (Couette flow)
With reference to figure 7.3, consider two plane surfaces, at a distance d, with the upper surface moving with constant velocity U.

Make the hypothesis that the flow is unidirectional, $v_y = v_z = 0$; that flow is two-dimensional, thus derivatives along z are neglected; that flow is stationary, thus time derivatives are neglected, and that flow is due to the wall motion only without pressure gradient $\frac{\partial p}{\partial x} = 0$. The assumption of unidirectional flow implies, by the continuity equation, that the flow is also uniform

$$\frac{\partial v_x}{\partial x} + \frac{\partial v_y}{\partial y} + \frac{\partial v_z}{\partial z} = 0 \quad \Rightarrow \quad \frac{\partial v_x}{\partial x} = 0.$$

The Navier Stokes equation in the direction perpendicular to the direction of motion simply states that pressure does not vary along y and z; thus pressure is constant everywhere. The only left unknown is the longitudinal component of velocity as a function of the transversal position $v_x(y)$. The Navier-Stokes equation in the direction of the flow (taken as the x-direction) simplifies in

$$\frac{\partial^2 v_x}{\partial y^2} = 0. \tag{7.17}$$

that must be solved with boundary conditions due to adherence $v_x(0) = 0$ and $v_x(d) = U$.

The solution is immediate to find

$$v_x(y) = U\frac{y}{d}; \tag{7.18}$$

the velocity increases linearly from zero at the fixed wall to the value of the moving wall as shown in figure 7.3. The shear stress is constant

$$\tau = \mu\frac{dv_x}{dy} = \mu\frac{U}{d}; \tag{7.19}$$

as briefly shown in the section 1.2.

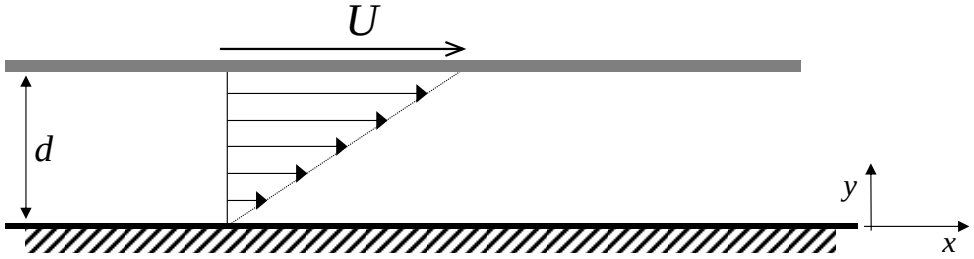

Figure 7.3. Flow induced by a moving wall.

(ii) Flow between parallel walls.
Consider the flow induced by a pressure gradient between two plane walls, at a distance d.

Make the hypothesis that the flow is unidirectional, two-dimensional, and stationary. Following the same argument used in the previous example, the continuity equation implies that the flow is also uniform. When the flow is uniform and unidirectional, the Navier Stokes equation in the transversal tells that pressure does not vary transversal to the direction of motion and that the transport term is identically zero in the direction of motion. Thus, Navier-Stokes becomes in the direction of motion (taken as the x-direction) is

$$\frac{1}{\rho}\frac{\partial p}{\partial x} = \nu\frac{\partial^2 v_x}{\partial y^2}. \tag{7.20}$$

that must be solved with boundary conditions due to adherence $v_x\left(\pm\frac{d}{2}\right) = 0$, where we have placed the x-axis as located in the mid-line between the two walls.

In this case the pressure gradient can be considered as the known quantity that forces the flow. For simplicity, call it $= -\frac{1}{\rho}\frac{\partial p}{\partial x}$, with the minus sign because pressure is higher upstream than downstream to induce a positive velocity. The solution to (7.20), being κ a constant, is immediate to find and it gives the parabolic profile

$$v_x(y) = \frac{\kappa}{2\nu}\left(\frac{d^2}{4} - y^2\right), \tag{7.21}$$

with maximum value at the mid-line between the walls. The shear stress corresponding to the parabolic profile (7.21) is linear

$$\tau = \mu\frac{dv_x}{dy} = -\rho\kappa y = \frac{\partial p}{\partial x}y \tag{7.22}$$

taking its maximum value $\tau = \pm\rho\kappa\frac{d}{2}$ with opposite sign on the opposite walls.

7.3. Steady Uniform Flow in a Circular Vessel (Poiseuille Flow)

The previous flow field was presented just to introduce the case of higher applied relevance of steady uniform flow in a circular rectilinear vessel. This case represents the effective flow that establishes under steady conditions in many actual vessels of the circulation. It thus applies to veins, where flow is approximately steady, as well as to the mean flow in some arteries or in slowly varying unsteady flows (as explained later in this section).

With reference to figure 7.4, make the hypothesis that the flow is unidirectional, axially symmetric (circular symmetry), and stationary. Thus, as we have seen above, the continuity states that the velocity field is also uniform along the direction of the vessel, say the x direction. Pressure is constant transversally to the direction of motion and the transport term is identically zero in the direction of motion. The unknown is the stream-wise velocity that varies on the cross-section $v_x(y,z)$.

Under these hypotheses, the Navier-Stokes equations simplifies to

$$\frac{1}{\rho}\frac{\partial p}{\partial x} = \nu\left(\frac{\partial^2 v_x}{\partial y^2} + \frac{\partial^2 v_x}{\partial z^2}\right). \tag{7.23}$$

The additional assumption of axial symmetry means that the velocity does not vary along the circumference and we may write $v_x(y,z) = v_x(r)$ where $r = \sqrt{y^2+z^2}$. The viscous term in (7.3) can thus be further simplified passing from Cartesian coordinates (x,y,z) to cylindrical coordinates (x,r,θ) and ignoring the dependence from the angular position θ because of the axial symmetry

hypothesis. For this simplification, the derivatives in Cartesian coordinates *y* and *z* are transformed into derivative with respect to the radial coordinate *r* by

$$\frac{\partial}{\partial y} = \frac{\partial r}{\partial y}\frac{\partial}{\partial r}$$
$$\frac{\partial^2}{\partial y^2} = \frac{\partial}{\partial y}\left(\frac{\partial r}{\partial y}\frac{\partial}{\partial r}\right) = \frac{\partial^2 r}{\partial y^2}\frac{\partial}{\partial r} + \left(\frac{\partial r}{\partial y}\right)^2\frac{\partial^2}{\partial r^2}$$

where

$$\frac{\partial r}{\partial y} = \frac{y}{r}, \quad \frac{\partial^2 r}{\partial y^2} = \frac{1}{r} - \frac{y^2}{r^3}.$$

The same can be written by analogy for the z-coordinate to give

$$\frac{\partial^2}{\partial y^2} + \frac{\partial^2}{\partial z^2} = \left(\frac{\partial^2 r}{\partial y^2} + \frac{\partial^2 r}{\partial z^2}\right)\frac{\partial}{\partial r} + \left[\left(\frac{\partial r}{\partial y}\right)^2 + \left(\frac{\partial r}{\partial z}\right)^2\right]\frac{\partial^2}{\partial r^2} = \frac{1}{r}\frac{\partial}{\partial r} + \frac{\partial^2}{\partial r^2} = \frac{1}{r}\frac{\partial}{\partial r}\left(r\frac{\partial}{\partial r}\right).$$

In cylindrical axially symmetric coordinates, equation (7.23) can thus be rewritten as

$$\frac{1}{\rho}\frac{\partial p}{\partial x} = \nu\frac{1}{r}\frac{\partial}{\partial r}\left(r\frac{\partial v_x}{\partial r}\right). \tag{7.24}$$

The version of the Navier-Stokes equation simplified for this case (7.24) can be solved for the unknown velocity profile $v_x(r)$, in correspondence to a given pressure gradient that represent the driving force to the flow, $\kappa = -\frac{1}{\rho}\frac{\partial p}{\partial x}$.

Figure 7.4. Flow in a circular vessel.

The adherence boundary condition in this case is $v_x(R) = 0$, and we notice that, differently from the case between two walls discussed above, there is only one boundary condition for the second order differential equation (7.24). This is a common consequence of the transformation from Cartesian to cylindrical coordinates because the other boundary at $r = 0$ is not a physical boundary, it is rather a singular point for the presence of the factor $\frac{1}{r}$ arising in the coordinate transformation. Here a regularity condition $|v_x(0)| < \infty$ must be applied and it takes the place of the second boundary condition.

Rewrite (7.24) as

$$-\frac{\kappa}{\nu}r = \frac{\partial}{\partial r}\left(r\frac{\partial v_x}{\partial r}\right),$$

and integrate over *r*

$$-\frac{\kappa}{2\nu}r^2 = r\frac{\partial v_x}{\partial r} + A,$$

where A is an integration constant, thus

$$-\frac{\kappa}{2\nu}r = \frac{\partial v_x}{\partial r} + \frac{A}{r}.$$

Integrate again

$$-\frac{\kappa}{4\nu}r^2 = v_x(r) + A\log(r) + B,$$

where B is another integration constant. For the regularity condition $A = 0$, and using the boundary condition at the wall $B = -\frac{\kappa}{4\nu}R^2$.

The solution eventually is

$$v_x(r) = \frac{\kappa}{4\nu}(R^2 - r^2); \tag{7.25}$$

which corresponds to a paraboloid solid profile with maximum velocity at the center of the vessel decreasing to zero at the wall as shown in figure 7.5.

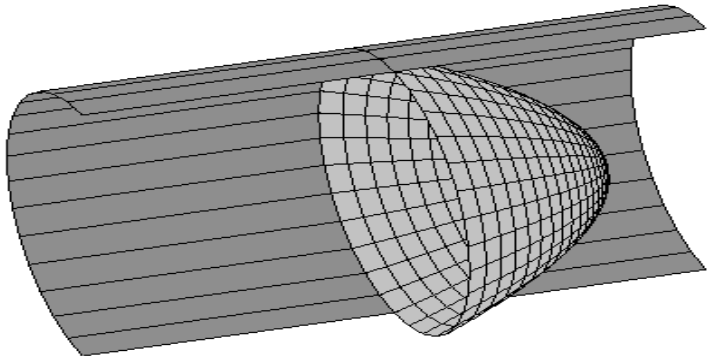

Figure 7.5. Velocity profile in a circular vessel.

The corresponding wall shear stress is

$$\tau_w = \tau(R) = \mu\frac{dv_x}{dr}\Big|_R = -\rho\kappa\frac{R}{2} = \frac{R}{2}\frac{\partial p}{\partial x}, \tag{7.26}$$

which represent the friction at the wall.

The flowing discharge can be computed by integration of (7.25)

$$Q = 2\pi\int_0^R v_x r dr = \frac{\pi}{8}\frac{\kappa R^4}{\nu};$$

and the average velocity

$$U = \frac{Q}{\pi R^2} = \frac{1}{8}\frac{\kappa R^2}{\nu}. \tag{7.27}$$

Equation (7.27) is also important as it provides a relationship between the forcing pressure gradient (the cause) and the resulting mean velocity (the effect). Using (7.27) the solution profile (7.25) can be expressed in terms of the mean velocity instead of pressure gradient

$$v_x(r) = 2U\left(1 - \frac{r^2}{R^2}\right); \tag{7.28}$$

which also shows that the maximum velocity at the center of the duct, $r = 0$, is equal to $2U$, twice the mean velocity.

In this case, where the Navier-Stokes equation could be solved exactly, it is immediate computing the momentum velocity-correction factor β that appeared in (5.6)

$$\beta = \frac{2\pi \int_0^R v_x^2 r dr}{\pi R^2 U^2} = 8\int_0^1 (1 - s^2) s ds = \frac{4}{3}. \tag{7.29}$$

It is worth to remark that given a flow rate Q, the pressure loss per unit length increases with the fourth power of the vessel diameter

$$\kappa = -\frac{1}{\rho}\frac{\partial p}{\partial x} = \frac{8\nu Q}{\pi R^4};$$

it is therefore natural to recognize that the decrease of the vessel size is accompanied in the vascular network by division of the vessel into multiple smaller vessels each bringing a much smaller discharges.

The steady flow solution (7.25) or (7.28) is the result of a balance (7.24) between the force to move the fluid due to the pressure gradient pushing over the vessel area, $\pi R^2 \frac{\partial p}{\partial x}$, and the viscous friction at the vessel wall that resists to the motion $2\pi R \tau_w$. In other terms, this flow is associated with continuous pressure loss due to viscous friction.

We have seen in the previous chapter that local energy dissipation represent a fraction of the available kinetic energy. Here too, the *distributed* energy dissipation can be expresses proportional to the available kinetic energy: energy dissipation per unit length is the pressure gradient (kinetic energy is constant) thus

$$-\frac{dp}{dx} = f(Re)\frac{\rho U^2}{2D},$$

where f is a dimensionless friction coefficient (the minus sign is introduced to have positive quantities and a positive friction factor). This formula was previously introduced by dimensional arguments in equation (1.13), where it was also shown that the friction coefficient must depend on the Reynolds number, Re. In this case, where we have solved the dynamical equations, it is possible to determine the function $f(Re)$. Using the relationship (7.27) obtained from the flow solution, the friction factor for Poiseuille flow is

$$f(Re) = \frac{64}{Re}; \tag{7.30}$$

where the exact definition of the Reynolds number for this application is

$$Re = \frac{UD}{\nu}.$$

Equation (7.30) shows that the smaller the Reynolds number and the higher are the energy losses due to friction; vice versa, when the Reynolds number is high, viscous losses decrease asymptotically to zero. The Reynolds number represents a proper dimensionless ratio telling how a flow is viscous; therefore, it is of fundamental importance for classifying the type of flow. It represents a ratio between the kinetic energy available to the flow and its ability to dissipate energy. The smaller the Reynolds number the more the flow is a viscous smooth one, energy is low with respect to the ability to

dissipate. The higher the Reynolds number and the more vigorous and energetic the flow. We will see shortly that when the Reynolds number is higher than a certain threshold the flow is so vigorous with respect to its ability to dissipate that a simple viscous mechanism is insufficient to balance. In this case, flow develops turbulence to increase viscous dissipation.

7.4. Oscillatory and Pulsatile Uniform Flow in a Circular Vessel

Blood motion in cardiovascular vessels, can be close to steady only in small capillaries and veins. In large arteries, flow normally presents a pulsatile behavior, which can be seen as given by a mean motion plus a fluctuation of comparable entity. Let us now move forward here and consider the solutions of unsteady flows, starting from simple cases and progressing toward more realistic ones.

(i) Sinusoidal Oscillatory flow

Consider the case of flow given by an oscillatory pressure gradient of the sinusoidal type

$$\frac{1}{\rho}\frac{\partial p}{\partial x} = \kappa \sin \omega t, \tag{7.31}$$

where the frequency $\omega = \frac{2\pi}{T}$ and T is the period of the oscillation. Under the identical hypothesis used for the Poiseuille flow and only removing the assumption of steady flow, the unknown is the unsteady velocity $v_x(t,r)$ that obeys the Navier-Stokes equation

$$\frac{\partial v_x}{\partial t} + \kappa \sin \omega t = \nu \frac{1}{r}\frac{\partial}{\partial r}\left(r\frac{\partial v_x}{\partial r}\right), \tag{7.32}$$

with no-slip boundary condition at the wall, $v_x(t,R) = 0$, and regularity condition at *r=0*. The linearity of equation (7.32) tells that that the solution must be time periodic with the same frequency, ω, like (7.31) although possibly a different phase (not just a *sin*). The solution of equation (7.32) with its boundary conditions can be obtained analytically as (Schlichting, 1979)

$$v_x(t,r) = \frac{\kappa}{\omega}\left[1 - \frac{J_0\left(r\sqrt{\frac{-i\omega}{\nu}}\right)}{J_0\left(R\sqrt{\frac{-i\omega}{\nu}}\right)}\right]e^{i\omega t}, \tag{7.33}$$

where $J_0(x)$ is the Bessel function of 1st type of order 0. The denominator in solution (7.33) permits to satisfy the boundary condition. The amplitude of the oscillation is given by the ratio $\frac{\kappa}{\omega}$, it is higher for high pressure gradient and for slow oscillations. The term in square bracket is a complex number that modifies the phase of the flow, along the radial coordinate *r*.

To better understand this point, solution (7.33) can be preferably expressed in terms of dimensionless parameters as

$$v_x(t,r) = U\left[1 - \frac{J_0\left(\frac{r}{R}W\sqrt{\frac{-i\pi}{2}}\right)}{J_0\left(W\sqrt{\frac{-i\pi}{2}}\right)}\right]e^{i2\pi\frac{t}{T}}, \tag{7.34}$$

where $U = \frac{\kappa}{\omega}$ here represents the maximum velocity during the oscillation and

$$W = R\sqrt{\frac{\omega}{\nu}\frac{2}{\pi}} = \frac{D}{\sqrt{\nu T}}, \tag{7.35}$$

is the *Womersley number* that gives a measure of the degree of unsteadiness of the oscillation.

The Womersley number can be understood as the ratio between the vessel diameter and a measure of the thickness of the boundary layer that develops during the period T of the oscillation. Indeed we have seen before that the thickness of a boundary layer reaches in a time t a value proportional $\sqrt{\nu t}$; in this case the boundary layer is allowed to grow for a time proportional to T , therefore the denominator of (7.35), $\sqrt{\nu T}$, is a measure of the maximum thickness that the boundary layer can reach. Velocity profiles at different values of the Womersley number are shown in figure 7.6. When W is small, the oscillation is slow, the boundary layer has the time to fill the entire vessel. The term in brackets is close to unity and the flow is a sequence of velocity profiles close to the Poiseuille type that is in phase with the pressure gradient because of the linear relationship between velocity and pressure gradient in Poiseuille solution. On the opposite end, when W is large, the oscillation is rapid, the viscous adherence has not enough time to affect the internal regions of the wall. The viscous boundary layer is limited to a thin region near the wall while the center of the vessel moves nearly as a uniform profile with marginal influence of viscosity. The viscous layer near the wall is in phase with the external forcing and gets progressively out of phase away from the wall because pressure gradient here balances with velocity time derivative rather than velocity itself.

A Reynolds number can also be introduced for the oscillatory flows using the peak velocity as $Re = \frac{UD}{\nu}$, that tells how intense is the bulk flow with respect to the ability of viscous dissipation.

In unsteady periodic flows, it is sometime useful to introduce another dimensionless number, the Strouhal number (see also equation (1.14)), defined as

$$St = \frac{D}{UT} = \frac{W^2}{Re}. \tag{7.36}$$

The Strouhal number represents a dimensionless frequency of the oscillation. It can be appreciated that the length travelled by particles during an oscillation is proportional to UT (equal to $UT/2\pi$ in sinusoidal oscillation); therefore the Strouhal number can be seen as the ratio between the diameter and a measure of the distance travelled by particles. Thus for high St, the oscillations are rapid and fluid particles oscillate for length smaller than the diameter; low St means that particles travel several diameters during each oscillation.

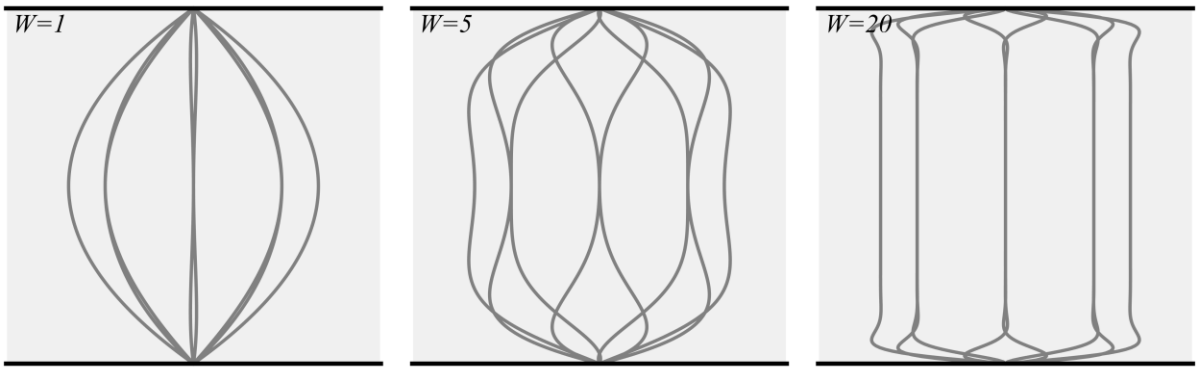

Figure 7.6. Oscillatory velocity profile in a circular vessel at different Womersley number.

(ii) Pulsatile flows

The oscillatory solution describe above is useful to understand the main phenomena entering into play in generally period flow. Indeed, flow in cardiovascular vessels is usually pulsatile: unsteady,

periodic in time, with non-zero time-average velocity. Pulsatile flows is a combination of steady flow and a series of sinusoidal oscillations. Under the hypothesis of unidirectional flow, the transport term in the Navier-Stokes equation is absent and equations are linear (see (7.24) and (7.32)). Therefore the solution corresponding to an arbitrary time-periodic pressure gradient

$$\frac{1}{\rho}\frac{\partial p}{\partial x} = -\kappa_0 + \sum_n \kappa_n e^{i2\pi n\frac{t}{T}}, \tag{7.37}$$

or an arbitrary mean velocity

$$U(t) = U_0 + \sum_n U_n e^{i2\pi n\frac{t}{T}}, \tag{7.38}$$

can be obtained by appropriate linear combination of solution (7.25) and (7.33), or (7.28) and (7.34).

In pulsatile flows, the Womersley number is usually defined with the main period $W = \frac{D}{\sqrt{\nu T}}$, while the Reynolds number $Re = \frac{UD}{\nu}$ is defined using U as either the time-average velocity U_0 or, more commonly, the peak velocity whose value depends on the details of the oscillatory components.

The solutions for pulsatile flow are then given by a Poisuille parabolic flow made with the mean velocity plus the individual solutions of sinusoidal flows (like those in figure 7.6). Examples of pulsatile flows solutions, given by a mean flow and a single sinusoidal oscillation of amplitude equal to the mean flow, are shown in figure 7.7 for a same average velocity and different values of the Womersley number. For low values of W the velocity profile is a sequence of Poiseuille solutions evaluated with the instantaneous values of the mean velocity; on the opposite end, as W increases, the solution presents an inversion of the boundary layer flow in the annulus near the wall.

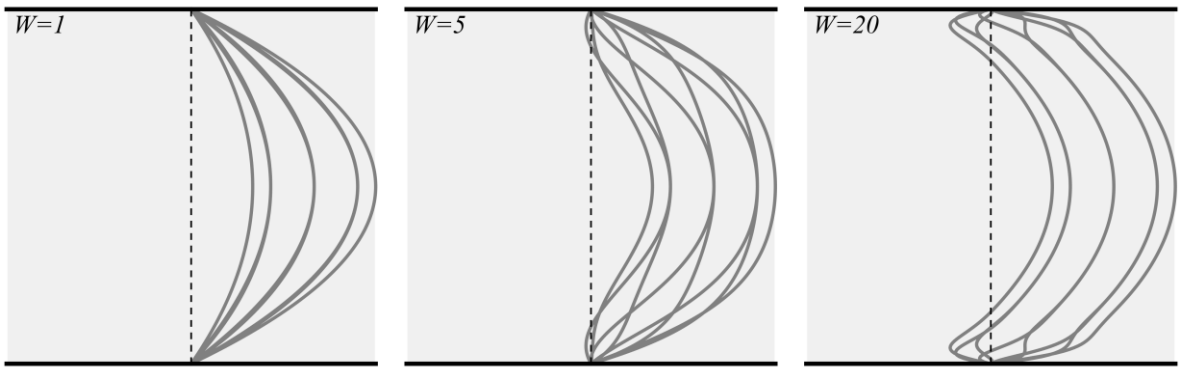

Figure 7.7. Pulsatile velocity profile in a circular vessel at different Womersley numbers (mean velocity ranges from 0 to *U*).

To give an idea of the order of magnitude, the following table provide indications of typical values for these dimensionless numbers in main vessels. It shows that flow is effectively unsteady in major arteries of clinical interest while it becomes well described by the Poisueille solution in smaller vessels as well as in veins.

	U [cm/s]	D [cm]	Re	W	St
Aorta	100	3	10000	20	0.04
Middle arteries	30	1	1000	5	0.05
Small arteries	5	0.2	30	1	0.05
Arterioles	0.1	<0.1	<0.5	<0.5	~1

8. Elements of Turbulent Flow

8.1. Introduction to Turbulence

We briefly anticipated that the Reynolds number represents the ratio between available kinetic energy and ability to dissipate it by regular friction. When the Reynolds number exceeds a certain threshold the kinetic energy can be excessively high, or the ability to dissipate can be insufficient, that the regular motion is unable to reach a balance between incoming energy and dissipation. This point was introduced in the famous experiment performed by Osborne Reynolds (performed back in 1883) describing the transition from laminar to turbulent flow in a circular pipe under steady and uniform conditions (Reynolds, 1894, 1883).

In this experiment, water was allowed to flow in a glass-walled (transparent) pipe with varying mean velocity and a small jet of dye was released at the center of the pipe near the inlet. When velocity was small enough, dye trajectory was rectilinear. This type of motion was said to be "laminar"; fluid motion is unidirectional and uniform in agreement with the hypothesis used for Poiseuille solution; thus, the velocity field was described by that solution (7.25).

When velocity approached a certain critical threshold, the dye trajectories started to display a slightly wavy pattern indicating that the flow is not perfectly laminar. As velocity further increased above a critical value, the dye rapidly mixes and spreads filling the entire pipe. This type of flow was said "turbulent"; velocities are irregular in space and in time with an apparently random behavior.

It is evident that any kinematic flow property (like, for example, the amplitude of turbulent fluctuations) must depend on the size of the circular pipe, measured by its diameter D, by the intensity of the flow, given by the mean velocity U, and by the properties of the flow, which in Newtonian flow are summarized by the kinematic viscosity ν. There were no other parameters that could be varied in the experiment. These are 3 parameters that are based on 2 dimensional units (length and time); dimensional analysis permits to show that any properly normalized dimensionless quantity can depends on a single dimensionless parameter constructed using such 3 dimensional parameters. The dimensionless parameter is the Reynolds number (this is were the name comes from) $Re = \frac{UD}{\nu}$. When the Reynolds number is below a critical values Re_{cr} the flow is laminar, when it is above the critical value the flow is turbulent. The transition from laminar to turbulence occurs over a small interval about $Re_{cr} \approx 2500$, although the exact figure depends on the degree of disturbance that are present in the experiment.

The same concept applies in other types of flow. For any flow arrangement there is a critical value of the Reynolds number build with an appropriate velocity scale U and an appropriate length scale L such that flow changes from laminar to turbulence regime when the Reynolds number exceeds the critical value for that arrangement. For flow behind a cylindrical obstacle, these scales are evidently the upstream velocity and the cylinder diameter. In a steady boundary layer developing over a flat plates, as discusses in section 7.1, the only external length scale available is the distance from the origin of the plate, thus also demonstrating that the laminar boundary layer remains stable only for a certain length from its origin.

For many years, the physical origin of turbulence was unclear. The laminar Poiseuille flow is a solution of the Navier-Stokes equation, thus, the observation that this solution does not realize may rise doubts on the validity of those equations for describing fluid motion in general. However, this is not the case. The Navier-Stokes equation is a non-linear equation; as such, it has not necessarily a unique solution and can admit multiple solutions to the same problem. In the case of pipe flow there

is one laminar solutions, that is steady uniform and unidirectional, and there are many others unsteady and irregular, turbulent solutions. When the Reynolds number is small enough, the viscous friction is large enough to damp the turbulent solution; thus, those turbulent solution are unstable as they would decay toward the laminar solution that is the only stable and physically realizable solution. Vice versa, when the Reynolds number is larger, the laminar solution becomes unstable because the flow has an excess of energy that cannot be dissipated through the simple linear friction, thus this solution does not realize physically. Any small disturbance to that solution tends to move the flow away from it, whereas turbulent solutions are stable and realizable. The selection of one or another of the many possible turbulent solutions depends on the details of the initial and boundary conditions. The solution can also jumps from one turbulent solution to another when disturbed by small perturbations that are unavoidably present in physical systems.

The point that deterministic equations like Navier-Stokes can give rise to apparently random solutions has been debated for years in the last decades; however, it was recognized that even much simpler deterministic non-linear equations could present analogous behavior (Davidson, 2004). This was described as the concept of deterministic "chaos" where the solution of deterministic equations present apparently random behavior (Feigenbaum, 1978). Probably the simpler equation is a difference equation (where time-derivative is replaced by a difference between discrete time instants) with no spatial dependence. Thus consider the variable u_k, with values in the open interval $0 < u_k < 1$, where k is the discrete time variable obeying the following evolution equation (May, 1976)

$$u_{k+1} = \lambda u_k (1 - u_k); \tag{8.1}$$

and λ is a parameter that plays a role analogous to the Reynolds number for this abstracted evolution equation. Equation (8.1) has a steady solutions, immediately found by setting $u_{k+1} = u_k$, which is $u_k = \frac{\lambda - 1}{\lambda}$ (the other solution $u_k = 0$ is out of the interval of definition). Until $\lambda < 3$ this solution is stable, any initial condition eventually converges to that. At larger values of λ the steady solutions becomes unstable, the system becomes unsteady, initially jumping alternatively between two values, between more values as λ increases, until for $\lambda = 4$ the solution oscillates randomly over the entire interval (0,1). The equation is deterministic; therefore, once the initial condition is set then the associate solution follows univocally, while different realizations are the result of setting different initial conditions. One can notice, however, that the solution at a certain time *k* is extremely sensitive to the value used as initial condition; extremely close initial conditions rapidly diverge and after a transient period give rise to macroscopically different solution. Initial differences can be limited to a far decimal digit, or the last significant digit in a numerical model, the smaller the difference the longer the transient, eventually the solutions diverge exponentially and become uncorrelated. This behavior is known as "Sensitivity to Initial Conditions" (SIC). Indeed, the smooth dependence of solution on initial/boundary conditions (that solutions relative to nearby conditions produce nearby solutions) is a property that is generally valid for linear systems only and does not necessarily applies to non-linear systems.

This behavior also applies to the Navier-Stokes equation, with the additional complexity that irregularities occur both over time and over the three spatial dimensions. This means that any small difference on initial or on boundary conditions can give rise to different turbulent solutions. Moreover, any small external perturbation is analogous to small changes to the initial condition for the following evolution and may drive the system across different turbulent solutions.

This means that an experiment about fluid turbulence performed under identical conditions produces different solutions because a laboratory cannot reproduce conditions that are exactly identical to

arbitrary accuracy. This is a fundamental conceptual problem that cannot be solved in principle, and in advances in numerical computations as well, because the boundary or initial conditions can be known with a finite accuracy only and such small uncertainty reflects to large differences in the solution. Moreover, numerical calculus uses a finite accuracy, that may be even different between different computers, and it can happen that numerical solutions of the same determinist equations produce different results. As a result, when talking about turbulent flows one cannot focus on an individual realization of that field, that is just one solution among infinite many others equally possible, and should rather pay attention to the main properties that are common to all turbulent realizations of that flow.

Physically, turbulence enhances energy dissipation and therefore it is normally a threat of excessive energy consumption in the vascular circulation. Another property is the unpredictability of its chaotic fluctuations that makes turbulent flows difficult to control, model, and manage. On the other side, turbulence has several positive implications; first of all, it makes life possible by enhancing mixing and diffusion. While viscous diffusion is an extremely efficient mechanism to distribute substances at very small scales, turbulent dispersion dominates mixing at larger scales. For example, viscous diffusion length, that grows proportionally to $\sqrt{\nu t}$, in water takes a few hundredth of a second to reach one millimeter, a few second for one centimeter, and over one hour for one meter. On the contrary, it is in everyone's experience that accelerated turbulent dispersion dominates the mixing and heat propagation at scales larger than, typically, a few millimeters. It is evident how turbulence is ubiquitous in nature and how it ensures the mixing that is experienced in everyday life.

8.2. Reynolds Equations

Turbulent flow are complex and irreproducible; nevertheless, the different realizations of turbulent flows under similar conditions present common characteristic, like the mean velocity or the amplitude of fluctuations. These properties are also those that present a practical interest. The most common strategy to tackle the problem of turbulence relies on statistical methods, searching for a description of the average motion (responsible for transport) and of its fluctuations (responsible for dispersion). This is such a common practice that the study of turbulence is often considered that of statistical fluid mechanics (Monin and Yaglom, 1971).

There are several different ways for defining average properties in turbulence, from spatial filtering to time filtering. The most straightforward approach is that of considering the mean velocity as time average over a period T that defines the separation between fluctuations due to turbulence and those caused by the large scale evolution in time. Indicating with angular brackets the averaging operator, we define the mean velocity as

$$\langle \boldsymbol{v}(\boldsymbol{x},t)\rangle = \frac{1}{T}\int_{-\frac{T}{2}}^{\frac{T}{2}} \boldsymbol{v}(\boldsymbol{x},t)dt\ , \tag{8.2}$$

and the fluctuating velocity

$$\boldsymbol{v}'(\boldsymbol{x},t) = \boldsymbol{v}(\boldsymbol{x},t) - \langle \boldsymbol{v}(\boldsymbol{x},t)\rangle\ ; \tag{8.3}$$

such that the actual velocity is the sum of the mean plus the fluctuating components $v = \langle \boldsymbol{v}\rangle + \boldsymbol{v}'$.

We can now try to write the equations for the mean velocity applying the average operator to the continuity and to the Navier-Stokes equations. Applying the mean operator to the continuity equation gives

$$\langle \nabla \cdot \boldsymbol{v} \rangle = \nabla \cdot \langle \boldsymbol{v} \rangle = 0 \,, \tag{8.4}$$

which tells that the mean velocity is also a divergence-free field. By difference, it is immediate to verify that also the fluctuating velocity field is divergence-free

$$\nabla \cdot \boldsymbol{v} = \nabla \cdot (\langle \boldsymbol{v} \rangle + \boldsymbol{v}') = \nabla \cdot \langle \boldsymbol{v} \rangle + \nabla \cdot \boldsymbol{v}' = \nabla \cdot \boldsymbol{v}' = 0 \,. \tag{8.5}$$

The same approach can be applied to the Navier-Stokes equation. To make it simple, consider the *x*-component of the equation written in a Cartesian system of coordinates, see equation (5.35), that is averaged to give

$$\langle \frac{\partial v_x}{\partial t} \rangle + \langle \boldsymbol{v} \cdot \nabla v_x \rangle = -\frac{1}{\rho} \langle \frac{\partial p}{\partial x} \rangle + \nu \langle \nabla^2 v_x \rangle,$$

and can be rewritten exchanging the derivative and the averaging operator

$$\frac{\partial \langle v_x \rangle}{\partial t} + \langle \boldsymbol{v} \cdot \nabla v_x \rangle = -\frac{1}{\rho} \frac{\partial \langle p \rangle}{\partial x} + \nu \nabla^2 \langle v_x \rangle. \tag{8.6}$$

The second terms is non-linear and does not allow a simplification based on the exchanged between average and derivatives. Let's us look at this term in details

$$\begin{aligned}
\langle \boldsymbol{v} \cdot \nabla v_x \rangle = & \\
= \; & \langle (\langle v_x \rangle + v_x{}') \frac{\partial (\langle v_x \rangle + v_x{}')}{\partial x} + \left(\langle v_y \rangle + v_y{}' \right) \frac{\partial (\langle v_x \rangle + v_x{}')}{\partial y} + (\langle v_z \rangle + v_z{}') \frac{\partial (\langle v_x \rangle + v_x{}')}{\partial z} \rangle = \\
= \; & \langle \langle v_x \rangle \frac{\partial \langle v_x \rangle}{\partial x} \rangle + \langle \langle v_y \rangle \frac{\partial \langle v_x \rangle}{\partial y} \rangle + \langle \langle v_z \rangle \frac{\partial \langle v_x \rangle}{\partial z} \rangle + \\
& + \langle \langle v_x \rangle \frac{\partial v_x{}'}{\partial x} \rangle + \langle \langle v_y \rangle \frac{\partial v_x{}'}{\partial y} \rangle + \langle \langle v_z \rangle \frac{\partial v_x{}'}{\partial z} \rangle + \\
& + \langle v_x{}' \frac{\partial \langle v_x \rangle}{\partial x} \rangle + \langle v_y{}' \frac{\partial \langle v_x \rangle}{\partial y} \rangle + \langle v_z{}' \frac{\partial \langle v_x \rangle}{\partial z} \rangle + \\
& + \langle v_x{}' \frac{\partial v_x{}'}{\partial x} \rangle + \langle v_y{}' \frac{\partial v_x{}'}{\partial y} \rangle + \langle v_z{}' \frac{\partial v_x{}'}{\partial z} \rangle \,.
\end{aligned}$$

These terms can be simplified further by realizing that the average values can be taken out of the average operator, because they behave like a constant with respect to the integral in the averaging operation. Therefore, we can rewrite the last equality

$$\begin{aligned}
\langle \boldsymbol{v} \cdot \nabla v_x \rangle = & \\
= \; & \langle v_x \rangle \frac{\partial \langle v_x \rangle}{\partial x} + \langle v_y \rangle \frac{\partial \langle v_x \rangle}{\partial y} + \langle v_z \rangle \frac{\partial \langle v_x \rangle}{\partial z} + \\
& + \langle v_x \rangle \frac{\partial \langle v_x{}' \rangle}{\partial x} + \langle v_y \rangle \frac{\partial \langle v_x{}' \rangle}{\partial y} + \langle v_z \rangle \frac{\partial \langle v_x{}' \rangle}{\partial z} + \\
& + \langle v_x{}' \rangle \frac{\partial \langle v_x \rangle}{\partial x} + \langle v_y{}' \rangle \frac{\partial \langle v_x \rangle}{\partial y} + \langle v_z{}' \rangle \frac{\partial \langle v_x \rangle}{\partial z} + \\
& + \langle v_x{}' \frac{\partial v_x{}'}{\partial x} \rangle + \langle v_y{}' \frac{\partial v_x{}'}{\partial y} \rangle + \langle v_z{}' \frac{\partial v_x{}'}{\partial z} \rangle \,.
\end{aligned}$$

It is immediate to notice that the first term on the right-hand-side is the transport equation written for the mean velocity. The second and third terms are both zero because they contain the mean of the fluctuating components that are zero by definition. Last terms can be simplified by adding the average of a null terms $v_x \, \nabla \cdot \boldsymbol{v}'$ that is zero because of (8.5); thus the equality can be rewritten

$$\begin{aligned}\langle \boldsymbol{v} \cdot \nabla v_x \rangle = \; & \langle \boldsymbol{v} \rangle \cdot \nabla \langle v_x \rangle + \\ & + \langle {v_x}' \frac{\partial v_x'}{\partial x} \rangle + \langle {v_y}' \frac{\partial v_x'}{\partial y} \rangle + \langle {v_z}' \frac{\partial v_x'}{\partial z} \rangle + \\ & + \langle {v_x}' \frac{\partial v_x'}{\partial x} \rangle + \langle {v_x}' \frac{\partial v_y'}{\partial y} \rangle + \langle {v_x}' \frac{\partial v_z'}{\partial z} \rangle \\ = \; & \langle \boldsymbol{v} \rangle \cdot \nabla \langle v_x \rangle + \frac{\partial \langle v_x' v_x' \rangle}{\partial x} + \frac{\partial \langle v_x' v_y' \rangle}{\partial y} + \frac{\partial \langle v_x' v_z' \rangle}{\partial z};\end{aligned}$$

where we used the product of derivatives in the last passage.

This result can be reinserted in the original equation (8.6) and rewritten in vector terms to better highlight the new structure of the equation

$$\frac{\partial \langle \boldsymbol{v} \rangle}{\partial t} + \langle \boldsymbol{v} \rangle \cdot \nabla \langle \boldsymbol{v} \rangle = -\frac{1}{\rho} \nabla \langle p \rangle + \nu \nabla^2 \langle \boldsymbol{v} \rangle + \frac{1}{\rho} \nabla \cdot \mathbb{T}_{\boldsymbol{R}}. \tag{8.7}$$

where the last term is written using the symmetric Reynolds stress tensor defined by

$$\mathbb{T}_{\boldsymbol{R}ij} = -\rho \langle {v_i}' {v_j}' \rangle; \tag{8.8}$$

Equation (8.7) is the Reynolds' equation. It corresponds to the Navier-Stokes equation when expressed in terms of mean velocity. The Reynolds equation differs from the Navier-Stokes equation for the additional terms that contains the Reynolds stress. Interestingly, the Reynolds stress term has exactly the same form of the stress tensor terms previously found in the Cauchy equation (5.30); however, this equation is for the mean velocity, that is not the physical velocity but only a mathematical filter of it. The Reynolds stresses therefore are not real stresses experienced by physical fluid elements, they are fictitious stresses that represent the influence of the fluctuating velocities on the mean velocities. It would represent the energy that is lost the mean flow because it is transferred into the fluctuations during the filter period T.

The Reynolds equation produces simpler, smoother solutions because of the enhanced dissipative mechanism introduced by the Reynolds stresses, thus avoiding the contemporary presence of many interleaving scales within the flow. This simplification is payed, on the other side, by the fact that the Reynolds equation is not closed: it includes 6 further unknowns, the Reynolds stresses, that cannot be obtained by the equation itself. The appearance of novel unknowns in the averaged equation is what is known as the *closure problem* of turbulence. Either equations are complicated and unsolvable (Navier-Stokes) o they are not closed (Reynolds, as well as many other filtered equation derived from Navier-Stokes) because they present additional unknown terms.

There are numerous models to provide a closure to the Reynolds equation by adding additional equations for the terms (8.8). It must be remarked, however, that all these models are not obtained from first conservation principles; thus closure models are not approximations, they are not accurate in general and rely on numerous empirical coefficients. They are more reliable in canonical flows of practical relevance where extensive experimental and numerical studies permitted to establish reliable models. In general, the closure problem is still open, although several advances have been performed during last decades to allow numerical solutions of turbulent flows (Sagaut, 2006).

8.3. Turbulent flow over a wall

A turbulent flow of paramount applied interest is that flowing near a surface under the hypothesis that the mean flow is steady and unidirectional. It cannot be solved exactly as it was done for laminar flows; nevertheless, some result can be achieved by properly combining all information available.

Following (Monin and Yaglom, 1971), consider turbulent flow over a flat surface as sketched in figure 8.1. Assume that the flow is steady and two-dimensional, on average, thus derivatives of mean quantities along z and t are zero, and that the mean flow is unidirectional, $\langle v_y \rangle = \langle v_z \rangle = 0$. By continuity we have the only unknown is the x-component of the mean velocity that can vary with the distance y from the wall: $\langle v_x(y) \rangle$.

The Reynolds equations along the transversal direction simply state that the mean pressure $\langle p \rangle$ is constant transversal to the mean flow, as can be immediately verified. The x-component of the Reynolds equation

$$\frac{\partial \langle v_x \rangle}{\partial t} + \langle v_x \rangle \cdot \frac{\partial \langle v_x \rangle}{\partial x} + \langle v_y \rangle \cdot \frac{\partial \langle v_x \rangle}{\partial y} + \langle v_z \rangle \cdot \frac{\partial \langle v_x \rangle}{\partial z} = \\ = -\frac{1}{\rho}\frac{\partial \langle p \rangle}{\partial x} + \nu \left(\frac{\partial^2 \langle v_x \rangle}{\partial x^2} + \frac{\partial^2 \langle v_x \rangle}{\partial y^2} + \frac{\partial^2 \langle v_x \rangle}{\partial z^2} \right) - \frac{\partial \langle v_x{}' v_x{}' \rangle}{\partial x} - \frac{\partial \langle v_x{}' v_y{}' \rangle}{\partial y} - \frac{\partial \langle v_x{}' v_z{}' \rangle}{\partial z},$$

simplifies with these assumptions to

$$\nu \frac{\partial^2 \langle v_x \rangle}{\partial y^2} - \frac{\partial \langle v_x{}' v_y{}' \rangle}{\partial y} = \frac{1}{\rho}\frac{\partial \langle p \rangle}{\partial x}.$$

Make the additional assumption that the mean pressure gradient is zero; thus that the motion is driven by the presence of a velocity away from the wall. However, it can be demonstrated that the presence of a mean pressure gradient would affect the value of velocity but without a direct influence on the profile of velocity. In this simple formulation the Reynolds equation provide the following relationship

$$\nu \frac{\partial^2 \langle v_x \rangle}{\partial y^2} - \frac{\partial \langle v_x{}' v_y{}' \rangle}{\partial y} = 0. \tag{8.9}$$

Both terms present a derivative along y; after integration we have

$$\nu \frac{\partial \langle v_x \rangle}{\partial y} - \langle v_x{}' v_y{}' \rangle = constant.$$

this constant has the dimension of a velocity square and it is commonly written as u_*^2

$$\nu \frac{\partial \langle v_x \rangle}{\partial y} - \langle v_x{}' v_y{}' \rangle = u_*^2 \tag{8.10}$$

where u_* is called the *friction velocity* whose physical meaning will be clear shortly.

Equation (8.10) tells that there is a property of the turbulent wall flow, that we call the square of the friction velocity, that is constant over the entire velocity profile, from the wall to above the wall. Looking carefully to the two terms in (8.10) we can recognize that, when multiplied with the density ρ, they represent the mean viscous stress $\langle \tau_{xy} \rangle$ and the turbulent Reynolds stress $\mathbb{T}_{\boldsymbol{R}_{xy}}$, respectively. Therefore, equation (8.10) tells that the total stress, given by the sum of viscous plus the turbulent stresses, is constant over the turbulent profile; the former dominates close to the wall, where turbulence stress reduces approaching is the wall where velocities are zero, while the turbulent stress dominates away from the wall as shown in figure 8.1. Equation (8.10) is valid also at the wall where turbulent stress is zero because velocity and its fluctuations are zero and the viscous stress is

$$\tau_0 = \rho \nu \left. \frac{\partial \langle v_x \rangle}{\partial y} \right|_{y=0} = \rho u_*^2 \, . \tag{8.11}$$

Equation (8.11) tells that the friction velocity is given by

$$u_* = \sqrt{\frac{\tau_0}{\rho}}. \tag{8.12}$$

Consider now the limiting situation very close to the wall. Here viscous stress dominates and equation (8.10) can be approximated as

$$\nu \frac{\partial \langle v_x \rangle}{\partial y} \cong u_*^2;$$

which can be integrated, with boundary condition $\langle v_x(0) \rangle = 0$, to give the velocity profile very close to the wall

$$\frac{\langle v_x \rangle}{u_*} \cong \frac{u_*}{\nu} y; \tag{8.13}$$

showing that velocity grows linearly from the wall. Expression (8.13) indicates the existence of a viscous length scale, given by $y_* = \frac{\nu}{u_*}$, at which distance $\langle v_x(y_*) \rangle \cong u_*$, that provides the length scale of this inner layer where viscosity is important.

Far from the wall, at distances much larger than such length scale, $y \gg y_*$, the turbulent stress dominates over the viscous one. Equation (8.10) does not allows to solve the velocity profile in this limit; nevertheless, we can confidently assume that the variations in the velocity profile (its y-derivative) should not depend explicitly on viscosity. Thus, in first approximation, the velocity gradient can only depend on the turbulent stress, which is estimated from (8.10) by the friction velocity, and by the distance from the wall that is a length scale of the spatial amplitude of turbulent fluctuation. Functionally we can write

$$\frac{\partial \langle v_x \rangle}{\partial y} = \mathrm{f}(u_*, y). \tag{8.14}$$

Dimensional analysis of (8.14) allows simplifying it in the following form

$$\frac{\partial \langle v_x \rangle}{\partial y} = \frac{1}{k} \frac{u_*}{y}. \tag{8.15}$$

where k is an unknown constant. This constant is known as the Von Karman constant, it was estimated experimentally to take the value $k \cong 0.4$ in most turbulent wall flows. Integration of (8.15) gives

$$\langle v_x \rangle = \frac{u_*}{k} \ln\left(\frac{y}{y_0}\right); \tag{8.16}$$

where y_0 is the integration constant that is unknown because there is no boundary condition that can be enforces given that this profile is not valid at the wall. The integration constant y_0 is a length and should be expressed proportional to the only existing length scale, found in (8.13), as $y_0 = \frac{1}{a} \frac{\nu}{u_*}$ where now the dimensionless unknown is a. With this substitution, equation (8.16) is rewritten in a form analogous to (8.13) as

$$\frac{\langle v_x \rangle}{u_*} = \frac{1}{k} \ln\left(a \frac{u_*}{\nu} y\right); \tag{8.17}$$

where the coefficient a is unknown and should be evaluated for the different cases. The solution (8.17), although obtained with several approximations and hypotheses, was demonstrated to be a very good representation of real wall-bounded turbulent flows under numerous different configurations, with or without pressure gradients, and in different geometries. It is valid for wind blowing over the sea or over a town, for water flowing in rivers as well as in cylindrical pipes, for example. A general

feature of the profile (8.17), sketched in figure 8.1, is its slow modulation; it is very slow varying after an initial steep region close to the wall. Therefore, the turbulent profiles are commonly very flat in contrast with the laminar parabolic profile.

The velocity profile in equation (8.17) is not an exact solution; it presents two dimensionless coefficients, k and a that must be estimated experimentally, and the friction velocity u_* that provides the intensity of the actual flow. Friction velocity was defined by (8.12) and it is the only velocity scale available in this context of generic flow without reference to conduits discharge or external velocities. However, once the details of the flow are provided, the friction velocity can be obtained from macroscopic measurable quantities. For example, in a conduit, the friction velocity can be related to the pressure gradient that induces the mean flow. To this aim, consider a steady and uniform turbulent flow inside a vessel of constant cross-section, the global balance of momentum between two sections has zero inertial and zero flux of momentum terms, it simply states a balance between the force due to pressure difference and the resistance due to wall shear stress

$$\tau_0 C = -\frac{\partial \langle p \rangle}{\partial x} A \,, \tag{8.18}$$

where C and A are the perimeter and the area of the vessel, respectively; equal to πD and $\frac{\pi}{4} D^2$ in a circular vessel of diameter D. Use (8.12) and (8.18) to obtain the friction velocity in terms of the pressure gradient,

$$u_* = \sqrt{-\frac{1}{\rho}\frac{\partial \langle p \rangle}{\partial x}\frac{A}{C}} = \sqrt{-\frac{1}{\rho}\frac{\partial \langle p \rangle}{\partial x}\frac{D}{4}} \,. \tag{8.19}$$

with the second equality valid for a circular vessel only.

We can also move further and use the previous results to build the relationship between friction velocity, or pressure gradient, and average velocity in a vessel of diameter D as follows. The logarithmic profile is valid for a large portion of the duct. Therefore, there must be a certain distance from the wall y where the local velocity is equal to the average velocity U in the duct. Express this distance as proportional to the duct diameter $y = a'D$, with a' an unknown constant; we can write in formulas that a value a' must exist such that $\langle v_x(a'D) \rangle = U$. Using (8.17) this condition becomes

$$\frac{U}{u_*} = \frac{1}{k} \ln\left(b \frac{UD}{\nu} \frac{u_*}{U} \right); \tag{8.20}$$

where b is the new unknown constant ($b = aa'$), which was experimentally estimated in circular vessels to be $b \cong 1.13$.

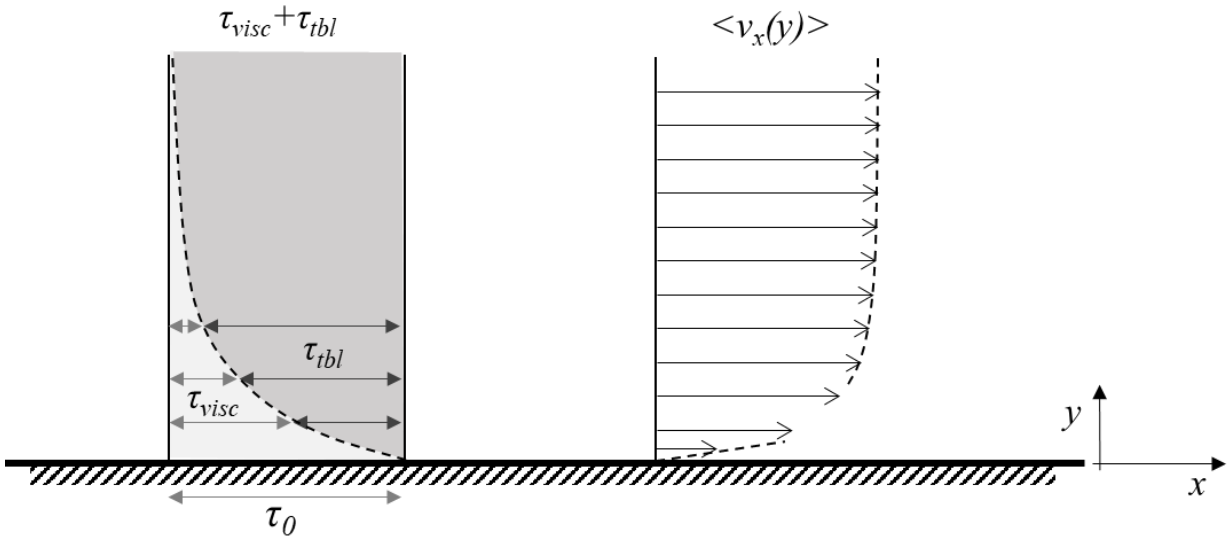

Figure 8.1. Turbulent flow over a flat surface.

Equation (8.20) provides a relationship between mean velocity and pressure gradient (or friction velocity). It is common habit introducing a friction coefficient, the dimensionless Chezy coefficient, as the ratio between mean and friction velocities, $C = \frac{U}{u_*}$. Using (8.20) the Chezy friction coefficient can be estimated in turbulent flows as

$$C = \frac{1}{k}\ln\left(b\frac{Re}{C}\right); \tag{8.21}$$

which is an implicit expression for $C(Re)$. The Chezy friction coefficient has the general role identical to the friction coefficient $f(Re)$ previously introduced in (1.13), with the two related by

$$C = \sqrt{\frac{8}{f}}, \quad f = \frac{8}{C^2}; \tag{8.22}$$

The friction coefficient was evaluated in (7.30) for the Poiseuille flow; thus the Chezy coefficient in Poiseuille flow is $= \sqrt{\frac{Re}{8}}$. The two friction coefficients can be used interchangeably, depending on the traditions in different contexts, regions or disciplines.

In unsteady and in spatially non-uniform flows, expressions for the wall shear stress and for the energy losses are not available in general, few results are in laminar flows (like those in section 7.4) and almost none in turbulent flows. The previous evaluations permit to have initial estimates for steady uniform turbulent flows.

9. Quasi Unidirectional Flow in Large Vessels

9.1. Mass Balance in Tapering and Branching Arteries

Tapered geometry, with area decreasing downstream, and branches, extracting flow from the main vessel, are characteristic elements in many arteries. Let us verify what mass balance tells about these situations. Consider first a tapered vessel and assume the duct as undeformable. The discharge $Q = UA$ is constant along the vessel, thus when area A decreases velocity U must increase following mass balance equation

$$\frac{dQ}{dx} = A\frac{dU}{dx} + U\frac{dA}{dx} = 0\ , \tag{9.1}$$

from which the velocity rate of increase would be

$$\frac{dU}{dx} = -\frac{Q}{A^2}\frac{dA}{dx} > 0\ . \tag{9.2}$$

This result does not realize physiologically because velocity must decrease when the vessel size decreases to avoid excessive friction.

Indeed, in real arteries the discharge decreases downstream $\frac{dQ}{dx} < 0$ in virtue of the side branches. At the same time, the velocity must decrease downstream $\frac{dU}{dx} < 0$ to avoid increase of friction. These considerations give a relationship between area reduction and discharge reduction. Extract the velocity gradient from mass balance (9.1) and impose that, differently from (9.2) it must be negative

$$\frac{dU}{dx} = \frac{1}{A}\frac{dQ}{dx} - \frac{Q}{A^2}\frac{dA}{dx} < 0\ . \tag{9.3}$$

Condition (9.3) can be restated as

$$-\frac{1}{Q}\frac{dQ}{dx} > -\frac{1}{A}\frac{dA}{dx}\ . \tag{9.4}$$

telling that the relative (percentage) reduction of discharge must be larger than the relative reduction of area.

A similar argument can be applied to bifurcations. Consider a vessel with area A_0 and discharge $Q_0 = U_0A_0$, where U_0 is the velocity, that bifurcates into two equal daughter vessels, each of area A_1 and discharge $Q_1 = U_1A_1$. Mass conservation tells

$$U_0A_0 = 2U_1A_1\ ; \tag{9.5}$$

where, as discussed before, we want the condition that velocity reduces in smaller vessels, $U_1 < U_0$ when $A_1 < A_0$. Using (9.5) this implies that

$$\frac{U_0}{U_1} = \frac{2A_1}{A_0} > 1\ . \tag{9.6}$$

Thus, although the individual daughter vessels reduce their size, the sum of their areas must increase. The total cross section area increase downstream at every branching.

To get an ideas of this geometric effect, consider the diameter of the Aorta, the first artery after the heart, whose diameter is approximately 3 cm. The total cross section of blood vessel at the root of Aorta is approximately $A_{Aorta} \approx 7\ cm^2$ where flow has a velocity about $U_{Aorta} \approx 1\ m/s$, thus a corresponding discharge $Q \approx 700\ \mathrm{cm}^3/s$. A similar discharge must cross the entire cross section of

the vasculature at any level of branching. Consider that at the capillary level blood velocity is smaller than 1 mm/s. This means that the total cross-section of capillary bed is close to 1 m^2.

9.2. Flow in Curved Vessels

The motion of a fluid in a curved in curved vessel presents some differences with respect to the laminar flow in a straight vessel (Poiseuille flow), because fluid particles cannot proceed by parallel trajectories given that particles on the inner side of the bend would travel a shorter path than those on the external side.

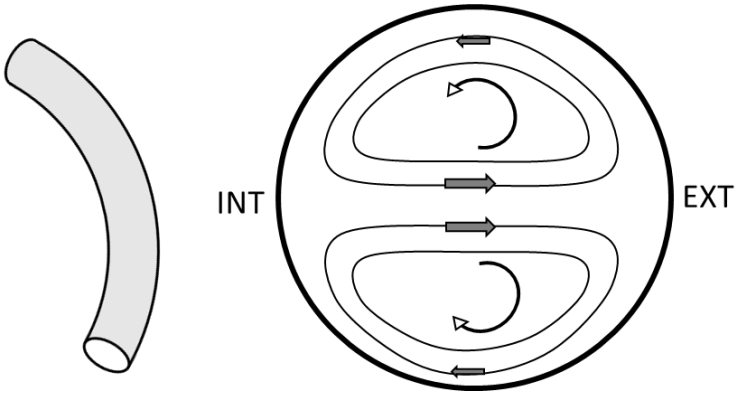

Figure 9.1. Flow in a curved vessel.

From a dynamic perspective, fluid particles are subjected to centrifugal acceleration, proportional to the square of their local velocity and inversely proportional to the curvature of the trajectory, v^2/R. Particles on the internal side have smaller radius of curvature and those near the center of the vessel have a higher velocity. Therefore, a pressure gradient develop transversally to the main flow direction pushing towards the external side across the center of the vessel. Then, for conservation of mass, flow returns from the external side to the internal side along the walls. This gives rise to a circulatory patterns of velocity on planes transversal to the main flow, as sketched in figure 9.1, which are called "secondary circulations" (Pedley, 1980).

Flow in curved vessels always develops secondary circulations. These take the form of two symmetric circulating cells when the curvature is planar, thus the system presents a mirror symmetry relative to the plane containing the curve. Most arteries, however, present a double curvature, mathematically described as curvature and torsion like a portion of a helical duct. A helical curve cannot be contained in a plane; it presents a radius of curvature on a plane and a torsion that depart from that plane. For example, a helix developing along the z direction can be described by its coordinates $x = R\cos\vartheta$, $y = R\sin\vartheta$, $z = c\vartheta$, along a generic parametric coordinate ϑ. When $c = 0$, the curve is planar and can be approximated locally by a portion of a circumference of radius R (curvature $\frac{1}{R}$ and no torsion). When $c \neq 0$ the curve cannot lay on a plane because it presents a torsion and can be approximated locally by a helix with curvature $\frac{R}{R^2+c^2}$, and torsion $\frac{c}{R^2+c^2}$. In presence of a torsion, the symmetry of the two cells is altered depending on the degree of torsion. and one secondary circulatory cell becomes wider tha the other.

Flow in real, doubly curved, arteries is composed of the main stream wise motion plus a rotation, due to the dominance of one cell to the other. The result of such a combination is that fluid particles move

downstream along helical trajectories. This is remarkably noticeable in the aortic arch like that shows in figure 9.2. Helical trajectories develop also in many bifurcations, like the carotid and the iliac bifurcations. Helical trajectories are considered to have a physiological significance because they permit a higher wash-out of the whose vessel and reduce the development of stagnation regions, which give higher chance of aggregation and development of arteriosclerosis (Caro et al., 1996).

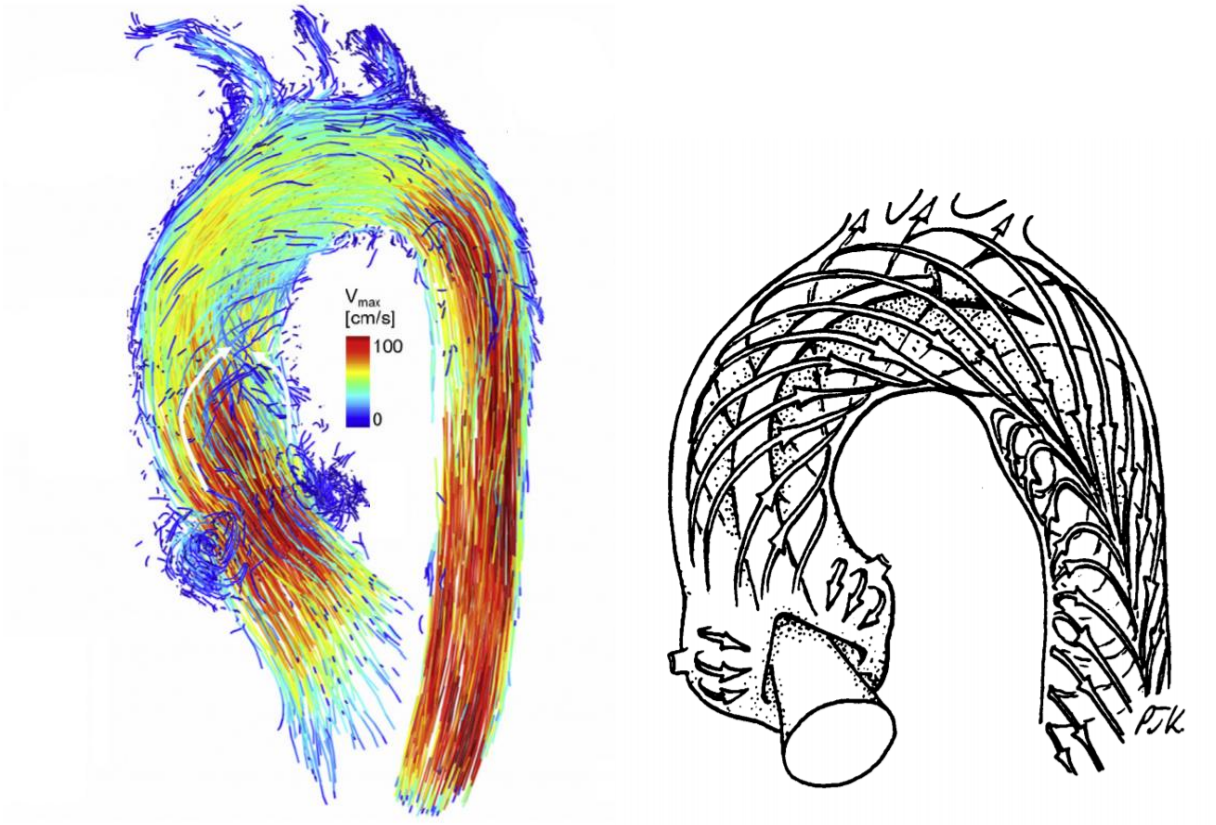

Figure 9.2. Helical trajectories in the Aortic arch. Reconstruction with magnetic resonance (left), and sketch (right). Adapted from: Oechtering et al. J Thorac Cardiovasc Surg 2020. DOI:10.1016/j.jtcvs.2019.02.127, and Kilner et al. Circulation 1993. DOI:10.1161/01.CIR.88.5.2235.

9.3. Flow in Elastic Vessels

Arteries are elastic and deform in virtue of the pressure changes due to the flowing blood inside the vessel. In order to analyze the interaction between vessel elasticity and fluid flow let us first analyze how the deformation occurs in presence of a change in pressure.

Consider a vessel or diameter D and thickness s, assumed small, subjected to a pressure increase dp inside its lumen. Vessel deformation obeys the law of motion for the elastic material, that is simplified into the equilibrium of forces, and the constitutive equation describing the relation between internal stress and deformation. With reference to figure 9.3, internal stresses are indicated by τ and are assumed constant over the thickness. Thus, the equilibrium equation is

$$\tau 2s = dpD \ . \tag{9.7}$$

Equilibrium (9.7) is evaluated in the undeformed configuration, thus making the assumption that deformations are small (rigorously speaking, infinitesimal); arterial deformation is usually less than 10% and this approximation is acceptable in this context. The constitutive equation, for small unidimensional deformations, gives the following relationship between stress and deformation

$$\tau = E\frac{dD}{D}\,; \tag{9.8}$$

where E is the Young modulus of elasticity that describes the elastic behavior of the tissue. Combination of (9.7) and (9.8) permits to relate the increase of pressure with the deformation

$$\frac{dD}{D} = \frac{dp\,D}{2Es}\,. \tag{9.9}$$

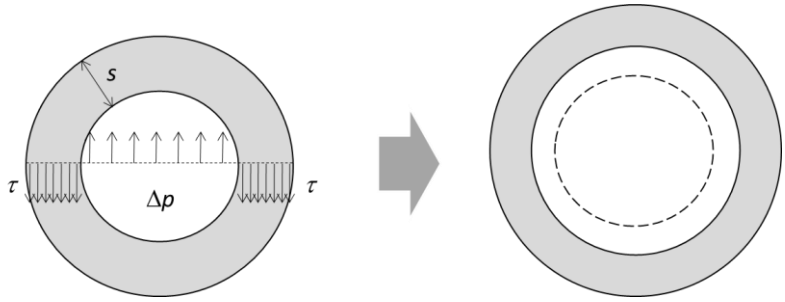

Figure 9.3. Deformation of an elastic vessel.

Then, mass conservation, permits to evaluate the change of thickness, that for small thickness gives

$$\frac{ds}{s} = -\frac{dD}{D}\,. \tag{9.10}$$

With this small background on solid mechanics, we can analyze the phenomenon of wave propagation in elastic vessels that applies to small pressure pulsations.

Consider the equation of continuity (4.7) and of motion (5.18) for a vessel

$$\begin{cases} \dfrac{dA}{dt} + U\dfrac{\partial A}{\partial x} + A\dfrac{\partial U}{\partial x} = 0\,, \\ \dfrac{dU}{dt} + U\dfrac{\partial U}{\partial x} + \dfrac{1}{\rho}\dfrac{\partial p}{\partial x} = 0\,. \end{cases} \tag{9.11}$$

In writing the second of (9.11) we made the additional assumption that friction is negligible, as it does not alter qualitatively the propagation phenomenon and would only produces an attenuation of the propagating wave.

The additional relationship needed here is the coupling between vessel size, A, and fluid pressure, p, that we can write in general, assuming uniform properties along the vessel, as a function $A(p)$, one simple example being equation (9.9). The existence of a relationship $A(p)$ permits rewriting any derivative of the vessel area, in time or space, in term of derivative of pressure

$$\frac{dA}{dx,t} = \frac{dA}{dp}\frac{dp}{dx,t}\,. \tag{9.12}$$

where the function $\frac{dA}{dp}$ characterizes the vessel elastic response. For example, in the case of infinitesimal deformation of the linearly elastic vessel discussed above, this function is obtained by the relationship (9.9) that can be recast as

$$\frac{dA}{dp} = \frac{AD}{Es} . \tag{9.13}$$

Let us simplify equations (9.11) for propagation phenomena assuming that the wave propagation velocity, the celerity c, is much larger than the physical fluid velocity, $c \gg U$. This means that the second (convective) term in both equations (9.11) can be neglected with respect to the first term because when changes in time are mainly imputable to a phenomenon of propagation then $\frac{d}{dt} \approx c\frac{d}{dx} \gg U\frac{d}{dx}$. In this approximation, and using (9.12), the system (9.11) can be rewritten

$$\begin{cases} \frac{1}{A}\frac{dA}{dp}\frac{dp}{dt} + \frac{\partial U}{\partial x} = 0 , \\ \frac{dU}{dt} + \frac{1}{\rho}\frac{\partial p}{\partial x} = 0 . \end{cases} \tag{9.14}$$

Now take the time derivative of the former and subtract the space derivative of the latter; then make the additional assumption that the term $\frac{1}{A}\frac{dA}{dp}$ is a property of the vessel that can be considered as slowly and little varying along the vessel (with respect to the variation of pressure itself), and we can neglect its space derivative. We obtain the equation for pressure

$$\frac{1}{A}\frac{dA}{dp}\frac{d^2p}{dt^2} - \frac{1}{\rho}\frac{d^2p}{dx^2} = 0 .$$

This can be rewritten in canonical form as

$$\frac{d^2p}{dt^2} - c^2\frac{d^2p}{dx^2} = 0 ; \tag{9.15}$$

which is the well-known wave equation where

$$c = \sqrt{\frac{A}{\rho}\frac{dp}{dA}} \cong \sqrt{\frac{Es}{\rho D}} . \tag{9.16}$$

is the celerity of the wave; the second equality in (9.16) being valid for the limit case of infinitesimal deformation discussed above.

The general solution of the wave equation (9.15) is

$$p(t,x) = p(x \pm ct) . \tag{9.17}$$

which represents rigid propagation of the initial pressure fields without change of shape.

For reference, using the second equality (9.16) its is possible to estimate the celerity in Aorts, where $E \approx 10^5 N/m^2$ and $s/D \approx 0.1$, between 3 to 5 m/s. Smaller vessels are relatively more rigid and celerity increases to about 10 m/s in peripheral arteries. The celerity formula (9.16) is often used to estimate the Young modulus of arteries, or directly their rigidity, which is a pathological degeneration typical of ageing. Celerity is measured by recoding the pressure peak at different positions along the vasculature whose time shift divided by the distance between the measurement points give celerity.

The linear analysis of pressure pulse propagation presented here is based on several assumption. A general nonlinear treatment is complicated and out of the present scope, more extensive analysis can be found elsewhere (Pedley, 1980). However, it is instructive to mention how the approximations would affect the general solution (9.17). The tube-law (9.13), and thus the celerity (9.16), is not constant and the vessel is more rigid when more deformed; this means that celerity is higher in correspondence to higher pressure values. Thus pressure pulse is faster in locations where pressure is

higher and slower where it is lower; this means that the peaks of the pressure wave move faster and give rise to a sharpening of the front side of the pressure wave. The transport term, that was neglected assuming velocity much smaller than celerity, would also contribute to deform the wave shape. Ultimately, a non-zero friction would produce the attenuation of the propagating wave that would be smoothed out downstream.

9.4. Impulse Propagation at a Bifurcation

At bifurcations, the pressure wave is partly transmitted downstream into the daughter vessels and partly reflected backwards. Thus, at a bifurcation there is the incident wave (*i*) moving downward, the reflected wave (*r*) propagating upward and the two transmitted waves (t_1 and t_2) downward.

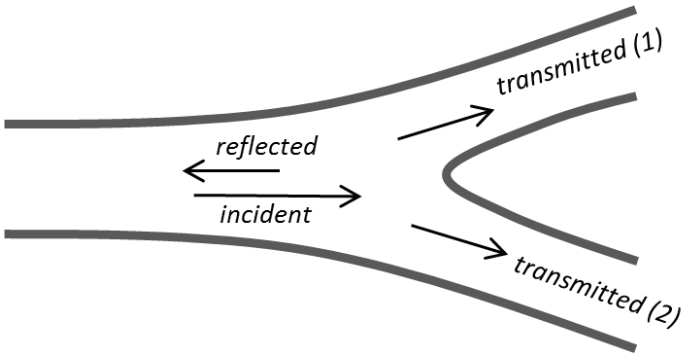

Figure 9.4. Wave propagation at a bifurcation.

In order to quantify, we can express the continuity of pressure at the junction, stating that pressure takes the same values when seen from the different vessels

$$p_i + p_r = p_{t1} = p_{t2} \; ; \tag{9.18}$$

and the conservation of mass that gives a relationship among discharges

$$Q_i - Q_r = Q_{t1} + Q_{t2} \; . \tag{9.19}$$

There are 4 unknown pressure and (9.18) provides two equations relating them; in order to move forward and use (9.19) let us find a relationship between pressure and discharge.

Consider a generic sinusoidal pressure wave $p(x,t) = F_p e^{i\omega(x-ct)}$ and the corresponding velocity wave $U(x,t) = F_U e^{i\omega(x-ct)}$; substituting them into either continuity of motion equation (9.14) we obtain that $F_U = \frac{F_p}{\rho c}$, thus that the discharge can be related to pressure through

$$Q = \frac{A}{\rho c} p \; . \tag{9.20}$$

This relationship between flow and pressure is commonly expressed

$$Q = \frac{p}{Z}, \quad Z = \frac{\rho c}{A}; \tag{9.21}$$

introducing the concept of impedance, Z, that is a characteristic of a vessel.

Substituting (9.21) in (9.19), this and (9.18) give a system of 3 equations

$$\begin{cases} p_i + p_r = p_{t1} \\ p_i + p_r = p_{t2} \\ \frac{p_i - p_r}{Z_0} = \frac{p_{t1}}{Z_1} + \frac{p_{t2}}{Z_2} \end{cases}; \tag{9.22}$$

where the subscript 0 stands for the parent vessel and the numbers for the two daughters. Substituting the first equations into the third we obtain a single equation relating incident and reflected waves

$$\frac{p_i - p_r}{Z_0} = \frac{p_i + p_r}{Z_1} + \frac{p_i + p_r}{Z_2}.$$

This can be rewritten introducing the coefficient of reflection R

$$\frac{p_r}{p_i} = R, \quad R = \frac{\frac{1}{Z_0} - \frac{1}{Z_1} - \frac{1}{Z_2}}{\frac{1}{Z_0} + \frac{1}{Z_1} + \frac{1}{Z_2}}. \tag{9.23}$$

and a coefficient of transmission can also be obtained after substituting into the first equations in (9.22).

A perfect bifurcation would be able to transmit the pressure pulse downstream with no reflection, $R = 0$, which realizes when $\frac{A_0}{c_0} = \frac{A_1}{c_1} + \frac{A_2}{c_2}$. We know (remind equation 9,6) that $A_1 + A_2 > A_0$, and that the celerity in a smaller vessel is usually higher, therefore in real bifurcation the reflection is effectively small, although non zero. Thus, most of the pressure pulse is transmitted downstream and only in small part reflected upstream.

An important place where reflected waves can be effective is the pulse propagation along the aorta where it encounters the iliac bifurcation. This phenomenon is sketched in figure 9.5. The incident pressure wave (*i*) starts from the aortic root and reaches the bifurcation after a time T *(*which is typically about 0.1 s, given by the ratio between the length of the aorta, say something about 50 cm, and the celerity, say about 5 m/s). At this point, the reflected wave (*r*) travels backwards from the bifurcation and reaches the aortic root after a time $2T$. Therefore, the pressure pulse that one measures at the root is the sum of the incident pressure wave, that is given by ventricular contraction and is made of a single impulse, plus the reflected wave that is similar to the incident wave, but it is lower in amplitude and delayed of $2T$. Physiologically, the backward travelling waves sustains the pressure at the aortic root after the initial impulse has passed and (with multiple reflections) ensures its slower decay during diastole. This higher pressure helps maintaining the aortic valve close and it is believed to help providing allowance to the coronary flow during diastole. There are, however, other mechanism involved and it is still unclear whether the role of reflection is fundamental or secondary. In any case, it is important to be aware that the time profile of pressure measured at any place does not reflect only the primary cause generating pressure (like ventricular contraction at the aortic root), it also included the contribution of reflected waves.

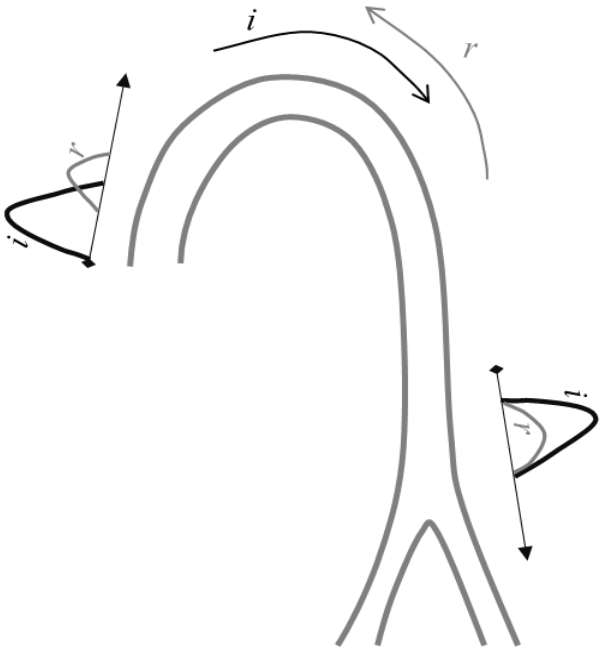

Figure 9.5. Wave reflection in the Aorta.

9.5. Collapsible Vessels

Arteries present a positive transmural pressure and typically operate under stretched conditions. There are, however, some other biological districts where internal pressure can become lower than the external value and the vessel be subjected to contraction. A contracted vessel maintains the circular geometry for small contractions only, then it undergoes to a bending instability and collapses reducing sharply its area as shown in the generic "tube law" sketched in figure 9.6. A collapsed vessel gives high resistance to the flow and increased decrease of pressure.

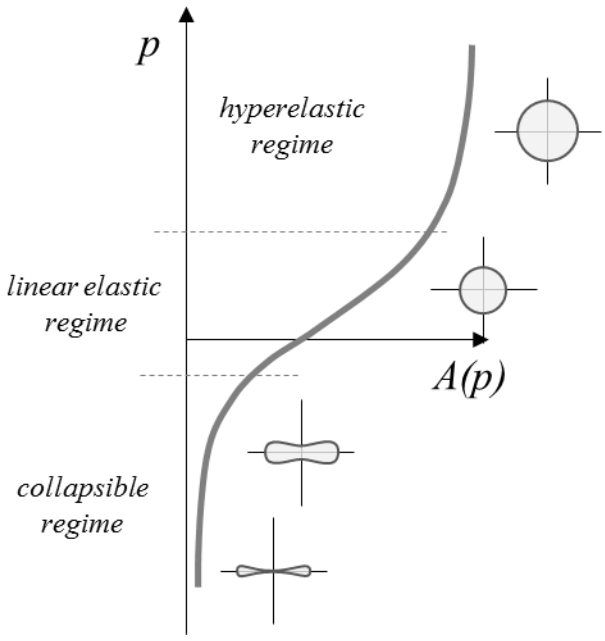

Figure 9.6. Tube law for collapsible vessels.

To exemplify possible implication, consider a vessel where flow starts with a given upstream transmural pressure p_0 at $x = 0$ that decreases downstream, for example following the Poiseuille law

$$p(x) = p_0 - \frac{128}{\pi}\mu\frac{Q}{D^4}x \ . \tag{9.24}$$

If the discharge Q increases, the pressure reduction is more pronounced along the vessels and the diameter decreases as well. Under certain conditions, when the upstream pressure is relatively low or the vessel is long enough, transmural pressure can become negative and, from the tube law, collapse. This further increases the pressure losses and decreases the pressure up to collapsing the vessel and not allowing for the flowing of the discharge.

This phenomenon is called “flow limitation” (Pedley, 1980): when the system increases the upstream pressure to try pushing a higher discharge, it may lead to more pressure losses than how pressure was increased upstream. Thus, pressure gets further reduced downstream and lead to the collapse of the vessel that does not allow flow passage. Flow limitation typically occurs in airways, where one cannot blow more than a limited air rate otherwise the airways collapse and blowing is reduced. It can occurs in male urination. It can also occur in long veins and was much studied in the giraffe jugular vein (Pedley et al., 1996).

D. ADVANCED ANALYSIS OF SEPARATED FLOW

10. Vorticity and Boundary Layer Separation

10.1. Dynamics of Vorticity

The fluid velocity was assumed so far as the fundamental quantity for describing fluid motion. Velocity is the most immediate and intuitive vector field to describe flows; however, it is not able to immediately evidence the underlying dynamical structure of a flow field, like stresses, mixing or turbulence, that depend on velocity gradients. The weakness of a description based on velocity alone is particularly critical when the fluid motion features the presence of vortex structures. In general, *vorticity* is the preferable fundamental quantity for the analysis of incompressible fluid dynamics.

Vorticity vector field was previously introduced through equations (3.6-3.7); it is mathematically defined as the *curl* is of the velocity field

$$\boldsymbol{\omega}(\boldsymbol{x}) = \nabla \times \boldsymbol{v} \; ; \tag{10.1}$$

and represents the local rotation rate of fluid particles. More than that, it allows emphasizing the structure that hides behind the flow field; it also represents a complete description of the flow and allows recovering the whole velocity field once the boundary conditions are imposed.

The interpretation of vorticity is particularly intuitive in two-dimensional flows, when only the *x* and *y* components of the velocity field exist. In this case, vorticity has only the component *z*, perpendicular to the plane of motion, $\omega = \frac{\partial v_y}{\partial x} - \frac{\partial v_x}{\partial y}$, and physically corresponds to (twice) the local angular velocity of a fluid particle. In fact, a positive vorticity corresponds to a vertical velocity, v_y, increasing horizontally, along *x*, and a horizontal velocity v_x, decreasing vertically. It is easy to understand, see figure 10.1 (leftmost sketch), that this type of velocity differences about a point represents a rotational motion.

The relevance of vorticity is not limited to local rotation. The spatial distribution of vorticity characterizes the different possible types of fluid motion, that is why vorticity is commonly considered the skeleton of the flow field and the fundamental quantity to define the flow structures as shown in figure 10.1. A *vortex* can be loosely described as a motion that possesses circular or swirling streamlines; more correctly, a vortex is actually a region of compact vorticity, a circulatory motion surrounds a region where vorticity has accumulated. In addition to vortices, the vorticity map allows recognition of any basic flow structure. A shear layer, that is an elongated layer of friction between streams with different velocities, is actually a layer of vorticity, a *vortex layer*. The boundary layer discussed previously is a vortex layer adjacent to the wall that develops because of the velocity difference between the outer flow and the fluid attached to the wall for viscous adherence. The intensity of a vortex is normally measured by its *circulation*, normally indicated with Γ, that is the integral of the velocity along a closed circuit surrounding the vortex that, by the Stokes theorem (3.9), is equivalent to the integral of all the vorticity over the vortex area contained inside the circuit. The intensity of a vortex layer is measured by the difference of velocity, the *velocity jump*, commonly indicated by γ, between the flow above and below the layer; equivalent to the line integral of the vorticity across the layer. Vortices and vortex-layers are the fundamental vorticity structure in flow fields. Their different three-dimensional arrangements and combinations give rise to the complexities of all evolving flows. The analysis of the vorticity field allows a more intimate descriptions of the motion of incompressible fluids (Kheradvar and Pedrizzetti, 2012; Panton, 2013).

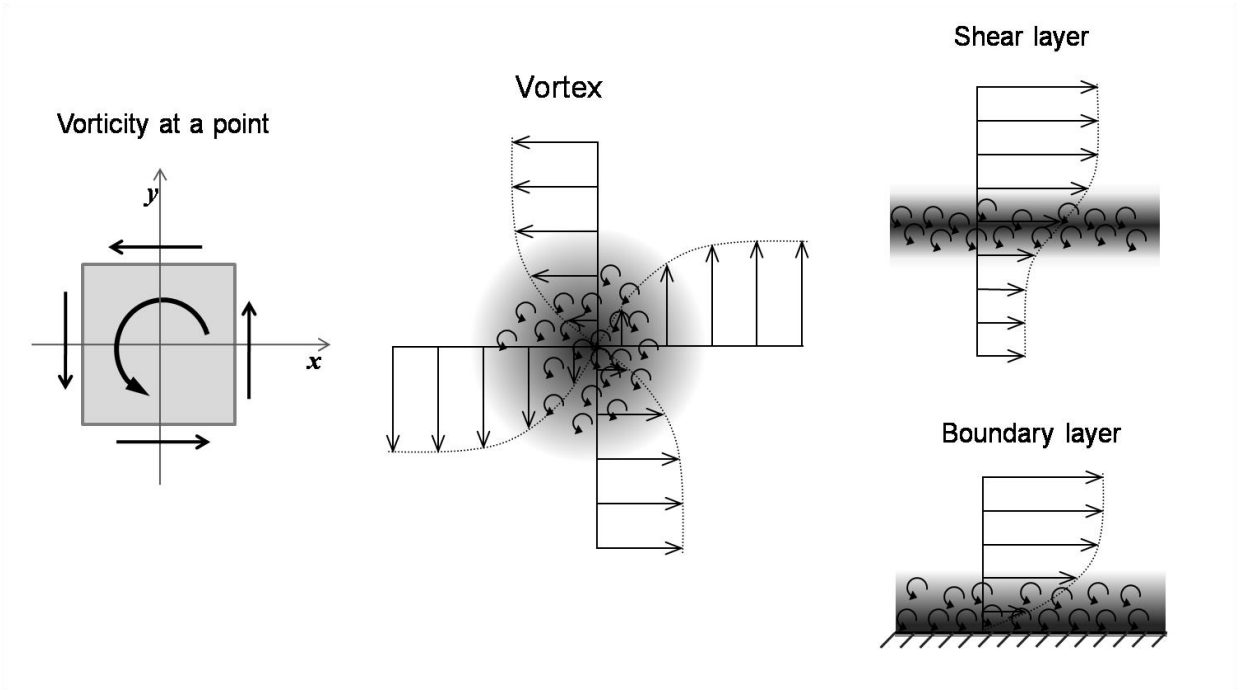

Figure 10.1. Vorticity corresponds to the local rotation of a fluid particle. The spatial distribution of vorticity gives rise to different flow structures. An accumulation of vorticity in a compact region corresponds to a vortex; an elongated distribution of vorticity corresponds to a shear layer that, when it is adjacent to the wall, is a boundary layer.

The significance of vorticity can be best appreciated by the decomposition, due to Helmholtz and Stokes, of the complete velocity field as the sum of one *irrotational* component $\boldsymbol{v}_{irr} = \nabla\phi$, expressed as a gradient of a scalar potential, plus a rotational component $\boldsymbol{v}_{rot} = \nabla \times \boldsymbol{\psi}$ expressed as the curl of a vector *streamfunction* field.

$$\boldsymbol{v} = \nabla\phi + \nabla \times \boldsymbol{\psi} \, . \tag{10.2}$$

The rotational component accounts for the whole vorticity in the flow field, while the irrotational velocity is independent from the vorticity content. Indeed, if one takes the curl of the velocity (10.2) the curl of a gradient is identically zero, and the vorticity is due to the rotational field only. Taking the curl of (10.2) we obtain an equation relating vorticity and streamfunction

$$\boldsymbol{\omega} = \nabla \times (\nabla \times \boldsymbol{\psi}) \, ; \tag{10.3}$$

showing that the irrotational velocity is not involved in vorticity.

Vice versa, the irrotational component of the velocity field is particularly simple in incompressible flows, which follows from the conservation of mass only (continuity constraint), and does not involves the equation of motion. It is immediate to verify taking the divergence of (10.2) that the divergence of a curl is identically zero. The rotational field automatically satisfies the continuity that becomes one equation for the potential only

$$\nabla \cdot \boldsymbol{v} = 0 \quad \Longrightarrow \quad \nabla^2\phi = 0 \, . \tag{10.4}$$

The linear second order equation (10.4) for the potential is of the elliptic type that is known as the Laplace equation. The Laplace equation has a unique solution and can be solved by numerous means. Conceptually, this means that the irrotational flow helps to satisfy the instantaneous balance of mass

without any evolutionary mechanism, without fluid dynamics, only kinematic congruence due to mass conservation. A flow without vorticity thus gives rise to an irrotational velocity field only that can be specified without involving the balance of momentum. The equation of motion can be then employed, when required, to derive the pressure distribution corresponding to the known the velocity field. In the case of irrotational flow, this can be performed with the simple Bernoulli equation for an ideal flow because energy dissipation is absent in an irrotational flow. In fact, the viscous term of the Navier-Stokes equation, $\nabla^2\boldsymbol{v}$, which can be written for an incompressible flow as $\nabla \times \boldsymbol{\omega}$, is identically zero for a flow without vorticity.

The velocity decomposition is the key tool to recognize the role of vortices in a flow because only the dynamics of vorticity involves the balance of momentum. A vortex, as said, is a region where vorticity has accumulated; *a vortex is not necessarily a region exhibiting circulatory motion*. It may appear as such or the circulatory pattern may remain hidden behind an irrotational contribution that covers its rotary features as shown in figure 10.2. The velocity field corresponding to an isolated vortex is purely rotational, its streamlines rotate about the vortex and describe a circulatory motion. When an irrotational contribution adds on top of the same vortex flow, it may modify the apparent vortex signature in terms of streamlines. To explain this point, let us consider the same vortex of figure 10.2 (left) with an additional uniform flow, a rigid translational motion from top to bottom that is evidently an irrotational component and does not affect the value of vorticity and of shear rate anywhere. The resulting flow fields are shown in figure 10.2 for increasing values of the uniform motion (central and rightmost panels). The three fields of figure 10.2 presents exactly the same vortex, the same gradients of velocity at all points. The rotational velocity field is always the same, corresponding to the leftmost picture, only an irrotational flow is added to the others; nevertheless, from a superficial qualitative view in term of streamlines the underlying vortex may not be equally recognizable.

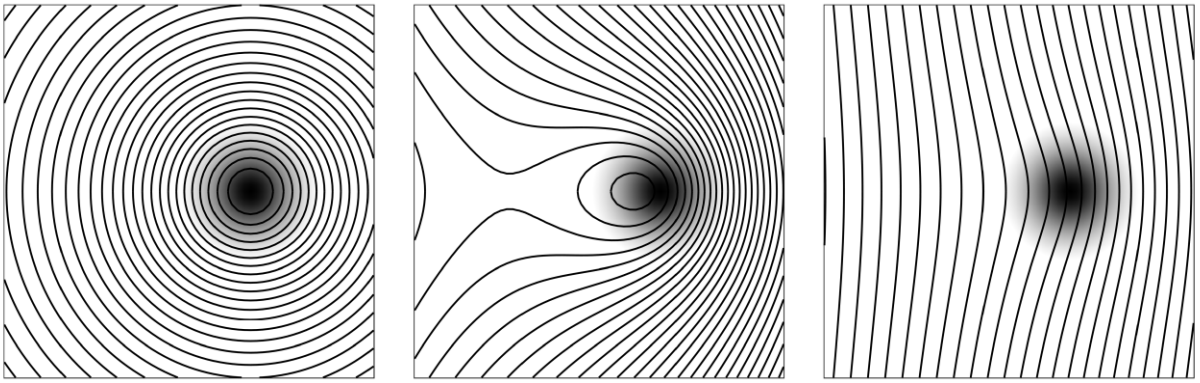

Figure 10.2. A vortex is a region where vorticity has accumulated; it is not necessarily a region exhibiting circulatory motion. A flow made of a vortex only is made of circular streamlines (left panel). The streamlines are modified when a uniform vertical flow of moderate (centre) ad high intensity (right panel) is added. In the three panels the vortex is unchanged, and so is shear in the flow.

Fluid dynamics phenomena related to evolutionary dynamics, friction, dissipation, forces, boundary layer, vortex formation etc., are dominated by the rotational part of the velocity field, while the irrotational contribution may have a role in terms of transport and mass conservation only. Therefore, a flow field can be evaluated from the dynamics of the vorticity, plus an irrotational contribution to adjust mass conservation according to boundary conditions. This is why, when the flow field is not simple or mostly unidirectional, vorticity, and vortices in which vorticity organizes, is the fundamental quantity to understand the flow evolution.

The vorticity is thus the fundamental quantity for describing a fluid flow. From the knowledge of the vorticity field only, the entire flow field inside a given geometry can be reconstructed (technically, by inversion of equation 10.3). It is therefore tempting to analyze the dynamics of a fluid motion following the dynamics of the vorticity itself. This is often useful because vorticity occupies only a small fraction of the flow field, and takes standard shapes that allow their immediate characterization.

The vorticity field has the further simplifying property that it obeys the same zero-divergence constraint of the velocity in an incompressible fluid: vorticity is a field with zero divergence (simply because the divergence of a curl is zero by definition)

$$\nabla \cdot \boldsymbol{\omega} = 0 \,. \tag{10.5}$$

This means that the vorticity field cannot take arbitrary geometric shapes. Therefore vorticity typically develops in terms of vortex tubes (whose associated velocity circulates around the tube) or of vortex layers (associated with a difference of velocity, a shear rate, across the layer). Moreover, the total vorticity contained inside a vortex tube is conserved like the discharge in a tube of flow: a vortex tube cannot terminate abruptly, and must either be a closed ring or terminate by spreading into a vortex layer. Thus we will use this knowledge to get a deeper description of complex cardiovascular flows.

Vorticity is an evolving field that follows deterministic evolutionary laws. Their mathematical expression can be immediately derived from the conservation of momentum: namely, the Navier-Stokes equation (5.35) rewritten in terms of vorticity. Indeed, taking the curl of the Navier-Stokes equation (5.35), and reminding that derivatives are linear operators and derivatives can be exchanged with the curl operator, we get

$$\frac{\partial \boldsymbol{\omega}}{\partial t} + \nabla \times (\boldsymbol{v} \cdot \nabla \boldsymbol{v}) = \nu \nabla^2 \boldsymbol{\omega}; \tag{10.6}$$

where the pressure term, like any other conservative force, disappears because the curl of a gradient is identically zero. The second term in (10.6) requires some care. Consider the *x*-component of this term in a system of Cartesian coordinates

$$\begin{aligned} \nabla \times (\boldsymbol{v} \cdot \nabla \boldsymbol{v})|_x \quad &= \frac{\partial}{\partial y}\left(v_x \frac{\partial v_z}{\partial x} + v_y \frac{\partial v_z}{\partial y} + v_z \frac{\partial v_z}{\partial z}\right) - \frac{\partial}{\partial z}\left(v_x \frac{\partial v_y}{\partial x} + v_y \frac{\partial v_y}{\partial y} + v_z \frac{\partial v_y}{\partial z}\right) = \\ &= v_x \frac{\partial}{\partial x}\left(\frac{\partial v_z}{\partial y} - \frac{\partial v_y}{\partial z}\right) + v_y \frac{\partial}{\partial y}\left(\frac{\partial v_z}{\partial y} - \frac{\partial v_y}{\partial z}\right) + v_z \frac{\partial}{\partial z}\left(\frac{\partial v_z}{\partial y} - \frac{\partial v_y}{\partial z}\right) + \\ &+ \frac{\partial v_x}{\partial y}\frac{\partial v_z}{\partial x} + \frac{\partial v_y}{\partial y}\frac{\partial v_z}{\partial y} + \frac{\partial v_z}{\partial y}\frac{\partial v_z}{\partial z} - \frac{\partial v_x}{\partial z}\frac{\partial v_y}{\partial x} - \frac{\partial v_y}{\partial z}\frac{\partial v_y}{\partial y} - \frac{\partial v_z}{\partial z}\frac{\partial v_y}{\partial z} \,. \end{aligned}$$

Recognize now that the terms in bracket are the *x* vorticity component, and use the continuity equation to group 2nd and 3rd terms and 5th and 6th terms in last line as follows

$$\begin{aligned} \nabla \times (\boldsymbol{v} \cdot \nabla \boldsymbol{v})|_x \quad &= \boldsymbol{v} \cdot \nabla \omega_x + \frac{\partial v_x}{\partial y}\frac{\partial v_z}{\partial x} + \left(\frac{\partial v_y}{\partial y} + \frac{\partial v_z}{\partial z}\right)\frac{\partial v_z}{\partial y} - \frac{\partial v_x}{\partial z}\frac{\partial v_y}{\partial x} - \frac{\partial v_y}{\partial z}\left(\frac{\partial v_y}{\partial y} + \frac{\partial v_z}{\partial z}\right) = \\ &= \boldsymbol{v} \cdot \nabla \omega_x + \frac{\partial v_x}{\partial y}\frac{\partial v_z}{\partial x} - \frac{\partial v_x}{\partial x}\frac{\partial v_z}{\partial y} - \frac{\partial v_x}{\partial z}\frac{\partial v_y}{\partial x} + \frac{\partial v_y}{\partial z}\frac{\partial v_x}{\partial x} = \\ &= \boldsymbol{v} \cdot \nabla \omega_x + \frac{\partial v_x}{\partial y}\frac{\partial v_z}{\partial x} - \frac{\partial v_x}{\partial x}\frac{\partial v_z}{\partial y} - \frac{\partial v_x}{\partial z}\frac{\partial v_y}{\partial x} + \frac{\partial v_y}{\partial z}\frac{\partial v_x}{\partial x} + \left(\frac{\partial v_x}{\partial y}\frac{\partial v_x}{\partial z} - \frac{\partial v_x}{\partial y}\frac{\partial v_x}{\partial z}\right) ; \end{aligned}$$

where in the last passage we added a terms that equal to zero. Now group the terms properly to give

$$\begin{aligned} \nabla \times (\boldsymbol{v} \cdot \nabla \boldsymbol{v})|_x \quad &= \boldsymbol{v} \cdot \nabla \omega_x - \frac{\partial v_x}{\partial x}\left(\frac{\partial v_z}{\partial y} - \frac{\partial v_y}{\partial z}\right) - \frac{\partial v_x}{\partial y}\left(\frac{\partial v_x}{\partial z} - \frac{\partial v_z}{\partial x}\right) - \frac{\partial v_x}{\partial z}\left(\frac{\partial v_y}{\partial x} - \frac{\partial v_x}{\partial y}\right) = \\ &= \boldsymbol{v} \cdot \nabla \omega_x - \boldsymbol{\omega} \cdot \nabla v_x \end{aligned}$$

Reinserting this result into (10.6) gives the *vorticity equation*

$$\frac{\partial \boldsymbol{\omega}}{\partial t} + \boldsymbol{v} \cdot \nabla \boldsymbol{\omega} = \boldsymbol{\omega} \cdot \nabla \boldsymbol{v} + \nu \nabla^2 \boldsymbol{\omega}; \tag{10.7}$$

which represents the Navier-Stokes equation expressed in terms of vorticity.

Despite the apparent mathematical complexity, the simple qualitative inspection of this equation permits to extract some important concepts regarding vortex dynamics. For example, it can be immediately recognized that the vorticity equation does not contain the pressure (or any conservative force like gravity). In fact, the distribution of pressure has no direct influence on vortex dynamics; on the contrary, however, pressure depends on vorticity that rules friction and energy losses.

A first property of the vorticity evolution is that if vorticity is zero at one instant it remains zero afterwards. This is seen by inspection of equation (10.7) where all terms are identically zero when vorticity is zero thus its time derivative is also null. This states that vorticity cannot be created inside the fluid, thus it can only be generated at the interface between the fluid and the boundary. This apparently simple fact is a fundamental element for the study of vortex dynamics: in incompressible flows vorticity does not appear spontaneously within the fluid, *the only place where vorticity can be created is at the boundary between fluid and tissue*. Indeed, the issue of the generation of vorticity, and vortex formation in particular, is a key one and it will carefully discussed in the next section.

Equation (10.7) tells that, once vorticity is somehow generated, it is subjected to few possible evolutionary phenomena. The primary one is that vorticity is transported with the flow as if it were a passive tracer (although not effectively passive, because velocity is related to vorticity itself). This phenomenon is provided by the two terms on the left hand side of (10.7) that represent the Lagrangian time derivative of vorticity over a particle moving with the flow. The first term is the time variation of vorticity at the fixed position crossed by the particle; the second term gives an increase of vorticity when a particle points in a direction along which vorticity grows (i.e. when velocity is aligned with a positive gradient of vorticity). They take a form analogous to, for example, the first two terms in equation Navier-Stokes equation (5.35), describing the acceleration on a moving particle. Therefore, vorticity moves with the local fluid velocity, like a tracer, and can further change its value in virtue of additional phenomena ruled by the two terms on the right hand side of (8.2).

The first represents the phenomenon of increase of vorticity by *vortex stretching*. Consider a small cylinder of fluid along whose axis the velocity increases, thus velocity is lower at the base and higher at the top of the cylinder; as time proceeds the cylinder elongates, it is stretched by the velocity gradient (and shrunk in the transversal direction for the conservation of mass). Well, the vorticity vector behaves in the identical manner as material fluid, when fluid is stretched the vorticity vector is stretched as well and the vorticity value increases. This term represents the stretching and turning of vortex lines as if they were lines of fluid. A further important aspect of this term is that it is exactly zero in a two-dimensional flow. In a two-dimensional flow, the vorticity is perpendicular to the plane of motion and there is no velocity gradient out of plane: vorticity stretching is intrinsically a three-dimensional effect.

Before turning the attention to the last term containing the viscous effects, let us recapitulate the dynamics of vorticity in absence of viscous effects. First, an element of fluid that contains no vorticity remains without vorticity afterwards. This is the first of the three Helmholtz's laws for inviscid flow. Then, the vorticity is a vector that behaves like a small string element of fluid. It moves with the flow and it is stretched and tilted with it. This is essentially the second Helmholtz's law. The third law, follows from the fact that vorticity is a field with zero divergence and the total vorticity contained

inside a vortex tube (or a vortex filament, when the tube is thin) is conserved along the filament while it moves with the flow.

The picture becomes extremely simple and intuitive in a two-dimensional flow, or in a motion that is locally approximately two-dimensional. In this case, the vorticity vector has a unique nonzero component perpendicular to the plane of motion, therefore it loses its vector character and can be considered as a scalar. Stretching is absent and vorticity is simply transported with the flow. The value of vorticity is stuck onto the individual fluid particles, vorticity simply accumulates into vortex patches, redistributes into vortex layer, accordingly to the motion of fluid particles.

The last, viscous term in the vorticity equation (10.7) introduces the effects of friction and energy dissipation in terms of vorticity. The action of viscosity on vorticity is analogous to that of heat diffusion or diffusion of a tracer like ink or smoke. The distribution of vorticity is smoothed out by viscosity; a sharp vortex reduces progressively its local strength while it widens its size in a way that the total vorticity is conserved. In general, the diffusion process is of a simple interpretation. Like in any diffusive process, the rate of diffusion is higher in presence of sharp vorticity gradients, therefore the magnitude of viscous dissipation become increasingly relevant where vorticity presents changes over short distances. This leads to the most important aspect of energy losses in fluid motion: *viscous dissipation is most effective at small scales*. Viscous diffusion, for example, gives rise to the annihilation of close patches of opposite sign vorticity. This has a peculiar consequence in three-dimensions when two opposite-sign vortex filaments get in contact, the opposite-sign vorticity locally annihilates and oppositely pointing vortex lines (that cannot terminate into the flow) reconnect. The viscous reconnection phenomenon is the underlying mechanism leading to topological changes, metamorphoses of three-dimensional vortex structures, and increased dissipation by turbulence.

In summary, the dynamics of vorticity is made by its transport with the fluid elements, intensification by three-dimensional straining of such fluid elements, and smoothing by viscous diffusion. A dynamics that see vorticity arranged into tubular and sheet-like structures ensuring a continuity of vortex lines. Some exemplary realizations of vorticity dynamics will be discussed later; before then, however, it is necessary to address the aspect of the generation of vorticity.

10.2. Boundary layer separation and vortex formation

As said above, in incompressible flows vorticity cannot be generated within the fluid. Vorticity can only develop from the wall in consequence of viscous adherence between the fluid and the bounding tissue. Vorticity is produced because of the no-slip condition at the interface between the fluid and the solid surface; it then progressively diffuses away from the wall through the viscous diffusion mechanism to produce a layer of vorticity at the boundary. The boundary layer thickness corresponds to the length at which the viscous diffusion penetrates into the flow, which is proportional to $\sqrt{\nu t}$ as taught from equation (7.12). The boundary layer was introduced in chapter 7 as the region adjacent to the wall where the velocity rises from the zero value that it takes at the boundary to a finite value away from it. However, its interpretation as a vorticity layer is more intuitive for addressing vortex formation processes.

The boundary layer has a fundamental importance in fluid mechanics as it represents the *unique* source of vorticity in a flow field. Consider the a set of Cartesian coordinates at the wall, with x and y parallel to the wall and z perpendicular to it, at the wall the normal vorticity vanishes for the adherence condition and the others take a simple form

$$\omega_x = \frac{\partial v_z}{\partial y} - \frac{\partial v_y}{\partial z} = -\frac{\partial v_y}{\partial z} ,$$
$$\omega_y = \frac{\partial v_x}{\partial z} - \frac{\partial v_z}{\partial z} = +\frac{\partial v_x}{\partial z} ,$$
$$\omega_z = \frac{\partial v_y}{\partial x} - \frac{\partial v_x}{\partial y} = 0 ;$$

therefore, assuming x as the local direction of the velocity, the adherence generates the vorticity component ω_y perpendicular to it (as if the flow moves over wheels, with vorticity representing their axis) and vorticity generation begins, locally, as a two-dimensional phenomenon. It is also immediate to recognize that the components of vorticity at the wall correspond to the wall shear rate and, after multiplication with viscosity, to the wall shear stress (WSS)

$$\begin{aligned} \mathrm{WSS_x} &= \tau_{0_x} = \mu\omega_y , \\ \mathrm{WSS_y} &= \tau_{0_y} = -\mu\omega_x ; \end{aligned} \qquad (10.8)$$

Which, we'll show later, takes particular relevance in cardiovascular physio-pathology. Therefore the wall vorticity is often employed interchangeably with wall shear rate (sometimes, given the constancy of viscosity, also with wall shear stress).

In small vessels, the thickness of the boundary layer is comparable to the diameter and fills the entire flow field. At such small scales, as found in arterioles and capillaries, viscous diffusion is the dominant phenomenon; vorticity is generated for adherence and quickly diffuses into the whole domain and compact vortices, with rare exceptions, are absent. On the contrary, in large blood vessels or inside the cardiac chambers, the boundary layer often remains thin and is capable to penetrate for diffusion over a small fraction of the vessel size. Indeed, until it remains attached to the wall, it has a relatively minor influence to the flow and only represents a viscous slipping cushion for the outside motion. However, under many circumstances, it happens that such a thin boundary layer separates from the wall and enters into the bulk flow. This is the process of *boundary layer separation*, when thin layers of intense vorticity enter into the flow and give local accumulation of vorticity and eventually to the formation of compact vortex structures.

Boundary layer separation is normally a consequence of the local deceleration of the flow. The process of boundary layer separation is sketched graphically in figure 10.3. When flow decelerates, the upper edge of the boundary layer is subjected to deceleration as well and, because of incompressibility, when the longitudinal velocity decreases downstream the vertical velocity must increase from the zero value at the wall and produces the growth of the thickness of the vortex layer at the same location. This tongue of vorticity is lifted and strained by the outside flow while the vorticity value at the wall below decreases. As this process progresses, opposite sign wall vorticity appears and a secondary boundary layer develops below the separating shear layer. The separation point at the wall, from where the separation streamline departs, corresponds to the place where vorticity is zero. The secondary vorticity is itself decelerated in its backward motion and is lifted up. Eventually, it cuts the connection between the original boundary layer and the separating vorticity that detaches and enters into the flow. This follows because the local velocity transports vorticity but the latter is not a passive tracer, it is made of velocity gradients that, when transported, alter the underlying structure of the flow itself. Figure 10.3 shows qualitative velocity profiles and streamlines that develop in correspondence of the separating vorticity field.

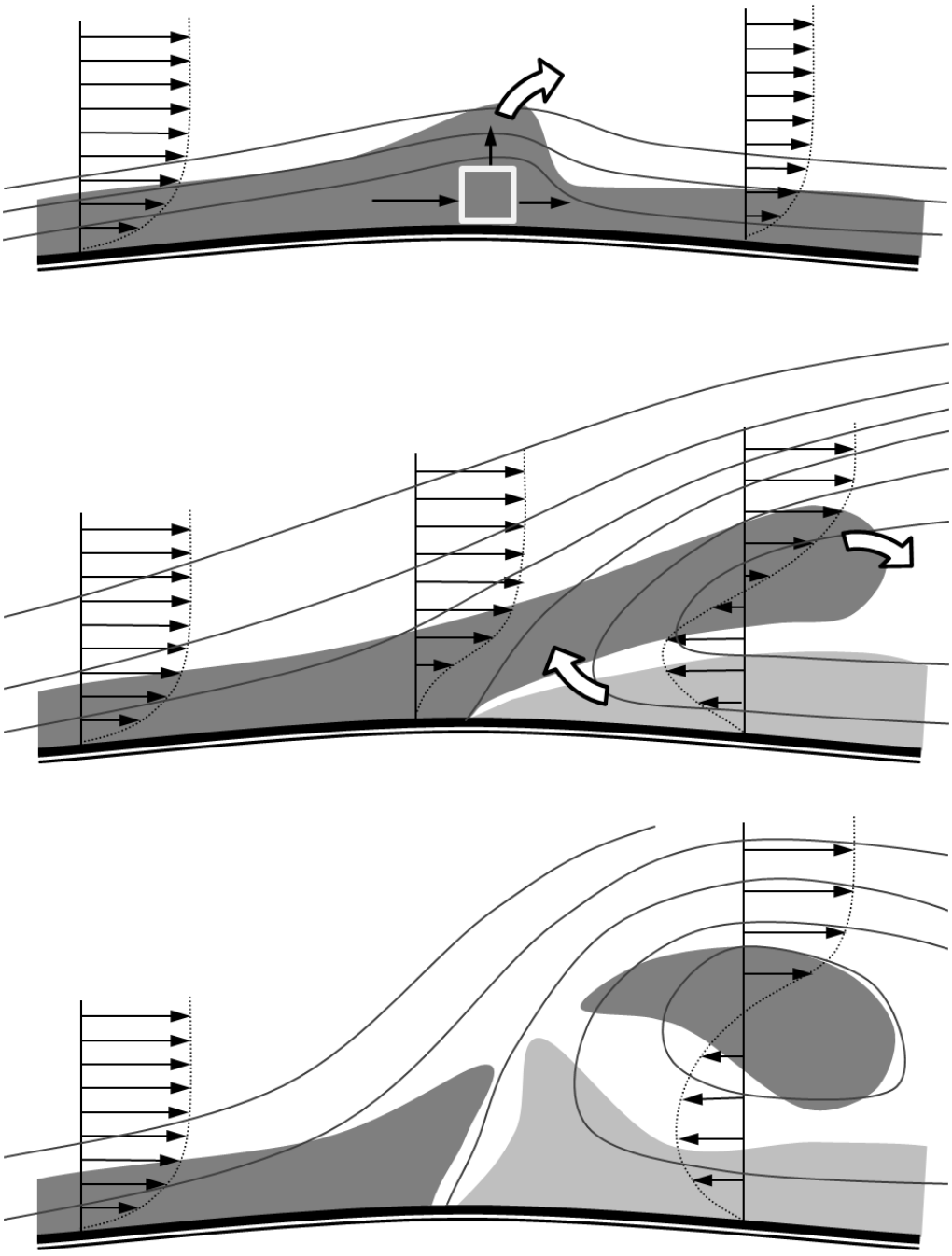

Figure 10.3. Sketch of the boundary layer separation process. The dark gray indicates layers with clockwise vorticity, the light gray is counter-clockwise; streamlines and velocity profiles are drawn. The deceleration of the flow produces a local thickening of the boundary layer due to mass conservation balance (upper panel). Such emerging vorticity is therefore lifted and transported downstream by the external flow (see arrows). A shear layer then extends away from the wall and produces a secondary boundary layer, with oppositely rotating vorticity (mid panel). The separated clockwise vorticity tends to roll-up while the secondary layer lifts up for the same initial mechanism, because it backward motion is decelerating (see arrows). Eventually, the separating vortex layer detaches from the boundary layer and becomes an independent vortex structure.

Boundary layer separation is thus a consequence of the local deceleration of the flow. In other terms, separation develops in presence of an *adverse pressure gradient* (pressure growing downstream) that pushes from downstream and decelerates the stream. The most common way to have an adverse pressure gradient is that of a geometric change: a positive curvature of the wall, like an enlargement in a vessel. In this case, the velocity decreases, for mass conservation, kinetic energy decreases and the value of pressure increases for the Bernoulli balance. Therefore, boundary layer separation develops behind a stenosis, or at the entrance of an aneurism. An extreme case of geometric change is that of a sharp edge, this is often found at the entrance of a side-branching vessel, and certainly on the trailing edge of the leaflets of the cardiac valves. In the case of sharp edges, the flow deceleration is so local that the position of boundary layer separation is definitely localizable at the edge. The vorticity that developed on the upstream side detaches at the sharp edge and leaves the tissue tangentially.

The process of boundary layer separation involves a competition between the tendency of vorticity layers to become progressively sharper and their tendency to become thicker for viscous diffusion. Therefore, sharp well recognizable vortices are generated in large vessels where the role of viscous diffusion is smaller. Vice versa, in small vessels, the process of boundary separation is often inhibited by the dominance of diffusion that quickly smooths out the vorticity.

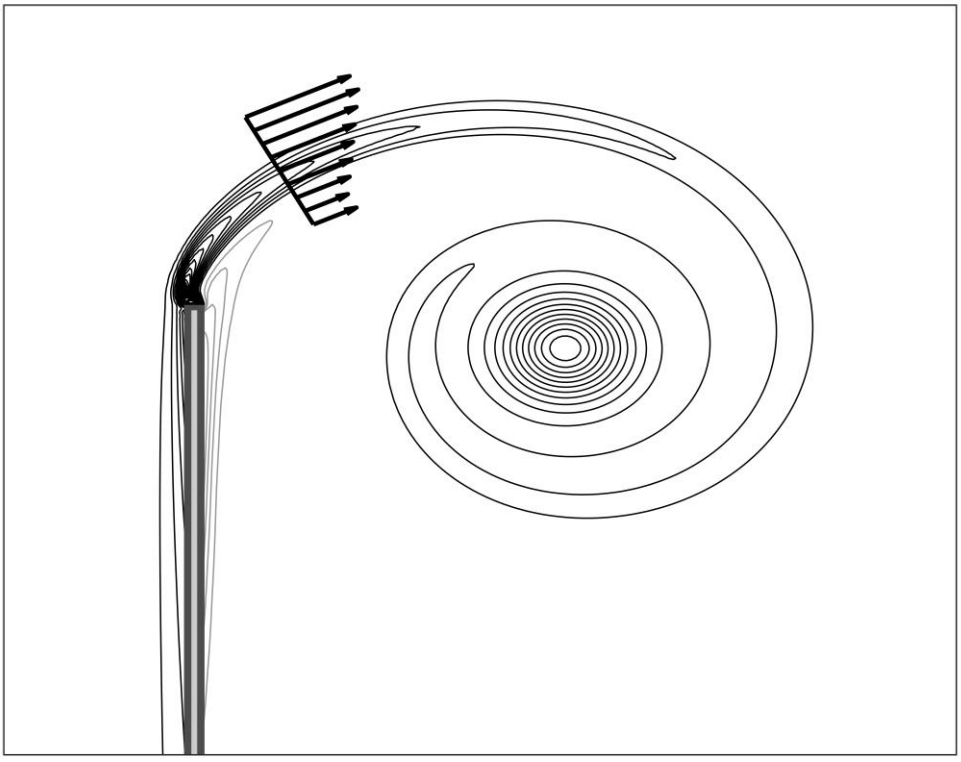

Figure 10.4. Vortex formation from a sharp edge obstacle. The shear layer separates from the upstream "wetted" wall and rolls-up into a spiral. The tight turns in the inner part of the spiral spread for viscous diffusion into the inner core of the formed vortex.

Geometric changes are not the unique possible sources for the development of a flow deceleration. Immediately downstream of branch sucking fluid away from a main vessel, the velocity reduces and

an adverse pressure gradient develops. Similarly, boundary layer separation develops for the so-called *splash* effect, when a jet reaches a wall and produces high velocity streamlines that decelerate when they are deflected along the wall. Finally, the local flow deceleration is often produced by previously separated vortices. A vortex that gets close to a wall gives rise to a localized increase (or reduction, depending on its circulation) of the flow velocity at the wall below, and a corresponding deceleration immediately downstream (or upstream). The vortex-induced boundary layer separation is a frequent phenomenon that may become particularly critical in some applications. In fact, the area of principal separation is often localizable and properly protected, whereas a separation induced downstream due to a previously separated vortex may occur at unexpected locations.

The separation of the boundary layer represents the starting phase of the vortex formation process. The featuring property of any shear layer is the difference of velocity between its two sides: the farther side of shear layer that detaches from the wall moves with a speed that is higher than the side closer to the wall. Therefore, the separating shear layer curves on itself and eventually rolls-up into a tight spiral shape. Now, during the rolling-up process, the distance between two successive turns of the vortex layer progressively reduces, with the closest neighboring turns at the center of the spiral. The viscous diffusion process smears out this tight spiraling structure into by a compact inner core with a smooth distribution of vorticity. The roll-up and the formation of an isolated vortex behind a sharp edge obstacle are shown in figure 10.4.

The vortex formation from a smooth surface is still described by the picture given above, where a few additional elements of complexity can be emphasized. First, the actual position of separation depends on the local flow structure; it cannot be preliminarily identified and may even change during time. Furthermore, the separation from a smooth surface is inevitably accompanied by a more direct interaction between the forming vortex and the nearby wall when the viscous dissipation effects normally support the formation of smoother vortex structures.

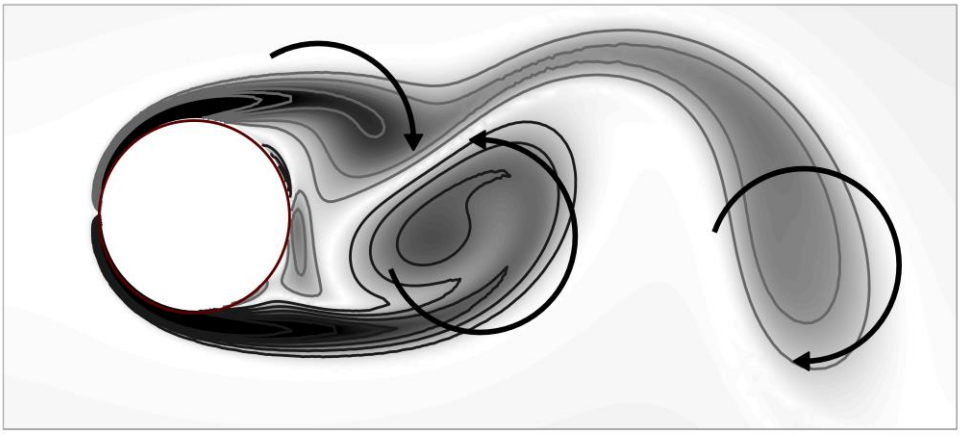

Figure 10.5. Formation of vortices behind a circular cylinder. Oppositely rotating vortices separate from the two sides of the body in an alternating sequence. The previously separated clockwise vortex detached from the upper wall translated downstream, a counter-clockwise vortex has been formed from the lower wall, and a novel clockwise vortex is under formation from the wall above.

One typical example of the external separation from the smooth surface of a bluff body is shown in figure 10.5 featuring the formation of oppositely rotating vortices from the two sides of a circular cylinder. In such an example, vortices interact and influence the opposite separation process

eventually producing a sequence of alternating vortices known as the von Karman street that is usually found behind bluff bodies. The development of alternating vortices is quite a common phenomenon when previously separated vortices may influence vortex formation in nearby regions. It is also present, with some differences, in internal flows when a vortex formed on one side of a vessel creates a vortex-induced separation on a facing wall. That, in turn, may induce a weaker further separation in a sort of wavy pattern extending and decaying downstream.

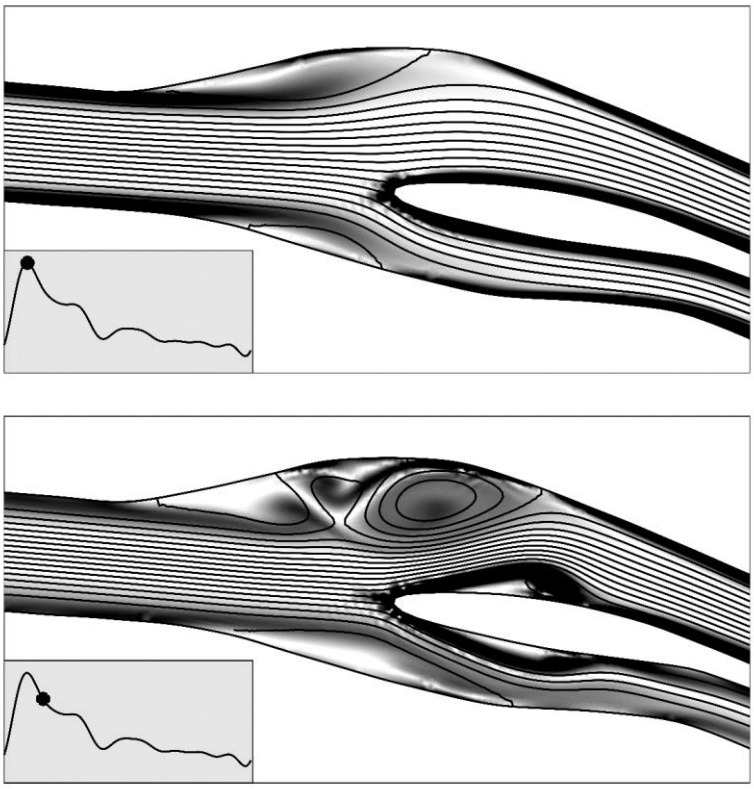

Figure 10.6. Formation of vortices in a model of a carotid bifurcation. The accelerating systolic flow (upper panel, at peak systole) leads to a smooth boundary layer separation at the carotid bulb. After the peak (lower panel) the vortex just formed at the bulb either interacts with the bulb boundary layer creating multiple small vortices, and gives rise to a vortex-induced secondary separation in the oppositely facing wall of the internal carotid artery. The same phenomena in a much weaker version are noticeable also on the opposite side at the entrance in the external carotid artery.

The internal separation, with the following formation of a vortex inside of a vessel is in general a smoother phenomenon because the presence of confining walls does not allow vortices to grow into large structures, keeps vortices more constrained within smaller scales and is more influenced by viscous diffusion. Nevertheless, the presence of a vortex inside a vessel may change the entire flow. It has a blocking effect that locally deviates the streamlines modify the wall shear stress distribution, possibly producing further separations. It changes the unsteady pressure drop and in a branching duct, it may affect the relative flows division in the daughter vessels. An example is given in figure 10.6 that reports the vortex formation in the bulb of a carotid bifurcation. During the systolic acceleration, the boundary layer separates tangentially from the common carotid artery and develops a smooth roll-up within the bulb close to the nearby wall. During deceleration, the formed vortex locally affects the wall shear stress inside the bulb with multiple opposite sign wall vorticity. It has a blocking effect

that deviates the streamlines at the entrance of the internal carotid artery into a faster jet. It produces secondary vortex-induced separation inside the internal carotid; that eventually (not shown in the picture) gives a secondary vortex formation and a further small separation little downstream.

A peculiar phenomenon associated with the vortex formation process can be outlined when the flow enters from a small vessel into a large chamber forming a jet whose head is the forming vortex. Here, after the very initial roll-up phase, a measure of the length of such a jet is given by the product of Ut where U is the velocity at the opening and t is the time. In this case it is enlightening to define a dimensionless *vortex formation time*, VFT, as the ratio of the jet length with respect to the diameter of the opening D

$$VFT = \frac{Ut}{D}; \tag{10.9}$$

The formation time represents a dimensionless number that characterizes the progression of vortex growth and allows a unitary description under different conditions. In reality, the definition of formation time has a more profound physical meaning. The separating shear layer has a strength given by the jump of velocity between its two sides, given approximately by U, and translates downstream with a velocity that is something like the average of velocity on the two sides of the layer, which is $U/2$, thus it feeds the circulation Γ of the forming vortex at a rate

$$\frac{d\Gamma}{dt} \cong \frac{1}{2}U^2; \tag{10.10}$$

The formation time thus also represents the dimensionless measure of the vortex strength, the circulation Γ, normalized with UD. The definition (10.9) can be extended to the case when either U or D vary during time, by integration of the ratio U/D during the period of vortex formation

$$VFT = \int \frac{U(t)}{D(t)} dt.$$

10.3. Three-dimensional Vortices and their Interactions

The vortex formation process described above is given in terms of two-dimensional pictures. It allows an immediate and intuitive understanding of the fundamental phenomenon because the initial phase of any vortex formation process is, with rare exceptions, locally two-dimensional and the three-dimensional organization of the vorticity enters into play at some later stages.

The simplest case of three-dimensional vortex formation is that from a circular orifice, in that case vortex formation has a circular symmetry and the forming three-dimensional vortex tube has the shape of a ring. Vortex rings are well known objects of fluid dynamics, which are easily generated using a piston-cylinder apparatus. A vortex ring is a stable vortex structure, it has an axial symmetric and vortices with a shape close to a ring also tend to the axisymmetric shape by an internal homogenization. Because of their stability, vortex rings are often encountered in nature, including when puffing smoke out of the mouth.

Figure 10.7 shows one instant during the formation of a vortex ring behind a circular orifice. The vorticity distribution on a transversal section (left panel) shows the shear layer separating from the orifice that eventually rolls-up into the jet head; however it must be kept in mind that this planar picture corresponds to a three-dimensional vortex structure that is more difficult to represent on paper. The vortex ring corresponding to the vortex core is shown (right panel) to emphasize the main element of the three-dimensional vortex. In general, however, there is some ambiguity on the effective delineation of a vortex boundary. This is not a big issue in two-dimensional systems when the entire

vorticity field can be shown in color scale on the picture plane and the different elements of the vortex structure are immediately recognized, from the separating shear layer, to the rolling-up spiral, to the vortex core. However, this case is particularly simple because the vorticity has an axial symmetry and only the azimuthal component: this flow is conceptually planar. Nevertheless, its three-dimensional representation, on the right panel of figure 10.7, certainly contains less complete information, and the choice of the vortex core boundary severely influences the three-dimensional structure that is eventually visualized.

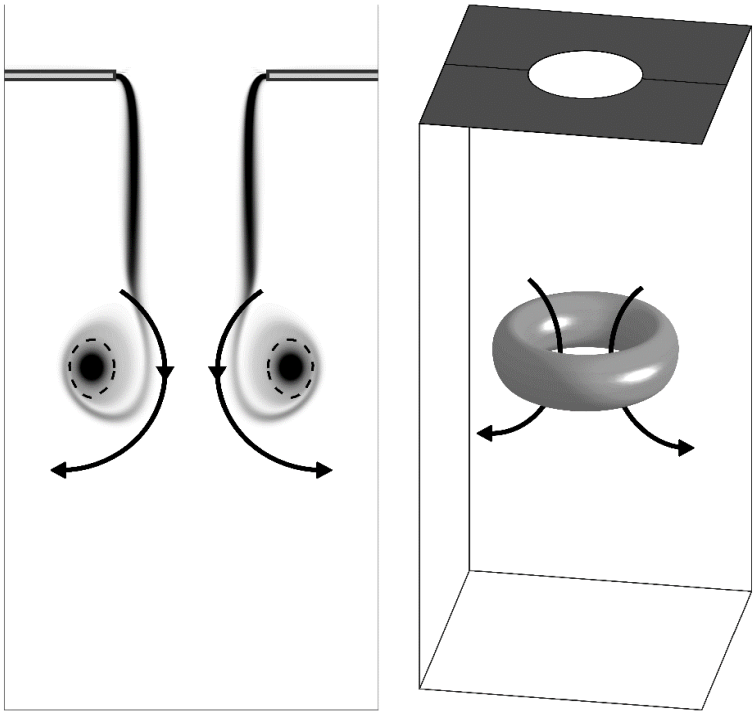

Figure 10.7. Formation of a vortex ring from a circular sharp orifice. Left panel: distribution of vorticity on a transversal cross-cut; the vortex core is indicated with a dashed line. Right panel: three-dimensional view of the vortex ring core.

A three-dimensional vortex ring present a *self-induced velocity* that is due to the curvature of the vorticity lines (lines everywhere tangent to the vorticity field). This follows from the relation between velocity and vorticity, a curved vortex tube corresponds to a velocity field made of a rotation around the tube, when the tube is curves this rotation also induces a translation of the tube itself. Thus, once formed, a ring continues to translate downstream for its own self-induced velocity field. Such a self-induced velocity gives rise to a peculiar limiting process of three-dimensional vortex formation: during its formation, the vortex ring is continuously fed by the rolling-up shear layer separating from the orifice edge, therefore its circulation grows and the self-induced vortex translation velocity of the vortex ring rises until it exceeds the velocity of the separating shear layer. At this point, the primary vortex detaches from the layer behind with a phenomenon known as *pinch-off*. At the same time the newly separated vorticity cannot reach the escaped vortex and eventually rolls-up in its wake. This limiting process occurs for a critical value of the vortex formation time that is about $VFT_{cr} \cong 4$. Above this limit, the vortex ring cannot grow as a unique structure and multiple vortices develop in its wake developing higher dissipation. It was found that the VFT in the human heart is close to this optimal limit and decreases in diseased hearts (Gharib et al., 2006).

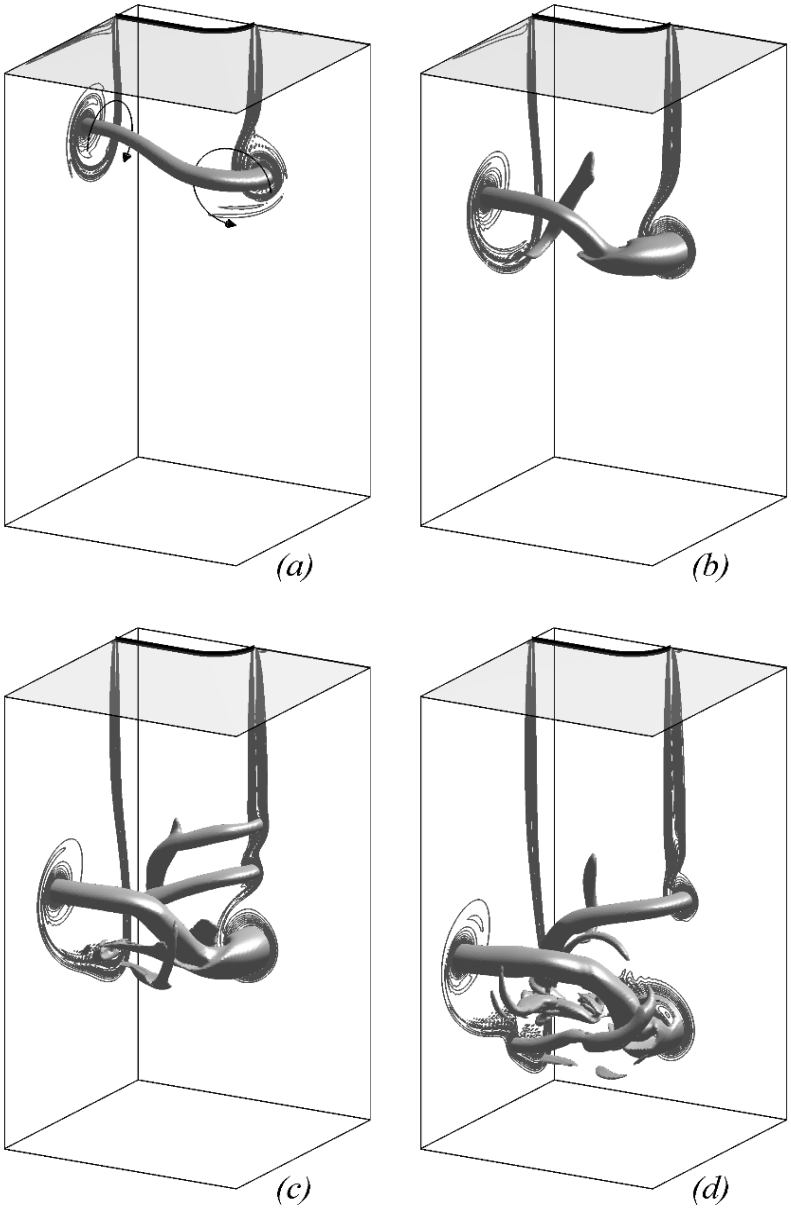

Figure 10.8. Three-dimensional vortex formation from a slender orifice at four instants in sequence. One quarter of the entire space is shown for graphic clarity (allowed by symmetry); the vorticity contours are reported on the side planes to help understating the three-dimensional arrangement of the principal vortex filaments. In the initial phase, the formed vortex loop presents a variable curvature and deforms because of the different self-induced translation speed; this leads to further deformations until the vortex structure loses its individuality and becomes a set of entangled three-dimensional elements that rapidly dissipate for viscosity (adapted from: Domenichini. J Fluid Mech 2011. DOI:10.1017/S0022112010004994).

The case of vortex ring formation after a circular opening represents the simplest case of three-dimensional vortex formation. Let us move forward and consider the flow across sharp edge orifices with a slender shape. In this case, the opening has a variable curvature and the separating vortex will present a variable curvature as well. Therefore, the self-induced velocity, that is proportional to the curvature, will be different along the vortex tube and will progressively further deform it. When this deformation becomes high enough, the compact tubular vortex structure becomes unstable and breaks down into smaller elements, that in turn deform into even smaller ones, until they are dissipated for

viscous effects. Commonly, vortex formation from a three-dimensional geometry gives rise to irregularly shaped structures, which become unstable and undergo to a rapid energy dissipation. One exemplary case of the three-dimensional vortex formation from a slender orifice is shown in figure 10.8 (Domenichini, 2011).

The three-dimensional vortex formation from smooth surfaces, after a constriction like a stenosis or in a vessel enlargement, introduces additional elements of complexity that do not allow drawing a simple unitary picture of the involved phenomena. The initial instants following boundary layer separation and initial roll-up are essentially two-dimensional with a moderate influence from the three-dimensional structure. Afterward, the three-dimensional development leads to widely different results depending on the separating geometry, the interaction with the nearby walls and with other surrounding vortices .

Before moving further, it is important to remark that the vortex formation process is not just a kinematic adjustment of the flow but it has dynamical consequences. The generation of a vortex is associated with the development of a force on the walls from where the vortex originates; this "vortex force" is given by the rate of growth of the vortex impulse (Saffman, 1992)

$$\boldsymbol{F} = \frac{d\boldsymbol{I}}{dt}, \quad \boldsymbol{I} = \rho \int \boldsymbol{\omega} \times \boldsymbol{x}\, dV; \tag{10.11}$$

where the integral is non zero only where the vortex (vorticity) is present. To clarify this point, consider the case of generating a vortex ring, which represent the roughly early stage of many three-dimensional vortex formation processes. The vortex impulse of a vortex ring of circulation Γ and radius R has only the component directed along the vessel axis, say x, (perpendicular to the plane containing the ring) which is $I_x = \rho\Gamma\pi R^2$; therefore, given that the radius does not vary or varies very slowly during the formation process, the force is proportional to the rate of growth of the vortex

$$F_x \cong \rho\pi R^2 \frac{d\Gamma}{dt} \cong \frac{\pi}{2}\rho R^2 U^2; \tag{10.12}$$

that, using (10.10) turns out to be proportional to the square velocity. This vortex force is due to the unsteadiness of the formation process. In a pulsatile flow, the vortex force (10.11), or (10.12), produces a continuous hammering onto the tissues where the vortex develops.

The ideal vortex formation picture described above is complicated when two or more vortices come nearby each other, because they likely interact in an intense and irreversible manner. The interaction of vortices involves many different and very complicated phenomena. In the simple case of two-dimensional vortices that come in close encounter, they reciprocally induce such a rotation velocity each other. When such vortices have the same sign they rotate together one around the other, winding up one over the other to eventually merge into a single larger one made by the sum of them. On the contrary, two vortices with opposite circulation, a vortex pair, translate together for the self-induced velocity (similarly to what a vortex ring does) along a straight or curved path depending on the relative strengths. Again, the differential velocity inside each single vortex produces the winding up of one's vorticity on other, however such vorticity strips are of opposite sign and do not merge rather they annihilate each other and reduce the individual vortices' strength.

The interaction between three-dimensional vortex structures occurs prevalently between two oppositely rotating portions of vortex tubes (because they are more likely driven one toward the other, while concordant 3D tubes tend to separate) and begins with the local interaction between the closest elements. One example of the interaction between two identical vortex rings is shown in figure 10.9. Initially, the local interaction is approximately the two-dimensional: the nearby oppositely rotating

tubular elements induce the velocity each other and try to translate away. This produces a local stretching of the three-dimensional vortex tube, a stretching that accelerates while the tubes become closer and would locally wind up one another. The interacting structures develop increasingly small scales until viscous diffusion becomes a dominant effect, at this point the *reconnection of vortex lines* occurs: adjacent opposite vorticity is annihilated by dissipation and the vortex tubes tend to fuse one onto the other.

The interaction between two identical vortices, like that shown in figure 10.9, may result into a complete vortex reconnection and a relatively simple new vortex tube. More often, however, one vortex is stronger than the other is, only part of its tubular structure can reconnect with the other weaker vortex and the incomplete reconnection gives rise to new vortices with a complex branched geometry (see also figure 10.8 where some vortex reconnection occurs). In general, the vortex structure resulting from the fusion of previous interacting vortices, typically presents a very irregular geometry. Differential curvatures, that give sharply variable self-induced velocity and local motion, and differential vorticity strength, that give axial flow along the tube, tend to rapidly further deform the vortex, produce further reconnections and gives rise to smaller vorticity structures. In other terms, an irregular three-dimensional vortex structure is overall unstable, tends to destroy itself, and it is short lived. The more a vortex is regular, like a vortex ring, the more it remains coherent and lasts longer.

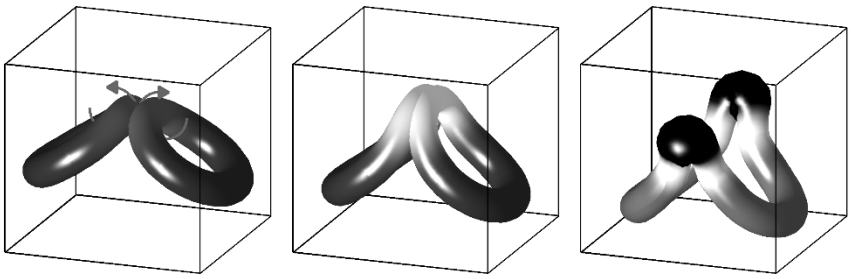

Figure 10.9. Vortex interaction between two identical impacting vortex rings; the brightness of the filament indicates the strength of the corresponding vorticity. When oppositely rotating vortex tubes get close, they produce a local vortex stretching due to the self-induced velocity (from left to central panels). During stretching, the boundary between the vortices becomes locally sharper until the filaments fuse one into the other for viscous effect (from central to right panels). After vortex reconnection a new structure is formed, typically its geometry is irregular, the vortex is often unstable and short lived..

Vortices also interact with the nearby walls; a phenomenon that is particularly relevant in closed systems like cardiovascular vessels. The vortex-wall interaction can be divided into two different phenomena: the *irrotational interaction*, that is a consequence of the wall impermeability; and the *viscous interaction* with the vorticity in the boundary layer. Let us consider the two effects separately.

First, an isolated vortex induces a rotary motion where streamlines are circular. When such a vortex approaches an impermeable wall, the streamlines must deform to avoid crossing the boundary. With reference to figure 10.10 (left panel), the modification of the flow field that satisfies the impermeability condition can be immediately constructed simply by symmetry considerations. It is the irrotational flow that would be induced by an *image vortex* of opposite circulation placed symmetrically below the wall. Such an image vortex gives a velocity perpendicular to the wall that is opposite to that of the real vortex, and thus ensures that the fluid does not penetrate into it. On the contrary, the tangential velocity has the same sign of that due to the real vortex and therefore the velocity adjacent to the wall increases (*splash effect*). In addition, the image vortex also induces a

velocity to the real vortex that accelerates or decelerates (depending on the direction of the circulation) with respect to the background flow because of this *image effect*. For example, a (clockwise) vortex that just formed from a wall underneath is decelerated by the image below the same wall, while it accelerates when it approaches a wall on the opposite side.

Second, in addition to the image effect, a vortex near a wall also influences the development of the boundary layer because of the viscous adherence condition at such a wall. A vortex creates a local velocity gradient along the wall, acceleration followed by deceleration. This perturbation, as previously discussed, may give rise to a vortex-induced boundary layer separation and to the formation of secondary vortices as it is sketched in figure 10.10 (right panel).

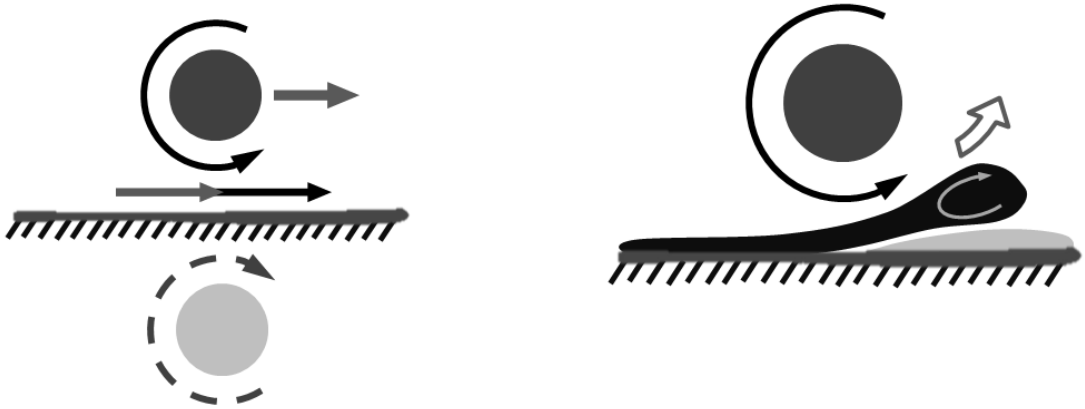

Figure 10.10. The interaction of a vortex with the wall produces two separate effects. First (left panel), the condition of impermeability is satisfied by a distortion to the vortex-induced flow that is equivalent to having an opposite vortex placed symmetrically below the wall. The presence of such a "image" vortex increases the tangential velocity next to the wall, and induces a translation velocity to the otherwise still vortex. The second effect (right panel) is due to viscous adherence, the development of a boundary layer and eventually a vortex-induced separation..

When the vortex-boundary interaction described above applies to a tract of a three-dimensional vortex tube, it eventually affects the following three-dimensional dynamics. First, the image effect gives a local stretching and deformation of a vortex filament. Second, when the vortex gets closer, it eventually interacts directly with the vortex-induced vorticity distribution. This is an interaction between oppositely circulating vorticity. That gives rise to the local wind-up of the wall vorticity around the approaching vortex and to reconnection with its vortex lines. Eventually, the vortex crops by dissipation in the regions closer to the wall, this unbalances the three-dimensional vortex structures that tends to rapidly further deform and develop small structures that are eventually dissipated.

10.4. A Further Account to Turbulence

Let us enter smoothly into the physics of turbulence by deepening a little further the concept introduced in chapter 8. We've said there that the interaction between two vortices first deforms the overall, *large scale* geometry of the vortex loops then, after sequences of reconnections, breaking of vortices and further deformations, it eventually transforms the original vorticity into several irregular

small structures. Such *small scale* elements present sharp velocity gradient, viscous friction, and are rapidly dissipated.

Physically, on average, vortices of the size of the large scales are continuously formed from the surrounding boundary; these large vortices are unstable and produce progressively smaller flow structures until they are small enough to produce dissipation. The resulting flow witnesses the simultaneous presence of these large structures with others of all intermediate sizes from these down to the smallest vortices dominated by viscosity. A measure of the complexity of such a flow can be provided by from the amount of such contemporary vortices, measured by the ratio between the largest scale, say L (given by the diameter of the pipe, or the size of the obstacle, for example), and the smallest friction-dominated one, that we indicate with η. When L is comparable to η, the flow is a regular one because the generated vorticity is smoothed out by viscosity; this is what happens in small vessels. When L is much larger than η, the flow presents changes over a large number of intermediate scales from L to progressively small size up to the smallest scales η. The order of magnitude of this complexity can be estimated in statistically steady turbulence from the phenomenological theory due to Kolmogorov in 1941 (Davidson, 2004; Frisch, 1995).

A flux of energy, indicated with ε, is injected in the flow at a scale close to L, say the energy of a vortex formed after an obstacle. When $L \gg \eta$, the large generated vortex breaks down into smaller vortices, which in turn then break down into smaller ones and so on. In other terms, the energy rate feeding the generation of the large vortex transfers to smaller scales with essentially no dissipation, and it is eventually dissipated when the smallest vortices approach the viscous scale η. Therefore, the energy rate ε is also the rate of energy dissipation. It can be hypothesized that at small enough scales turbulence becomes locally uniform and isotropic, independent on the details of how turbulence was generated. Thus, the fluctuations of velocity depend only on the energy rate that arrives from large scales and is transferred to the small scales. From dimensional arguments, the rate of injection of kinetic energy in the large scales is proportional to the kinetic energy, proportional to U^2, divided by the time to transport such energy away, proportional to $\frac{L}{U}$, thus it can be estimated (as order of magnitude) by

$$\varepsilon \sim \frac{U^3}{L}. \tag{10.13}$$

In such uniform and isotropic conditions, the viscous scale will depend solely on the amount of energy flux and by viscosity

$$\eta = f(\varepsilon, \nu). \tag{10.14}$$

This is a dimensional equation involving two units. By dimensional analysis, it is immediate to obtain the estimate

$$\eta \sim \left(\frac{\nu^3}{\varepsilon}\right)^{\frac{1}{4}}. \tag{10.15}$$

The viscous scaled defined by (10.15) is also called the Kolmogorov scale. The degree of complexity of turbulent flows is represented by the amount of interleaving scales and can be estimated by the ratio

$$\frac{L}{\eta} \sim \frac{L\varepsilon^{\frac{1}{4}}}{\nu^{\frac{3}{4}}} \sim \left(\frac{LU}{\nu}\right)^{\frac{3}{4}} = Re^{\frac{3}{4}}. \tag{10.16}$$

that is proportional to the Reynolds number. That again represents the measure of a distance between the scale of available energy and viscous dissipation scale.

As a further remark, these estimates demonstrate how the Navier-Stokes equations, that do not allow general analytical treatments, may be difficult to be tackled even by numerical approaches when turbulence develops. Numerical solutions are based on a spatial discretization and it requires accuracy up to about the Kolmogorov scale to possibly reproduce the details of dissipative phenomena. Therefore, the space spanning the entire length of interest, of size proportional to L, must be sampled with resolution η. Thus, the number of points η along any spatial direction must be not smaller than L/η and the total number of points required in three-dimensions is something like

$$N^3 \approx \left(\frac{L}{\eta}\right)^3 = Re^{\frac{9}{4}}. \qquad (10.17)$$

The estimate (10.17) sets a limit to the actual feasibility of numerical solution of turbulent flows at large Reynolds number. Due to this limitation, turbulence literature was mainly based on solution of the Reynolds equations, or different version of them based on different averaging/filtering (Sagaut, 2006) introducing a "closure" model for the unknown terms appearing therein as discussed in section 8.2. All such closure methods are however approximate and their reliability limited to relatively simple flows. As a result, turbulence remains an open challenge and it is important to build a physical picture of possible turbulent phenomena in flows of interest.

In general, we may think of turbulence as a system of entangles and interacting vortex elements of disparate sizes. Ranging from the large size generated by the boundaries, to the smaller size where the flow is smoothed out by viscous effects. Understanding that turbulence is generated by a sequence of interacting three-dimensional vortices allows its description in terms of the *energy cascade* described above. An external energy input (like a pressure difference across a valve) pushes a fluid across an orifice or along an irregular vessel bend. The flow thus generates energetic vortices whose size is comparable with that of the container. These large vortices interact and produce smaller eddies, that further interact producing turbulent eddies of progressively smaller size capable to dissipate kinetic energy into heat. At the lower end of this energy cascade, energy very small eddies are entirely dissipated and do not generate anything smaller.

An increased friction between fluid elements and enhanced energy dissipation with respect to regular fluid motion characterizes turbulence. In fact, the development of turbulence is the strategy used by fluids to dissipate the excess energy. When a fluid motion presents a large kinetic energy (high velocity), the fluid may be unable in a regular motion to maintain equilibrium between viscous dissipation and the external energy source, in that case it increases the particle paths by developing swirling motions and small scales with higher shear rate to increases viscous dissipation up to equilibrium. The Reynolds number represents, through (10.16), the ratio between the kinetic energy introduced in the large scales, proportional to ρU^2, and their ability to dissipate with shear stress, grossly estimable as proportional to $\rho \nu U/L$. When the Reynolds number increases above a certain threshold, smaller scales develop to enhance dissipation. In other words, regular flow becomes unstable and turbulence appears. That's why every realization of flow motion presents a critical value of the Reynolds number above which the motion develops turbulence.

In the cardiovascular system, turbulent flows are rarely encountered. The largest scales of motion achievable in the arterial network cannot exceed the vessel size, of a few centimeters at most. The Reynolds number is normally well below one thousand, with the exception of the very largest vessels. The flow in the ascending Aortic and, sometime, in the left ventricular cavity can reach values of the

Reynolds number up to some thousands. When turbulence develops, it is weak turbulence with an energetic level that does not influence dramatically the main dynamics. It should be remarked, that the highest levels of turbulence, if any, in an unsteady pulsatile flow are recorded during the deceleration after the peak of the flow. In fact, although the instantaneous Reynolds number has decreased, the flow has been filled with energy during the maximum velocity and has to dissipate such energy during deceleration. Deceleration enhances instability phenomena that supports turbulence.

Weak turbulence may develop in the diastolic filling of the left ventricle when the mitral jet impacts onto the walls, as it may occur with a large cardiac output. The most frequent appearance of turbulence occurs in the aortic artery, particularly in the ascending part. Here the tri-leaflet geometry of the aortic valve provokes a rather complex three-dimensional vortex formation that, associated with the large Reynolds number (roughly from 3000 to 8000 at peak systole), produces weak turbulence.

Boundary layer separation, vortex dynamics and weak turbulence represent key elements in the interaction between fluid flow and surrounding tissues in large vessels. Understanding these fundamental phenomena is necessary to allow proper interpretations of fluid dynamics in cardiovascular regions of interest. They are particularly relevant for pathological developments and will be discussed in the next chapters.

11. Separated Flow in Large Arteries

11.1. Arteriosclerosis and boundary layer separation

Arteriosclerosis is the deposition of substances transported with blood on the internal walls of the arteries provoking a progressive reduction of their lumen. The initial phase of arteriosclerosis can be imputed to multiple causes, like the inflammation of the arterial wall giving a thickening of intima-media layer, pathologies of the endothelium reducing its protective function, or just the progressive deposition of fat material. The individual arteriosclerotic risk level depends on numerous causes ranging from the properties of substances transported with blood to the affinity of these with endothelium. Besides those biological reasons, certain characteristics of fluid dynamics play a fundamental role, possibly for the starting and certainly for the progression of arteriosclerosis, and represents a sure risk factor for its development (Caro et al., 1969).

Flow and surrounding tissues can interact only though the exchange of dynamic actions: forces and stresses. Blood flow interacts with the endothelial layer of the arteries though the wall shear stress (WSS), which is recognized to have a primary role in the development of arteriosclerosis. On the biological side, an abnormal WSS on the endothelium triggers a signaling that induces vascular inflammation (Chen et al., 2019). On a more mechanical side, the endothelium is made of elongates cells that are kept aligned with the flow by the normal wall shear stress. When the wall shear stress is abnormal and not directed along the vessel, stresses may progressively alter this alignment of endothelial cells that get randomly oriented. In that case, the endothelium becomes rougher and more prone to deposition of fat material transported with the blood.

Wall shear stress changes during the heartbeat and several measures were introduced to relate anomalous wall shear stress and arteriosclerosis. The most immediate is the value of the time-averaged wall shear stress averaged during the heartbeat, of duration *T*,

$$\mathrm{TAWSS} = \frac{1}{T}\int_0^T \mathrm{WSS}dt \; ; \tag{11.1}$$

low or negative values of TAWSS where shown to correlate with atherosclerosis. More modern indices were also introduced to better underline the importance of reversal of WSS for pathology (Lee et al., 2009); one of those is the oscillating shear index (OSI) that is defined

$$\mathrm{OSI} = 1 - \frac{\left|\int_0^T \mathrm{WSS}dt\right|}{\int_0^T |\mathrm{WSS}|dt} \; ; \tag{11.2}$$

that is close to zero when the WSS is always positive and increases towards 1 when negative WSS develop.

The WSS quantity contained in (11.1) and (11.2) refers to the stream wise component. In general, the wall shear stress is a vector tangent to the endothelium, as shown in formula (10.8). Vector quantities are more difficult to be synthesized into simple indicators accounting to complex physiological phenomena; for example, the presence of helical flow, discussed above in section 9.2, may influence the development of stagnating regions and the development of atherosclerosis (Morbiducci et al., 2011). The general rule is that the risk of atherosclerosis is related to anomalous wall shear stress on the endothelium, high fluctuation and spatial gradient, especially when stresses are not aligned with the main flow direction.

It is evident that boundary layer separation and vortex formation are the key cause to the development of flow reversal and anomalous wall shear stress. Additionally, regions with flow reversal are

associated with higher blood stagnation and material aggregation. Therefore, the location of boundary layer separation are considered regions with higher risk of atherosclerosis.

It is fundamental to be aware of which regions may, at least qualitatively, present higher chances of developing boundary layer separation and thus higher risk of atherosclerotic developments. Boundary layer separation typically occurs in those regions where velocity decreases along the wall; figure 11.1 displays some typical geometric conditions where this is can happen.

Separation is largely expected after a vessel narrowing, which can happens in presence of stenosis, the outcome of progressive atherosclerosis, or at an enlargement, which is typically due to the wakening of arterial wall leading to aneurysms; both cases will be discussed in more details later. Boundary layer separation can also occur under physiological condition for example at a bifurcation. In particular the carotid bifurcation presents an enlargement (carotid sinus) on the side of the internal carotid and is a region at risk. In general, however, any branching leads to local flow decelerations that may give rise to boundary layer separation. We have also seen that a vortex, after its formation, interacts with the wall and gives rise to secondary boundary layer separation. Therefore, any important boundary layer separation may provoke secondary separation and create regions at risk even somehow away from those regions considered critical by geometric consideration only.

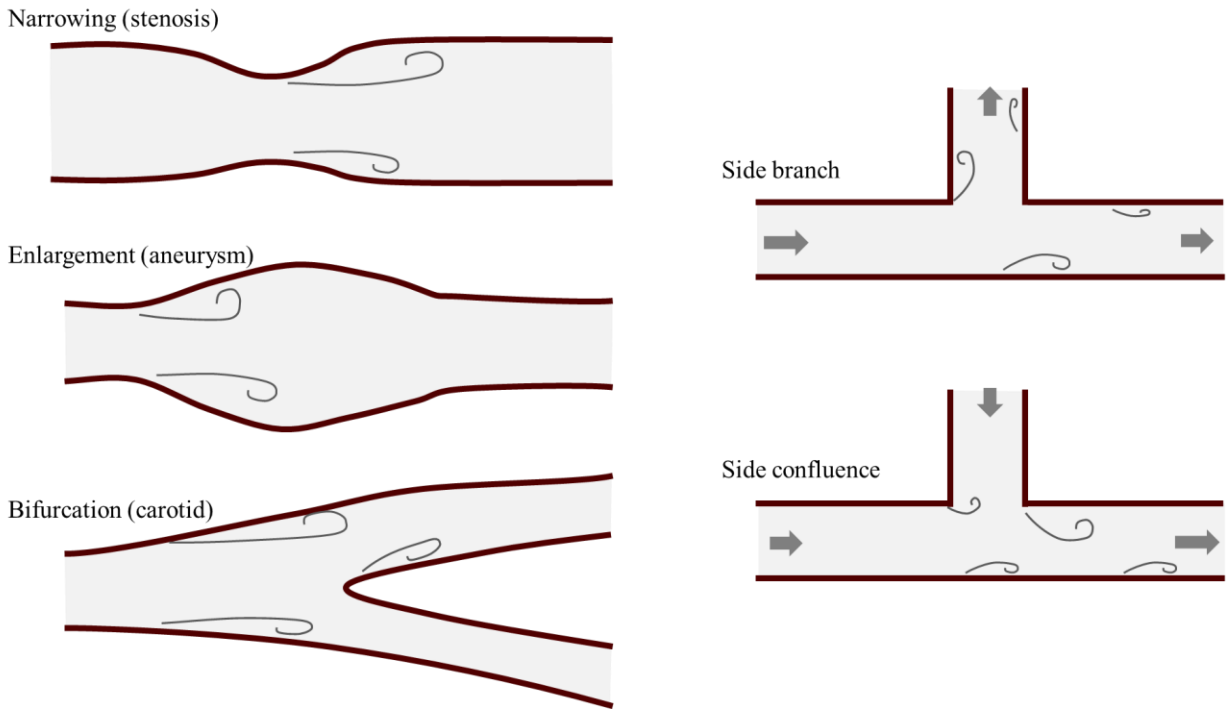

Figure 11.1. Regions with higher chances of boundary layer separation, which are also higher risk of atherosclerosis.

11.2. Stenosis

Stenosis is a pathological conditions corresponding to the reduction of arterial lumen due to atherosclerosis. From a mechanical, fluid dynamics, perspective it can start from a small disturbance in the flow that reduces the wall shear stress and facilitates further deposition of material. This reduction of the vessel size provokes boundary layer separation and further disturbance that in turn reduces the wall shear stress downstream and enhances deposition. The narrowing of the vessel reduces the blood availability in the organs served by that vessel; eventually the stenosis can even

lead to a blockage of the vessel and give rise to ischemic phenomenon to the downstream regions. Stenotic narrowing is a self-sustained phenomenon where the growth helps further growth; therefore, it is extremely unlikely to record a reduction of stenosis during time.

Stenosis reduced the flow and causes ischemia to the regions whose blood (oxygen) allowance is given by that vessel. Sometimes, secondary circulation can partially overcome this issue although secondary allowance is rarely sufficient ensure efficiency when the oxygen request increase, because of exercise or stress, above a minimum rate.

Figure 11.2. Development of arteriosclerosis and stenosis in an artery (Source: *Anatomical Travelogue*).

Fluid dynamics in presence of a stenosis is characterized by boundary layer separation and generation of a deformed vortex ring downstream the stenosis. This gives disturbed flow therein and further risk of atherosclerosis development.

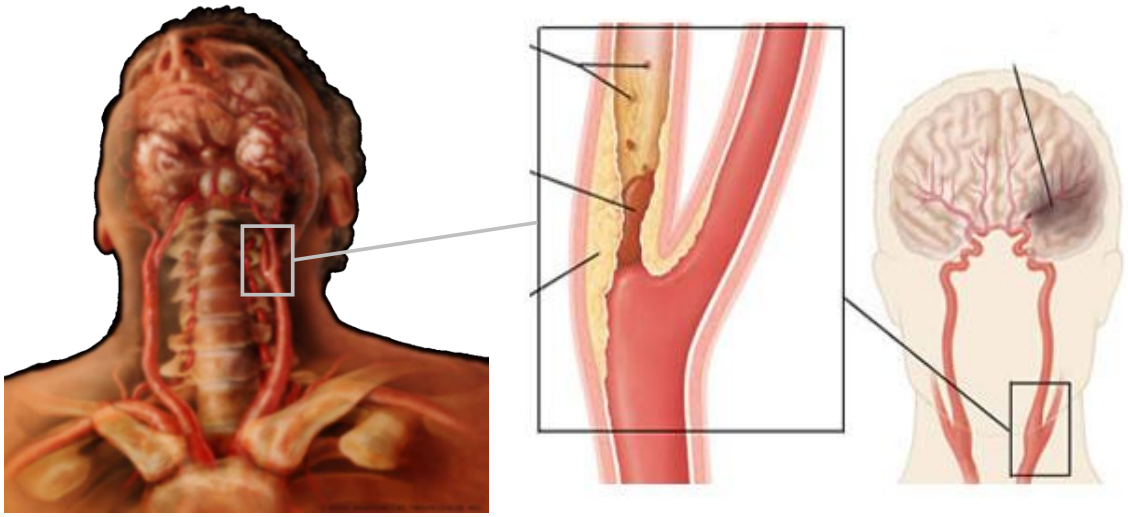

Figure 11.3. Stenosis in the carotid artery (Source left picture: *Anatomical Travelogue;* center and right pictures: *https://mychart.geisinger.org/Staywel/html/Inpatient/3,83084.html*).

In addition to the partial or total blockage of the vessel, the main risk of a stenosis is its partial breaking with the release of a small fragment (a thrombus) that is transported downstream. Along the branching arterial network vessels becomes progressively smaller until such a transported element is unable to pass through and at a certain level it is blocked in a vessels, closing it and not allowing blood availability to the tissues perfused by that. For this reason stenosis are also studied to assess its "vulnerability" to break up and release fragments. This depends whether the stenosis is well perfused,

it is hard passive material or it is composed of different materials. The process of stenosis rupture can be influenced by the entity of vortex formation as we have seen above, in equation (10.11), that it gives rise to dynamic hammering that may help to making the stenosis unstable and release material.

One typical site at risk of stenosis are the two carotid bifurcations (symmetric on the two sides of the neck) as shown in figure 11.3. The right or left common carotid artery divides into the external carotid artery, bringing blood to the muscles of the face, and the internal carotid artery bringing blood to the brain. The latter is the most important and it is the vessel at higher risk of atherosclerosis because it starts from the side of the carotid sinus where separation can occur naturally and it is particularly prone to development of stenosis. The consequence of stenosis at the internal carotid is the reduction of blood allowance to the brain. Its partial breaking can have consequences like ictus, which can be severe or temporary (TIA, transient ischemic attach) or be fatal leading to death.

Carotid sinus is so prone to development of the atherosclerotic plaque that it is commonly monitored as an indicator for the predisposition of individuals to develop stenosis in the other parts of the arterial network. Its analysis is also relatively easy because the carotid is a superficial artery on the neck and can visualized with good quality by simple ultrasound imaging (Doppler echography).

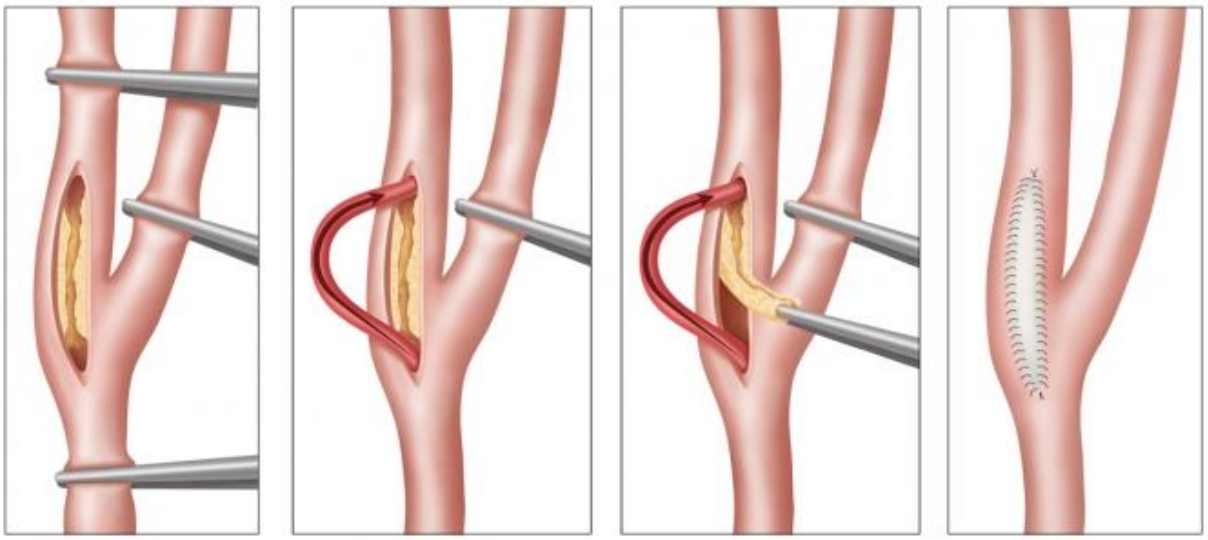

Figure 11.4. Carotid endarterectomy surgery (Source: *https://holesterin.wiki/lechenie/operatsiya-na-sonnoj-arterii*).

Therapeutic strategies for carotid stenosis at the early stage are made of blood thinners to reduce the risk of further aggregation and growth. When the stenosis is relevant or at risk of rupture, therapies are based on surgery or endovascular surgery. In either cases, the therapeutic procedure and its outcome must take into account the alterations they induced on fluid dynamics. Carotid endarterectomy is a common surgical approach to remove the arteriosclerotic plaque at or near the carotid bifurcation. Its diffusion also follows the relatively simple access to the carotid bifurcation. The procedure is schematically sketched in figure 11.4. The carotid lumen, once the blood transit is temporarily deviated, is accessed through a longitudinal cut on the arterial wall. The material is then removed and the artery is sutured. During the suture, a small patch is commonly added to the artery wall to avoid a reduction of the lumen of the sutured artery. Evidently, the shape of such a patch influences the geometry of the reconstructed vessel, therefore the distribution of wall shear stress, which in turn influences the risk of re-stenosis after surgery. Patches are made large enough to ensure

a good passage of blood; however, they must not be too large to avoid local enlargements and boundary layer separation. Which is a major risk factor, by the fluid dynamics perspective, to the therapeutic outcome. Monitoring the flow in the reconstructed artery, for example with color Doppler ultrasound, is important to assess the risk associated with fluid dynamics.

Invasive surgical therapies are often substituted by endovascular procedures; shown schematically in figure 11.5. The endovascular approach is commonly preferable to subjects with additional risk factors, like aged patients. In this case, the vessel is accesses by a guided catheter that releases an endovascular prosthesis (stent). A balloon is expanded pressing the plaque at the wall, without removing it, and a prosthesis is placed on the expanded vessel restoring a sufficient lumen to allow blood passage. This prosthesis alters the vessel geometry and creates an elasticity mismatch. These changes affects the fluid dynamics and the interaction between flow and tissue, which may in turn alter the distribution of wall shear stress. Cases of restenosis are observed and may sometime be imputable to the alteration of blood motion, which should be monitored as a measure of the quality of the therapy.

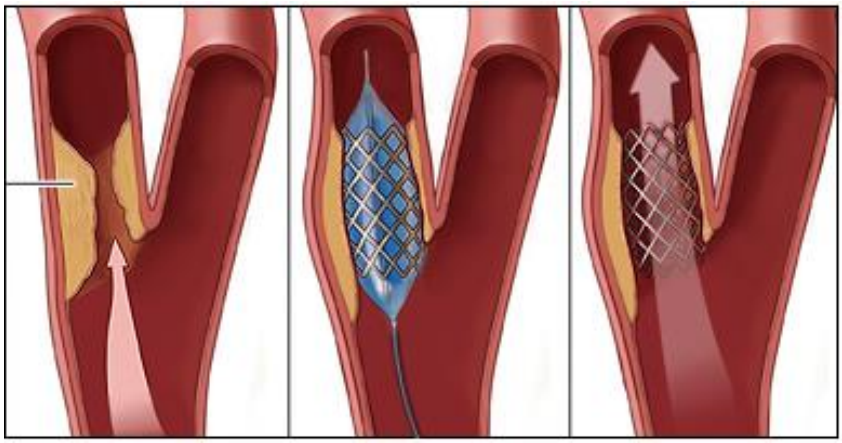

Figure 11.5. Carotid endovascular prosthesis (Source: https://creationcenter.org/wp-content/uploads/2020/03/Practitioners-Handbook-Final.pdf).

Another major site at risk of stenosis is the coronary tree. Coronaries are the arteries that bring oxygenated blood to the myocardium, the heart muscle. The two main coronaries, the right and left coronary arteries (RCA and LCA), originate just behind the aortic valve from two of the three sinuses of Valsalva (better described in chapter 13). Thus the heart pumps blood from the left ventricle cavity into the Aorta and, right after the aortic valve, part of that blood return to the heart to feed its own myocardium. As shown in figure 11.6, the RCA feeds the myocardium on the side of the right ventricle, the LCA divides into circumflex and in the anterior and posterior interventricular arteries to feed the left ventricle and the interventricular septum.

We previously discussed carotid stenosis as a life threatening disease because it reduces blood allowance to the brain: Similarly, coronary stenosis is a life threatening disease because reduces blood allowance to the heart. The consequence of a coronary stenosis (see figure 11.7) is the ischemia (reduction of oxygen) to the myocardium that, for this reason, reduces its ability to contract. When the stenosis blockage is almost complete, the oxygen allowance is reduces to near zero and the region of muscle perfused by that coronary undergoes to myocardial infarction. When the lack of oxygen persists for some time that tissue dies and becomes necrotic.

Myocardial ischemia, or infarction, affects the ability of the heart muscle to contract, thus the ability of the heart to pump blood into circulation.

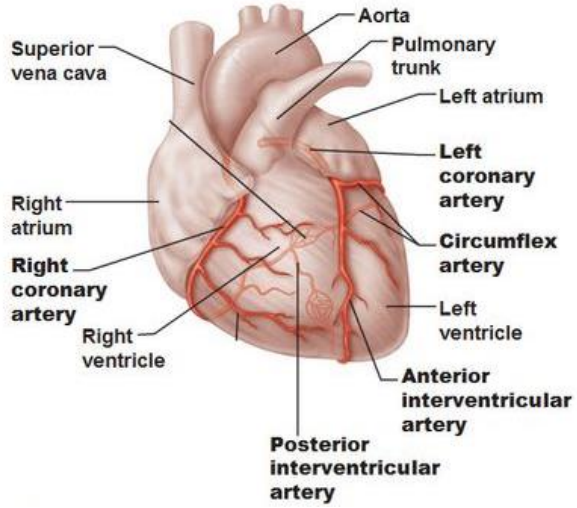

Figure 11.6. Major coronary arteries that supply blood to the myocardium (Source: http://pshs.psd202.org/documents/bzetterg/1581440857.pdf).

An extended infarction, due to stenosis in a large upstream artery, leads to the inability for the heart to pump enough blood and can lead to death if not recovered rapidly before the infarcted tissue dies. A small infarction or ischemia, are primarily detected in terms of reduction of the cardiac function; thus their symptoms are those of a cardiac disease, and they are first detected by cardiac dysfunction, although they originate from a vascular disease.

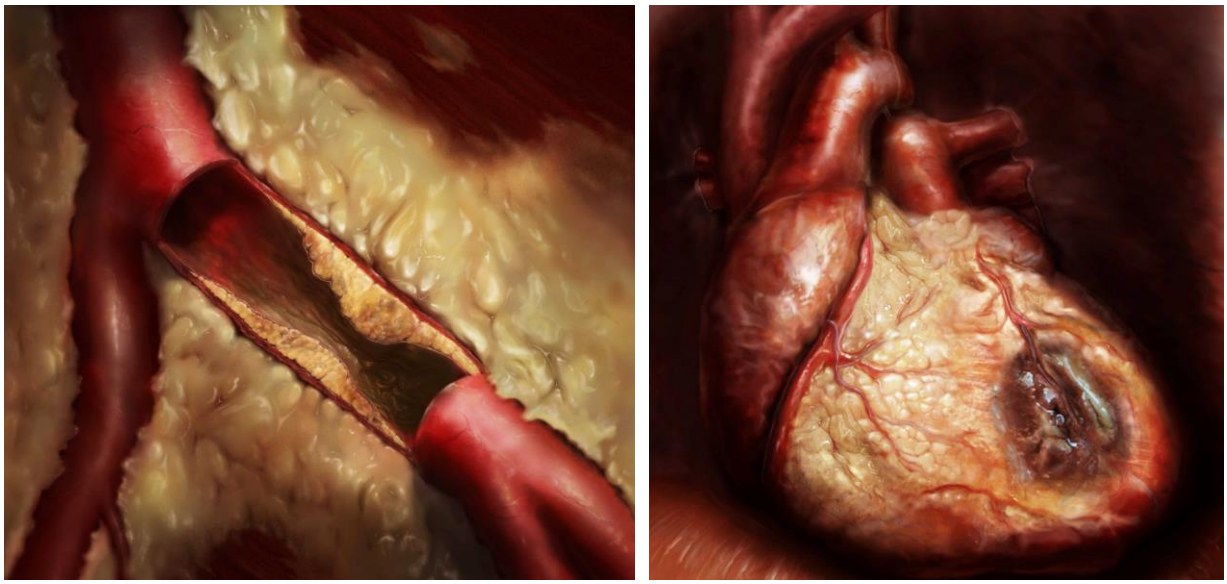

Figure 11.7. Coronary stenosis (left) and myocardial infarction (right) artery (Source: *Anatomical Travelogue*).

The most common approach to recognize the presence of myocardial ischemia is thus that of echocardiography to observed whether some region of the wall present reduced contraction.

Sometime, the blood allowance is sufficient for an approximately normal contraction at rest, while it becomes insufficient under stress or exercise. Therefore, it is also common to perform a stress echocardiography (by exercise, or using pharmacologic stress in patients who cannot perform exercise) to recognize contraction abnormality in presence of a higher demand of oxygen. This occurs in presence of small stenosis as well as when some blood is able to reach the region through secondary circulation. Suspected coronary stenosis are then verified by coronary angiography that permits to visualize the blood flowing into the coronary tree and thus the lumens of the coronary arteries.

Therapies for coronary stenosis are those of blood thinners to avoid their progression. Surgical approach is that of coronary by-pass as shown in figure 11.8. After a by-pass, the blood flow can be disturbed at the junctions that can become regions at further risk of stenosis. Much more common, however, is now the endovascular procedure. The procedure is shown schematically in figure 11.9: the vessel is reached by a guided catheter from the Aorta that expands the endovascular prosthesis and a prosthesis (stent) remains in position after the catheter is released. The changes in geometry and elasticity about the stent position may sometime disturb the fluid dynamics and alter the distribution of wall shear stress. However, these are subjects at risk, where cases of restenosis are not more frequent than those of new stenosis, and are commonly kept under periodic control.

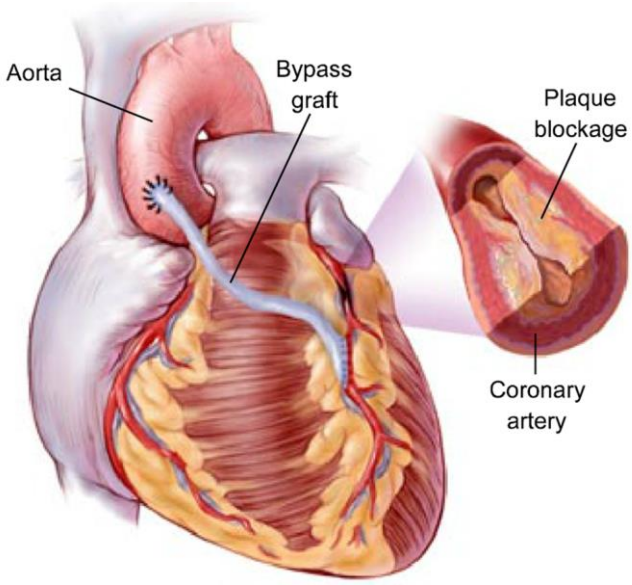

Figure 11.8. By-pass coronary surgery artery (Source: Ruszkowski, 2015. DOI:10.14288/1.0166664).

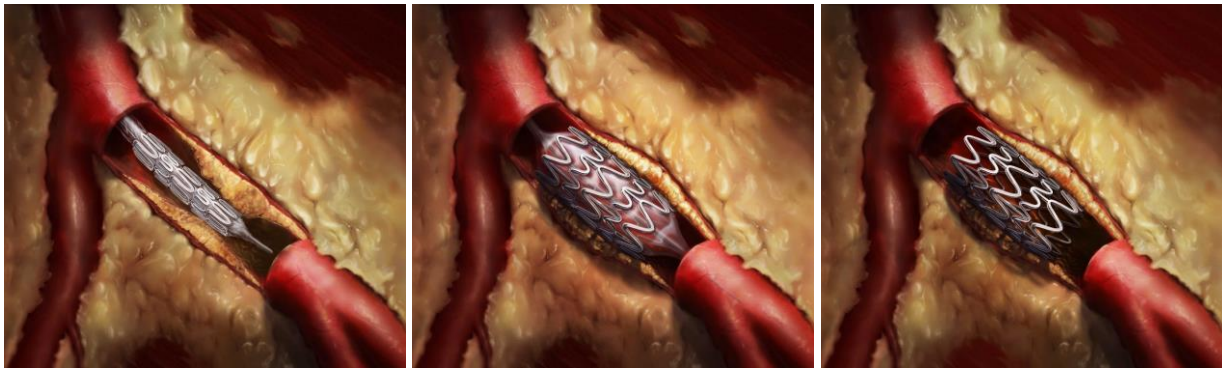

Figure 11.9. Endovascular coronary surgery artery (Source: *Anatomical Travelogue*).

Carotid and coronary stenosis are most common; however, stenosis can develop in numerous other arterial positions. Examples are the branches on the aortic root, or the iliac bifurcation. Nowadays, most arteries are solved by endovascular procedures, whose technology is continuously advancing. Stent are available for about any dimension and shape, and multiple stents can also be combined to reconstruct bifurcations and multiple branching. Typically, patients who developed a stenosis are subjects with higher predisposition to atherosclerosis. Therefore, alteration of the fluid dynamics in such patients must be carefully monitored in those sites where boundary layer separation is likely or is observed.

11.3. Aneurism

Aneurism is a local enlargement of the vessel with consequent thinning and weakening of the stretched tissue and that presents risk of rupture. Aneurysm are more frequent in the Aorta, at all levels, and in the brain arteries. The main issue associated with aneurysm is that in most cases they do not give flow impairment and do not produce symptoms. Therefore, they are detected by specific searches (for inheritance or other risk factors) or, frequently, by chance. However, when the aneurysm undergo to a rupture in many cases it can be fatal.

Schematically, aneurysms are divided into two main geometric types as shown in figure 11.10. The fusiform aneurysm is a dilatation of the entire vessel that is characterized by a diameter large than normal; the saccular aneurysm is a side bulging of the vessel tissue that generates a balloon-like protrusion. Evidently, the categorization is not necessarily so sharp and all intermediate conditions may also exist.

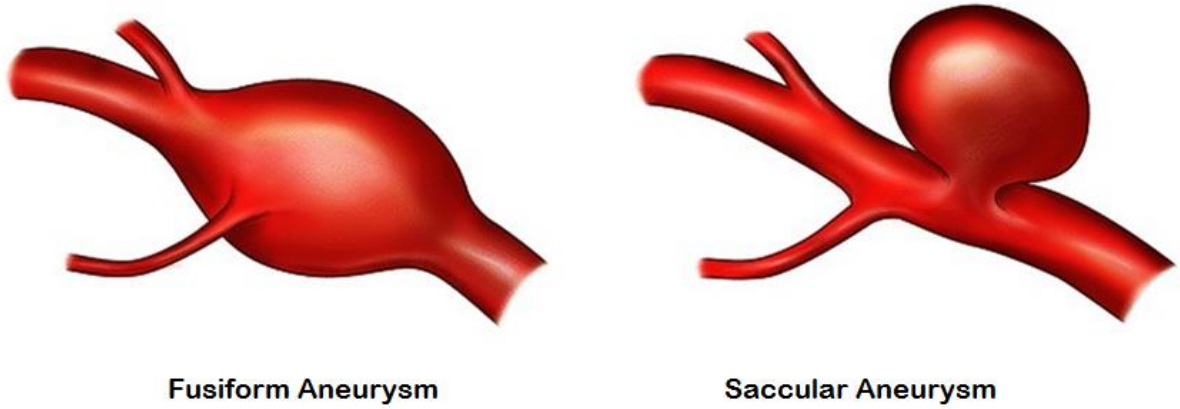

Figure 11.10. Type of aneurysms (Source: Withers et al. Applied Health Economics and Health Policy 2013. DOI:10.1007/s40258-012-0005-x).

The fluid dynamics inside an aneurysm depends from details of its specific shape. Fusiform geometries usually present a central jet due to boundary layer separation at the expansion and recirculating regions at the enlargement. The jet may or may not be aligned with the distal vessel and possibly impact on the side wall of the aneurysm. In a saccular geometry, the flow is mainly stagnating therein with more or less wash-out of the blood. Therefore, the first fluid dynamics phenomenon in aneurysms is the presence of stagnation areas, that may form thrombi when there is not enough exchange of blood with the main flow. The second important phenomenon is the impact

of the jet on the side wall provoking overpressure in the splash area; an impact occurring at every heartbeat thus hammering on a wall that is already thin and weak increasing its risk of rupture.

The birth of aneurysms can be imputable to the local weakening of the tissue. This phenomenon is sometime related to alteration of the local fluid mechanics that creates overpressure or shear stress at the wall. More frequently, however, this follows an alteration of the tissue itself for multiple causes and often follows genetic predisposition. The progression and development of the aneurysm is primarily due to the continuing presence of the causes that generated it. Progression, however, can also be imputable to the specific alteration of the fluid dynamics therein. The major risk is its rupture that can bring to ictus (brain aneurysm) and internal hemorrhage, which in turn can lead to sudden death.

A typical sites for the development of aneurysm is the Aorta. In the aortic root, a wall deformation in the proximal part of the ascending Aorta can follow from genetic causes or also be a consequence of anomalies in the aortic valve. In the latter case, the valve jet may presents high velocity that are deviated toward the aortic wall, because the orifice area is small and tilted. The impact of the jet on the wall creates high shear that can weaken the epithelium and produces a continuous hammering, every heartbeat, on such wall. This type of aneurysm is sometime associated with the presence of bi-leaflet aortic valves, whose opening may provokes a laterally directed fast jet. In the aortic arch, including part of the ascending and descending Aorta, the aneurysm develops mainly because of genetic alteration of the wall tissue. The abdominal Aorta above to the iliac bifurcation, as shown in figure 11.11, is one of the most frequent for the formation of aneurysms, which deserved an own acronym AAA, for Abdominal Aortic Aneurysm.

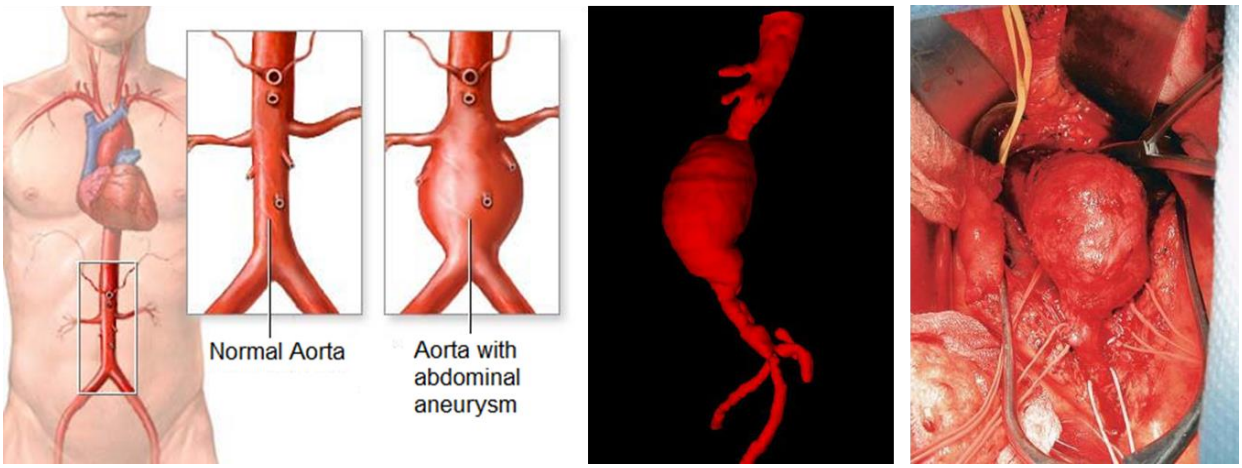

Figure 11.11. Abdominal aortic aneurysm (AAA), of fusiform type. Sketch (left), reconstruction from Angio MR (center), picture before surgery (right). (Source: left image: Demirci. Technical University of Munich, 2011. Corpus ID: 116163160. Central image: Antignani and Schachter. Journal of Non Invasive Vascular Investigation 2016. DOI:10.24966/NIVI-7400/100004. Right image: https://www.diariomedico.com/medicina/cirugia-general/la-terapia-endovascular-para-reparar-los-aneurismas-de-aorta-abdominal-reduce-el-riesgo-de-mortalidad-al-mes.html)

Fluid dynamics plays a role for the progression of the aneurysm. Consider a saccular aneurysm first. The flow may occur mostly along the vessel, without significant exchange with the side expansion; for example, when the bulge is very lateral and the opening is small and aligned with the vessel wall as sketched in the left side of figure 11.12. In this case, a thrombus can likely develop inside the aneurysm and remains therein to somehow protect the bulged wall. This aneurysm is stable, by a fluid

dynamic point of view, because flow is not expected to induce its growth. On the opposite, when the main flow partly enters into the side bulge, as shown on the right of sketch of figure 11.12, it can provoke additional shear and epithelial damage, it does not allow coagulation of blood, thus keeps the bulge camera active. In this case, the aneurysm is unstable, by a fluid dynamic perspective, because it is expected to progress and to present an increasing risk of rupture. Similar evaluations can be brought forward about fusiform aneurisms. In these case the complete coagulation is less common. Here, the deviation of the main flow, as shown in figure 11.13, and its potential impact in the wall is more important for assessing stability properties to aneurysm progression.

Fluid dynamics, however, is rarely used clinically to categorize the risk of progression or rupture of aneurysm. Currently, this is essentially based on the size of expansion only. However, the progression of imaging techniques now allow evaluation of intra-aneurysm blood velocity vector field and novel solutions are under development to improve the categorization and support diagnosis and therapeutic planning (Chung and Cebral, 2015).

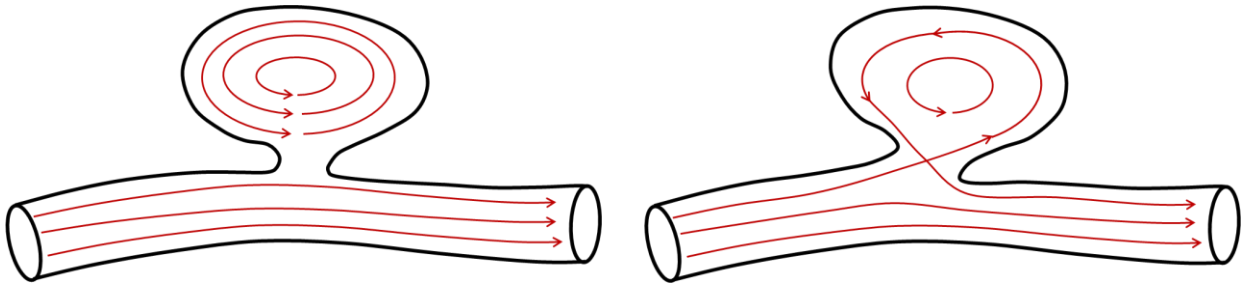

Figure 11.12. Flow in a saccular aneurysm where the aneurysm is separated from main flow (left) or when it exchanges blood and provokes shear inside the aneurysm.

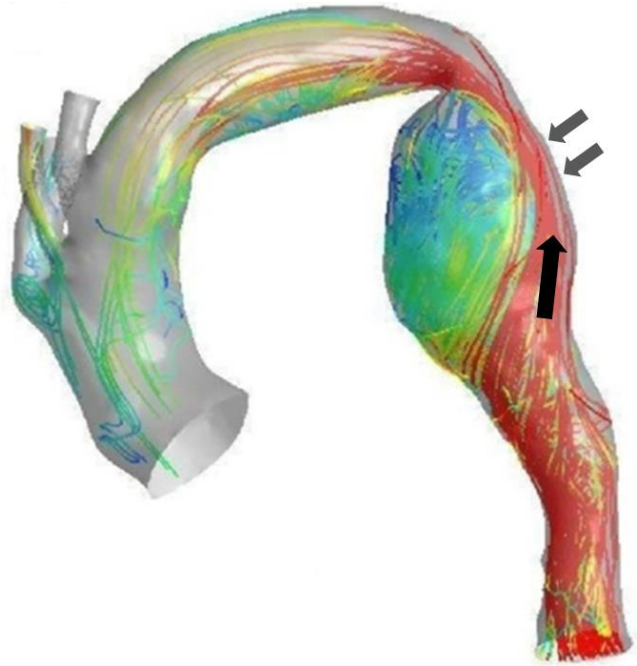

Figure 11.13. Flow in an aortic fusiform aneurysm where the deviated flow impacts on the side wall (Source: http://irc.cs.sdu.edu.cn/vis/course/ppt/20151022.pdf).

Once an aneurysm has been detected, there is no specific pharmacological therapeutic treatments (beside those for associated risk factors, like high blood pressure). The periodic control is crucial to monitor its progression. Therapies are essentially of surgical or of the endo-surgical type as sketched in figure 11.14. Surgery is performed through bandage or, more likely, removal of the aneurysm and replacement with a prosthesis. Endovascular surgery is performed by inserting a stent in the vessel. After the insertion of the endovascular prosthesis, as shown in figure 11.15, the blood flows through the prosthesis while stagnating blood is left to coagulate in the lateral expansions that is excluded from the circulation.

We said above that the causes of aneurysm formation are genetic or due to regional alteration of either tissue or flow properties. The surgical repair solves the effects but does not removes the causes that led to aneurism development. Therefore, frequent controls are important after surgical therapy close to the repaired vessel where tissues can have sub-optimal mechanical properties, as well as in other sites at risk. Monitoring is mainly performed looking at the vessel geometry; however, it also important to verify the presence of anomalies in the flowing blood that witnesses abnormal dynamics and possibly associated risk factors (Ziegler et al., 2019).

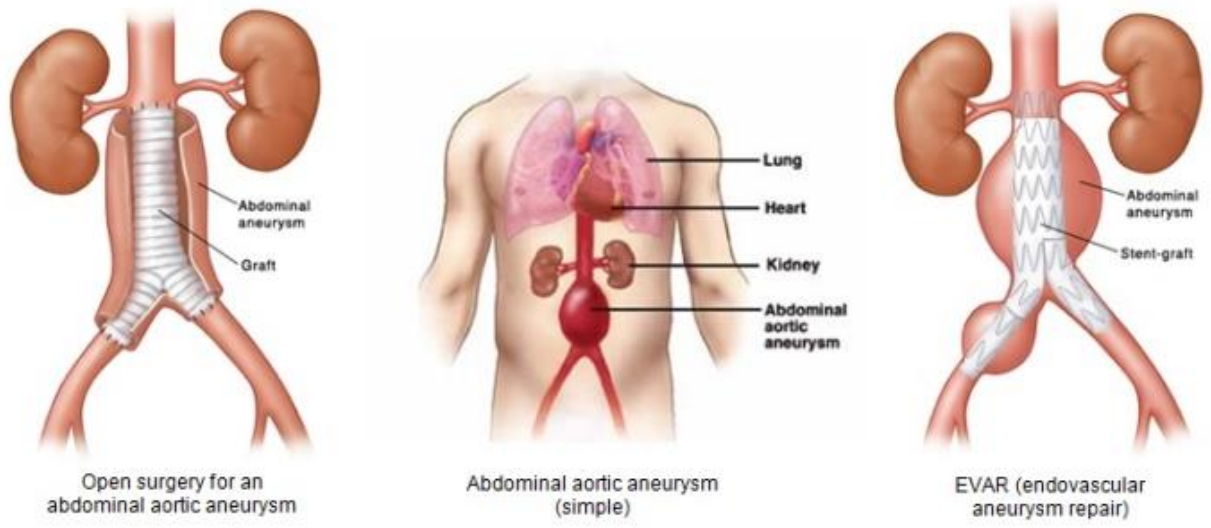

Figure 11.14. Surgical (left) and endovascular surgical (right) treatment of an abdominal aortic aneurism (Source: https://drpraveenchandra.com/abdominal-aortic-aneurysm.html).

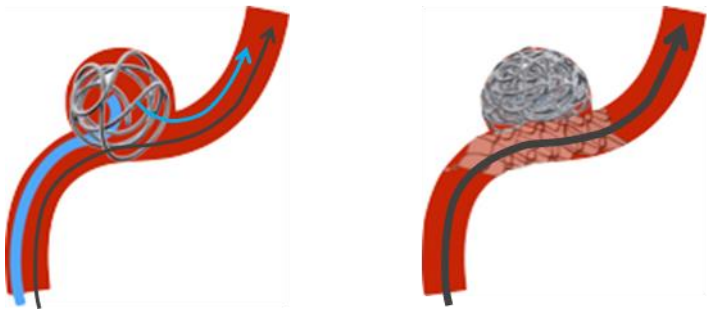

Figure 11.15. Changes in the fluid dynamics from before (left) to after (right) endovascular surgery of a saccular aneurysm.

12. Cardiac Mechanics I: Fluid Dynamics in the Cardiac Chambers

12.1. Cardiac electro-mechanical cycle

The heart is an organ than contains two biological pumping systems, the right heart and the left heart. Each individual heart is composed of an atrium that receives low pressure blood and is connected to the respective ventricle that pumps at the corresponding arterial pressure blood into the circulation. The left and right sides work synergistically in the whole heart and they present similar timing of their activity. They are also arranged in series along the circulatory network. The left heart pumps oxygenated blood in the primary circulation that, after oxygen release to all body, terminates into the right side of the heart. The right heart pumps de-oxygenated blood in the pulmonary circulation, where it entrains new oxygen and, that terminates in the left heart. Therefore, for blood incompressibility, each side pumps the same amount of blood volume in the circulation. The main difference is that the pumping work is performed a significantly different arterial pressure that on the right side, pressure in the pulmonary artery typically ranges between 5 and 20 mmHg whereas on the left side pressure in aorta is much higher and varies from 80 to 120 mmHg.

The heart anatomy, with indication of the blood flow pattern, is shown in figure 12.1.

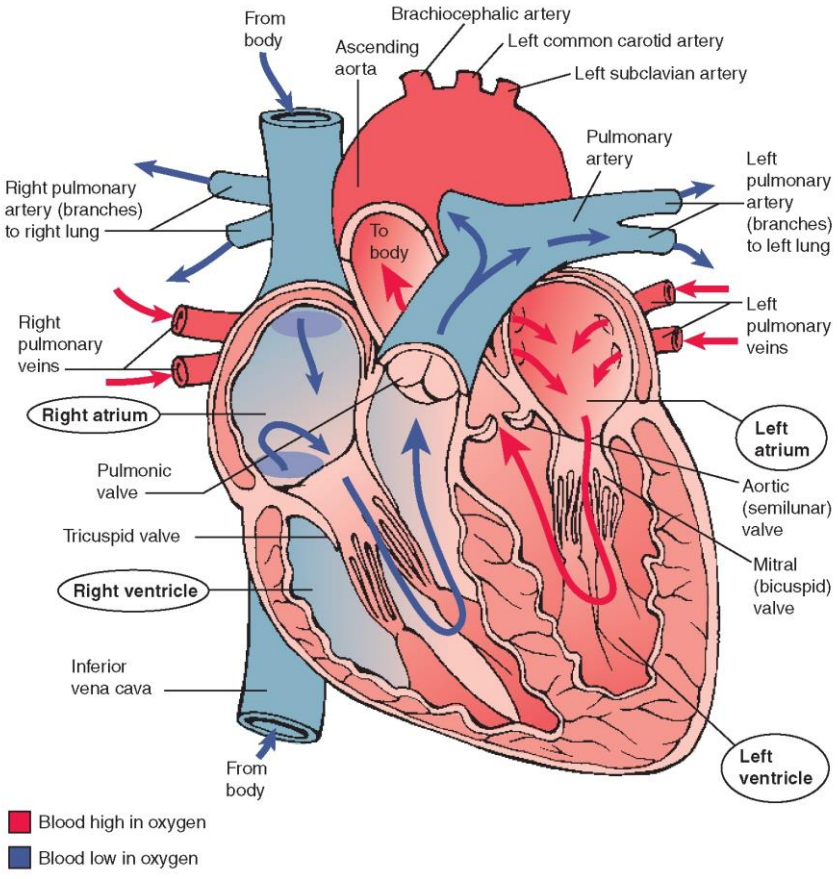

Figure 12.1. Heart anatomy and blood flow paths (Source: http://medicinebtg.com).

On left side, the pulmonary veins coming from the lungs bring oxygenated blood in the left atrium. The left atrium connects to the left ventricle through the mitral valve, a valve with two leaflets (bicuspid valve) that opens into the left ventricle and avoids backflow. To this aim, despite the high pressure difference that can develop between left ventricle and left atrium, leaflets are retained from

opening into the atrium by the chordae tendineae that connect the tips of the valvular leaflets to the inside of the ventricle wall that in a bump region called papillary muscles. A thick myocardial muscle surrounds the left ventricle and permits its contraction to vigorously pump blood into the Aorta, the first artery of the primary circulation, to work against the high aortic pressure (80-120 mmHg). The aortic valve is placed at the base of the ventricle, on the right side of the mitral valve, and separates the left ventricle from the aortic artery. It is a tricuspid valve (with three leaflets) that avoids backflow, for the relatively lower pressure difference from Aorta to the left ventricle, by the closure of the three leaflets with the tips aligned downstream. On the right side, the right atrium receives poorly oxygenated blood from the inferior and superior venae cavae, and connects to the right ventricle through the tricuspid valve. The right ventricle is surrounded by thin myocardium and pushes blood through the pulmonary valve, into the pulmonary artery. The right ventricle produces the same volume rate than the left, but it works against much the lower pressure in the pulmonary arteries (5-20 mmHg). Geometrically, the left ventricle has roughly the shape of a prolate spheroid and the right ventricle wraps around it on the right side, for about 45 degrees, in a triangular shape. The two ventricles are separated by a part of the myocardium called the interventricular septum.

The left ventricle (LV) is the principal mechanical element of the human heart. It has the function of a volumetric pump that receives low pressure blood from the venous system through the left atrium and ejects it with higher pressure through the aortic valve into the primary arterial system. The LV chamber is surrounded by a muscular tissue, the myocardium, that operates in a sequence of mostly passive relaxations, when it receives the blood, and active contractions to push it into the circulation. Given the fundamental mechanical function of the heart, the myocardial tissue deformation and the blood flow inside the LV represent a central issue of clinical evaluations.

LV function can be described, in global terms, as comprised of three interconnected elements: the *electric cycle*, this is associated with the volumetric changes in an *electric-mechanical cycle* that, in turn, interacts with the pressure to produce *mechanical work*.

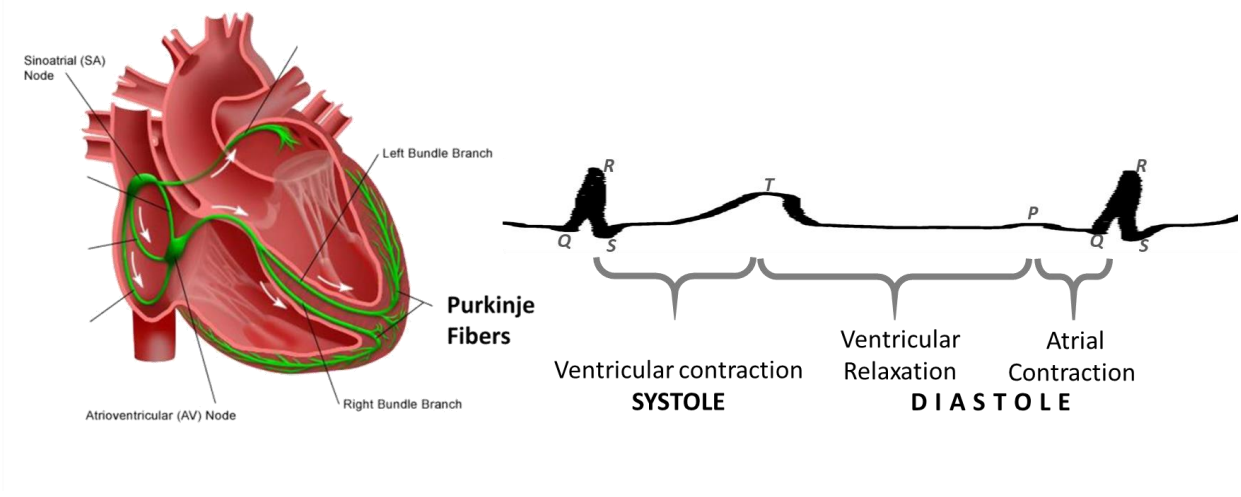

Figure 12.2. The electric cycle. Left: fibers transmitting the electric impulse, right: ECG (Source left side: https://image1.slideserve.com/2374428/slide31-l.jpg).

Cardiac *electric cycle* develops by the propagation of the electric signal that produces the mechanical contraction of the individual myocardial cells and eventually give rise to the volumetric reduction of the chambers. For this reason, the cardiac cycle is commonly referred as an electro-mechanical cycle. The electrocardiogram (ECG) records the polarization and de-polarization of the muscular fibers, due

to electrical voltage difference, which correspond to the beginning of fibers contraction and relaxation, respectively. One typical ECG trace is reported in figure 12.2 with the main electric conduction system. The electrical stimulation starts from the sinoatrial node placed about the tip of the atrium (on the right side) and propagates into the myocardium surrounding the two atria. It produces polarization and consequent shortening of the muscular fibers: the *atrial contraction*; which pushed some blood into the ventricle; this weak polarization is noticeable in the ECG by a small peak that is called the P-wave. The electrical conduction converges into the atrio-ventricular node, placed between the ventricle and the atrium where it slows-down before propagating rapidly into the ventricles' branches. The QRS complex in the ECG indicates the polarization of the ventricular myocardial fibers, after which the ventricular contraction develops. The ventricular contraction, or *systole*, pushes blood in the circulation. When contraction is completed the muscular fibers depolarize, revealed by the T-wave in the ECG, and relax allowing the blood to fill the ventricle during *diastole*. Diastole is then completed by the following atrial contraction.

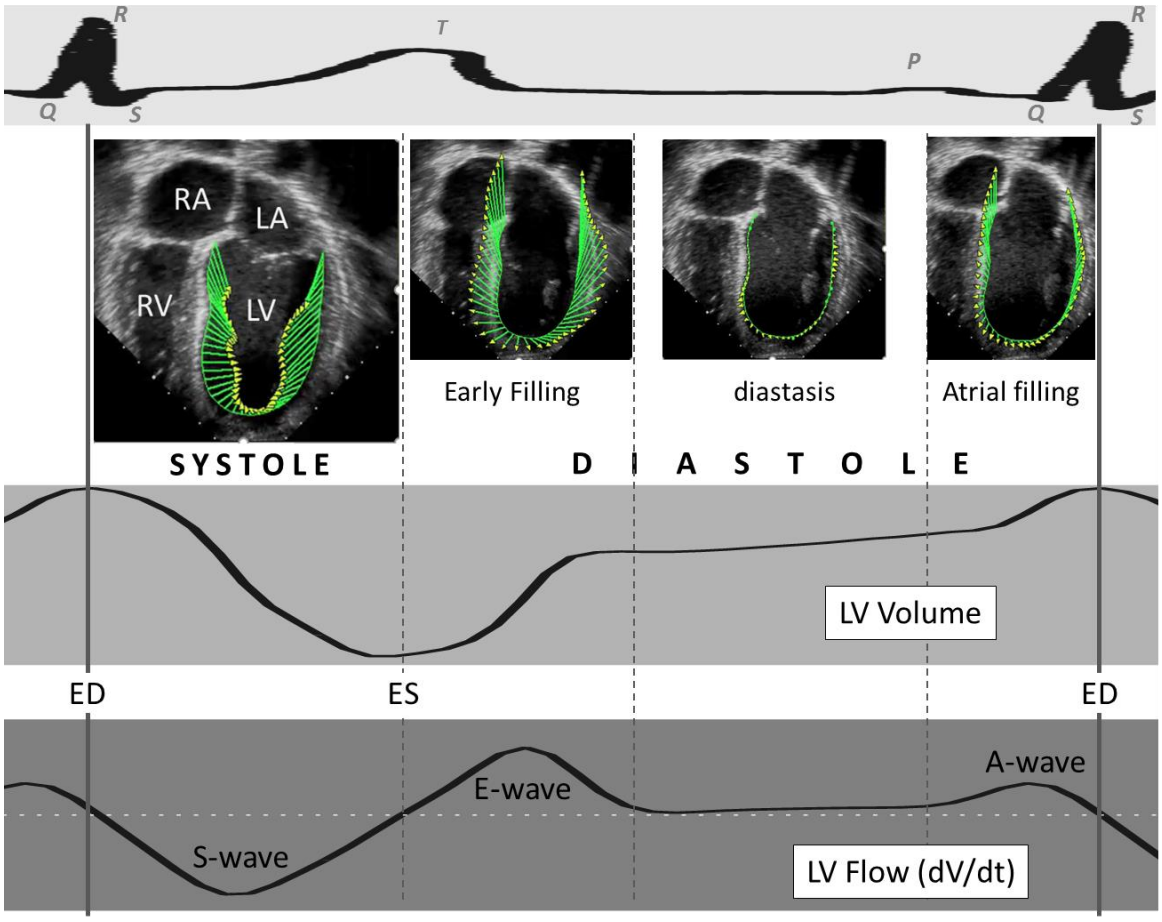

Figure 12.3. The electro-mechanical cycle.

The electric cycle has a parallel mechanical cycle of ventricular filling and ejection to give rise to the *electric-mechanical cycle*. We will keep the focus on the LV, unless otherwise specified, that is the most energetic element of the human heart; however, the right ventricle follows in parallel an analogous process. With reference to figure 12.3, we can correlate the electric cycle with the mechanical activity. During systole the LV contracts, the mitral valve is closed, its volume decreases and flow is ejected (S-wave) at systolic pressure through the Aorta. Then the myocardium relaxes, pressure decreases below that of the left atrium, aortic valve closes, mitral valve opens and blood

flows into the LV that increases its volume. This is the early filling phase, the E-wave terminates when the atrial and ventricular pressure become comparable and flow into the ventricle is very small during diastasis. Afterwards, the atrial contraction completes the LV filling (A-wave) and the diastolic phase.

The volumetric function of the LV is primarily described through parameters as those of a volumetric pump. The volume at end-diastole, V_{ED}, is the maximum size of the LV chamber that then contracts to reach a minimum value at end-systole, V_{ES}. Therefore the stroke volume $SV = V_{ED} - V_{ES}$ is the volume of blood ejected by the LV into the circulation, as well as the volume entering during diastole. The SV is the volume the passes through each cross-section of the circulatory network during one heartbeat.

The SV is commonly normalized with the to provide a dimensionless measure of the entity of the contraction relative to the available volume. This measure is defined *ejection fraction*

$$EF = \frac{V_{ED} - V_{ES}}{V_{ED}} = \frac{SV}{V_{ED}}; \tag{12.1}$$

which represents the most common clinical parameter to assess the LV function. Evaluation of EF requires the evaluation of LV volumes, which can be performed with numerous methods based on imaging, from echocardiography to MRI and others. In normal hearts the EF is usually about 65%, and considered abnormal when it falls below 55% (although exact figures depend on the measurement method). The reduction of the EF commonly reveals the presence of a cardiac dysfunction, although there are also pathologies that present a preserved EF.

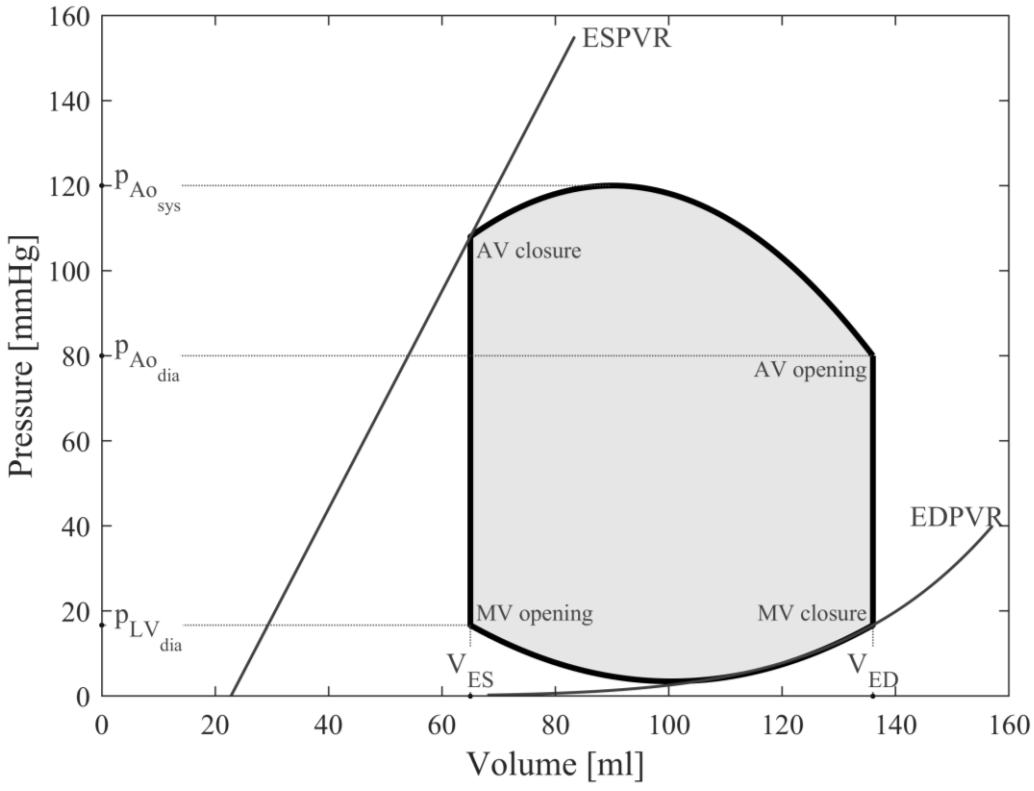

Figure 12.4. Pressure-volume loop in a normal left ventricle.

A deeper understanding of LV mechanical function must include the role of pressure to identify the effective *mechanical work* associated to the electric-mechanical cycle. Pressure inside the left ventricle reaches its maximum value during the systolic contraction, when it has to overcome the systolic pressure inside the aortic artery (normally about 120 mmHg) and reduces during the contraction to values comparable to the diastolic pressure in the aorta (about 80 mmHg). After the closure of the aortic valve, and opening of the mitral valve, the pressure inside the ventricle during diastole falls to the low value that are found in the left atrium, reaching a minimum slightly above 0 mmHg. The interplay between pressure and volume leads to an interpretation in terms of isothermal thermodynamic process that can represents by a pressure-volume loop as sketched in figure 12.4 for a normal subject. The loop is bounded above and below by the end-systolic pressure-volume relationship (ESPVR) that contains and contains the end-systolic point, and its end-siastolic counterparts. These are related to the concept of elastance that is out of the scope of these notes, more details can be found elsewhere (Berne and Levy, 1997).

The pressure-volume loop must be run in the counter-clockwise direction. The upper curve represents the systolic contraction when volume reduces from end-diastole to end-systole with pressure reaching its maximum about half the way. The lower curve corresponds to the diastolic LV expansion. The approximately vertical lines connecting the two curves represents the quick transition between the closure of one valve and the opening of the other when volume is approximately constant and pressure changes abruptly.

The pressure-volume loop is relevant for the evaluation of the mechanical work of the ventricle. The instantaneous power associated to a volume of fluid, that represents the time derivative of the mechanical work, is defined as the scalar product between acting force and velocity. In the case of a volume of fluid $V(t)$ with no volumetric forces, the only force is the pressure that acts normally to its bounding surface $S(t)$, and the total power is

$$\mathcal{P}(t) = \int_S \; p\boldsymbol{v} \cdot \boldsymbol{n} \, dS \, . \tag{12.2}$$

Pressure can be confidently assumed as approximately constant in the chamber with a value $p(t)$; in this case it can be taken out of the integral and the integral is identically zero in an incompressible fluid for mass conservation (4.3). This results is informative when one considers that the wall is given by the tissue boundary and the open parts where fluid flows $S = S_b + S_{open}$. Equation (12.2) can be rewritten as

$$p \int_{S_b} \boldsymbol{v}_b \cdot \boldsymbol{n} \, dS + \int_{S_{open}} \boldsymbol{v}_f \cdot \boldsymbol{n} \, dS = 0;$$

and including the boundary of the open part

$$p \int_S \; \boldsymbol{v}_b \cdot \boldsymbol{n} \, dS = -p \int_{S_{open}} \left(\boldsymbol{v}_f - \boldsymbol{v}_b\right) \cdot \boldsymbol{n} \, dS.$$

The first integral represents the volumetric rate and equation (12.2) becomes

$$p \frac{dV}{dt} = -p \int_{S_{open}} \boldsymbol{v}_{\boldsymbol{f_r}} \cdot \boldsymbol{n} \, dS \, . \tag{12.3}$$

where $\boldsymbol{v}_{\boldsymbol{f_r}} = \boldsymbol{v}_f - \boldsymbol{v}_b$ is the fluid velocity relative to the (possibly moving) volume boundary. Equation (12.3) shows that the power required by the myocardium to change the volume against the pressure is equal to the power of the fluid leaving the LV cavity against the same pressure. It further

tells the total mechanical work performed by the LV during one heartbeat is the area of the pressure-volume loop; which is mainly due to the mechanical work during systole

$$\mathcal{W}_{sys} = \int_{V_{ES}}^{V_{ED}} p \, dV \cong \bar{p}_{sys} \, \mathrm{SV} \, . \tag{12.4}$$

where $\bar{p}_{sys}$ is the average value of aortic pressure during systole.

The properties described so far provide information about the overall mechanical performance of the LV associated to fluid motion. However, these are only global properties and do not account to the fluid dynamics inside the left ventricle that influence its effective performance.

12.2. Fluid dynamics inside the left ventricle (with mention to the other chambers)

Heart function is about creating and sustaining motion of blood. The previously discussed electro-mechanical cycle has therefore its ultimate effect on the dynamics of blood flowing through the LV from mitral to aortic valve.

Despite this apparent simplicity of the heart cycle, the fluid dynamics inside the left ventricle is a very intense dynamical phenomenon and represents a fundamental element in cardiac function. The incoming jet that enters the LV develops impulsively; within a few hundreds of second, it reaches speeds above the meter per second to enter a few centimeters long cavity. Then, just as rapidly, flow must reverse the direction of motion of 180° to re-direct toward the aorta where it will exit at the same high speed. The diastolic jet develops boundary layer separation from the tips of the mitral valve and immediately gives rise to a swirling motion within the cavity, as exemplified in figure 12.5. The mitral orifice is slightly offset with respect to the ideal ventricular axis for which the jet redirects towards the lateral wall and gives rise to an asymmetrical swirling structure. The underlying phenomenon is that of the formation of a vortex ring, both during the E-wave and during the A-wave, which then dissipates and stretched toward the outflow tract at the beginning of systole.

The flow pattern in a normal LV was extensively described in literature (Kilner et al., 2000; Pedrizzetti and Domenichini, 2005). It can be qualitatively understood in terms of vortex dynamics. In brief, and with reference to figure 12.5, the inflow jet during the diastolic E-wave enters through the mitral valve and develops of a ring-like vortex structure below the valve, which represents the jet heart. This vortex is slight displaced with respect to the chamber because the mitral valve is not central; the vortex ring slows down on the side closer to the boundary (the posterior-lateral wall, behind the shorter mitral valve leaflet) for image effect. The ring thus tilts with one side remaining more upstream while the other reaches the center of the chamber; by the velocity perspective, the jet deviates toward the opposite wall (the anterior-septal wall, behind the longer leaflet). Shortly, the vortex induces boundary layer separation on the same side where it is closer to the boundary and dissipation is enhanced therein. Eventually, the vorticity remains stronger about the center of the chamber where a rotatory motion develops. The same phenomenon develops, in weaker form, during the A-wave, which feeds the previously developed dynamics. Sometime, this process is so intense that it may be accompanied by vortex instabilities giving rise to weakly turbulent flow. Typically, at the end of diastole, the blood presents a weak rotation with velocity directed upward on the side below the outflow tract. This facilitates the blood ejection into the aorta during the following contraction and avoid sharp dissipation during early systolic ejection.

The length of the jet, the phenomena associated with its impact on the endocardial tissue, as well as the development and dynamics of the vortex structure inside the cardiac chamber, depend on various physiological and pato-physiological factors. A fundamental role is given by the size and the

geometry of the chamber and its synergistic contraction and elastic relaxation, as well as the geometry of the mitral valve orifice. All these concurring elements can alter the picture discussed above, making the vortex a stable structure maintaining kinetic energy or an unstable structure that creates turbulence. It must also be considered that blood is an incompressible medium. All myocardial regions must work in harmonic synergy to push blood toward the aortic exit and receive blood evenly; an incorrect timing of contraction or relaxation in one region of the wall has the result of pushing blood toward the other region, thus creating intraventricular pressure gradients that are not appropriate to create blood motion.

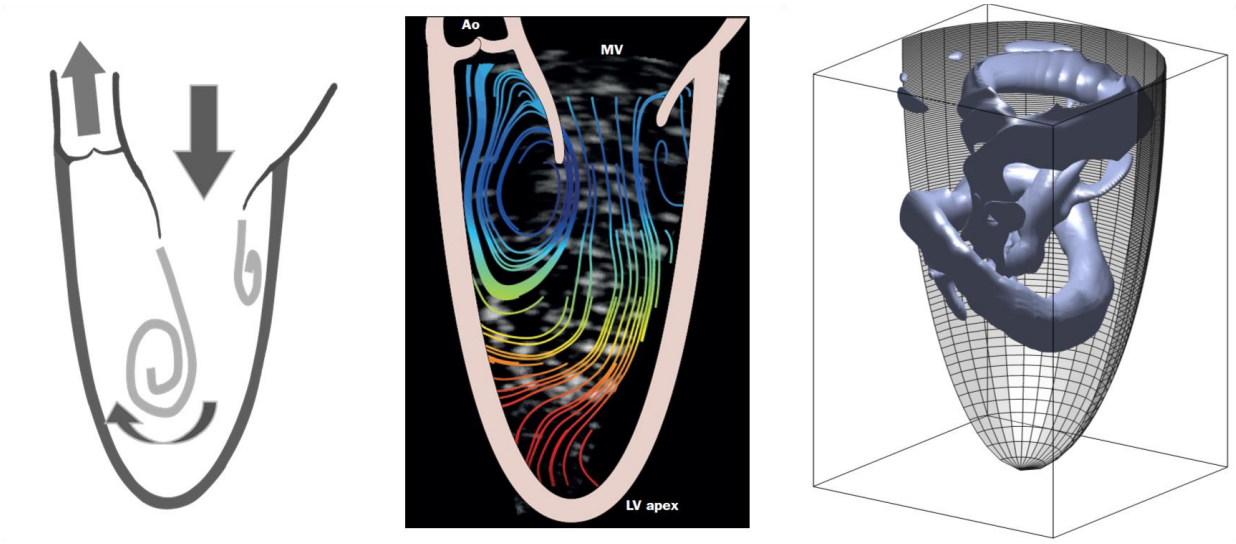

Figure 12.5. Blood motion inside the left ventricle during diastolic filling. Sketch (left), streamlines on the central longitudinal plane reconstructed from echocardiography (center), three-dimensional vorticity structure computed by numerical simulations (right). (Source: Left, Pedrizzetti and Domenichini. Phys Rev Lett 2005. DOI:10.1103/PhysRevLett.95.108101. Center, Pedrizzetti et al. Nature Reviews Cardiology 2014. DOI:14; doi:10.1038/nrcardio.2014.75).

Following the description of the featuring phenomena of LV fluid dynamics we can briefly mention what is known about the other chambers (Kilner et al., 2000). Blood motion in the left atrium is driven by the pulmonary veins that enter the atrium transversally. Very much dependent from the angle of attach of these veins, the resulting flow can take a rotary motion or be more irregular and weakly turbulent; when the mitral valve opens this possibly rotary motion flows down into the left ventricle in a funnel-like patters. These considerations are extracted from few visualizations and not much more is known (Park et al., 2013). Similarly, little is known about the right atrium that receives blood from the inferior and superior cavae veins, they are supposed to produce a rotary motion and can give rise to turbulence depending on the orientation of the two jets.

The right ventricle (RV) presents a peculiar shape that is elusive to visualization methods and limits the possibility to assess RV function. Although the RV has a streamlined geometry, the role of fluid dynamics in RV function is largely unknown. Currently there are only few works performed with respect to characterization of RV fluid dynamics, although RV function has been shown to be a major determinant of clinical outcome in numerous cardiac dysfunction including congenital heart diseases. Additionally, it is worth to mention that, because the circulation system is a closed one, the volume of blood ejected from the RV must be equal to that ejected by the LV.

The flow field in the RV presents some qualitative differences with respect to the LV due to the different and peculiar RV geometry (Fredriksson et al., 2011; Mangual et al., 2012). The diastolic

filling presents some analogy to that in the LV with the development of a ring-like vortex structure behind the tricuspid valve during the inflow; this vortex interacts with the close boundaries of this smaller chamber, particularly on the septal side. The vorticity remains mainly in the region from below the valve to the apex and does not spread much in the region toward the outflow. During systolic contraction, the remaining vorticity extends along the converging outflow tract adding a slightly helical pattern to the otherwise largely irrotational velocity field.

The fluid dynamics inside the LV (as well as in the other chambers) plays a critical role in two fundamental aspects. The first is a kinematic aspect, about the efficiency of the flow transit; the second is a dynamic aspect, about the exchange of forces between fluid and surrounding tissues (Pedrizzetti and Domenichini, 2015).

(i) Kinematic aspects: Flow transit

The quality of flow transit corresponds to mapping the time of residence of blood elements inside the chamber and the formation of regions with limited exchange of mass. The presence of stagnation regions reduces the wash-out of blood in the LV and represents a risk factor for thrombus formation; especially when the higher residence time is accompanied by a high shear stress that can trigger aggregation mechanisms.

Major advanced along this aspect point were achieved by processing 3D phase-contrast MRI acquisitions, usually called 4D Flow MRI, that provides the 3D velocity vector field in the entire LV (with the limitation of moderate time and space resolution, and of having results for an average heartbeat instead of real-time). There, one approach proposed to subdivide the LV end-diastolic volume, V_{ED}, into 4 sub-volumes depending on whether they reside more or less that one heartbeat in the LV chamber, as follows (Bolger et al., 2007). The direct flow, V_{direct}, is the volume of blood that entered during diastole and transits directly to the aortic outlet during the following systole, thus residing less than one heartbeat in the LV. The retained volume, $V_{retained}$, is the part that entered during diastole that is not ejected during the following systole. The delayed volume, $V_{delayed}$, was already present in the LV at the beginning of diastole and is then ejected during the following systole. Finally, the residual volume, $V_{residual}$, that was present in the LV and yet not ejected in the next systole. In a formula, the V_{ED} is divided as

$$V_{ED} = V_{direct} + V_{delayed} + V_{retained} + V_{residual} \,. \qquad (12.5)$$

The first two terms on the right hand side are the volumes that are the ejected during systole, the stroke volume, $SV = V_{direct} + V_{delayed}$, and by difference with (12.5), the other two terms are those remaining in the LV at the end of the systolic ejection, $V_{ES} = V_{retained} + V_{residual}$. At the same time, the stroke volume also corresponds to the terms that enter during diastole $SV = V_{direct} + V_{retained}$, meaning that $V_{retained} = V_{delayed}$, up to measurement errors. These linear relationships among the four sub-volumes in Eq. (12.5) allows to recover three of them from the knowledge of a single one (typically V_{direct}, but any other could be used). For example, the measurement of V_{direct} provide information of the percentage of blood that transits across the LV without residing more that 1 heartbeat; it is then immediate to obtain the $V_{residual} = V_{ES} - SV + V_{direct}$ that stagnates at least two beats inside the chamber. It was shown that the direct flow component was reduced in dilated dysfunctional LVs with respect to normal hearts while the residual component increase; showing a detrimental flow transit and higher risk of thrombus formation (Carlhäll and Bolger, 2010).

The analysis of flow transit and residence time is relevant for recognizing stagnating regions and helping to stratify the risk of thrombus formation. A more systematic approach to recognize stagnation regions can be obtained by resolving a simple transport-diffusion equation for the a passive

scalar that corresponds to individual blood particles "marked" at a certain instant during the cardiac cycle and computing their wash-out as time progresses . Call $C(\boldsymbol{x}, t)$ the concentration of particles, the diffusion-transport equation is

$$\frac{\partial C}{\partial t} + \boldsymbol{v} \cdot \nabla C = D\nabla^2 C; \tag{12.6}$$

that can be solved with relative ease, numerically, once the velocity field $\boldsymbol{v}(\boldsymbol{x}, t)$ is known. This can be solved, for example, starting from end-systole with the condition that $C(0) = 1$ everywhere in the LV volume. The concentration will decrease after every heartbeat of a percentage that depends on the quality of blood wash-out. The average value of concentration $\bar{C}(t)$ is a curve that is $\bar{C}_0 = 1$ initially and decreases after every heartbeat (typically exponentially). It is immediate to see that the concentration after one heartbeat, at the following systole, corresponds to the ratio $\bar{C}_1 = \mathrm{V}_{\mathrm{residual}}/\mathrm{V}_{\mathrm{ES}}$. , Therefore the sub-volumes of equation (12.5) can be recovered by the first term of the wash-out curve. This approach, however, produces a curve, instead of a single value, which provides a more comprehensive information of the wash-out process. In dilated ventricles, the curve decays more slowly and in presence of stagnation regions the tail of the curve is sustained for long time because the region with blood stasis is more difficult to wash-out.

This approach can also provide maps of concentration or, with minor changes, of the residence time. It can also be combined with the entity of shear stress, to weight the measure of stagnation with the potential degree of biological activation for developing thrombus. Clinical studies along this line are still at an early stages; however they are promising for providing quantitative measures of the risk of thrombus formation and better modulate the anticoagulation therapy in subjects at risk (Seo et al., 2016).

(ii) Dynamic aspects: Hemodynamic forces or intraventricular pressure gradients

Hemodynamic forces are the forces acting on blood to produce acceleration. The field of the hemodynamic force per unit volume $\boldsymbol{f}(\boldsymbol{x}, t)$ can be computed from the fluid acceleration, once the intraventricular velocity field $\boldsymbol{v}(\boldsymbol{x}, t)$ is known, as

$$\boldsymbol{f} = \rho\left(\frac{\partial \boldsymbol{v}}{\partial t} + \boldsymbol{v} \cdot \nabla \boldsymbol{v}\right). \tag{12.7}$$

This hemodynamic force field is essentially equivalent to the intraventricular pressure gradient field (*IVPG*), ∇p, which is known from literature (with measures made by catheter in animals) to play a fundamental in LV function (Courtois et al., 1988; Guerra et al., 2013). Indeed, the ∇p field can be obtained after rearrangement of the Navier-Stokes equation as

$$\nabla p = -\rho\left(\frac{\partial \boldsymbol{v}}{\partial t} + \boldsymbol{v} \cdot \nabla \boldsymbol{v}\right) + \mu\nabla^2 \boldsymbol{v}, \tag{12.8}$$

which differs from (12.7) for the contribution of the viscous friction (last term) that, however, is usually negligible along the short intra-chamber paths.

In alternative to (12.8), the relative pressure field, up to a constant value (e.g. the average pressure) that can change in time, can be obtained by solving the Poisson's equation

$$\nabla^2 p = -\rho\nabla \cdot (\boldsymbol{v} \cdot \nabla \boldsymbol{v}) \tag{12.9}$$

obtained by taking the divergence of Eq. (12.8). When solving (12.9), however, care must be taken in imposing appropriate boundary conditions because this is a second order equation on pressure and the average pressure gradient (tri-linear terms in pressure) is solution of the homogeneous Laplace operator and its value follows from the boundary conditions only.

Hemodynamic forces, or IVPGs, drive blood motion during both ventricular ejection and ventricular filling as shown in figure 12.6. They represent the ultimate result of LV deformation and play a central role in cardiac function that governs blood flow. Moreover, flow-mediated forces influence and participate to cardiac adaptation in presence of pathologies. Despite their potential relevance, hemodynamic forces or IVPGs have never been utilized in clinical cardiology due to the complexity of their acquisition.

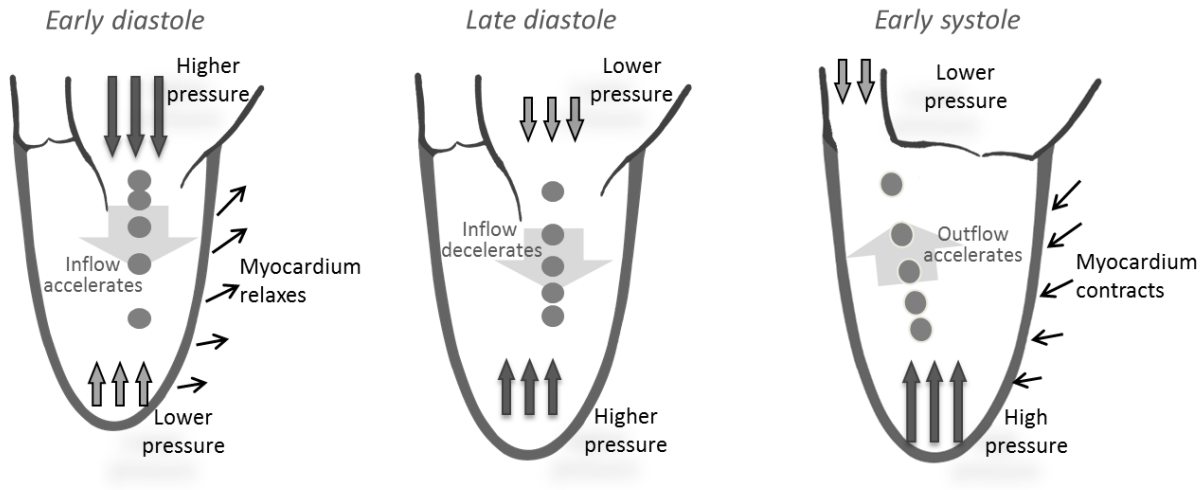

Figure 12.6. Relationship between pressure gradient and flow acceleration in phases of the cardiac cycle.

The usage of hemodynamic forces has been recently renewed with the introduction of novel imaging techniques able to estimate the intraventricular velocities non-invasively(Arvidsson et al., 2018; Eriksson et al., 2017; Pedrizzetti et al., 2016). Clinical results are under way and much promising as a physics-based indicator of sub-clinical physiological changes and a predictor of cardiovascular diseases. Lately, it was recognized that the integral value of hemodynamic forces can be obtained on the basis of the tissue dynamics without the need to know the velocity field inside the chamber. Using the formulation (5.3) for the balance of momentum in integral form, one can estimate the global force vector

$$\boldsymbol{F}(t) = \rho \int_S \; \boldsymbol{x}\left(\frac{\partial \boldsymbol{v}}{\partial t}\cdot \boldsymbol{n}\right) + \boldsymbol{v}(\boldsymbol{v}\cdot \boldsymbol{n})\, dS, \tag{12.10}$$

which includes all forces acting on the fluid volume bounded by the surface S. The bounding surface contains both the closed part, where fluid velocity coincides with that of the tissue, and the open (valvular) boundary where velocity is that effectively of blood. This approach is limited to global force value, but it can be applied to all standard imaging technologies.

In addition to the more established analysis of flow transit and dynamical interaction, there are further aspects of intraventricular flow that may play a role for the efficiency of LV function. Some authors analyzed the kinetic energy

$$KE = \frac{1}{2}\rho \int_V |\boldsymbol{v}|^2\, dV, \tag{12.11}$$

to describe the energetic level of LV flow; other the properties (size, position, strength) of the vortex formation. A possibly relevant property is the amount of dissipation of kinetic energy, given by the time integration of the rate of kinetic energy dissipation given in equation (6.2), that reflects the

energetic efficiency of blood flow pattern. The amount of energy dissipated by viscous friction inside the LV is certainly negligible with respect to that lost along the entire systemic circulation. Nevertheless, high levels of dissipation is commonly imputable to the presence of turbulence, and turbulence-induced fluctuations of pressure and wall shear stress (not directly measurable by current imaging technology that has not enough spatial and time-resolution) represent uncomfortable stresses to the myocardial tissue. These can influence its physiological feedback and eventually its adaptation (Pedrizzetti et al., 2014) although no clinical demonstration is available, yet.

12.3. Fluid dynamics in cardiac pathology

Pathologies of the left ventricle can be roughly classified, by a mechanical viewpoint, as those due to a reduced myocardial contraction (perfusion defect) or to a general inability to properly deliver an appropriate contraction/relaxation rhythm that can progressively lead to the syndrome of heart failure. Further pathologies are imputable to dysfunctions of electrical conduction; some of these can be purely neurological defects, like fibrillations, some others can lead to improper contraction or relaxation and are broadly included in the class of heart failure. A separate class of dysfunctions are those whose primary cause is imputable to pathologies of cardiac valves, which are discussed later in dedicated sections. It should altogether keep in mind that many such pathologies are inter-related and the present classification is driven by discussion on intraventricular fluid dynamics more than on clinical scenarios.

(i) Perfusion defects (myocardial ischemia)

The most known pathology of the left ventricle is ischemia, whose extreme consequence is the myocardial infarction: a regional loss of myocardial contraction that is a consequence of the reduction of myocardial perfusion due to coronary stenosis. This is, therefore, a byproduct of vascular disease; when blood flow is reduces inside a coronary artery for its partial or total stenosis, the myocardial territory perfused by that vessel receives less oxygen allowance and reduces its contractile ability.

The ischemic disease is commonly considered a systolic dysfunction because the myocardium is unable to properly contract during systole. However, by first principles, this is a vascular disease that should be treated at the vascular level as we have discusses in the previous chapter. Nevertheless, it becomes evident for inability of the myocardium to contract properly and it is often diagnosed by cardiac evaluations first.

Ischemic diseases present themselves with a reduction of the EF; this reduction is mostly due to regional contractile defect in the poorly perfused myocardial region, which can be recognized by cardiac imaging methods allowing visualization and quantification of myocardial motion. When this defect is small, it can be difficult to recognize under normal conditions and may become appreciable only under stress condition, thus requiring imaging performed under exercise of pharmacologic stress. In alternative, perfusion defects can be evaluated by perfusion imaging techniques, available in nuclear imaging, MRI and, sometime, echocardiography. When recognized, they are eventually evaluated by coronary angiography to assess the presence of coronary stenosis as discussed previously.

Intraventricular fluid dynamics is also affected by myocardial ischemia. Blood near a segment characterized by a reduced motility is more stagnant, especially when this is near the LV apex. This gives a reduction of wash-out and increased risk of thrombi. It also creates an imbalance in the intraventricular forces with over-stresses in some regions, even distant from the infarcted zone. Over-stresses, or anomalous stresses, can progressively induce a feedback and ventricular adaptation that alters the LV geometry with potential further pathological implications.

Ischemia is typically solved by coronary endovascular surgery. However, when the solution is not complete, for example when there are multiple stenosis, some ischemia may remain and give ventricular imbalances. Similarly, when the ischemia has lasted for too long time, some regions of the myocardium may not be able to fully recover its contractile ability. In presence of such remaining imbalances may induce ventricular adaptation and progressive dysfunction (up to heart failure).

(ii) General mechanical dysfunction (heart failure)

Heart failure (HF) is the principal social threatening cardiac progressive dysfunction. It presents either as a primary pathology or as a consequence of numerous (almost all) primary diseases. It can be a consequence of partly recovered ischemia; it can follow electrical dysfunctions that do not allow a synchronous contraction; it can simply due to varied stiffness/thickness in the myocardium (for example due to hypertension or to fibrosis) that does not allow a uniform relaxation, to cite a few examples. On the other hand, it can develop as a primary disease following poor medical conditions. In any case, heart failure is the terminal stage of a progressive disease associated with impaired cardiac function.

The clinical syndrome of heart failure is associated with the development of ventricular remodeling: a modification of ventricular geometry that progressively alters its functional parameters whose final stage is the LV dilatation, known as dilated cardiomyopathy (DCM). Remodeling represents a physiologic adaptation feedback that often does not lead to a stable configuration rather to a progressively worsening of the cardiac function and eventually to failure. Despite modern treatments, hospitalization and death rate remains high, with nearly 50% of people diagnosed with heart failure dying within 5 years (Lloyd-Jones et al., 2002).

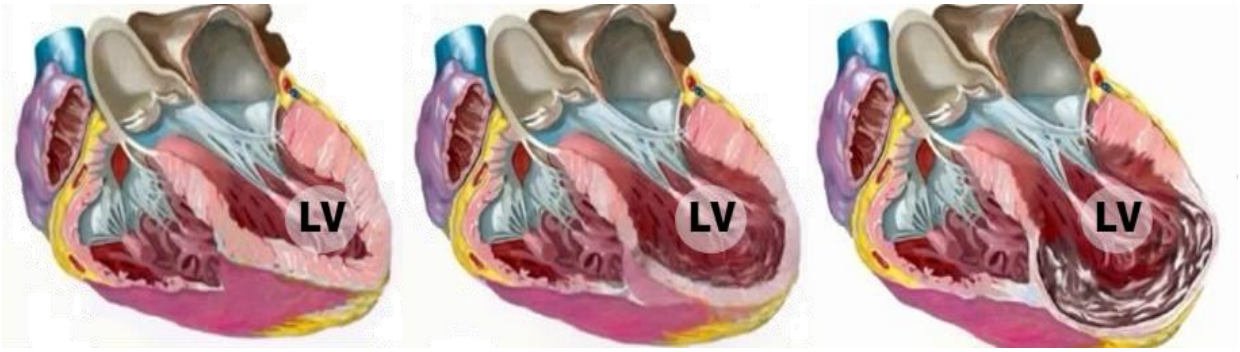

Figure 12.7. Progression of left ventricular (LV) remodelling after an ischemic event. Left side: a ventricle with normal geometry and a regional reduced contractility. Centre: a moderately dilated ventricle. Right: a dilated cardiomyopathy at the late stage of heart failure (Adapted from: Menicanti and Di Donato. Multimedia Manual of Cardio-Thoracic Surgery 2005. DOI:doi:10.1510/mmcts.2004.000596.

The physiological causes leading to LV remodeling (as exemplarily sketched in Figure 12.7 for a case of ischemia) are mainly ascribed to an increase of stress on the myocardial fibers (around an ischemic area, or because of hypertension etc.), which stimulates the growth and multiplication of cells giving rise to an increase of muscular thickness (hypertrophy) or extension (local dilatation). However this picture is unable to differentiate patients exhibiting differences in LV structure and function, it is not consistently predictive of the future risk of cardiac remodeling and does not clarify how a regional disease rapidly remodels the LV as whole. The availability of predictive models that can forecast progression or reversal of LV remodeling following initiation of therapeutic interventions would be

invaluable for overall risk stratification, improvement of preventive healthcare, and reduction of the perspective social burden.

Progressive disease and heart failure have numerous possible causes and can also develop in different ways, as shown in figure 12.8.

Heart failure is most commonly associated to ventricular dilatation (DCM). In this case, the myocardium is stretched and thinner. The heart muscle contract very little and is able to eject a sufficient SV with small contraction because of the large volume. The EF is well reduced, and we talk about HF with reduced ejection fraction (HFrEF), also referred to as systolic heart failure. In HFrEF, the intraventricular fluid dynamics is very weak; the SV is a small percentage of the chamber volume. Typically, blood flow takes either a continuous weak rotary motion, when the inflow is aligned to feed the central vortex, or it presents a weak turbulence. In both cases, flow is featured by stasis and thrombus risk. Intraventricular hemodynamic forces are reduced and incoherent.

Another type of HF is associated with thickening and/or stiffening of the myocardium. The ventricular volume is about normal and the pumping parameters are also normal but the ventricle does not relax properly during ventricular filling because of its stiffness. The EF is thus preserved, usually because the ventricle is hypertrophic and the inward thickening helps supporting systolic ejection. volume reduction. In this case, that is more difficult to recognize, we talk about HF with preserved ejection fraction (HFpEF), also referred to as diastolic heart failure. Intraventricular blood flow in this case is more similar to normal; however, dynamical difference reflecting the altered flow pattern are expected although not studied, yet.

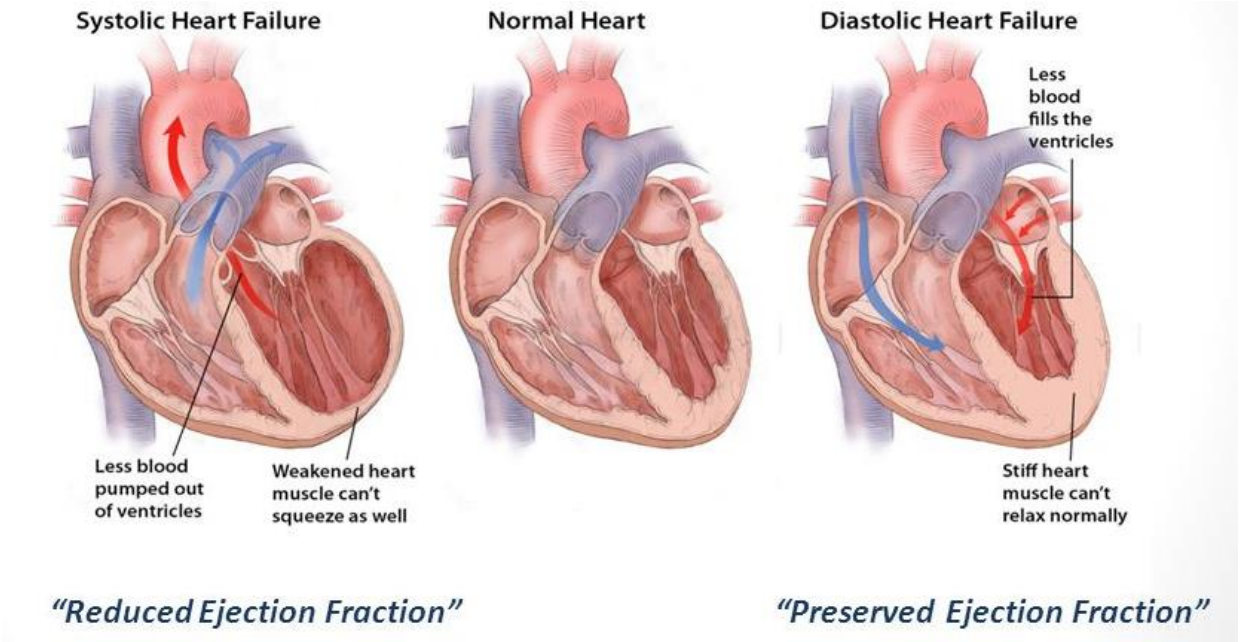

Figure 12.8. Types of remodeling and heart failure (Source: https://medhero.wordpress.com/2017/02/14/heart-failure).

The causes leading to LV remodeling are still largely incomplete. During the progression, there are changes in the pumping function. These can be noticed by a reduction of systolic trust, as well as by changes in the relative intensity between diastolic E-wave and A-wave, with an extra-burst by atrial contraction when early filling is insufficient, or alteration of timing of acceleration and decays of

individual phases. Clinicians use the combination of numerous indicators trying to figure out the specific pathological scenario; however the comprehensive mechanical picture is still missing.

It has been recently shown that alteration in the intraventricular fluid dynamics are observable well before the tissue has undergone to noticeable often-irreversible changes. Given the incompressible nature of blood, in a cardiac chamber that is filled with blood, every segment is somehow in touch with the others and, as a result, the blood inertia associated with the rapid acceleration-deceleration about one region can instantaneously influence distant regions. The role of flow on cardiac remodeling has been considered in the past only through global indicators like volumetric changes, the inflow velocity of E- and A-wave, or combinations thereof. The absence of more specific fluid dynamics indicators is mainly due to the lack of technologies able to evaluate intraventricular fluid dynamics with sufficient ease and reliability.

Normal intraventricular fluid dynamics is known to be associated to a physiologically stable cardiac function that does not lead to remodeling. Vice versa, a progressive disease corresponds to a physiologically unstable state that is expected to proceed further away from normality. As shown schematically in figure 12.9, an alteration of intraventricular fluid dynamics induces alteration of forces and shear stress on the tissue, these can trigger adaptation feedbacks and bring to progressive dysfunction (Pasipoularides, 2015). In an initial phase, the alteration of flow-mediated stresses may lead to stiffening of the myocardial tissue that sometime is associated to the increase of myocardial thickness (hypertrophy). This can be a condition going to HFpEF, or it can be just a a quick passage toward progressive tissue dilatation with further reduction of LV function and eventually going to the more common HFrEF.

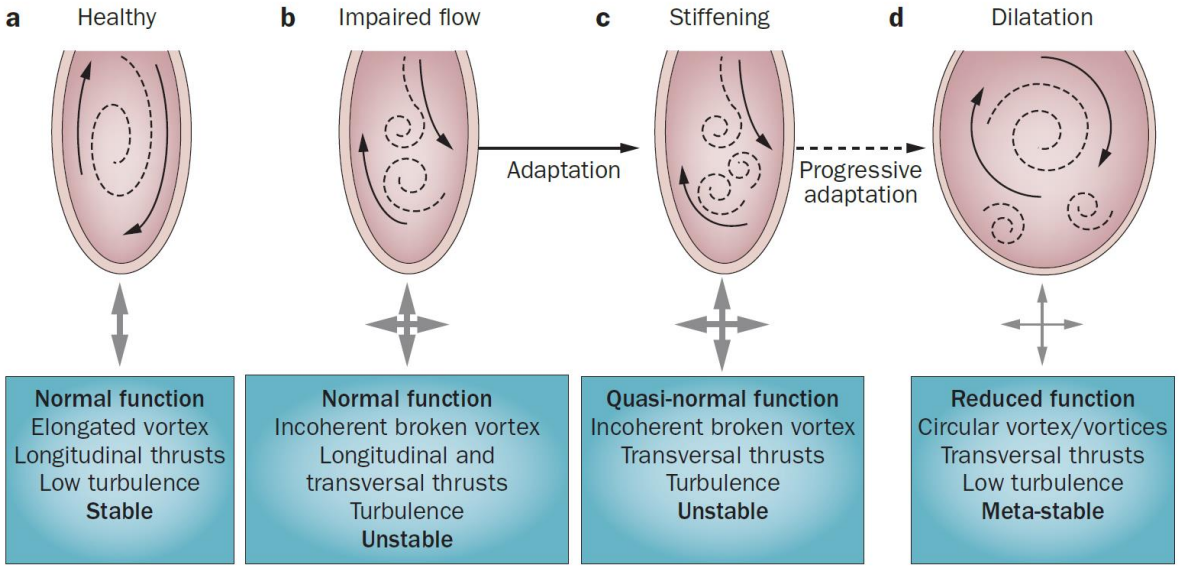

Figure 12.9. Flow-mediated path toward heart failure (Source: Pedrizzetti et al. Nature Reviews Cardiology 2014. DOI:10.1038/nrcardio.2014.75).

Therapies for heart failure are complicated as they should go to the cause leading to remodeling. Moreover, HF often involves dysfunction in physiologically related organs and, therefore, precise guidelines are not available, and therapies are varied.

Multipoint pace makers were shown to be one successful option in many cases, especially when HF is associated with a disturbed electrical activity (either as a cause or a consequence of HF), because they permit to restore a synchrony in LV contraction and relaxation. This approach, called cardiac resynchronization

therapy (CRT), requires the definition of stimulation intervals in the pace-maker to ensure optimal therapeutic outcome. Typically, they can be chosen by electric conduction optimization or though synchronization of myocardial tissue motion. However, the rate of success is still low (nearly 40% patients do not benefit of CRT). Fluid dynamics offers a global perspective to define the proper contraction pattern, by ensuring that the hemodynamic forces are maximized and properly aligned along the base-apex direction. However, studies are currently in progress to verify effective clinical relationships. This concept can, however, be generalized to evaluate the normality of cardiac function after the acute cause that may, or may not, lead to heart failure. These include endovascular prosthesis, valvular repair or transplant, and so on.

Intraventricular fluid dynamics appears as the first mechanical factor modified after, even minor and unnoticeable, alteration of cardiac function. As such, it appears a promising central element for the prediction of progressive disease or of therapeutic outcomes (Pedrizzetti et al., 2015).

13. Cardiac Mechanics II: Heart Valves and Congenital Defects

The heart contains four valves, as sketched in figure 13.1. Two of them are atrioventricular valves, the mitral valve on the left side and the tricuspid on the right side; the other two valves are for the communication from the ventricle to the circulation, the aortic valve and the pulmonary valve for the left and right ventricles, respectively. The main function of the cardiac valve is to allow flow in one direction and prevent backflow.

During systole, the ventricles contract and eject blood through the aortic and pulmonary valves, for the LV and RV, respectively, while the other valves remain closed. Ventricular contraction is made of an inward motion of the ventricular endocardial surface, combined with a shortening of the base-apex length. Given that the apex is relatively fixed, shortening is obtained by the motion of the entire valvular plane downward. Vice versa, during diastolic ventricular expansion, the ventricles expand and the valvular plane moves upwards. This upward-downward motion creates a relative velocity at the valve that supports ventricular filling-emptying and helps anticipating valvular opening and closure. It must otherwise reminded that the velocity measured just above and below the valves can be non-zero when the valves are closed because of the motion of the valve itself.

Despite their overall common function, cardiac valves present important differences, due to the actual anatomical position and to the fluid dynamics operating conditions. The therapeutic solution can also be very different. We discuss here the two main valves sited on the left side, as the valves on the right side are much less studied and their solutions are mostly borrowed from the left ones.

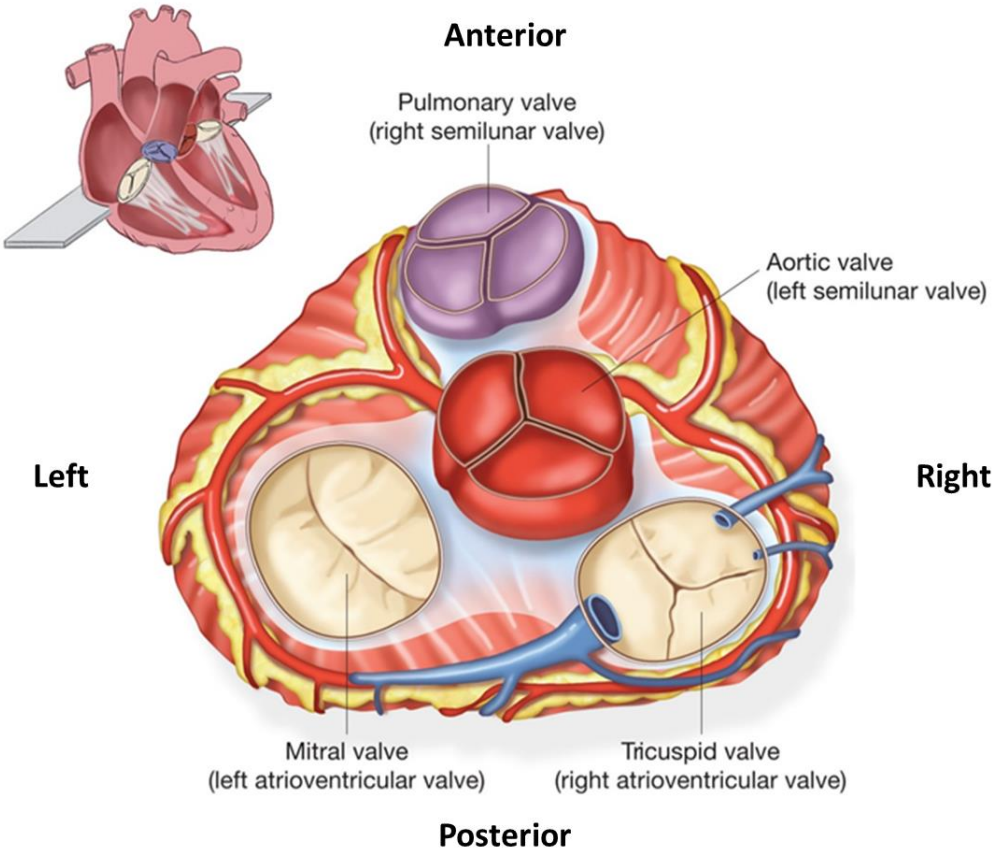

Figure 13.1. Valvular plane containing the 4 cardiac valves (seen from top of ventricles). (Source: https://www.anatomynote.com/human-anatomy/heart/heart-valve-anatomy)

13.1. Aortic valve

Aortic valve is situated in the left ventricular outflow tract where the aorta begins. It consists of three lunar-shaped flaps of tissue, referred to as cusps. The leaflets of the aortic valve are attached partially to the muscular walls of the LV. The aortic valve is crossed by flow ejected from the LV into Aorta during systole and its function is of preventing backwards flow into the LV during diastole when the aortic remains closed. Once it is closed, the cusps are coapting, aligned and separate the LV from the aorta. Artistic representations of the aortic valve are shown in figure 13.2.

The anatomy and function of the aortic valve have inspired studies for the past 600 years beginning with Leonardo da Vinci who studied aortic valve and the role of the sinuses of Valsalva. The Valsalva sinuses are dilatations in the aortic wall, just behind the valve, in correspondence of each of the semilunar cusps of the aortic valve. Generally, there are three aortic sinuses, the left, the right and the posterior, each one in correspondence of a leaflet. The left aortic sinus gives rise to the left coronary artery, and the right aortic sinus gives rise to the right coronary artery, while no vessels arise from the posterior aortic sinus, which is known as the non-coronary sinus.

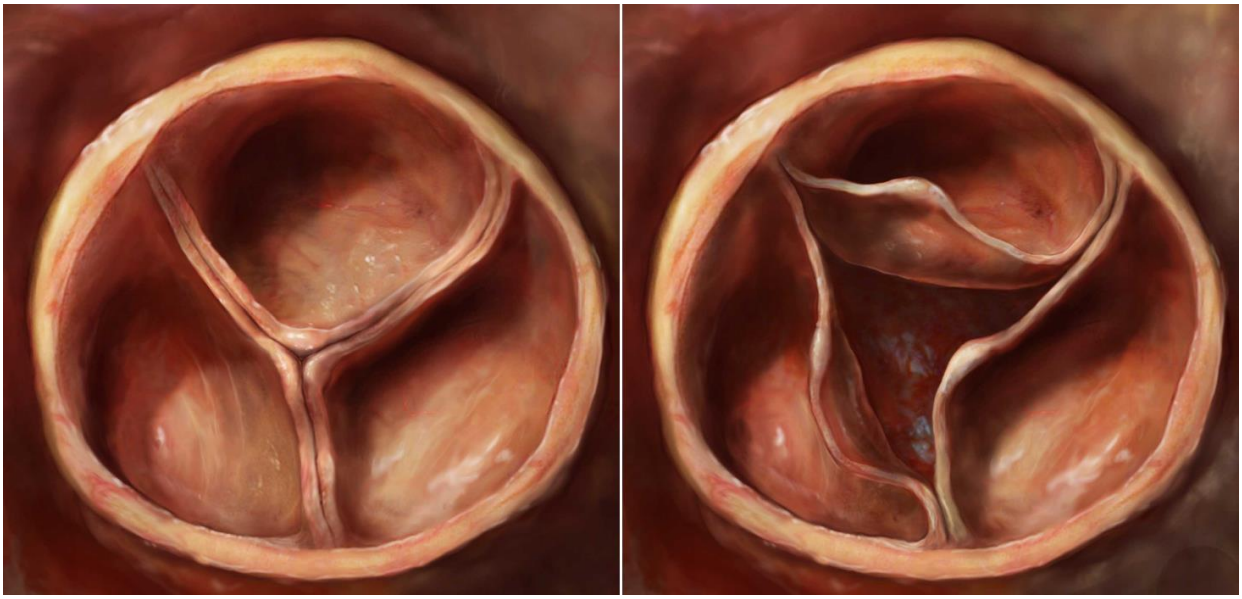

Figure 13.2. Aortic valves, closed (left) and while opening (right). (Source: *Anatomical Travelogue*).

The aortic jet presents as a turbulent jet with Reynolds number that can reach about 10,000 (velocity near 2 m/s and orifice diameter about 2 cm). It is probably the only fully turbulent flow in the circulatory system. The Strouhal number is about 10^{-2}, thus the jet is well above 10 diameters long.

Given the enlargement at the Valsalva sinuses, and the close-to-triangular shape of the open valve, the systolic flow separated from the nearly straight edge given by each of the open leaflet and detaches downstream as a free shear layer that rolls-up forming a vortex structure that develops main recirculation in the Valsalva sinuses. The role of vortex formation in the sinuses is not completely understood, yet. This backflow was initially considered to help the leaflet closure at the end of systole; it is also expected to facilitate the flow into the coronaries. More likely, the coronary flow is principally driven by the backflow that develops near the boundary during diastolic deceleration while the bulk flow, at the center of Aorta still moves downstream, and by the reflected pressure wave. Surely, the presence of the Valsalva sinuses prevents the leaflet to touch the aortic wall and to close of the coronary entrance.

The aortic jet exists from a rounded triangular orifice into the center of the Aorta thus, despite its strength, it does not interferes directly with the aortic walls; the jet then develops into helical streamlines when going through the aortic arch as shown in figure 13.3 (left side).

Normal aortic valve is tricuspid; however, a significant percentage of the population (about 2%) is born with a bicuspid aortic valve (BAV) where two leaflets are not fully separated or they are totally fused as one. One possible effect of BAV is the reduced orifice size when the valve is open, giving rise to even stronger jet and possible higher resistance to the ejection requiring an extra effort to the LV with consequences similarly to what happens in valvular stenosis (discussed below). Another important possible phenomenon related to a BAV is the asymmetric opening of the unequal leaflets, which may deviate the jet towards the aortic wall. This increases the risk of damaging the wall and developing aneurisms in the aortic root. An example of flow recorded (by MRI) in normal and BAV individuals is shown in figure 13.3. BAV subjects can have a normal life; however, given the additional risk factors, they must be monitored to ensure absence of progressive diseases development.

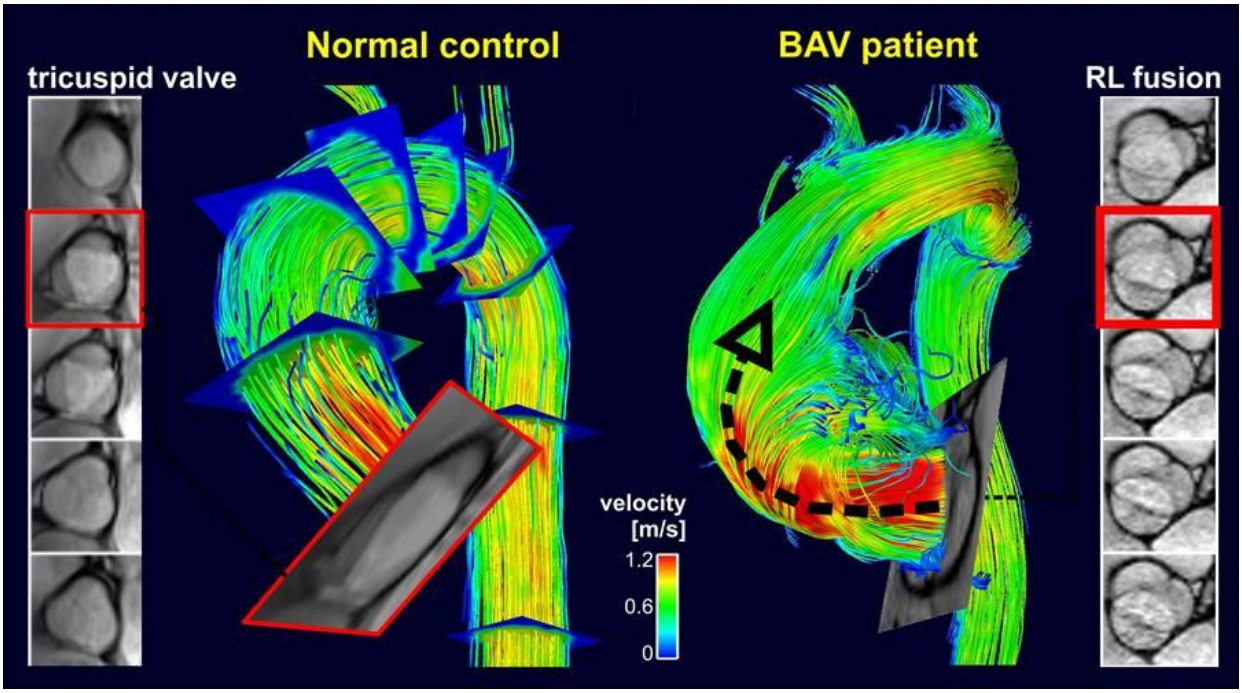

Figure 13.3. Aortic jet under normal valve (left) and for bi-leaflet aortic valve (right). (Source: Bissell, et al. Circ. Cardiovasc. Imaging 2013. DOI:10.1161/CIRCIMAGING.113.000528)

13.2. Pathologies of the aortic valve

Major valvular pathologies can be roughly grouped, from a mechanical standpoint, as those due to valvular *stenosis* or to valvular *insufficiency*.

Valvular stenosis is a reduction of the valvular orifice due to calcification of the valve leaflets that makes them less elastic and more difficult to open as sketched and shown in figure 13.4. Valvular stenosis thus reduces the effective orifice area and provokes a stronger jet entering into the Aorta, with velocities that can reach several meters per second, which means higher turbulence and risk of damage to the arterial wall when such jet is deviated.

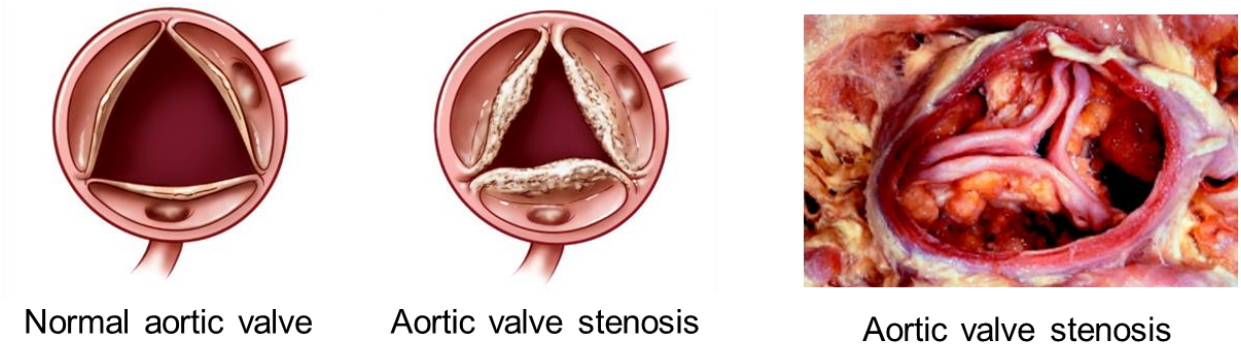

Figure 13.4. Aortic valve stenosis (Source: left, https://intermountainhealthcare.org/services/heart-care/conditions/aortic-valve-stenosis; right, https://relaped.com/asociacion-del-tiempo-entre-los-picos-de-presion-sistolica-del-ventriculo-izquierdo-y-la-aorta-con-la-gravedad-de-la-estenosis-aortica-y-la-calcificacion-de-la-valvula-aortica).

The major consequence imputable to valvular stenosis is the higher energetic resistance to ejection: higher pressure drop across the aortic valve that, at peak systole, is proportional to the square of velocity, see equation (6.10). This additional pressure loss can be significant (if velocity is in m/s, pressure loss in mmHg is given by $4v^2$) and it is totally in charge of the LV as it occurs immediately at its exit. This means that the ventricle requires to build up a higher pressure to get the same output pressure in the Aorta. In turn, LV requires an extra effort and the myocardium is subjected to higher stresses. Such a condition can likely give rise to tissue stiffening and possibly to LV dilatation setting the path toward heart failure as discussed before.

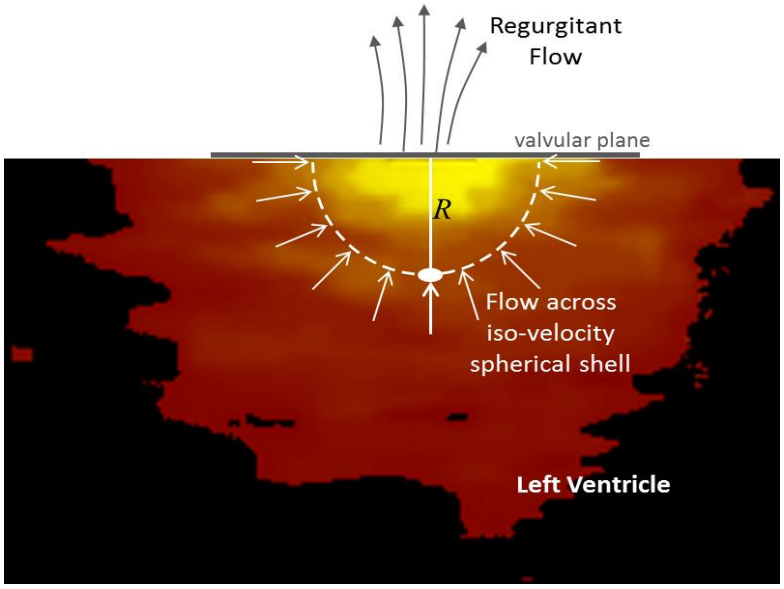

Figure 13.5. PISA method to estimate the regurgitating flow from color Doppler echocardiographic image proximal to the insufficient orifice.

The other major pathology of aortic valve is valvular insufficiency. In valvular insufficiency, the leaflets are looser, or the valve is dilated, and leaflets coaptation is insufficient; as a result the leaflets are unable to properly close the valve during diastole giving rise to valvular *regurgitation*. Valvular regurgitation means that, during LV filling, when the LV pressure decreases and blood flows in

through the Mitral valve, some flow also enters into the LV back from Aorta. This means that part of the net LV pumping effort is wasted because a percentage of the ejected blood is returned to LV itself.

Measuring the entity of the regurgitated volume is the principal mean to assess the severity of aortic insufficiency. This can be performed by phase-contrast MRI, recording the velocity across a plane just above or below the valve; this is the most accurate option although a relatively time-consuming procedure that is performed on patients requiring an accurate evaluation of the regurgitated volumne. A simpler, less accurate, approach used for a preliminary screening is by color Doppler echocardiography that permits to look at the color map of the vertical component of blood velocity. The regurgitating jet downstream the valve is not measurable because velocities are too high and disturbed; instead the color Doppler image proximally to the regurgitation orifice shows a smooth pattern corresponding to a smoothly converging flow that can be somehow analyzed. The most common method, called Proximal Isosurface Velocity Area (PISA), hypothesizes that the converging upstream velocity is axially symmetric; therefore the value of the Doppler (vertical) velocity, v_{Doppler}, at an upstream distance R on the axis can be assumed to be equal to the radial velocity over a hemispherical shell as shown in figure 13.5. Therefore, the regurgitating discharge is obtained, by continuity, as that crossing the shell

$$Q_{peak} = 2\pi R^2 v_{\text{Doppler}}. \tag{13.1}$$

This gives the regurgitating flow rate at peak diastole; it would require a time integration to be transformed in volume. The regurgitated volume, V_{regurg}, is often estimated by other means; typically, recording the time profile of the mitral inflow velocity (by pulsed-wave Doppler) and assuming a proportionality between velocity peak value (v_{peak}) and velocity time integral (VTI) that can be performed in most echographs; $V_{regurg} = \text{VTI} \times Q_{peak}/v_{\text{peak}}$.

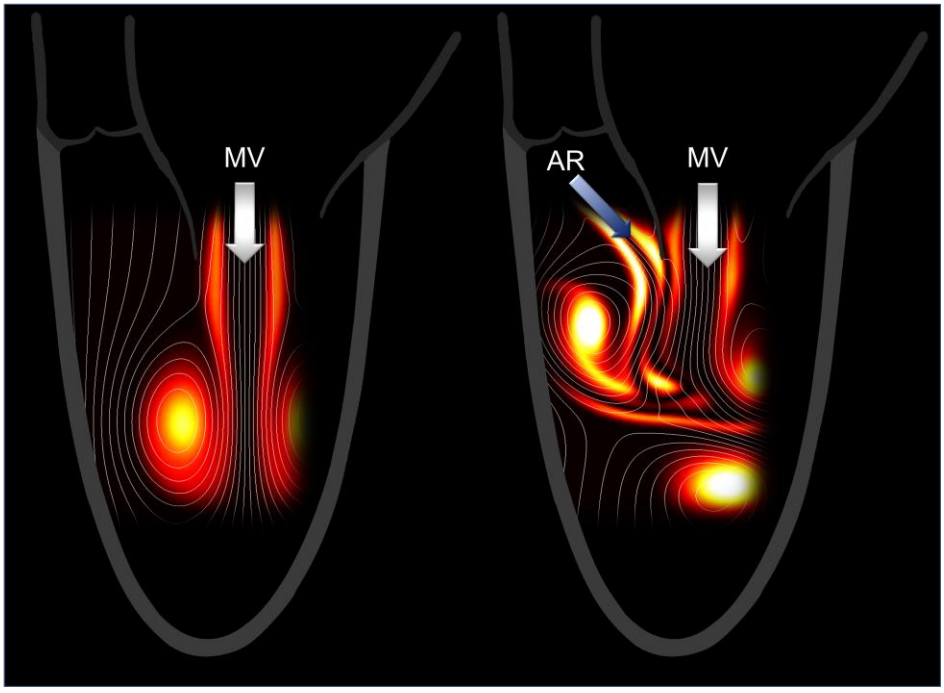

Figure 13.6. Flow in the LV in presence of Aortic valve regurgitation (Partly from: Pedrizzetti and Sengupta. Eur Heart J, Cardiovasc Imag 2015. DOI:10.1093/ehjci/jev070).

The entire PISA approach is very approximate, some further improvement has been introduced by most vendors of ultrasound equipment by using 3D color Doppler data and corrections for irregular orifices. It has the merit to be a quick procedure feasible routinely; nevertheless, it should be repeated to improve reliability of results and used as a preliminary information only and not as a rigorous measurement.

The entity of regurgitation is not the only matter responsible for the clinical severity of the insufficiency. Aortic regurgitating jet can conflict with the mitral inflow as shown in figure 13.6, giving rise to turbulence and disturbed LV filling that may further affect the LV function. Some studies suggested that the severity of aortic regurgitations could be measured by evaluating the degree of irregularity of the intraventricular flow during diastole; however, this was only a suggestion and clinical results are still inconclusive (Pedrizzetti and Sengupta, 2015).

Because of aortic insufficiency, the LV tends to dilate for the extra volumetric load coming from the regurgitated blood volume. At the same time, the reduction of net flow downstream in the Aorta induces metabolic feedback to stimulate the LV pumping to allow the necessary blood in the circulation. This requirement of an abnormal an extra effort to a LV, that was already increasing its volume, sets again the path toward heart failure.

The therapeutic solutions to aortic stenosis as well to aortic regurgitation are those of surgical valvular repair or, most commonly, valvular replacement. Surgical valvular replacement contemplates the substitution of the diseased valve with a prosthetic one that is directly sutured in its place. This type of surgery may also include the substitution of the aortic root with a prosthetic vessel.

Figure 13.7. Prosthetic valves: bi-leaflet mechanical valve (left) and the same with prosthetic vessel (right). (Source: https://www.cryolife.com).

Several types of prosthetic mechanical valves were introduced in the past and are still designed. Currently the most common is the bi-leaflet mechanical valve; which ensures life-long duration, depicted in figure 13.7. However, due to the hardness of the material, mechanical valve produce the phenomenon known as hemolysis: they break red blood cells that induce coagulation for repair and higher risk of thrombus formation. For this reason, they also require life-long anticoagulant medication. Mechanical valves also largely alter the fluid dynamics downstream the valve. The aortic jet presents multiple shear layers with altered vortex formation process and higher turbulence. The relationship between the three leaflets and three Valsalva sinuses is broken thus other contraindications may accompany such an implant. A more natural alternative is that of biological

valves that do not require anticoagulant and better mimic the original natural geometry and reproduces the natural fluid dynamics behind the valve. Biological valves, on the other side, are not guaranteed for life-long duration although technological improvements give confidence for their reliability.

Figure 13.8. Trans-catheter aortic valve implant procedure (top panel), a few example trans-catheter prostheses (lbottom panel). (Source: top, Auricchio et al. Computer Methods in Biomechanics and Biomedical Engineering 2013. DOI:10.1080/10255842.2012.746676; bottom, Piazza et al. JACC, Cardiovascular Interventions 2011. DOI:10.1016/j.jcin.2011.03.016).

With the advent of trans-catheter approach to valvular replacement, that rapidly grew from the early 2000 (Bourantas and Serruys, 2014), the surgical procedure of valvular replacement has become less frequent. Since then, the most widely used solution that avoids open surgery is the Trans-catheter Aortic Valve Implant (TAVI), or equivalently called Trans-catheter Aortic Valve Replacement (TAVR). In TAVI the valve is placed inside an endovascular prosthesis that can be positioned by catheter avoiding surgery. In this procedure, the previous valve is initially squashed at the wall, and then the new valve is expanded and placed over the previous one, as shown in figure 13.8 (top sequence). The number TAVI prostheses available is continuously increasing (Piazza et al., 2011), a few examples is shown in figure 13.8 (bottom panel).

The resulting fluid dynamics after TAVI is very similar to that of a biological valve and does no exhibit drastic changes from that of a natural aortic valve. A critical effect can be the presence of para-valvular blood leakage when the new valve does not adhere perfectly to the side tissues and allows small blood passing in the small gaps between the tissue and the implanted valve. This may

give rise to a para-valvular regurgitation. As a consequence of increasing time after TAVI, it is occasionally required to intervene over a previously installed failing trans-catheter valve by a novel TAVI on top of the previous one. This procedure, called valve-in-valve, presents similar criticalities in fluid dynamics terms.

13.3. Mitral valve

Mitral valve is the bi-leaflet valve that connects the left atrial chamber to the left ventricle. The valve consists of two leaflets of unequal size, with a coaptation between the two that takes a D-shape, as artistically shown in figure 13.9. The anterior leaflet is the largest, positioned between the mitral orifice and the left ventricular outflow tract, while the smaller posterior leaflet is placed to the left of the mitral orifice close to the posterior-lateral wall.

The leaflets edges are connected to the papillary muscles via cord-like tendons, called chordae tendineae, that prevent valvular opening toward the atrium. The chordae tendineae are required to hold the leaflets during systole in presence of a high pressure difference between the LV, which develops a high systolic pressure, and the low left atrial pressure. While the aortic valve is inside a tubular shape vessel, the Mitral valve is contained in the atrioventricular plane; here, the Mitral valve is surrounded by a fibrous annulus, that approximates a hyperbolic paraboloid similar to a riding saddle, which modulates its shape during the heartbeat.

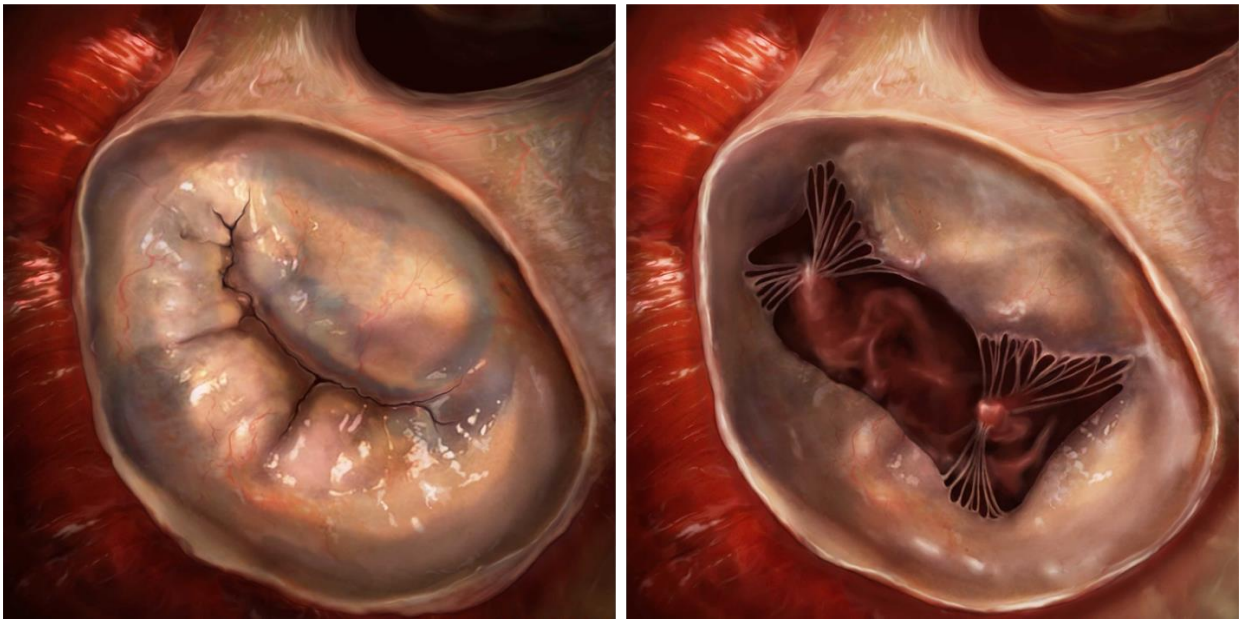

Figure 13.9. Mitral valve, close (left) and open (right) showing the chordae tendineae attaching the leaflets to the papillary muscles inside the ventricle (Source: *Anatomical Travelogue*).

The transmitral flow is characterized by two impulses, the early filling wave (E) and the atrial contraction (A). Before the early filling, at the end of systole, the ejected flow decelerates and LV pressure is lower at the apex than at the LV base. At the passage between systole and diastole, the myocardial contractile elements are deactivated and release the stored elastic energy, this results in further pressure drop inside the LV whose response is the opening of mitral valve. Both these two mechanisms about the transition between systole and diastole are associated with a lower pressure at the apex than at the LV base and both actively contribute to early ventricular filling impulse. Afterwards, before the end of diastole, the electric stimulation starts with the atrial systole and the A-wave completes the LV filling. The relative entity of E and A-waves is an indicator of LV function.

The E and A peaks of mitral velocity are usually assessed by Doppler echocardiography; typically, E-wave velocity is some greater than the A-wave; this ratio is reversed when early filling is insufficient and additional effort is given by atrial contraction, suggesting diastolic dysfunction. This ratio is also reversed in normal fetal hearts before the cardiac maturation.

The anatomic asymmetry of the Mitral valve has a fundamental influence on the development of LV fluid dynamics. The vortex formation process is made of a distorted vortex ring that is stronger on the anterior side and weaker on the posterior; that deviates the ring towards the posterior side (because the anterior side has a higher self-induced velocity, while the posterior side is slowed down by the image vorticity at the wall). As a result, the larger leaflet on the anterior side helps to redirect the blood flow along the lateral-posterior wall. The anterior vortex eventually occupies most of the LV cavity and ensures the development of a proper circulation inside the LV (as previously shown in figure 12.4). Normal transmitral flow is usually laminar and relatively low in velocity (usually less than 100 cm/s); nevertheless the vortex formation creates vortical structures that are complex although not strictly turbulent.

13.4. Pathologies of the mitral valve

Like for the aortic valve, Mitral stenosis, shown in figure 13.10, is due to calcification and reduces the orifice size. The mitral jet presents higher velocities and can be deviated inside the LV. This can create disturbed even turbulent flow with higher energy dissipation and abnormal shear and pressure increase on regions of the wall. The narrower valve is also associated with the increase of transmitral pressure drop, with consequent impairment of LV filling, higher atrial pressure. The increased atrial pressure can influence back pulmonary circulation, produce pulmonary congestion and higher RV pressure. These effects can set the path towards diastolic heart failure and RV dilatation.

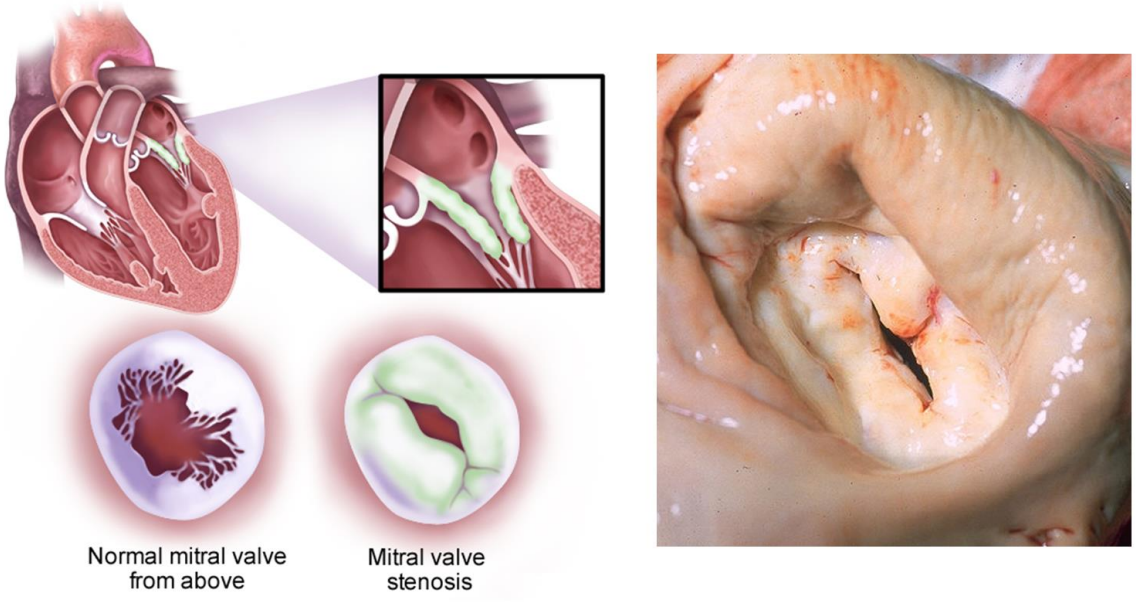

Figure 13.10. Mitral valve stenosis, sketch (left panel) and real image (right). (Source: left, https://medmovie.com/library_id/3255/topic/ahaw_0164i/; right, http://phil.cdc.gov/PHIL_Images/02051999/00015/20G0015_lores.jpg)

Mitral insufficiency can present as a secondary effect to LV dilatation; in this case the entire LV increases its volume and the mitral annulus also enlarges such that the leaflets are unable to cover the

entire mitral area allow backflow. Mitral insufficiency, however, frequently develops as a primary valvular disease in presence of Mitral valve prolapse. Mitral prolapse is due to the growth of the leaflets that become wider, longer and looser. The leaflets of the mitral valve bulge (prolapse) back into the left atrium for the LV pressure during systolic contraction, like a parachute held by the chordae tendineae at the edges. Prolapse is a frequent phenomenon giving no specific symptoms and not requiring treatment. However, it must be monitored because, as shown in figure 13.10, eventually the loose leaflets may not properly close the valve and allow blood flowing backward into the left atrium producing mitral valve regurgitation.

The severity of mitral regurgitation can be evaluated by measuring the regurgitated volume with the same imaging methods (MRI or echography) previously described for aortic valve regurgitation. Mitral regurgitation reduces the effectiveness of LV pumping because part of the stroke volume is not ejected into the Aorta and flows backwards into the left atrium. This induces metabolic feedbacks to increase LV pumping and stressing the LV, especially under exercise or stress. The most evident pathologic consequence of severe regurgitation is the dilatation of the left atrium, which must comply with the additional blood volume and is subjected to systolic LV pressure. When the atrial dilatation becomes important mitral prolapse requires treatment.

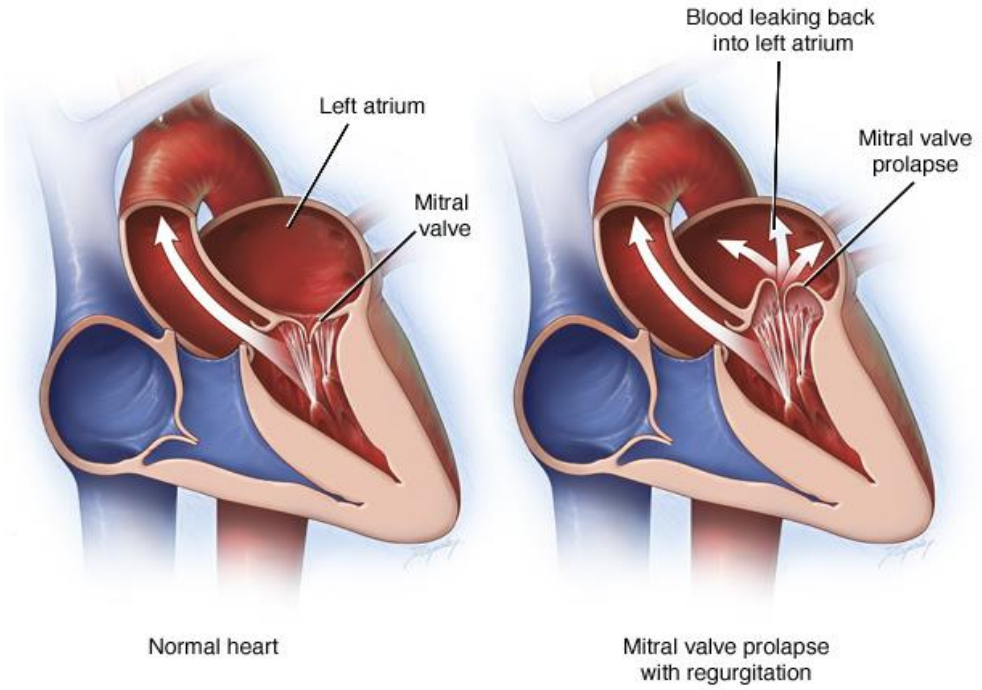

Figure 13.11. Mitral valve prolapse and regurgitation. (Source: https://www.quora.com/How-long-should-I-expect-a-reasonable-recovery-to-take-after-an-aortic-valve-replacement).

Pharmacologic treatments to mitral valve diseases can reduce the effects of this pathology but not heal the defect. A surgical solution to mitral valve stenosis or, sometime, prolapse is the replacement of the diseased valve with a prosthetic valve. As discussed for the aortic valve, prosthesis can be either biological or mechanical. A prosthetic valve alters the intraventricular fluid dynamics and can give rise to further problems in LV function. It was shown, see figure 13.12, that the symmetry of a mechanical bi-leaflet, in contrast with natural asymmetry of the Mitral valve, increase turbulence and may even reverse the vortical circulation inside the LV. However, as these observations are difficult to perform clinically, there are no indications on the consequences of such LV flow alterations.

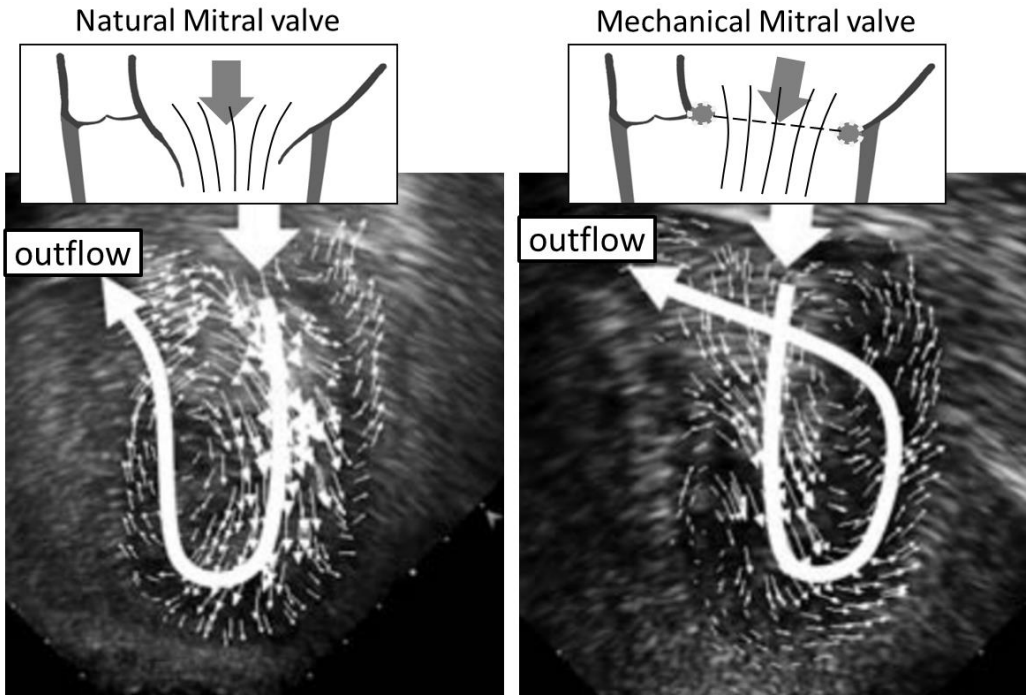

Figure 13.12. Flow redirection with bi-leaflet mechanical valve in mitral position. (Source: Pedrizzetti et al. Ann Biomed Eng 2010. DOI:10.1007/s10439-010-9928-2).

Balloon angioplasty is usually the first option for stenosis before other surgical options. To this aim, a balloon is inserted trans-catheter and expanded at the valve position to break the stenosis.

The most common surgical option for the mitral valve is mitral valve repair (MVR), which has evolved during the years and can be performed under different procedures (Cohn et al., 2015). This is the primary choice for prolapse, although it is performed in presence of stenosis as well. As shown in figure 13.13, MVR aims to recreate the natural valvular geometry removing the exceeding tissue and suturing the original tissue into a proper geometry. Often, MVR is performed including a new prosthetic mitral ring replacing the older one that can be dilated.

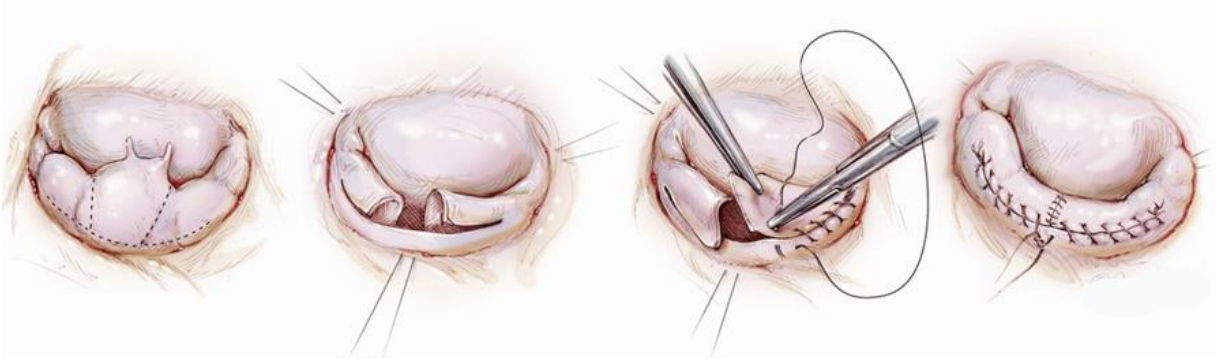

Figure 13.13. Mitral valve repair. (Source: Cohn et al. Ann Cardiothorac Surg 2015. DOI:10.3978/j.issn.2225-319X.2015.04.09).

The fluid dynamics after MVR can vary a lot depending the details of the surgical procedure. The primary end-point is represented by the reduction of regurgitation and the influence of repair to the

intraventriculat flow is rarely monitored. Nevertheless, the long terms outcome can vary substantially after similar MVR procedures and it is sometimes suggested that LV remodeling is influenced by the flow pattern that develops after repair. However, systematic evidences in this sense are not yet available.

Trans-catheter mitral valve repairs (TMVR) are less common than they are for aortic valve, because they present the complexity to anchor the prosthesis in the mitral plane, without a surrounding vessel as was available for the aortic valve. This solution started to be available in the late 2010s, clinical experience is lower than for TAVI and it has to face additional technical challenges (Regueiro et al., 2017). Nevertheless, the applications of TMVR are rapidly growing and novel technological solutions are in continuous progress.

One endovascular solution for reducing regurgitation in Mitral valve prolapse has been recently introduced. It consists of a "clip" (similar to a paper clip) introduced trans-catheter that sticks together the two leaflet thus transforming the wide prolapsed orifice in two small orifices, as shown in figure 13.14 (left), that do not allow regurgitation when closed. This methods is a trans-catheter version of a previous surgical solution called edge-to-edge repair that was then replaced by MVR. After Mitral clip, regurgitations is normally reduced or eliminated; however, this treatment dramatically alters the intraventricular fluid dynamics, as demonstrated since the introduction of edge-to-edge repair (Redaelli et al., 2001) and shown in figure 13.14 (right). The mitral jet transforms into two distinct jets diverging from the valve and impacting on the opposite walls, higher turbulence, varied shear stress and intraventricular pressure gradients. The long term clinical consequences of this alteration are still not verified. This solution is advised for critical Mitral regurgitations conditions and for patients that cannot undergo to other treatment options.

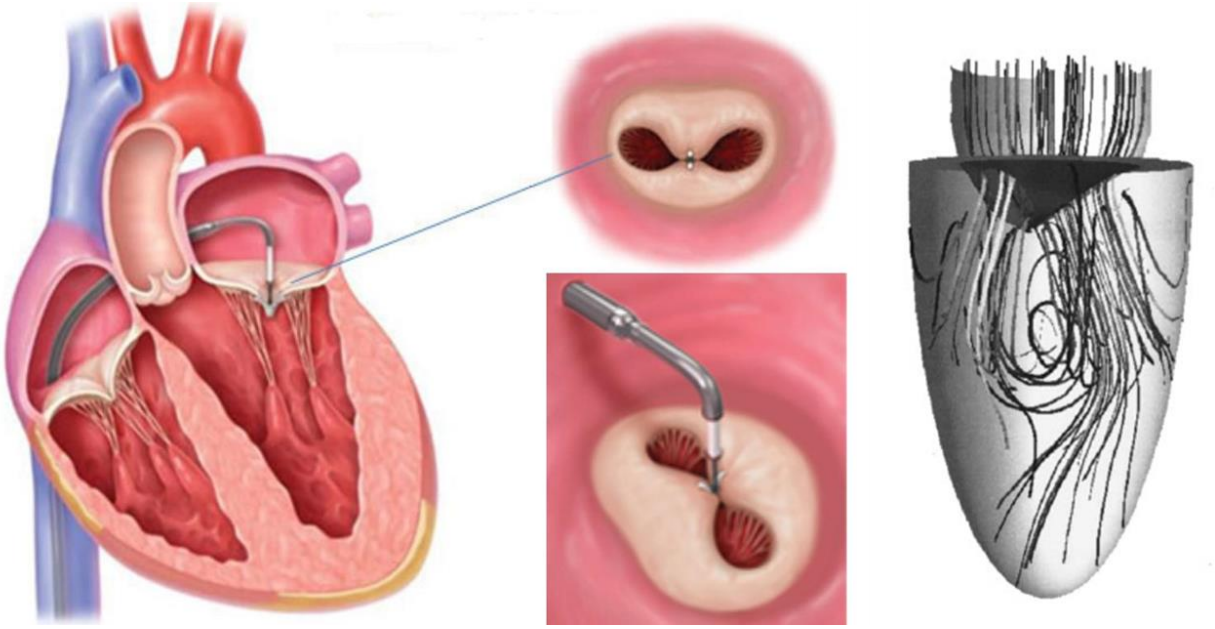

Figure 13.14. Mitral valve edge-to-edge repair with Mitral clip (left); flow after repair (right). (Source: left, https://www.cardiovascular360.it/emodinamica/strutturale/mitraclip; right, Redaelli et al. J Biomech Eng 2001. DOI: 10.1115/1.1408938)

13.5. A mention to congenital cardiac disease

Several diseases are related to congenital malformations of the heart, most of them related to pathological alterations of cardiac valves. This is a wide and complex topic that is out of the scope this basic text and not discussed here. However, it is worth mentioning the most common (frequency of 1 every 2000 children) severe congenital heart defects that is found in new born children: Tetralogy of Fallot, and Hypoplastic Left Heart Syndrome (HLHS).

The Tetralogy of Fallot (TOF) is a combination of four defects, interrelated and concurring, that directly influence the blood circulation in the heart. Each defects one can present with different degree of severity and in different combinations. The common result is low blood oxygenation, which can gives rise to cyanosis; for this reason, this defect is also called the "blue baby syndrome".

TOF is characterized by the followings malformations as graphically described in figure 13.15.

1. A defect in the interventricular septum that is not complete and allows passage of blood between RV and LV; this measn that part of the non-oxygenated RV blood can enter the LV and delivered into the circulation.
2. The pulmonary valve, at the RV outlet, is narrower thus reducing the amount of blood delivered toward the pulmonary circulation for oxygenation.
3. The Aorta is displaced towards the right side, because the basal part of the interventricular septum is absent, therefore it can receive either the oxygenated blood from the LV and part of the non-oxygenated blood ejected by the RV.
4. The communication between LV and RV and the narrower pulmonary valve provoke the increases of the RV pressure and hypertrophy of the RV wall that becomes thicker.

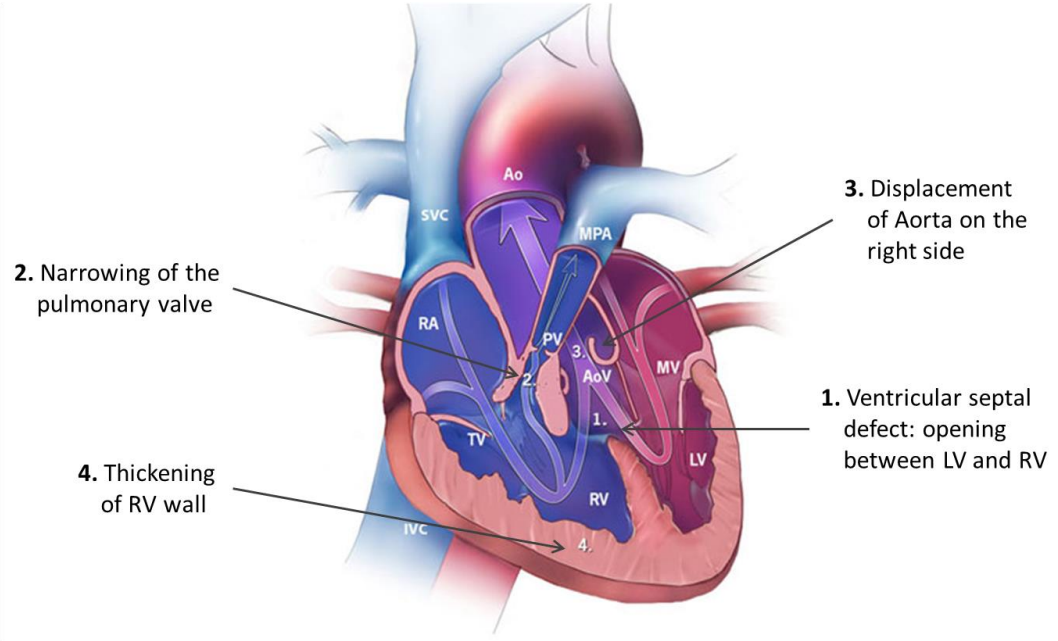

Figure 13.15. Tetralogy of Fallot. (Source: https://www.cdc.gov/ncbddd/heartdefects/tetralogyoffallot.html)

TOF typically requires open-heart surgery in the first years of life. The procedure involves increasing the size of the pulmonary valve and pulmonary arteries and repairing the ventricular septal defect.

The exact timing of surgery depends on the symptoms and size. Normally, surgery is delayed as much as possible in order to act on more grown heart. When surgery is made early, further surgery may be required to adapt the therapeutic repairs along with the increasing size of the heart.

The big challenge in TOF therapy is therefore to be able to anticipate the evolution of the disease, in order to better plan the timing of the various therapeutic activities. The dynamic analysis of intra-cardiac fluid dynamics was recognized to have a role in cardiac morphogenesis as well in cardiac development. Therefore, research is in progress to evaluate fluid dynamics in TOF patients, especially by 3D Phase-contrast MRI (4D flow MRI), with more centers under creation in numerous sites. The aim is of providing evaluations of the actual status of the cardiac circulation and, possibly, indications of the probable evolutions that can be precious for optimization of surgical choices and timing of therapy.

The Hypoplastic Left Heart Syndrome (HLHS) is a birth defect that occurs when the left side of the heart is underdeveloped; in this pathology, the LV is not formed or it is very small, and the ascending portion of the aorta is typically underdeveloped as well. These babies must undergo surgery immediately at birth because blood is not pumped in the primarily circulation.

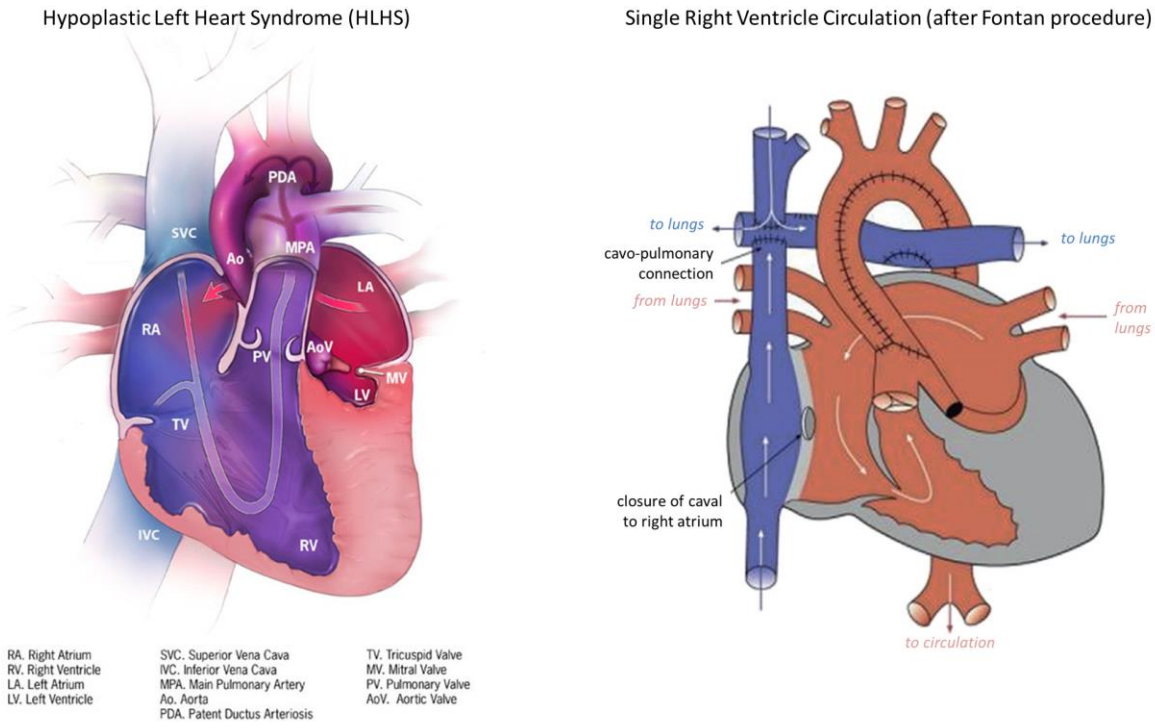

Figure 13.16. Hypoplastic Left Heart Syndrome (left), Single Right Ventricle circulation (right). (Source: left, https://en.wikipedia.org/wiki/Hypoplastic_left_heart_syndrome; right, Love B. JACC 2017. DOI:10.1016/j.jacc.2017.06.048)

A baby with hypoplastic left heart syndrome has to undergo to multiple surgeries in a particular order are needed to increase blood flow to the body and bypass the poorly functioning left side of the heart (Love, 2017). The right ventricle becomes the main pumping chamber to the body. These surgeries do not cure hypoplastic left heart syndrome, but help restore heart function. Soon after birth, babies undergo the first surgery (Norwood Procedure). This creates a new aorta connected to the right ventricle, such that the right ventricle is used to pump blood both to the pulmonary and the systemic

circulation. After a few months a an additional surgery is commonly required (Bi-directional Glenn Shunt) that creates a direct connection between the pulmonary artery and the superior vena cava. This reduces the work of the RV for the pulmonary circulation and increase it for the systemic circulation.

A final procedure (Fontan Procedure) is usually performed when the baby has about 3 years of age. In this final configuration the inferior an superior venae cavae are connected directly to the pulmonary artery (total cavo-pulmonary connection, TCPC) and the RV is completely bypassed and not used to pump blood into the lung. Pulmonary circulation is thus assumed to occur naturally, without the thrust from the RV, supported by the pressure available in the caval veins. The RV is then connected directly to the aorta and it is used for the systemic circulation. This final circulation, where the RV is transformed in the systemic ventricle, is commonly called one with single right ventricle (SRV).

REFERENCES

Arvidsson, P.M., Töger, J., Pedrizzetti, G., Heiberg, E., Borgquist, R., Carlsson, M., Arheden, H., 2018. Hemodynamic forces using 4D flow MRI: an independent biomarker of cardiac function in heart failure with left ventricular dyssynchrony? Am. J. Physiol. Circ. Physiol. ajpheart.00112.2018. https://doi.org/10.1152/ajpheart.00112.2018

Barenblatt, G.I., 2003. Scaling. Cambridge University Press.

Berne, R.M., Levy, M.N., 1997. Cardiovascular Physiology. Mosby-Year Book, Inc., St. Louis.

Bolger, A.F., Heiberg, E., Karlsson, M., Wigström, L., Engvall, J., Sigfridsson, A., Ebbers, T., Kvitting, J.P.E., Carlhäll, C.J., Wranne, B., 2007. Transit of blood flow through the human left ventricle mapped by cardiovascular magnetic resonance. J. Cardiovasc. Magn. Reson. 9, 741–747. https://doi.org/10.1080/10976640701544530

Bourantas, C. V., Serruys, P.W., 2014. Evolution of Transcatheter Aortic Valve Replacement. Circ. Res. 114, 1037–1051. https://doi.org/10.1161/CIRCRESAHA.114.302292

Carlhäll, C.J., Bolger, A., 2010. Passing strange flow in the failing ventricle. Circ. Hear. Fail. 3, 326–331. https://doi.org/10.1161/CIRCHEARTFAILURE.109.911867

Caro, C.G., Doorly, D.J., Tarnawski, M., Scott, K.T., Long, Q., Dumoulin, C.L., 1996. Non-Planar Curvature and Branching of Arteries and Non-Planar-Type Flow. Proc. Math. Phys. Eng. Sci. 452, 185–197.

Caro, C.G., Fitzgerald, J.M., Schroter, R.C., 1969. Arterial Wall Shear and Distribution of Early Atheroma in Man. Nature 223, 1159–1161. https://doi.org/10.1038/2231159a0

Chen, P.Y., Qin, L., Li, G., Wang, Z., Dahlman, J.E., Malagon-Lopez, J., Gujja, S., Cilfone, N.A., Kauffman, K.J., Sun, L., Sun, H., Zhang, X., Aryal, B., Canfran-Duque, A., Liu, R., Kusters, P., Sehgal, A., Jiao, Y., Anderson, D.G., Gulcher, J., Fernandez-Hernando, C., Lutgens, E., Schwartz, M.A., Pober, J.S., Chittenden, T.W., Tellides, G., Simons, M., 2019. Endothelial TGF-β signalling drives vascular inflammation and atherosclerosis. Nat. Metab. 1, 912–926. https://doi.org/10.1038/s42255-019-0102-3

Chung, B., Cebral, J.R., 2015. CFD for Evaluation and Treatment Planning of Aneurysms: Review of Proposed Clinical Uses and Their Challenges. Ann. Biomed. Eng. 43, 122–138. https://doi.org/10.1007/s10439-014-1093-6

Cohn, L.H., Tchantchaleishvili, V., Rajab, T.K., 2015. Evolution of the concept and practice of mitral valve repair. Ann. Cardiothorac. Surg. 4, 315–21. https://doi.org/10.3978/j.issn.2225-319X.2015.04.09

Courtois, M., Kovács, S.J., Ludbrook, P.A., 1988. Transmitral pressure-flow velocity relation. Importance of regional pressure gradients in the left ventricle during diastole. Circulation 78, 661–71. https://doi.org/10.1161/01.cir.78.3.661

Davidson, P.A., 2004. Turbulence: An Introduction for Scientists and Engineers. Oxford Uuniversity Press, New York.

Domenichini, F., 2011. Three-dimensional impulsive vortex formation from slender orifices. J. Fluid Mech. 666, 506–520. https://doi.org/10.1017/S0022112010004994

Eriksson, J., Zajac, J., Alehagen, U., Bolger, A.F., Ebbers, T., Carlhäll, C.-J., 2017. Left ventricular hemodynamic forces as a marker of mechanical dyssynchrony in heart failure patients with left bundle branch block. Sci. Rep. 7, 2971. https://doi.org/10.1038/s41598-017-03089-x

Feigenbaum, M.J., 1978. Quantitative universality for a class of nonlinear transformations. J. Stat. Phys. 19, 25–52. https://doi.org/10.1007/BF01020332

Firstenberg, M.S., Vandervoort, P.M., Greenberg, N.L., Smedira, N.G., McCarthy, P.M., Garcia, M.J., Thomas, J.D., 2000. Noninvasive estimation of transmitral pressure drop across the normal mitral valve in humans: Importance of convective and inertial forces during left ventricular filling. J. Am. Coll. Cardiol. 36, 1942–1949. https://doi.org/10.1016/S0735-1097(00)00963-3

Fredriksson, A.G., Zajac, J., Eriksson, J., Dyverfeldt, P., Bolger, A.F., Ebbers, T., Carlhäll, C.J., 2011. 4-D blood flow in the human right ventricle. Am. J. Physiol. - Hear. Circ. Physiol. 301, 2344–2350. https://doi.org/10.1152/ajpheart.00622.2011

Frisch, U., 1995. Turbulence. The Legacy of A. N. Kolmogorov. Cambridge University Press. https://doi.org/10.1017/CBO9781139170666

Fung, Y.C., 1997. Biomechanics: Circulation, 2nd ed. Springer-Verlag, New York.

Gharib, M., Rambod, E., Kheradvar, A., Sahn, D.J., Dabiri, J.O., 2006. Optimal vortex formation as an index of cardiac health. Proc. Natl. Acad. Sci. 103, 6305–6308. https://doi.org/10.1073/pnas.0600520103

Guerra, M., Brás-Silva, C., Amorim, M.J., Moura, C., Bastos, P., Leite-Moreira, A.F., 2013. Intraventricular pressure gradients in heart failure. Physiol. Res. 62, 479–487.

Kheradvar, A., Pedrizzetti, G., 2012. Vortex formation in the cardiovascular system, Vortex Formation in the Cardiovascular System. https://doi.org/10.1007/978-1-4471-2288-3

Kilner, P.J., Yang, G.Z., Wilkes, A.J., Mohiaddin, R.H., Firmin, D.N., Yacoub, M.H., 2000. Asymmetric redirection of flow through the heart. Nature 404, 759–61. https://doi.org/10.1038/35008075

Kundu, P.K., Cohen, I.M., Dowling, D.R., 2012. Fluid Mechanics, 5th ed. Academic Press.

Lee, S.W., Antiga, L., Steinman, D.A., 2009. Correlations among indicators of disturbed flow at the normal carotid bifurcation. J. Biomech. Eng. 131, 1–7. https://doi.org/10.1115/1.3127252

Lloyd-Jones, D.M., Larson, M.G., Leip, E.P., Beiser, A., D'Agostino, R.B., Kannel, W.B., Murabito, J.M., Vasan, R.S., Benjamin, E.J., Levy, D., 2002. Lifetime risk for developing congestive heart failure: The Framingham Heart Study. Circulation 106, 3068–3072. https://doi.org/10.1161/01.CIR.0000039105.49749.6F

Love, B.A., 2017. Transcatheter Superior Cavopulmonary Anastomosis: Interesting Technique, Limited Applicability. J. Am. Coll. Cardiol. 70, 753–755. https://doi.org/10.1016/j.jacc.2017.06.048

Mangual, J.O., Domenichini, F., Pedrizzetti, G., 2012. Describing the highly three dimensional right ventricle flow. Ann. Biomed. Eng. 40, 1790–1801. https://doi.org/10.1007/s10439-012-0540-5

May, R.M., 1976. Simple mathematical models with very complicated dynamics. Nature 261, 459–467. https://doi.org/10.1038/261459a0

Messner, A.M., Taylor, G.Q., 1980. Algorithm 550: Solid Polyhedron Measures [Z]. ACM Trans. Math. Softw. 6, 121–130. https://doi.org/10.1145/355873.355885

Monin, A.S., Yaglom, A.M., 1971. Statistical Fluid Mechanics: Volume 1. MIT Press.

Morbiducci, U., Ponzini, R., Rizzo, G., Cadioli, M., Esposito, A., Montevecchi, F.M., Redaelli, A., 2011. Mechanistic insight into the physiological relevance of helical blood flow in the human

aorta: An in vivo study. Biomech. Model. Mechanobiol. 10, 339–355. https://doi.org/10.1007/s10237-010-0238-2

Panton, R.L., 2013. Incompressible Flow, 4th ed. John Wiley & Sons, Inc., Hoboken, NJ, USA. https://doi.org/10.1002/9781118713075

Park, K.-H., Son, J.-W., Park, W.-J., Lee, S.-H., Kim, U., Park, J.-S., Shin, D.-G., Kim, Y.-J., Choi, J.-H., Houle, H., Vannan, M.A., Hong, G.-R., 2013. Characterization of the Left Atrial Vortex Flow by Two-Dimensional Transesophageal Contrast Echocardiography Using Particle Image Velocimetry. Ultrasound Med. Biol. 39, 62–71. https://doi.org/10.1016/j.ultrasmedbio.2012.08.013

Pasipoularides, A., 2015. Mechanotransduction Mechanisms for Intraventricular Diastolic Vortex Forces and Myocardial Deformations: Part 2. J. Cardiovasc. Transl. Res. 8, 293–318. https://doi.org/10.1007/s12265-015-9630-8

Pedley, T.J., 1980. The fluid dynamics of large blood vessels. Cambridge University Press.

Pedley, T.J., Brook, B.S., Seymour, R.S., 1996. Blood pressure and flow rate in the giraffe jugular vein. Philos. Trans. R. Soc. London. Ser. B Biol. Sci. 351, 855–866. https://doi.org/10.1098/rstb.1996.0080

Pedrizzetti, G., 2019. On the computation of hemodynamic forces in the heart chambers. J. Biomech. 109323. https://doi.org/10.1016/j.jbiomech.2019.109323

Pedrizzetti, G., Domenichini, F., 2015. Left Ventricular Fluid Mechanics: The Long Way from Theoretical Models to Clinical Applications. Ann. Biomed. Eng. 43, 26–40. https://doi.org/10.1007/s10439-014-1101-x

Pedrizzetti, G., Domenichini, F., 2005. Nature optimizes the swirling flow in the human left ventricle. Phys. Rev. Lett. 95, 1–4. https://doi.org/10.1103/PhysRevLett.95.108101

Pedrizzetti, G., La Canna, G., Alfieri, O., Tonti, G., 2014. The vortex—an early predictor of cardiovascular outcome? Nat. Rev. Cardiol. 11, 545–553. https://doi.org/10.1038/nrcardio.2014.75

Pedrizzetti, G., Martiniello, A.R., Bianchi, V., D'Onofrio, A., Caso, P., Tonti, G., 2016. Changes in electrical activation modify the orientation of left ventricular flow momentum: Novel observations using echocardiographic particle image velocimetry. Eur. Heart J. Cardiovasc. Imaging 17, 203–209. https://doi.org/10.1093/ehjci/jev137

Pedrizzetti, G., Martiniello, A.R., Bianchi, V., D'Onofrio, A., Caso, P., Tonti, G., D'Onofrio, A., Caso, P., Tonti, G., 2015. Cardiac fluid dynamics anticipates heart adaptation. J. Biomech. 48, 388–391. https://doi.org/10.1016/j.jbiomech.2014.11.049

Pedrizzetti, G., Sengupta, P.P.P., 2015. Vortex imaging: new information gain from tracking cardiac energy loss. Eur. Hear. J. - Cardiovasc. Imaging 16, 10–11. https://doi.org/10.1093/ehjci/jev070

Piazza, N., Bleiziffer, S., Brockmann, G., Hendrick, R., Deutsch, M.-A., Opitz, A., Mazzitelli, D., Tassani-Prell, P., Schreiber, C., Lange, R., 2011. Transcatheter Aortic Valve Implantation for Failing Surgical Aortic Bioprosthetic Valve. JACC Cardiovasc. Interv. 4, 721–732. https://doi.org/10.1016/j.jcin.2011.03.016

Redaelli, A., Guadagni, G., Fumero, R., Maisano, F., Alfieri, O., 2001. A computational study of the hemodynamics after "edge-to-edge" mitral valve repair. J. Biomech. Eng. 123, 565–570. https://doi.org/10.1115/1.1408938

Regueiro, A., Granada, J.F., Dagenais, F., Rodés-Cabau, J., 2017. Transcatheter Mitral Valve

Replacement: Insights From Early Clinical Experience and Future Challenges. J. Am. Coll. Cardiol. 69, 2175–2192. https://doi.org/10.1016/j.jacc.2017.02.045

Reynolds, O., 1894. II. On the dynamical theory of incompressible viscous fluids and the determination of the criterion. Proc. R. Soc. London 56, 40–45. https://doi.org/10.1098/rspl.1894.0075

Reynolds, O., 1883. III. An experimental investigation of the circumstances which determine whether the motion of water shall be direct or sinuous, and of the law of resistance in parallel channels. Proc. R. Soc. London 35, 84–99. https://doi.org/10.1098/rspl.1883.0018

Rubenstein, D.A., Yin, W., Frame, M.D., 2015. Biofluid Mechanics: An introduction to fluid mechanics, macrocirculation, microcirculation, 2nd ed. Academic Press.

Saffman, P.G., 1992. Vortex Dynamics. Cambridge University Press.

Sagaut, P., 2006. Large Eddy Simulation for Incompressible Flows, Scientific Computation. Springer-Verlag, Berlin/Heidelberg. https://doi.org/10.1007/b137536

Schlichting, H., 1979. Boundary-Layer Theory, VII editio. ed. McGraw-Hill.

Seo, J.H., Abd, T., George, R.T., Mittal, R., 2016. A Coupled Chemo-Fluidic Computational Model for Thrombogenesis in Infarcted Left Ventricles. Am. J. Physiol. - Hear. Circ. Physiol. 310, H1567–H1582. https://doi.org/10.1152/ajpheart.00855.2015

Tonti, G., Pedrizzetti, G., Trambaiolo, P., Salustri, A., 2001. Space and time dependency of inertial and convective contribution to the transmitral pressure drop during ventricular filling. J. Am. Coll. Cardiol. 38, 290–291. https://doi.org/10.1016/S0735-1097(01)01355-9

Ziegler, M., Welander, M., Lantz, J., Lindenberger, M., Bjarnegård, N., Karlsson, M., Ebbers, T., Länne, T., Dyverfeldt, P., 2019. Visualizing and quantifying flow stasis in abdominal aortic aneurysms in men using 4D flow MRI. Magn. Reson. Imaging 57, 103–110. https://doi.org/10.1016/j.mri.2018.11.003